# MODELING AND SIMULATION OF ABRASIVE FLOW MACHINING PROCESS

by

**RAJENDRA KUMAR JAIN**



DEPARTMENT OF MECHANICAL ENGINEERING

**INDIAN INSTITUTE OF TECHNOLOGY KANPUR**

May 1999

# MODELING AND SIMULATION OF ABRASIVE FLOW MACHINING PROCESS

*A Thesis Submitted*
*in Partial Fulfillment of the Requirement*
*for the Degree of*
**DOCTOR OF PHILOSOPHY**

by

**RAJENDRA KUMAR JAIN**

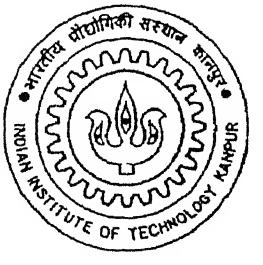


to the

**DEPARTMENT OF MECHANICAL ENGINEERING**

**INDIAN INSTITUTE OF TECHNOLOGY - KANPUR**

May 1999

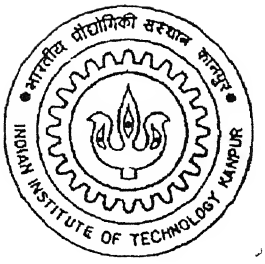


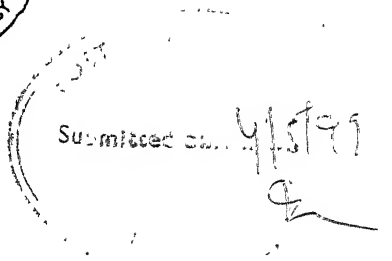


# CERTIFICATE

It is certified that the thesis work entitled ***Modeling and Simulation of Abrasive Flow Machining Process*** by **Rajendra Kumar Jain** has been carried out under my supervision and that it has not been submitted elsewhere for a degree.

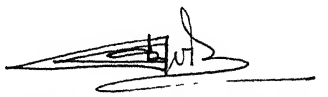

**( Prof. V. K. Jain )**

Department of Mechanical Engineering
Indian Institute of Technology
Kanpur 208 016, India

May 1999

# Acknowledgements

With warmest regards, I express my deepest gratitude and heartful thanks to my thesis supervisor Prof V K Jain for his authentic and invaluable guidance, scrupulous attention, constant encouragement, and inspiring advice throughout this course of research I owe much more than I can express to him for his support at every stage of the work

I am indebted to Prof G K Lal, Prof S K Choudhary, Prof P M Dixit, Prof Prashant Kumar, Prof K Murlidhar, Prof G Biswas, Prof M K Muju and Prof. P K Kalra for their valuable suggestions, cooperation and encouragement during the various phases of the work

My sincere thanks are due to Sri R M Jha, Sri H.P. Sharma and Sri Namdev of the manufacturing Science laboratory for their skillful and friendly rendering of all possible help in the setting up and conducting of the experiments

I am obliged to Madhav Institute of Technology and Science Gwalior for sponsoring me as Q.I P scholar and also Government of India for its financial support. I acknowledge the financial support from Department of Science and Technology, Govt of India and Widia (India) Limited, Banglore, for the project. Thanks are also due to Extrude Hone, USA for supplying abrasive media

I am also grateful to my seniors Dr Philip Koshy, Dr. V.N. Reddy, Dr. U S Dixit and Dr. Rajiv Gupta for suggestions, support and friendly environment provided by them

I extend many thanks to all my friends who have been supportive during the course of the work. The time I spent with Santosh kumar, Ramarao, Rammohan, G Adsul, Rangnath, Sunil, Kumaraswamy, Gautam Pohit, Ali, Nilesh, Mukul, Vinod, Ramesh . has been very exciting and enlightening as well, they really made life at IIT Kanpur memorable and great

I am greatly indebted to my parents, brothers and sister Bhavana for their love, patience and support, but for which this work would have hardly been possible.

I am beholden to my wife Anupama for the constant encouragement, tolerance and cheerful environment rendered.

Finally, I express my thanks to all those who helped me directly or indirectly for successful completion of this work.

Rajendra Kumar Jain

Dedicated to my father Sri C. L. Jain

# SYNOPSIS

The most labour intensive, uncontrollable area in the manufacturing of precision parts involves *final machining operations*, which frequently demand as much as 15% of the total manufacturing cost. The result of high quality finish on the parts is improved performance, 'running-in-period' of minimum duration, and considerable increase in the length of life of the component. Abrasive finishing process is usually employed as the last operation on the high value added components. It is imperative to achieve these processes economically with strategic consideration of the key influencing parameters.

Grinding, lapping, honing, and super finishing are *traditional methods of finishing*. But the applications of grinding, lapping, honing, super finishing, and other abrasive finishing processes are limited to the production of the workpieces of the basic forms such as flat, cylindrical etc. These conventional finishing processes are being pushed to their limits of performance and productivity in general, and in case of hard materials, and components of complicated shapes in particular. Hence, a need is being felt to develop a finishing process with wider bounds of application areas, better quality performance, and higher productivity. Abrasive flow machining is one of such processes.

**Abrasive flow machining** (AFM) is a non-traditional finishing process that is used for deburring, radiusing, surface finish improvement, polishing of irregular shaped passages, and removal of thermal machining recast layer. With today's focus on total automation in the flexible manufacturing system, AFM process offers both automation and flexibility in final machining operations. A key feature differentiating AFM from most of the other finishing processes is the ability to control and select the intensity and location of abrading through fixture design and abrasive media selection. Applications of this process include finishing of components in aerospace, automotive, dies, chemical processing and medical industries. Materials from soft aluminum to tough nickel alloys, ceramics and carbides have been successfully micro machined by this process. AFM process provides a high level of surface finish and close geometric tolerances with economically acceptable rate of surface generation for a wide range of industrial components. The ability of media in AFM process

to finish difficult to reach areas, to follow complex contours and to simultaneously work on multiple edges and surfaces, makes it more versatile than other finishing processes.

AFM removes small quantity of material by flowing a semisolid abrasive laden compound called **'media'** (abrasive particles uniformly suspended in viscous chemical compound) through or across the surfaces of the workpiece to be finished. Two vertically opposed cylinders extrude abrasive media back and forth through passages formed by the workpiece and tooling. The machining action compares to grinding or lapping operation as the media gently and uniformly abrades the surface or edges. The media acts as a *'self deformable stone'* having protruding abrasive particles acting as cutting tools.

AFM process is very much in its early stages of development. Sustained research is required to transform the process into a mature technology, for its successful induction into the industry. The thesis makes an attempt in this direction.

Both *theoretical and experimental studies* of abrasive flow machining are greatly *hampered* by the inherent random nature and multiplicity of variables. Not much information is available in the literature which deals with theoretical analysis of material removal mechanism in AFM. The relationship between process parameters and performance characteristics of the process are not completely known. There is a need to carry out systematic theoretical analysis of viscous media flow to determine the stresses and machining forces acting on the workpiece. This will help in modeling and proper understanding of the mechanics of the micro cutting process during AFM. The objective of the present work is to investigate the mechanism of AFM process and to study the effect of various process parameters on the process performance by experimentation and theoretical modeling.

The **specific objectives** to achieve the above mentioned goals are as follows :

- To conduct experiments to study the effects of various process parameters on material removal and surface roughness.
- To analyze the flow of media in AFM process using finite element method by considering the media as viscoelastic material.
- To develop a model to determine the material removal and surface finish in AFM process and to validate the developed model with the data obtained by experimentation.

- To develop a model for the topography of media and estimate the active grain density by microscopic technique; and to simulate the random surface generated in AFM process.
- To analyze the specific energy and thermal aspects of AFM process.
- Application of neural network in AFM process for modeling and optimization.

**Experiments** have been conducted on the AFM machine designed and fabricated at Indian Institute of Technology, Kanpur. Experiments have been planned using central composite rotatable design to get the useful inferences by performing minimum number of experiments. A fixture was designed to direct the media to flow in the desired areas. The process parameters considered are number of cycles, extrusion pressure, percentage concentration of abrasives and reduction ratio. Internal surfaces of mild steel workpieces with circular cross section have been finished using abrasive media (SiC abrasives mixed with polyborosiloxane carrier). Material removal increases with extrusion pressure, concentration of abrasives, reduction ratio and number of cycles. Surface roughness value decreases with increase in extrusion pressure, reduction ratio and concentration of abrasives for a specified number of cycles.

A model has been proposed for analysing media flow through the media cylinder and workpiece. The method involves the use of **finite element technique** to solve the governing equations in terms of primary variables (velocity and pressure). The theoretical analysis of media flow predicts the stresses developed during the flow. These computed stresses can be used to evaluate the machining forces. The model predicts the normal stresses at the workpiece surface with reasonable accuracy.

AFM is considered to be a scratching action performed by the abrasive grains in the flowing media. A **model** has been proposed to determine the material removal and generated surface roughness during AFM using abrasion theory. The model is based on accumulated plastic flow of material by repeated indentation by moving abrasive particles. The model includes the operating conditions of the process, e.g. abrasive size, extrusion pressure, workpiece material hardness and size of the workpiece to be machined. A good agreement is found between the experimental results and theoretical predictions. Material removal increases with increase in extrusion pressure and percentage concentration of

abrasives in the media. Surface roughness value decreases with increase in extrusion velocity / extrusion pressure, percentage and concentration of abrasives for a specified number of cycles.

Understanding of the process of generating finished surface is important for the control of the AFM process. Systematic modeling and analysis of AFM are greatly hampered by the inherent random nature and multiplicity of variables. Simulation technique can help to understand the mechanics of AFM process by allowing the effects of various process parameters. The concept of a newly developed, versatile **simulation model** which generates and statistically evaluates the interaction between spherical abrasives and workpiece surface is described. The simulation enables prediction of the roughness of the machined surfaces and material removal with reference to percentage concentration of abrasives, extrusion pressure of media, reduction ratio and number of cycles. The number of active grains and state of cutting edges are closely related to the AFM performance. The present stochastic simulation method is used to evaluate the active grain density. A microscopic technique is also used to estimate the number of active grain density at various mesh sizes and concentrations. The results obtained from stochastic simulation method agree well with the data obtained by microscopic technique.

A model has been proposed for the determination of **specific energy and tangential forces** in AFM process. The model includes the operating conditions of AFM e.g., grain size, applied pressure, hardness of workpiece material, number of cycles and active grain density. A simple model of **heat transfer in AFM** has also been developed that considers heat flow to the workpiece and abrasive media. The dependence of the workpiece temperature on the AFM parameters has been explored. The model also predicts the fraction of heat entering into the workpiece and media.

AFM process is too complicated to warrant appropriate analytical models and most of the time, analytical models are based on many assumptions, which contradict in reality. More importantly, it is sometimes difficult to adjust the parameters of the above mentioned models according to actual situation of the machining process. Therefore, neural networks which can map the input/output relationships and possess massive parallel computing capability, have attracted attention of researchers working in the area of AFM process. The thesis presents architecture of **back-propagation neural network model** for

prediction of material removal rate and surface roughness in AFM. In order to decide the structure of neural network, the rate of error convergence is checked by changing the number of hidden layers and also by adjusting the learning rate and momentum rate. The three layers back-propagation with four inputs, two outputs and nine hidden nodes is adopted for neural network. It is observed that learning could remarkably be enhanced by training the network with noise injected inputs. The results confirm the feasibility of this approach, and show a good agreement with experimental results for a wide range of machining conditions.

The neural network has also been used for **optimum selection of input parameters** of AFM process. First, a generalized back-propagation neural network is used to establish the process model. A second network, which parallelizes the Augmented Lagrange Multiplier algorithm, determines the corresponding optimal machining parameters by minimizing a performance index subject to appropriate operating constraints. An important consideration is that process optimization can be performed in the absence of process model and purely by experimental observations.

To validate the neural network results, optimization of the AFM process has been also performed using **genetic algorithm** (GA). Genetic algorithms are computerized search and optimization algorithms, based on the evolutionary process of biological organisms in nature. The optimization results of neural network coincide well with the results obtained by genetic algorithms and justify the neural network approach.

The thesis also outlines the possible avenues for future research in abrasive flow machining process.

**Organization of the thesis**

First chapter of the thesis comprises introduction of traditional finishing methods and their limitations, introduction and importance of abrasive flow machining process, review of literature, and scope and objective of the present work. Description of the experimental set-up, details of experimentation and the associated results constitute chapter 2 of the thesis. Chapter 3 presents a model for analysing the flow of AFM media using finite element technique. Modeling for material removal and surface roughness using abrasion theory is also described. A model for the topography of abrasive media and

estimation of active grain density by microscopic technique is described in chapter 4. A modified model to simulate the random surface generated and material removal in AFM is also discussed. Chapter 5 is devoted to forces, specific energy and thermal aspects of AFM. Chapter 6 deals with the modeling of AFM by neural networks. Optimization of AFM process by neural network and genetic algorithm is also presented. The conclusions drawn from the present work are enumerated in chapter 7. Possible avenues for future research in AFM are also outlined. The references and appendices are given at the end of the thesis.

# Contents

# List of Figures

# List of Tables

# Nomenclature

| | |
|---|---|
| [A} | matrix of A |
| {A} | column vector of A |
| $b$ | radius of the projected area of indentation, m |
| $b_s$ | side of a square cross section, m |
| [B] | matrix of differential coefficients of shape functions |
| $c_{pa}$ | specific heat of abrasive material, J/kg-K |
| $c_{pc}$ | specific heat of carrier polyborosiloxane, J/kg –K |
| $c_{pw}$ | specific heat of workpiece, J/kg-K |
| $C$ | percentage concentration of abrasives by weight |
| $d_g$ | diameter of abrasive grain, m |
| $d_w$ | diameter of workpiece to be finished, m |
| $f$ | average coefficient of friction |
| $F_{ng}$ | normal force acting on an abrasive grain, N |
| $F_t$ | total tangential force, N |
| $F_{tg}$ | tangential force acting on an abrasive grain, N |
| $\{F\}$ | global right hand side vector |
| $H_w$ | hardness of workpiece material, $N/m^2$ |
| $k_a$ | thermal conductivity of abrasives, $W/m^2 K$ |
| $k_c$ | thermal conductivity of carrier, $W/m^2 K$ |
| $k_m$ | thermal conductivity of media, $W/m^2 K$ |
| $k_w$ | thermal conductivity of workpiece, $W/m^2 K$ |
| $[K^e]$ | elemental coefficient matrix |
| [K] | global coefficient matrix |
| $l_s$ | stroke length, m |

workpiece length, m

actual contact length in $i$th stroke, m

mesh size of abrasive grains

active grain density, /mm$^2$

number of cycles

vector of boundary shape functions

column vector of bilinear shape functions for the approximation of pressure

matrix of biquardatic shape functions for the approximation of velocities

hydrostatic pressure (or pressure), N/m$^2$

extrusion pressure, N/m$^2$

heat flux, W/m$^2$

heat flux entering to the media, W/m$^2$

heat flux entering to the workpiece, W/m$^2$

radius of media cylinder , m

grain radius, m

radius of workpiece, m

cylindrical coordinates

fraction of total heat flux entering into the workpiece

surface roughness of the workpiece, $\mu$m

initial surface roughness of the workpiece, $\mu$m

reduction ratio

peak to valley roughness, $\mu$m

standard deviation

temperature, K

depth of indentation of abrasive into workpiece material, m

component of traction vector

specific energy, J/mm$^3$

| | |
|---|---|
| $V$ | volume of total material removed, $m^3$ |
| $V_a$ | volume of abrasives, $m^3$ |
| $V_i$ | volume of material removed in $i$th stroke, $m^3$ |
| $v_f$ | velocity of media across the workpiece, m/s |
| $v_p$ | velocity of piston or velocity of media flow at inlet, m/s |
| $v_i$ | component of velocity vector |
| $v_{j,k}$ | net internal activity levels of neuron j in layer k |
| $\{w^e\}$ | vector of elemental nodal weight functions for primary variables |
| $\{w_v^e\}$ | vector of elemental nodal weight functions for velocities |
| $\{w_p^e\}$ | vector of elemental nodal weight function for pressure |
| $\{w\}$ | global vector of nodal weight function |
| $w_{j,i,k}$ | synaptic weight vector between neuron $j$ in layer $(k-1)$ to neuron $i$ in layer $k$ |
| x,y,z | random variables defining grain position along axial, transverse and vertical directions |
| $y_{j,k}$ | function signal of the neuron $j$ in layer $k$ |
| W | Weissenberg number |

## Greek Symbols

| | |
|---|---|
| $\alpha$ | angle made by normal at tool surface with r-axis |
| $\alpha_n$ | momentum constant of neural network |
| $\alpha_w$ | thermal diffusivity of the workpiece material, $m^2/s$ |
| $\delta$ | local gradient of network |
| $\delta_{ij}$ | Kronecker's delta |
| $\dot{\varepsilon}_{ij}$ | strain rate tensor |
| $\eta$ | learning rate parameter |
| $\lambda$ | Relaxation time, s |
| $\lambda_1$ | Langrange multiplier |
| $\mu$ | viscosity function of the media, Pa s |

| | |
|---|---|
| $\mu$ | viscosity function of the media, Pa s |
| $\mu_o$ | constant used for non-dimensionalization of $\mu$ |
| $\rho_a$ | mass density of abrasives, kg/m$^3$ |
| $\rho_c$ | mass density of carrier, kg/m$^3$ |
| $\rho_m$ | mass density of media, kg/m$^3$ |
| $\sigma_{ij}$ | stress tensor |
| $\sigma_0$ | initial yield stress of the material, N/m$^2$ |
| $\sigma_n$ | normal stress, N/m$^2$ |
| $\tau_{ij}$ | deviatoric component of stress |
| $\Gamma$ | boundary of the domain |

# Chapter 1

## Introduction and Literature Review

### 1.1 Abrasive Fine Finishing

The most labour intensive, uncontrollable area in the manufacture of precision parts involves *final machining operations*, which frequently demand as much as 15% of the total manufacturing cost The cost of surface finish increases sharply for a roughness value of less than one micron. Surface finish has a vital influence on important functional properties such as wear resistance and power loss due to friction on most of the engineering components. When constant friction is required, the surfaces must be uniform and have a predictable wear rate. Surface finish can also affect part-to-part fit and tolerances. The result of high quality finish on the parts is improved performance, 'running-in-period' of minimum duration and considerable increase in the length of life of the component. These final machining operations are uncontrollable and if they are not carried out properly, performance of the machined component may be far from optimum. The dimensional and alignment accuracy and the quality of the surface finish are taken care of by finishing processes.

The need for high accuracy and high efficiency machining of difficult-to-machine materials is making the application of abrasive finishing technologies increasingly important Abrasive finishing process is usually employed as the last operation on the highly value added components. It is imperative to achieve these processes economically. This is generally possible with strategic consideration of the key influencing parameters.

Traditionally, single or multiple point tools with geometrically defined edges, such as turning and milling tools, have been considered for roughing and semi-finishing. For fine finishing, fine abrasives (be they loose or fixed) are invariably used in the components of the highest quality in terms of form and finish accuracy, and surface integrity. The basic idea of ***abrasive fine finishing processes*** is to use a large number of multipoint or random cutting edges with indefinite orientation and geometry for effective removal of material in the form of chips having sizes smaller than those obtained during finishing methods that use cutting tools with defined edges. Because of extremely thin chips produced in abrasive machining, it yields better surface finish, closer tolerances, more localized control,

generation of more intricate surface features, and machining of harder and difficult-to-machine materials [1,2] Unlike other machining processes, the failure of one cutting edge does not affect the process in abrasive machining. The abrasive tools are consequently quite stable. Compared with the defined cutting edge tool, the abrasive tool is less sensitive to interrupted cuts and variations in work hardness as well as the areas of the workpieces to be machined

Grinding, lapping, honing, and super finishing are commonly used methods of finishing. Lately, magnetic abrasive finishing (MAF) has also joined this class of abrasive finishing processes. Even though these processes are in use for various applications, each process has its limitations in producing the desired surface finish on the components. Some of them are discussed in the forth-coming sections.

## 1.2 Abrasive finishing processes

**Grinding** [3] is a finishing process, which uses abrasive wheel or tool made of large abrasive grains retained by bonding material. Although grinding is more efficient for removing material than other finishing methods, it is still difficult to achieve desired fine finish by grinding alone. Though the finish can be improved with the application of grinding wheels with fine grits, they get heavily loaded with debris during the grinding process. Hence, very frequent dressing is needed to remove the loading, which causes excessive wheel loss and interruption in production. Finishing of intricate parts by grinding requires expensive profile grinding wheels. Grinding of certain materials such as aluminum and brass is not possible as they cause quick loading of the grinding wheel, making grinding quite difficult. Grinding develops localized heat with potentially harmful effects on the integrity of the surface.

**Lapping** [4] is a low pressure abrading process, which is used for obtaining surface finish, and dimensional accuracy superior to that obtained by grinding and honing. Relatively low force is exerted on the workpiece that is usually held in a well supported manner, consequently lapping is often successfully applicable to brittle materials and fragile parts. The rate of stock removal is low due to low cutting speed and shallow penetration of fine abrasive grains into the workpiece surface. The material is removed by applying loose abrasive slurry between work material and close fitting surface called lap (Fig. 1.1) The abrasive grains follow a free continuously changing path over the

workpiece and produce a stress free surface by cutting action [5]. The shapes of the surfaces frequently worked by lapping are mostly limited to basic forms, such as flat, cylindrical (including slender tapers), and spherical. In lapping, to polish a three dimensional surface such as finishing of dies, the operation is usually manual. Also the accurate motions of lap and work are required, necessitating use of high precision set-up and linear actuators, increasing the cost

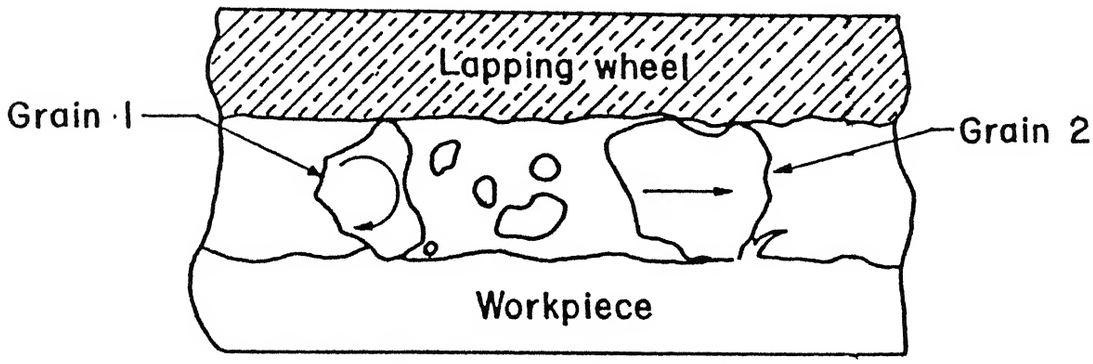


**Fig. 1.1 Schematic diagram of a lapping process**

**Honing** [6,7] is a low velocity abrasive machining process characterized by low cutting pressure and large area of contact The principle of honing, with the self-piloting tool automatically finding the neutral axis of the hole and developing the new surface in relation to that axis, are well-adapted for producing straightness and roundness by removing the least amount of material often within very short cycle time. Bonded abrasive stones are forced against the work surface, while a combination of rotary and traversing motions successively and repeatedly bring the entire work surface into contact with the stones (Fig. 1.2). It is employed to improve the accuracy of cylindrical, usually, internal surfaces. It also reduces or corrects geometric errors resulting from previous operations, such as machining, heat treating etc., with least possible amount of material removal. It is used in a wide variety of applications including engine cylinder walls, compressor bodies, valve bodies, bearings and hydraulic cylinders. The surface topography generated by honing can have a profound effect on tribological performance [7].

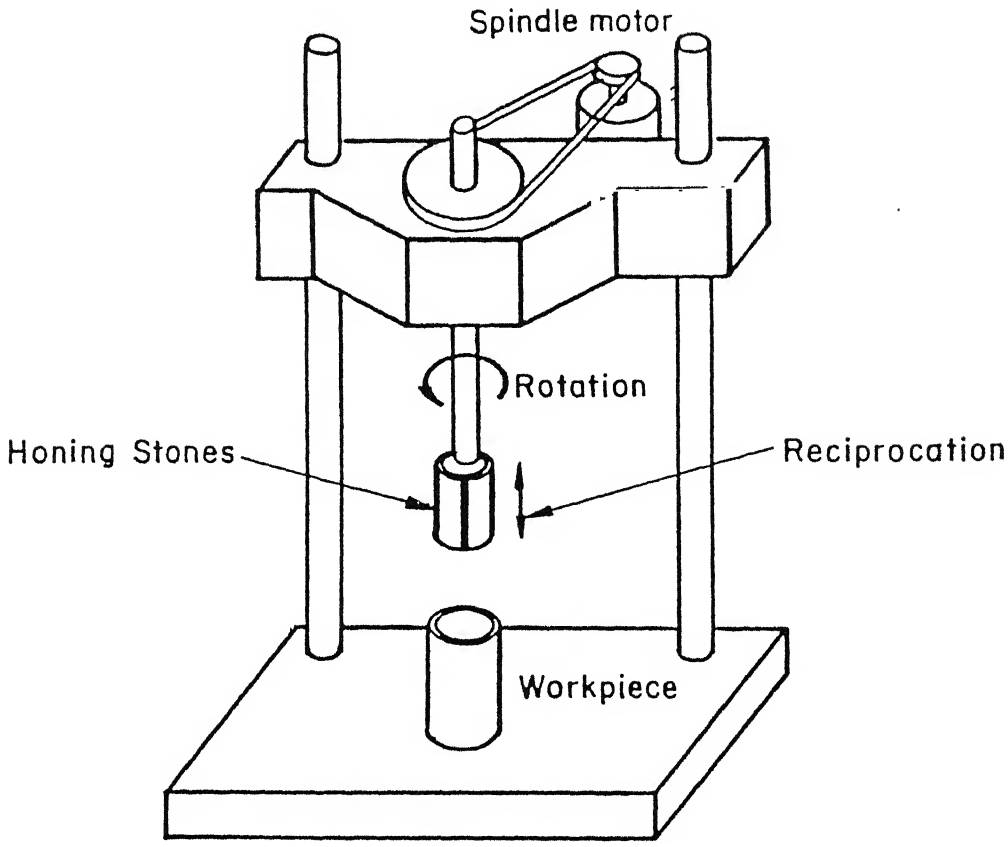


**Fig. 1.2 Illustration of bore honing**

**Superfinishing** [4] is an operation using bonded abrasive stones in a particular way to produce an extremely high quality surface finish. A very thin layer of material is removed in superfinishing. In this process, a very fine abrasive stick is fixed in a suitable holder and pressed against the surface of the workpiece with a light spring pressure. The stick is given a feeding and oscillating motion, and the workpiece is given rotating or reciprocating motion according to the requirement of the shape being machined In superfinishing operation, there occurs formation of sharp edge which is subjected to manual working.

In **magnetic abrasive finishing process** [8], granular magnetic abrasives composed of ferromagnetic materials (as iron particles) and abrasive grains (as $Al_2O_3$, SiC or diamond) are used as cutting tools and the necessary finishing pressure is applied by electro-mechanically generated magnetic field (Fig 1 3). The magnetic abrasives are joined to each other magnetically between magnetic poles along the lines of magnetic force, forming flexible magnetic abrasive brushes. When a workpiece with rotatory,

vibratory, and axial movement is inserted in such a magnetic field, surface and edge finishing are performed by these magnetic abrasive brushes. MAF can be used for finishing of tubes, external finishing of rods and finishing of flat surfaces made of ferromagnetic and non-ferromagnetic materials.

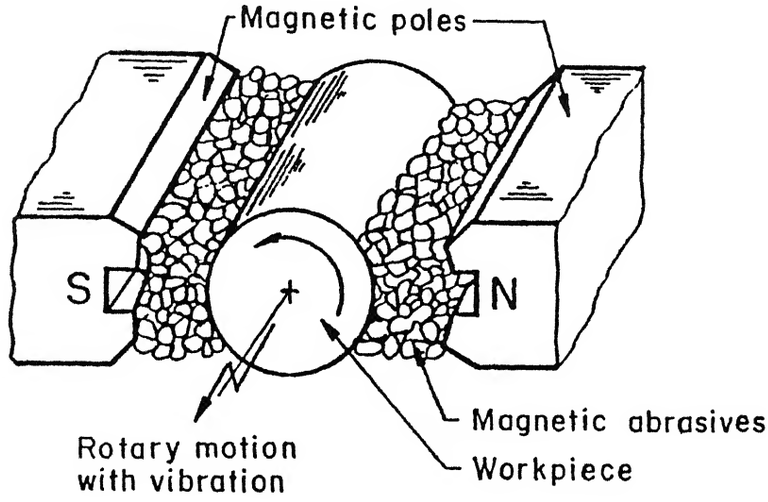


**Fig. 1.3 Schematic view of magnetic abrasive finishing (MAF) [8]**

But the applications of the grinding, lapping, honing, super finishing, magnetic abrasive machining and other abrasive finishing processes are limited to the production of the workpieces of the basic forms such as flat, cylindrical etc. These finishing processes are being pushed to their limits of performance and productivity in general, and in case of hard materials and components of complicated shapes in particular. Hence, a need is being felt to develop a finishing process with wider bounds of application areas, better quality performance and higher productivity. Abrasive flow machining is one of such processes. The characteristics of four important finishing processes are compared in Table 1.1.

The foregoing discussion clearly indicates that abrasive machining has a vital role to play in the finishing of industrial components. The work reported in this thesis is on a new process, called abrasive flow machining (AFM). The following section provides an introduction to this process, and a review of the relevant literature available.

**Table 1.1 Comparison of abrasive finishing processes.**

| S. N | Process features | Lapping | Honing | MAF | AFM |
|---|---|---|---|---|---|
| 1 | Surface finish, ($\mu$ m) | 0.25 - 0.1 [1] | 0 25 – 0.5 [1] | 0 04 [8] | 0 05 [17] |
| 2. | Dimensional tolerance, ($\mu$ m) | ± 0.5 [1] | ± 0.5 - 1.25 [1] | ± 0.5 [8] | ± 5 0 [17] |
| 3. | Material removal, (mm) | < 0 0025 [1] | 0.061 - 0.183 [1] | 0.002 - 0 007 [8] | 0.008 - 0.010 [9] |
| 4. | Pressure, (MPa) | 0.01 - 0.2 [1] | 1.0 – 3.0 [1] | 0 - 0.077 [8] | 0.69 - 22.0 [9] |
| 5. | Abrasive product type | Abrasive grain entrained in a liquid vehicle | Bonded abrasives | Magnetic abrasives Composed of ferromagnetic particles and Conventional abrasive grits | Semisolid abrasive media composed of viscoclatic carrier and abrasive grits |
| 6. | Work surface Configuration | Flat, cylindrical, and spherical surfaces | Cylindrical Surfaces | Flat and cylindrical surfaces | Inaccessible areas and complex Internal passages |

## 1.3 Abrasive Flow Machining (AFM) Process

With today's focus on total automation in the flexible manufacturing system, the abrasive flow machining process offers both automation and flexibility in final machining operations. AFM can be applied to an impressive range of finishing operations, providing uniform repeatable and predictable results A key feature differentiating AFM from most finishing processes is the ability to control and select the intensity and location of abrading through fixture design, media selection and process parameters. Abrasive flow machining is a non-traditional finishing process that is used to attain one or more of the following objectives:

- Uniform radius generation.

- Edge or intersection deburring
- Surface finish improvement
- Polishing of irregular shaped passages
- Removal of thermal machining recast layers
- Post processing of conventionally machined surfaces to eliminate residual stresses.

**Applications** of this process include finishing of components in aerospace, automotive, dies, chemical processing and medical industries. It is an appropriate process for pharmaceutical and semiconductor processing industries. Materials from soft aluminum to tough nickel alloys, ceramics and carbides have been successfully micro machined with the process [9]. AFM process provides a high level of surface finish and close geometric tolerances with economically acceptable rate of surface generation for a wide range of industrial components. The ability of media in AFM process to finish difficult to reach areas, to follow complex contours and to simultaneously work on multiple edges and surfaces, makes it more versatile than other finishing processes. Abrasive flow machining is a cool process, as opposed to grinding which develops localized heat with potentially harmful effects on the integrity of the surface.

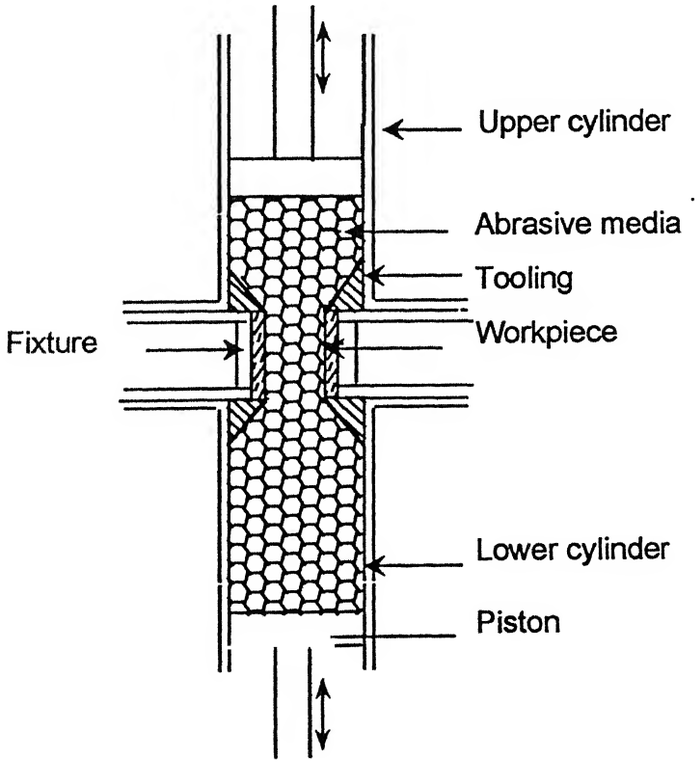


**Fig. 1.4 Schematic diagram of abrasive flow machining process**

AFM removes small quantity of material by flowing a semisolid abrasive laden compound called **'media'** (abrasive particles uniformly suspended in viscous chemical compound) through or across the surfaces of the workpiece to be finished [10]. Two vertically opposed cylinders extrude media back and forth through passages formed by the workpiece and tooling (Fig.1.4). The machining action compares to a grinding or lapping operation as the media gently and uniformly abrades the surfaces or edges. The media acts as a **'self deformable stone'** having protruding abrasive particles acting as cutting tools. The media is composed of semisolid carrier and abrasive grains. AFM systems designed for production applications often include part cleaning and unload/reload stations, media maintenance devices and cooling units.

In order to achieve the desired machining, the following process-influencing parameters should be considered.

1. **Setting parameters:** Extrusion pressure, velocity of flow of media, flow volume, and number of cycles.
2. **Tooling :** Shape and size, stiffness, stability and resulting media flow passage.
3. **Media :** Type and size of grains, concentration of abrasives, and type, rheology and viscosity of carrier.
4. **Workpiece :** Hardness, surface roughness, shape and stiffness.

The most commonly used abrasive grains are aluminum oxide ($AL_2O_3$), silicon carbide (SiC), boron carbide ($B_4C$) and diamond. Sometimes their mixture can also be used. The carrier is made by blending rubber like polymer with a gel like lubricating diluent, which can give desired velocity e.g. polyborosiloxane. Tooling design directs the media to flow in the desired area.

### 1.3.1 Unique characteristics of AFM process

AFM offers a number of unique and important features. Some of them are reported below [9,10,11].

1. Deburring, radiusing and polishing in one operation even in inaccessible areas.
2. Produces true round radii even on complex edges. Since the media confirms to the passage geometry, complex shapes can be processed as easily as simple one.
3. Reduces surface roughness by 75 to 90 percent on cast, machined or EDM'd surfaces.

4. Confidently produces close tolerances due to the selectivity and easy controllability of the process.
5 Processes dozens of holes or parts simultaneously in about the same time it would take to do just one.
6 Multiple passages can be processed simultaneously with uniform results. Cooling air holes on turbine disks and hundreds of holes in a combustion liner are deburred and radiused in one operation.
7. AFM maintains flexibility. The same machine can do a variety of jobs just by changing tooling, process settings and, if necessary, abrasive media.
8. Defects are removed or blended in pure grinding mode. There is no peening over or smearing of metal into the surface.
9. Jobs requiring hours of highly skilled hand polishing are processed in a few minutes automatically.
10. Process variables are easily controlled. Small changes in media flow rates, pressures, or volumes normally have little effect on results.

### 1.3.2 Applications of AFM

AFM is used for finishing of various components in wide range of industries. Some of them are given below [9,10,11].

**(a) Aerospace**

- Deburring of aircraft valve bodies and spools.
- Polishing and radiusing of blades, disks, hubs, shafts and air cooling holes in the turbine disk.
- Finishing accessory parts such as fuel spray nozzles, fuel control bodies and bearing components.
- Removing the recast layers in laser'd and EDM'd cooling holes on turbine disk and blades.

**(b) Dies**

- AFM has been successfully applied to polish extrusion, drawing, wire-forming, compacting and cold-heading dies.
- The process polishes surface in the direction of flow, producing a better quality and longer lasting dies with uniform surface and gently radiused edges.

**(c) Automotive**

- For deburring and polishing fuel injection systems, splines, gears, pumps, valves and fittings.
- AFM abrades, smoothes and polishes the surface of the two stroke cylinders and four stroke engine heads for improved air flow and better performance.

**(d) Chemical processing**

- To finish valves and fittings used for pharmaceutical and semi-conductor applications. AFM can easily reach inside the smaller fitting and valves, where access for hand polishing is very difficult.

Studley [12] presented applications of AFM process, e.g. finishing of hundreds of holes in a disk in one operation, uniform and controlled stock removal of cast blades with minimum dimensional change, resizing of cooling holes in aircraft engine combustion liners, finishing of turbine components which otherwise are very difficult to finish. The AFM process has been successfully applied for the components ranging from gears as small as 1.5 mm in diameter and orifice as small as 0.2 mm, to splined die having passages of 50 mm in diameter [9]. Some of the applications of AFM process for finishing various components in different industries are shown in Fig. 1.5 to Fig. 1.8.

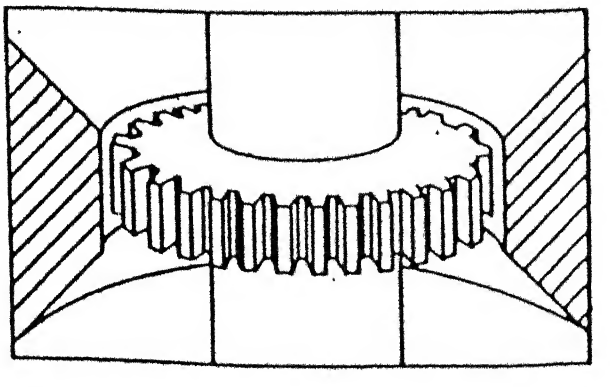

**Fig. 1.5 Deburring and polishing gear teeth [10]**

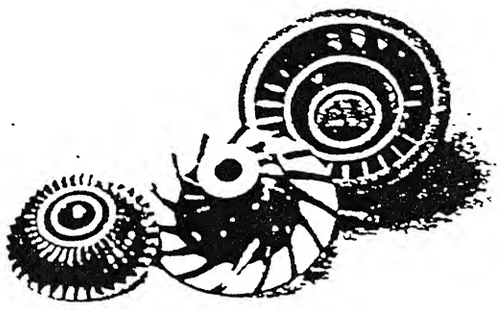

**Fig. 1.6 polishing of airfoil and gas path surfaces in turbine engine parts [15]**

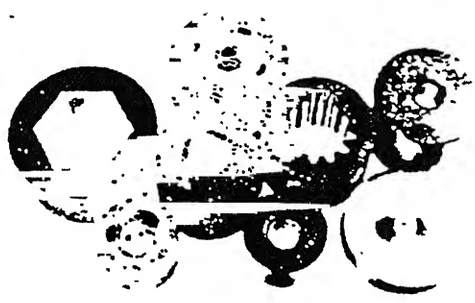

**Fig. 1.7 Polishing of both tool steel and tungsten carbide dies [15]**

**Fig. 1.8 Valves and fittings used for pharmaceutical and semiconductor applications [15]**

## 1.4 Literature Review

The Abrasive Flow Machining (AFM) process has been developed and brought to production stage in U. S A. during the years of 1966 to 1968. The process was initially used to perform critical deburring of aircraft valve bodies and spools, and production of burr free internal edges In 1978, AFM was reported as an alternative for hand polishing of extrusion dies at the International aluminum extrusion technology seminar in Atlanta, Georgia. Since that time, use of AFM for polishing of dies has developed as a way of satisfying stringent manufacturing requirements. AFM process is in its early stage of development; and the available published literature mainly deals with a qualitative description of the process and its applications. The review as given below, is presented in two parts, viz related to experimental findings and theoretical investigations.

### 1.4.1 Review of experimental studies

Many researchers conducted experimental studies to investigate the effects of the process parameters on the process performance. The effects of process variables like extrusion pressure, number of cycles, viscosity, concentration and mesh size of the abrasive media are discussed

Rhoades [9,10,11] studied the basic principle of AFM process and identified its process control parameters. The depth of cut primarily depends upon the size, relative hardness, sharpness of abrasive grains and extrusion pressure. The number of cuts made by abrasive particles located on the outer periphery of the slug (the media extruded through the workpiece, shown in Fig. 1.4) during one cycle, is a function of length of the media as it passes through the restriction, and size and concentration of abrasives in the media. The type of flow pattern to occur has been shown to depend upon the machine setting, media formulation, workpiece material and tooling configuration.

It is also reported [10,11] that higher viscosity media is to be used for uniformly abrading the walls of large passages and lower viscosity media is to be used for radiusing edges and for processing small passages. The effective life of the media depends on a number of factors including the initial batch quantity, the abrasive size and type, the flow speed and part properties and its configuration.

Przyklenk [13] described the effects of workpiece geometry, surface roughness and different media on process performance. He concluded that with small bore diameter more grains come in contact with the wall and material removal increases. The edge radius decreases if diameter and length of a bore increase. The share of abrasives in media, the grain size and viscosity of base media are the most important parameters which have influence on stock removal and media velocity. In comparison to this the influence of material, temperature, type of abrasive and bore geometry is small within the given limits It was also found that the media should not be allowed to achieve temperature more than $100^0$C to keep the viscosity of the media within certain limits. It is possible to use aluminum or polyurethane as material for the construction of fixtures.

For any working pressure the amount of abrasion that occurs is directly related to the slug length of flow. It has been shown that if the two passages of different areas are given the same volume flow, then the smaller passage abrades more than the large passage due to greater slug length of flow [14].

Perry [15] presented some principles and practices regarding AFM. He reported that abrasion is high where media velocity is high. If two holes have different diameters but equal total flow area, then they will get abraded equally. High viscosity media provides high material removal rate. Low viscosity is used for radiusing purpose. Likewise coarse abrasives are used for faster cutting and fine abrasives for flowing through small holes, or for highly polished finishes.

An increase in pressure and media viscosity increases material removal rate while surface finish value decreases [9,16-18]. Media viscosity combined with extrusion pressure relates directly to the media flow rate which affects the amount of abrasion, the uniformity of stock removal and edge radius size. Slow media flow rates are good for uniformly removing materials; high flow rates produce large radii [10]. It is found that for constant flow of volume, changes in media flow rate do not significantly affect material removal. With increasing number of cycles, material removal initially increases due to higher initial coarseness of the workpiece surface; but later on it decreases [17,19]. A study of the workpiece surfaces generated by AFM, with the help of scanning electron microscope photographs, indicates that there is significant improvement in the surface finish only within initial few cycles [16]. Among all studied process parameters, the

dominating one is percentage concentration of abrasives in media followed by abrasive mesh size, number of cycles and media flow speed [19].

The type of machining process used to prepare the specimens prior to AFM are found to significantly affect the improvement in surface finish [18]. The amount of material removed from the WEDM'd and milled surfaces are significantly different from that of turning and grinding [18], because these machining processes produce different micro surface contours. WEDM'd surfaces are better suited to AFM than turned and milled surfaces. The actual reason for this suitability needs further investigation. However, suspicion goes to the weak junctions between the recast layer and the parent material formed during WEDM.

Davies [20] reported the relationships between rheological behavior of polyborosiloxane-grit mixtures and their machining characteristics. It is observed from the experimental results that the relationship between number of extrusion cycles and changes in both the temperature and pressure drop depends upon the media type and polyborosiloxane-grit ratio. It is found that increase in the temperature results, decrease in viscosity of the media and increase in the volumetric flow rate. It has been observed from experimentation that viscosity of media increases with percentage concentration and decreases with the mesh size and temperature [21].

The physical properties of the media such as thermal conductivity, specific heat capacity and surface heat transfer coefficient of media have been experimentally determined by Fletcher [22]. These experimental values are also validated with the mathematical model of each property, which are then used in the calculation of thermal behavior of mixture as a function of material composition and temperature.

### 1.4.2 Review of theoretical investigations

AFM process is complex due to little understood behavior of the media, and the complicated and random nature of mechanical action of material removal. William and Rajurkar [17] used a stochastic modeling and analysis technique called data dependent system (DDS) to study the AFM generated surfaces. The DDS modeling procedure consists of fitting ARMA models by standard non-linear least square routines until the residual sum of squares of random disturbances can not be significantly reduced as determined by F-test criterion. Wave length decomposition of AFM surface profiles has

indicated the presence of two wavelengths, a large wavelength linked to the main path of the abrasive grains and a small wavelength linked to the cutting edges. Methods have been proposed to estimate the number of dynamic active grains involved in the cutting and the amount of abrasive grain wear per stroke. The number of active grains has been obtained by multiplying the frequency associated with the primary root from the DDS models by the time per stroke and dividing by the cross sectional area of the extrusion passage. The range of active grains found is very close to 280 to 600 reported for the grinding operations.

DDS modeling of the surface roughness profile data by Loveless et al. [18] indicated a general trend of AFM reducing the order of the ARMA models representing the surface. Green's function plots showed that AFM removed the signs of the original machining process of the workpiece surface.

Rajeshwar *et al.* [23] presented a mathematical model to determine the characteristics of the media flow during machining. The simulation model has been developed using the constitutive equations of Maxwell model describing non-Newtonian flow characteristics of the AFM media through cylindrical workpieces. Finite difference method was used to obtain the solution. It is observed that there exists linear relationship between the shear stress on the surface and thickness of the material removed determined experimentally.

Control systems may be added to monitor and control additional process parameters, such as media temperature, viscosity and flow speed of media, and wear of abrasives. The estimate of number of dynamic active grains may be useful as abrasive tool life criterion. It might also serve as an indicator that media has absorbed too much workpiece material and must be replaced [16]. These methods may aid in the off-line optimization of the process. They may also be useful as a part of on-line adaptive control or media replacement strategy for AFM, once they have been correlated with existing abrasive wear signals.

AFM process is very much in its early stages of development. Sustained research is required to transform the process into mature technology, for its successful induction into the industry. This thesis makes an attempt in this direction. The scope of the present work and organization of the thesis are described in the following sections.

## 1.5 Scope and Objectives of the Present Work

Although the investigations carried out by various researchers are very good; they seem to be rather lacking in theoretical treatment. Both theoretical and empirical studies of abrasive flow machining are greatly hampered by the inherent random nature and multiplicity of variables. Not much information is available in the literature, which deals with theoretical analysis of material removal mechanism in AFM. The relationship between process parameters and performance characteristics of the process are not completely known. The exact mechanism by which the individual abrasive particles accomplish material removal is only partially understood. There is a need to carry out systematic theoretical analysis of viscous media flow to determine the stresses and machining forces acting on the workpiece. This will help in modeling and proper understanding of the mechanics of the machining process during AFM.

The following are the specific objectives of the present work:

- To conduct experiments to study the effects of various process parameters on material removal and surface roughness.
- To analyze the flow of media in AFM process using **finite element method** by considering the media as viscoelastic material.
- To develop a model to determine the material removal and surface finish in AFM process and to validate it by comparing with the data obtained by experimentation.
- To develop a model for the topography of media and estimate active grain density by microscopic technique, and to simulate the random surface generated in AFM process.
- To analyze the specific energy and thermal aspects of AFM process.
- Modeling of AFM process by neural network, and optimization using neural network and genetic algorithm.

## 1.6 Organization of the Thesis

The total thesis write-up is divided into seven chapters and four appendices. First chapter of the thesis comprises introduction of traditional finishing methods and their limitations, introduction and importance of abrasive flow machining process, and review of literature. Based on the literature review, the scope and objectives of the present work are presented.

Description of the experimental set-up, details of experimentation and the associated results constitute chapter 2 of the thesis. **Experiments** have been conducted on the AFM machine designed and fabricated at Indian Institute of Technology, Kanpur. Experiments have been planned using central composite rotatable design to get the useful inferences by performing minimum number of experiments. A parametric study of process performance is also carried out.

Chapter 3 presents a model for analysis of media flow. The method involves the use of **finite element technique** to solve the governing equations in terms of primary variables (velocities and pressure). The theoretical analysis of media flow predicts the stresses developed during the flow.

Modeling for material removal and surface roughness using **abrasion theory** is also described in chapter 3. The model is based on accumulated plastic flow of material by repeated indentation by moving abrasive particles. The model includes the operating conditions of the process e.g. abrasive size, extrusion pressure, workpiece material hardness and size of the workpiece to be machined.

A **stochastic simulation method** using random sampling technique is proposed to evaluate the active grain density in chapter 4. A microscopic technique has also been used to estimate the number of active grain density at various mesh sizes and concentrations. The modified model to simulate the random surface generated and material removal in AFM is also discussed.

The chapter 5 is devoted to forces, specific energy and thermal aspects of AFM. A model has been proposed for the determination of **specific energy and tangential forces** in AFM process. A simple model of **heat transfer in AFM** has also been developed that considers heat flow to the workpiece and abrasive media.

Chapter 6 deals with the modeling of AFM by neural networks. The thesis presents an architecture of **back-propagation neural network model** for prediction of material removal rate and surface roughness in AFM.

The neural network has been used for **optimum selection of input parameters** of AFM process. Optimization of the AFM process has also been performed using **genetic algorithm** (GA). The optimization results of neural network are compared with the results obtained by genetic algorithms.

The conclusions drawn from the present work are enumerated in chapter 7. Possible avenues for future research in AFM are also outlined. The references and appendices are given at the end of the thesis.

# Chapter 2

# Experimentation

This chapter presents the effects of AFM process parameters on process performance determined experimentally. Experiments have been conducted on mild steel workpieces to determine the material removal and change in surface roughness under the specific machining conditions. The experiments have been planned according to central composite rotatable design. The effects of percentage concentration of abrasives, extrusion pressure, reduction ratio and number of cycles on material removal and surface roughness have been discussed. The following sections describe the experimental set-up and details of experimentation.

## 2.1 Working of AFM Set-up

The Abrasive Flow Machining set-up has been designed and fabricated at Manufacturing Science Lab., Indian Institute of Technology Kanpur, keeping in view the fundamental mechanism of the process and the basic requirements for research purposes. Media composed of silicon carbide abrasives (mesh size = 50-60) and polyborosiloxane carrier was used (Supplied by Extrude Hone Limited, U.S.A). Polyborosilixane carrier is soluble in acetone. Abrasive grains can be separated from media by dissolving the carrier in acetone. In AFM, media is extruded to and fro through the passage formed around the workpiece by utilizing two opposed piston media cylinders. The passage around the workpiece surface to be finished is formed by means of fixture arrangement.

The Abrasive Flow Machining set-up shown in Figures 2.1 and 2.2 consists of the following main components [24]

1. Media cylinders
2. Pistons
3. Hydraulic drive and controls
4. Workpiece fixture
5. Frame and housing.

## Media cylinders

The main function of the media cylinder (Fig. 2.2) is to embody the media at required extrusion pressure. It should also guide the piston movement. It can withstand pressures upto 100 bar. As the media is moving back and forth, the abrasion will take place on the cylinder inner surface. Hence, replaceable cylinder liners are also provided.

## Pistons

The piston acts to transmit the extrusion force applied by the piston rod of hydraulic cylinder to the abrasive media. It is used to extrude the media through the media cylinder to the workpiece. The main extruding surface is formed by the piston head, which accommodates two cast iron rings to provide sealing and reduce frictional resistance.

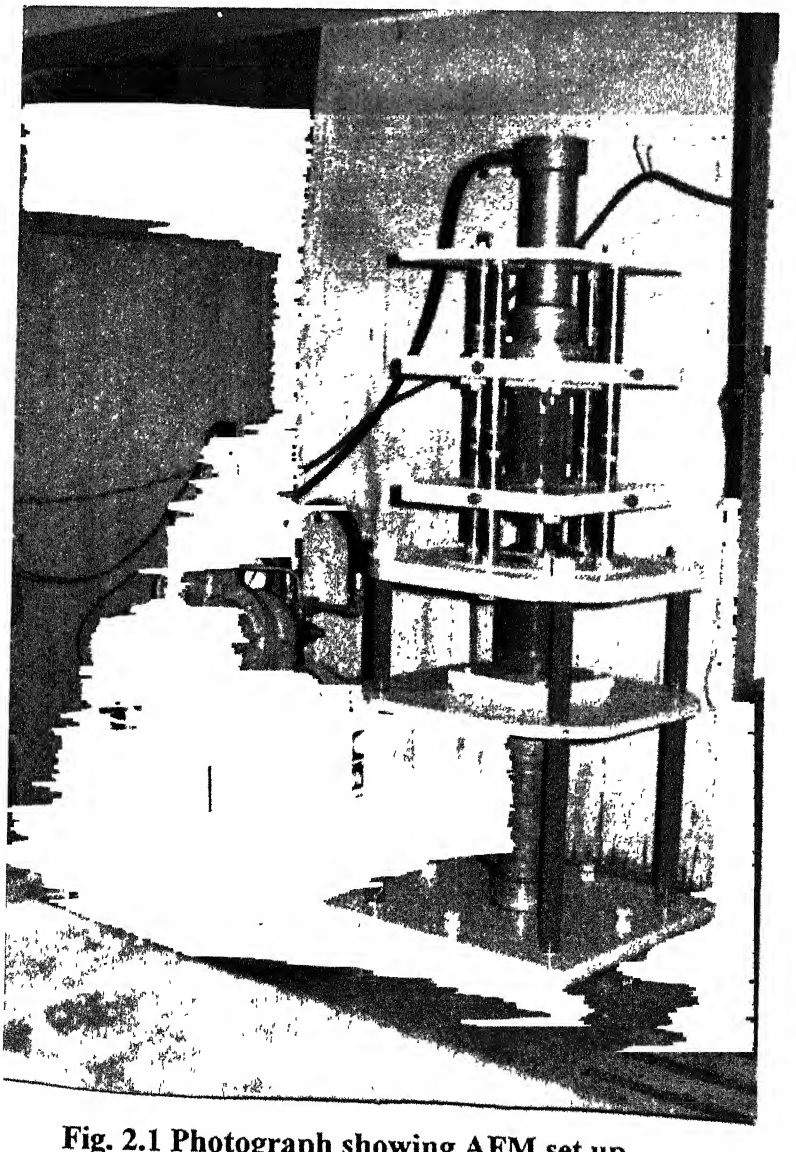

**Fig. 2.1 Photograph showing AFM set up**

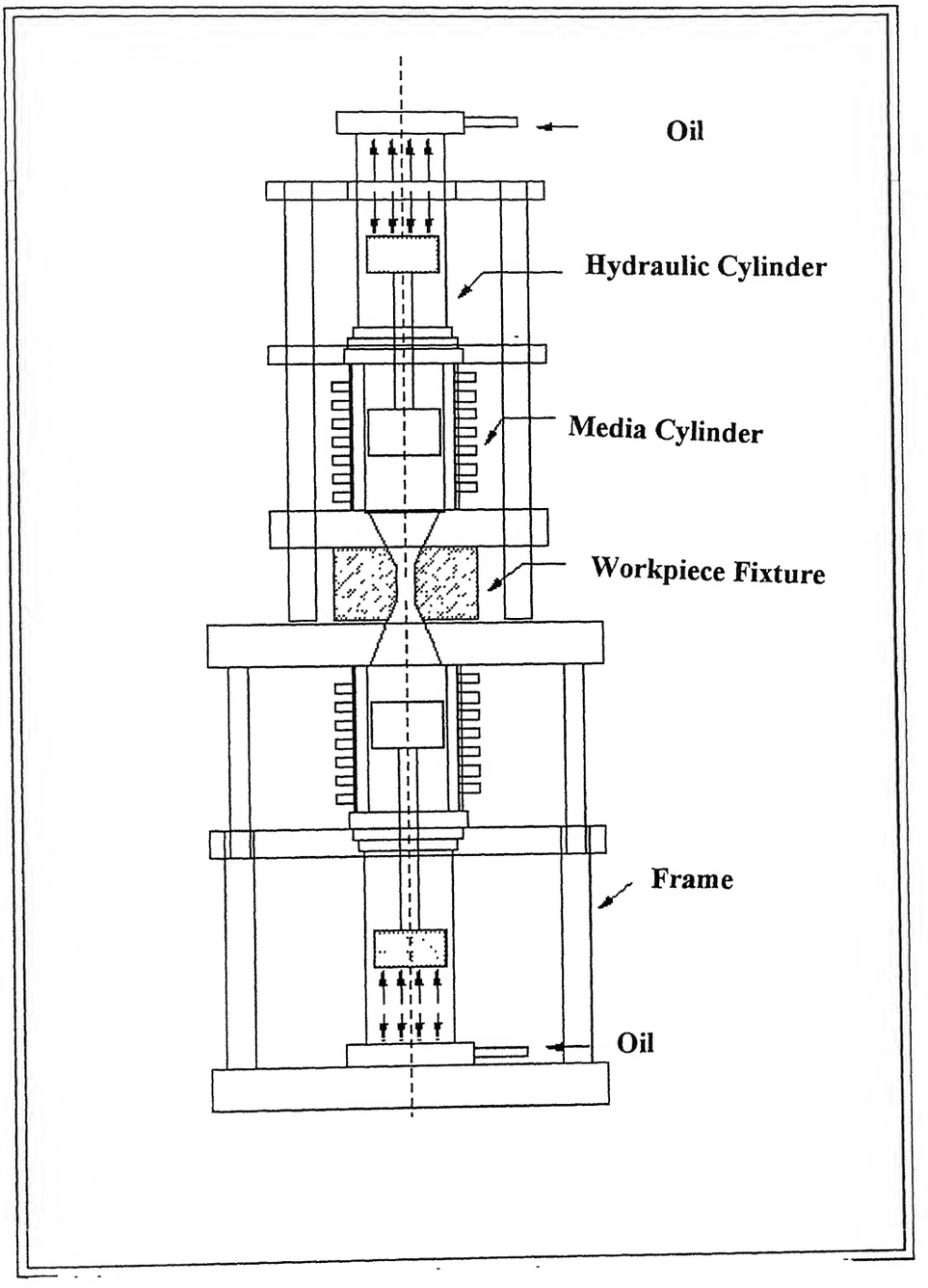


**Fig. 2.2 Kinematic configuration of the AFM experimental set-up [24]**

## Hydraulic drive and controls

In the AFM, the operations are powered by the hydraulic drive. The hydraulic system refers to the complete assembly of component parts that transmit and control the fluid power. Fig. 2.3 shows the block diagram of a hydraulic system. Fig 2.4 shows the hydraulic circuit which has following components.

1. Reservoir (R)
2 Strainer (S)
3 Variable delivery pump (VDP)
4. Flexible coupling
5 Electric motor (M)
6 Connectors
7 Relief valve (RV)
8. Check valve (CV)
9. 3-position 4-ways direction control valve (DCV)
10. Single acting cushioned cylinders (HCL & HC2)

The pump VDP withdraws oil from the inlet line C and delivers it to the outlet line D at a volumetrically uniform rate for any particular setting. The direction of flow is reversed by means of valve DCV so that line P is connected to either of the cylinder

To ensure that the maximum pressure is limited, a shunt line G is provided, communicating with reservoir R by way of relieve valve RV3. It is apparent that, with this arrangement, the rate of advance of the piston P1 is determined by the rate of withdrawal of oil from the hydraulic cylinder HC2. As oil is passed through the pump VDP at a volumetrically uniform rate, the piston would advance at uniform speed provided that the oil is incompressible.

During forward stroke of the cycle, oil enters from the port P of the direction control valve (DCV) and flows into the line A connected to check valve and relief valve for pressure control in the cylinders. Initially RV1 and RV2 are adjusted manually for a particular pressure. In forward stroke the oil passes from CV1 into HC1 till the pressure in the hydraulic cylinder HC2 reaches the adjusted pressure. As the pressure exceeds the adjusted value, the RV2 gets opened and oil comes out from HC2, making piston P1 traversing in downward direction. After completing forward stroke, the direction of DCV is reversed by relays and oil flow is reversed to complete one cycle.

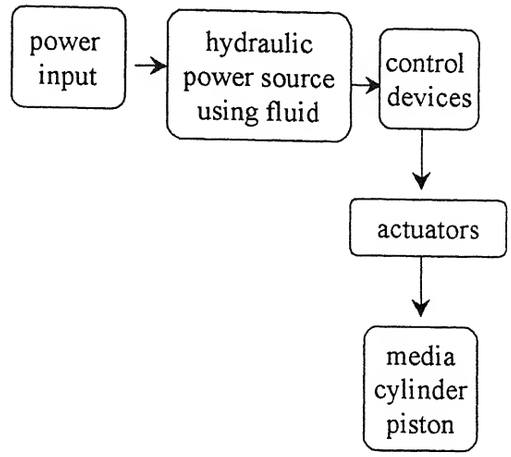


**Fig. 2.3 Block diagram of a hydraulic system**

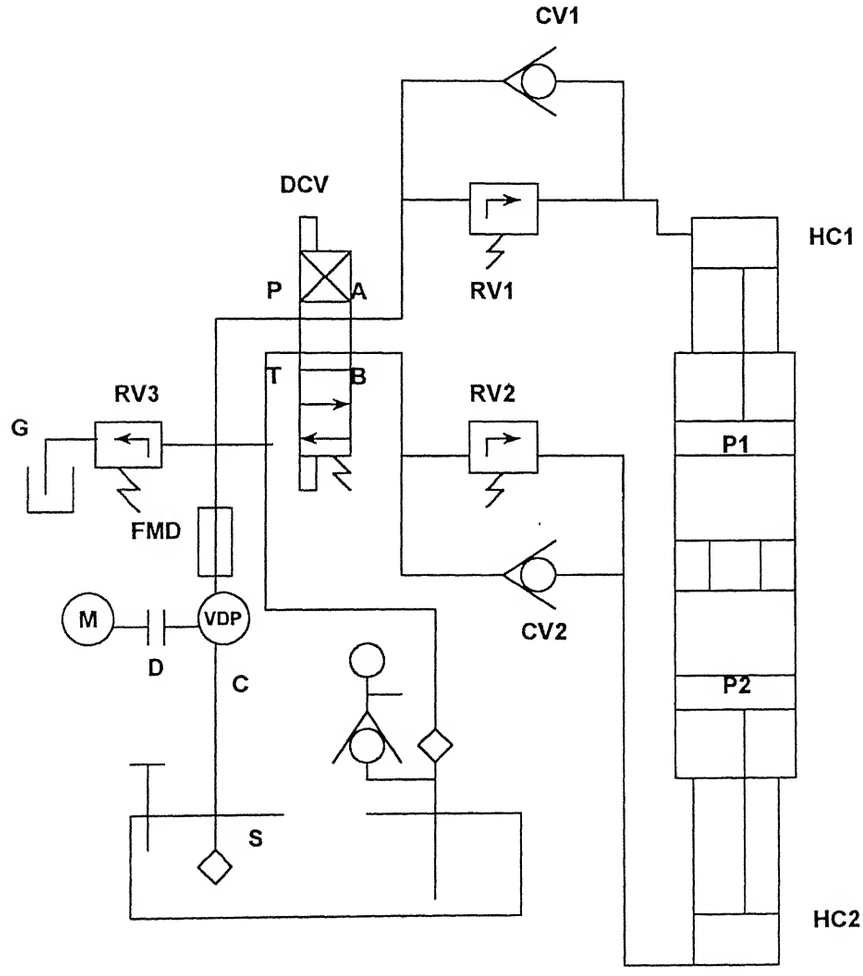


**Fig. 2.4 Hydraulic circuit for AFM set-up [24]**

### Workpiece fixture

The function of fixture or tooling is simply to hold the workpiece in position and to direct the flow of media to pass around the surface to be finished The design of the workpiece fixture is different for different shapes of workpieces. Keeping in the view the fixture design considerations, fixturing arrangement, as shown in Fig. 2.5 is fabricated to fulfill the requirements The fixture is fabricated for finishing internal surface of cylindrical workpiece The workpiece fixture consists of main body, which accommodates the workpiece and tooling The tooling is different for different internal diameter of workpiece to direct the abrasive media at a particular angle

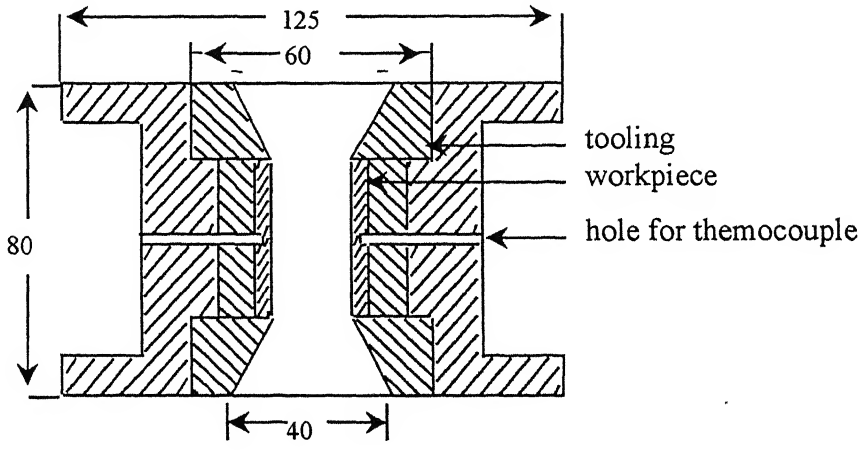


**Fig. 2.5 Schematic diagram of fixture used for AFM**

### Frame and housing

Frame and housing are used to accommodate media cylinders, hydraulic cylinders, workpiece fixture, etc together as a single unit. It is capable to withstand all kind of forces acting on it.

## 2.2 Procedure and Precautions to Conduct Experiments

The following **procedure** should be followed during experimentation on AFM set-up.

1 Abrasive media is filled tightly in media cylinder. It is preferred to fill the media in bottom cylinder, keeping piston in extreme bottom position.

2 Initial weight and surface roughness of the workpiece are measured before machining

3 Then, the workpiece is fixed in the fixture as shown in Fig 2 5 and the media is filled in the workpiece fixture

4 The top media cylinder assembly is lifted by the screw arrangement and the fixture (filled with media) is kept over the bottom media cylinder as shown in Fig 2 2 The fixture is tightened, so that no media should leak out during experimentation.

5 The motor is started, ensuring that the pressure is at 0 bar

6 The voltage is adjusted to approximately 6V in the DC power supply and then, the control mechanism for solenoids should be switch on to change the direction of flow of oil.

7. Keeping the control switch in neutral position, the pressure is increased to the required pressure by the pressure valve arrangement.

8 After this, the automatic control switch for solenoids is kept in on position and it automatically changes the direction of flow of the oil. One AFM cycle is completed when the media is extruded from the lower cylinder to the upper cylinder and back again to the lower cylinder.

9 After completing required number of cycles, the automatic control switch and motor are switched off.

10. After machining, the workpiece fixture and workpiece are taken out from AFM set-up, and the final weight and surface roughness of workpiece are measured

The following **precautions** should be observed while conducting experiments:

1. Before starting the experiments, it should be made sure that the control switches are working properly.

2 Fixture should be placed in alignment to the media cylinder.

3. The plates should be hold very tightly above the fixture, so that no media leaks out

4. Both manual and automatic switches provided for control of solenoids should not be kept 'on' at the same time. Otherwise it may damage total solenoid circuit.

5. Design of workpiece fixture should be such that the workpiece is held tightly. The workpiece should be cleaned after machining, but before weighing it.

## 2.3 Guidelines to Design Fixture / Tooling

The basic functions of the fixture / tooling for AFM process are as follows

- It should assure high accuracy of the parts.
- It should position the workpiece at the desired place and hold it tightly.
- It should guide media, and form the restriction passage so that the finishing takes place in the desired manner
- If possible, it should provide interchangeability.

To fulfill the above basic functions, fixture should contain the following components / elements:

- A sufficiently rigid body to withstand all types of loads coming on it.
- Locating elements to position the workpiece at a required place.
- Clamping elements to hold the work tightly.
- Elements for positioning a fixture on the AFM set-up.

## 2.4 Design of Experiments

Experiments conducted were planned using statistical techniques so that we get useful inferences by performing minimum number of experiments. If the yield or response 'y' is a function of the levels of quantitative variables then we may write [25],

$$y_u = \phi\ (x_{1u}, x_{2u}, \ldots\ldots, x_{ku}) + e_u \qquad (2.1)$$

where, $u = 1,2, \ldots ,N$ represent the N observations in the factorial experiment, and $x_{iu}$ represents the level of the $i$th vector in the $u$th observation

The function $\phi$ is called the response surface. The residual $e_u$ measures the experimental error of the $u^{th}$ observation. A knowledge of the function $\phi$ gives a complete summary of the results of the experiments and also enables us to predict the response for the values of the $x_{iu}$ that are not tested in the experiment. When the mathematical form of $\phi$ is not known, this function can sometimes be approximated satisfactorily, within the experimental region by a polynomial equation in the variables $x_{iu}$. The important criteria in selecting design for fitting a second order response surface is that the computations should

not be too difficult Considering desirable properties, Box and Hunter proposed the criteria of rotatability. In the experiments conducted for AFM process analysis, the Central Composite Rotatable Design [25] is used The general from of the quadratic polynomial fitted to the experimental data is given below

$$y_u = b_o + \sum_{i=1}^{k} b_i x_{iu} + \sum_{i=1}^{k} b_{ii} x_{iu}^2 + \sum_{i<j}^{k} b_{ij} x_{iu} x_{ju} \qquad (2.2)$$

where, k is no of variables and u is number of observation

From the results of any experiment, we can compute the standard error of $y_u$, at any point on the fitted surface The standard error will be a function of the co-ordinate $x_{iu}$ of the point In a rotatable design, this standard error is the same for all points that are at the same distance from the center of region This property is reasonable one to adopt for exploratory work, in which the experimenter does not know in advance how the response surface will orient itself with respect to the $x$-axis Consequently he has no rational basis for specifying that the standard error of $y_u$ should be smaller in some directions than the others

The design for four x - variables (say, $x_1$= extrusion pressure, $x_2$ = number of cycles, $x_3$ = reduction ratio, and $x_4$ = percentage concentration of abrasives) is shown in the appendix A (Table A.1). The columns headed $x_1$, $x_2$, $x_3$ and $x_4$, which specify the actual combination to be used, constitute the plan of experiment.

Subsequent steps are as follows.

1. The columns headed $x_0$, $x_1$, $x_2$, $x_3$, $x_4$, $x_1^2$, $x_2^2$, $x_3^2$, $x_4^2$, $x_1x_2$, $x_1x_3$, $x_1x_4$, $x_2x_3$, $x_2x_4$, $x_3x_4$ as shown in Table A.1 (Appendix A) are completed. The two way array with 16 columns and 31 rows comprises the X - matrix of the x-variables The corresponding values of the response $y$ are placed on the right.
2. The sum of products of each column in the matrix X with the column of y values are calculated. These sum of products are denoted by $(0y)$, $(1y)$, $(2y)$ and so on.
3 From the values of $(0y)$, $(1y)$, etc the regression coefficients are computed directly by the equations given below [25]. The only auxiliary quantity needed is $\sum(iiy)$, found by adding the crossproducts of all the squared terms with $y$.

$$
\begin{aligned}
&b_0 = 0\ 142857(0y) - 0\ 035714\sum iiy \\
&\sum iiy = (11y) + (22y) + (33y) + (44y) \\
&b_i = 0\ 041667(iy) \\
&b_{ii} = 0.031250(iiy) + 0.003720\sum(iiy) - 0\ 035714(0y) \\
&b_{ij} = 0\ 0625(ijy)
\end{aligned}
\qquad (2.3)
$$

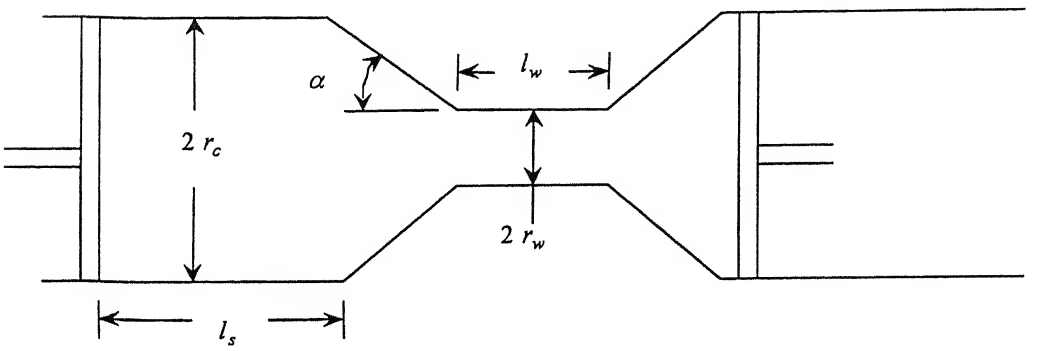


**Fig. 2.6 Illustration of AFM process**

In the present analysis of the experiments, the effect of four variables viz. pressure $p_e$, number of cycles $N$, percentage abrasive concentration by weight $C$, and reduction ratio $R_e$ are studied on material removal and change in surface finish. Reduction ratio $[R_e = 1-(r_w^2/r_c^2)]$ expresses the reduction in cross sectional area of flow of media. It is defined as the difference between cross sectional area of media cylinder and workpiece, divided by the cross sectional area of media cylinder. Here, $r_c$ is internal radius of media cylinder and $r_w$ is inner radius of cylindrical workpiece (Fig. 2.6). Slug length $l_m$ (this term is used in subsequent sections) varies with reduction ratio. It is defined as the length of media passed through workpiece in one stroke ($[l_m = l_s/(1-R_e)]$. Here, $l_s$ is length of stroke. Percentage concentration of abrasives by weight $C$ can be defined by the following equation.

$$
C = \left(\frac{\text{weight of abrasives}}{\text{total weight of abrasives and carrier}}\right) * 100 \qquad (2.4)
$$

A preliminary step is to set-up the relationship between the coded x - scales and the original scales in which the levels are recorded In design scale, the lowest and highest values of x are -2 0 and 2.0 So we take,

x = -2 0 when $p_e$ = 20 bar; $N$ =5 cycles, $C$ = 56 %, $R_e$ = 0 84

x =2 0 when $p_e$ = 80 bar, $N$ =25 cycles, $C$ = 76%, $R_e$ = 0 97

Then,

x = a + b * (variable)

'a' and 'b' are chosen to satisfy the desired conditions at the end of the scale

After substituting the lower and higher values of variables at original scale corresponding to –2 0 and 2.0, the following expressions, which describe the relation between x and original scale of variables, are obtained·

$x_1$ = -3.3333 +0.0666 $p_e$

$x_2$ = -3.0+ 0 2 $N$

$x_3$ = -27.8461538 + 0 3076923 $R_e$

$x_4$ = -13.2 + 0.2 $C$

where $x_1$, $x_2$, $x_3$ and $x_4$ denotes the values of x corresponding to pressure, number of cycles, reduction ratio and percentage concentration of abrasives respectively.

From these equations, extrusion pressure, number of cycles, reduction ratio and percentage concentration of abrasives in media corresponding to level x = -1, 0, 1 are determined.

The complete conversation is tabulated in Table 2.1.

Table 2.1 Conversion Table

| x | Extrusion pressure, bar | No. of cycles | Reduction Ratio, % | Concentration % |
|---|---|---|---|---|
| -2.0 | 20 | 5 | 84.00 | 56 0 |
| -1.0 | 35 | 10 | 87.25 | 61.0 |
| 0 0 | 50 | 15 | 90.50 | 66.0 |
| 1.0 | 65 | 20 | 93 75 | 71.0 |
| 2.0 | 80 | 25 | 97 00 | 76.0 |

With the above conversions, the experiments have been conducted according to the order given in the Table 2.2. The table also gives the responses – material removal and change in surface roughness ($\Delta R_a$), observed during experimentation. The experiments with lowest abrasive concentration have been conducted first, then in the increasing order of percentage concentration of abrasives, due to limited availability of media. For increasing percentage concentration of media, abrasives were mixed in the same media used in the previous experiments. Specifications of workpiece, abrasives and carrier used during experimentation are given in Appendix C.

**Table 2.2 Plan of experiments**

| | Designed parameters | | | | Responses | |
|---|---|---|---|---|---|---|
| Ex. No. | Pressure, bar | Number of cycles | Reduction ratio % | Concentration % | Material removal, g | $\Delta R_a$ (μm) |
| 1. | 50.0 | 15 | 90.50 | 56 | 0.0147 | 0.43 |
| 2 | 35.0 | 10 | 87.25 | 61 | 0.0090 | 0.35 |
| 3 | 65.0 | 10 | 87.25 | 61 | 0.0146 | 0.50 |
| 4 | 35.0 | 20 | 87.25 | 61 | 0.0177 | 0.52 |
| 5 | 65.0 | 20 | 87.25 | 61 | 0.0241 | 0.77 |
| 6. | 35.0 | 10 | 93.75 | 61 | 0.0123 | 0.56 |
| 7. | 65.0 | 10 | 93.75 | 61 | 0.0167 | 0.69 |
| 8. | 35.0 | 20 | 93.75 | 61 | 0.0214 | 0.73 |
| 9. | 65.0 | 20 | 93.75 | 61 | 0.0297 | 0.94 |
| 10. | 20.0 | 15 | 90.50 | 66 | 0.0075 | 0.32 |
| 11. | 80.0 | 15 | 90.50 | 66 | 0.0282 | 0.74 |
| 12. | 50.0 | 5 | 90.50 | 66 | 0.0065 | 0.31 |
| 13. | 50.0 | 25 | 90.50 | 66 | 0.0274 | 0.77 |
| 14. | 50.0 | 15 | 84.00 | 66 | 0.0063 | 0.36 |
| 15. | 50.0 | 15 | 97.00 | 66 | 0.0495 | 1.01 |
| 16. | 50.0 | 15 | 90.50 | 66 | 0.0217 | 0.61 |
| 17. | 50.0 | 15 | 90.50 | 66 | 0.0229 | 0.54 |

| | | | | | | |
|---|---|---|---|---|---|---|
| 18 | 50 0 | 15 | 90.50 | 66 | 0.0234 | 0 50 |
| 19. | 50.0 | 15 | 90 50 | 66 | 0.0211 | 0.59 |
| 20. | 50 0 | 15 | 90.50 | 66 | 0.0208 | 0.73 |
| 21 | 50.0 | 15 | 90.50 | 66 | 0.0205 | 0.64 |
| 22 | 50 0 | 15 | 90.50 | 66 | 0 0216 | 0.71 |
| 23. | 35 0 | 10 | 87.25 | 71 | 0.0117 | 0 45 |
| 24 | 65.0 | 10 | 87 25 | 71 | 0 0186 | 0 57 |
| 25 | 35 0 | 20 | 87.25 | 71 | 0 0197 | 0 65 |
| 26 | 65.0 | 20 | 87 25 | 71 | 0.0285 | 0.89 |
| 27 | 35 0 | 10 | 93.75 | 71 | 0.0209 | 0.54 |
| 28. | 65 0 | 10 | 93.75 | 71 | 0.0335 | 0.71 |
| 29 | 35.0 | 20 | 93.75 | 71 | 0.0363 | 0.79 |
| 30. | 65.0 | 20 | 93.75 | 71 | 0.0465 | 1.03 |
| 31 | 50.0 | 15.0 | 90.50 | 76 | 0 0279 | 0 85 |

## 2.5 Material Removal Measurement

The weight of the workpiece was measured using the available electronic weight balance "AFCOSET FX-400" having accuracy of 0.0001g. It is essential to clean the workpiece properly before measuring the weight By measuring the weight of the samples before and after machining, the material removed has been calculated by taking their difference. The data of material removal measurements are given in Table A.2 (Appendix A) and their average values in Table 2.2.

## 2.6 Surface Roughness Measurement

To study the change in surface texture due to various process parameters, the surface roughness measurements are essential. For this purpose, the instrument used was "TAYLOR HOBSON SURTRONIC 3P " having least count of 0.01μm. It gives on its digital scale the $R_a$, $R_y$ and $R_{tm}$ values. The improvement in surface finish has been determined by measuring $R_a$, $R_y$ and $R_{tm}$ values before and after machining.

$R_a$ is most widely used description of a surface. For determining $R_a$ value over a sampling length, a mean line is computed such as the area of the solid above the line is equal to the area of the void below. The arithmetic average of the deviation up and down from this theoretical mean line is $R_a$

$R_y$ is the distance from the highest peak to the deepest valley $R_y$ is useful for detecting the finishing problems, like pick-up or areas which have not cleaned up

$R_{tm}$ is also called $R_z$ DIN. For determining $R_{tm}$, the measured length is divided into five equal lengths and then average of the highest peak to the deepest valley of each of the five lengths is equal to $R_{tm}$ It is likely to be a slightly smaller than $R_y$ because one deeper is diminished by the finer finish of the other four values

The data of surface roughness measurements of workpiece surface before and after machining are given in Table A 3 (Appendix A). The data representing improvement in surface roughness are given in Table A.4 (Appendix A). The average of change in surface roughness ($\Delta R_a$) for each experiment is given in Table 2.2.

## 2.7 Response Surface Analysis (RSA)

The equation of general quadratic response surface for four variables is of the form

$$y = b_0 + b_1x_1 + b_2x_2 + b_3x_3 + b_4x_4 + b_{11}x_1^2 + b_{22}x_2^2 + b_{33}x_3^2 + b_{44}x_4^2 + b_{12}x_1x_2 + b_{13}x_1x_3 + b_{14}x_1x_4 + b_{23}x_2x_3 + b_{24}x_2x_4 + b_{34}x_3x_4 \quad (2.5)$$

where y is response under study. $b_0$, $b_1$, .... , $b_{34}$ are constants, and $x_1$, $x_2$, $x_3$ and $x_4$ are process variables as mentioned in section 2.4. The quadratic response surface for each response is obtained by calculating constants $b_0$, $b_1$, ....., $b_{34}$ of equation (2.5).

### 2.7.1 Material removal

The constants $b_0$, $b_1$, ....., $b_{34}$ are calculated from eqn. 2.3 using the responses of table A.2 (Appendix A) or table 2.2. The following response surface equation is obtained for material removal (MR).

$$MR = 21.714 + 4.358x_1 + 5.350x_2 + 6.658x_3 + 4.025x_4 - 0.703x_1^2 - 0.928x_2^2 + 1\ 808x_3^2 + 0.158x_4^2 + 0.262x_1x_2 + 0.487x_1x_3 + 0.862x_1x_4 + 0.900x_2x_3 + 0.375x_2x_4 + 2.750x_3x_4 \quad (2.6)$$

### 2.7.2 Surface roughness

The constants $b_0$, $b_1$, , $b_{34}$ are calculated from eqn 2.3 using the responses of change in surface roughness given in table A 4 (Appendix A) or table 2 2. The following response surface equation is obtained to predict a change in surface roughness ($\Delta R_a$) generated by AFM process

$$\Delta R_a = 0.617 + 0\ 101\ x_1 + 0\ 119\ x_2 + 0.107\ x_3 + 0\ 067 x_4 - 0.009\ x_1^2 - 0.006 x_2^2 + 0\ 029\ x_3^2 + 0.006\ x_4^2 + 0.023\ x_1x_2 - 0\ 0006\ x_1x_3 + 0.0018\ x_1x_4 + 0.0068\ x_2x_3 + 0\ 0093\ x_2x_4 - 0.0118 x_3x_4 \quad (2.7)$$

## 2.8 Results and Discussion

Responses have been calculated using response surface equations (2.6) and (2 7), which have been obtained from experiments based on central composite rotatable design, to study the effects of various parameters on material removal and change in surface roughness. In the following chapters, the results obtained using these eqns (2.6) and (2.7) are termed as response surface analysis (RSA) results. Figures 2.7 and 2 8 show that the experimental points are close to those predicted by RSA. Hence, RSA results can be considered as representatives of experimental results At the center point of the experimental design, eight experiments were carried out for same value of variables. As there is very little difference in the results for material removal and surface roughness values obtained during these eight experiments (Table 2.2), one can conclude that process repeatability is good.

### 2.8.1 Material removal

Figure 2 7 shows the effect of percentage concentration of abrasives by weight on material removal. As the percentage concentration of abrasives in media increases, material removal also increases, because higher concentration of abrasives results in higher number of active grains per unit area and hence higher material removal. Further,

grains can sustain larger cutting forces due to increase in viscosity of media at higher concentration.

It is found that material removal increases with increase in extrusion pressure (Fig 2.8). Depth of indentation increases with increase in extrusion pressure, which results in higher area of indentation of a grain and hence higher material removal occurs

Material removal also increases with increase in reduction ratio (Fig. 2.9), or due to increase in slug length of media passed per unit time. As volume of media passed across the workpiece in an AFM stroke is fixed, slug length of media passed across workpiece becomes more at low value of cross sectional area of workpiece and vice versa. At higher reduction ratio, the pressure acting on the workpiece surface is also higher, leading to higher depth of indentation. Both these factors result in higher material removal at higher reduction ratio.

Material removal value increases non-linearly with the number of cycles (Fig 2.10). The rate of material removal slightly decreases with the increase in number of cycles. This can be explained as follows Initially unfinished surface has sharp peaks, the peaks get machined and become comparatively flater after a few cycles of machining.

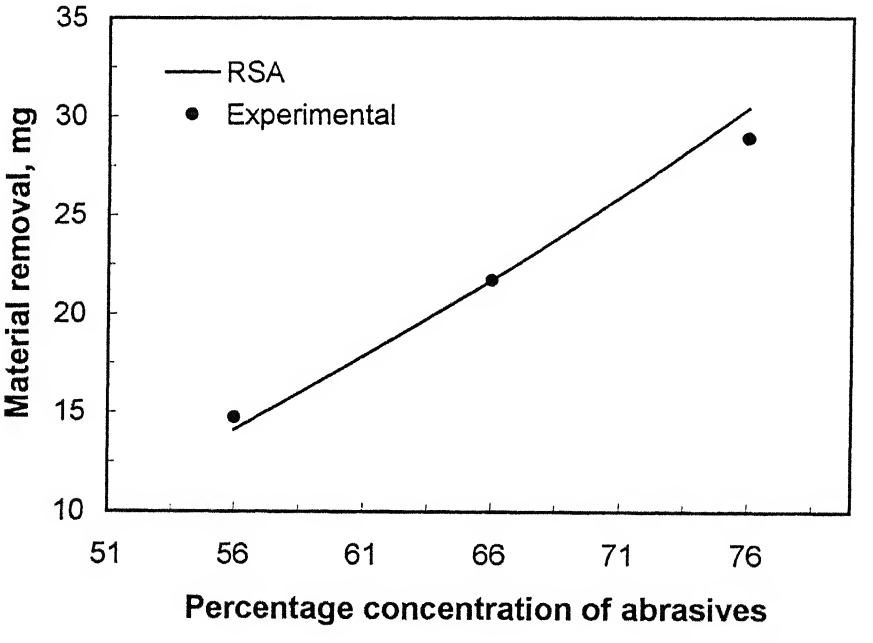


**Fig. 2.7 Variation of material removal with percentage concentration of abrasives ($p_e$ = 50 bar, $R_e$ = 0.905, $N$ =15 cycles)**

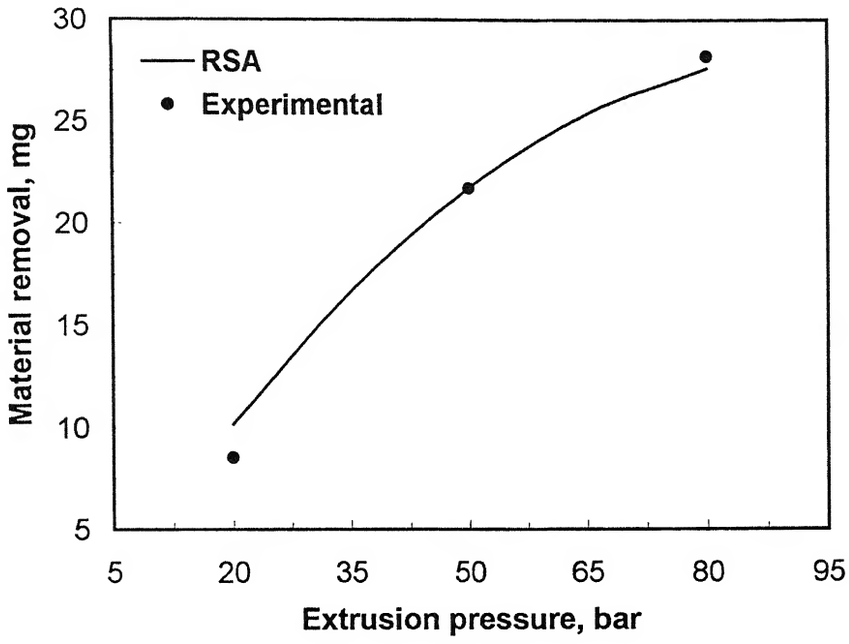


**Fig. 2.8 Variation of material removal with extrusion pressure**

**($R_e$ = 0.905, $N$ =15 cycles, $C$ = 66%)**

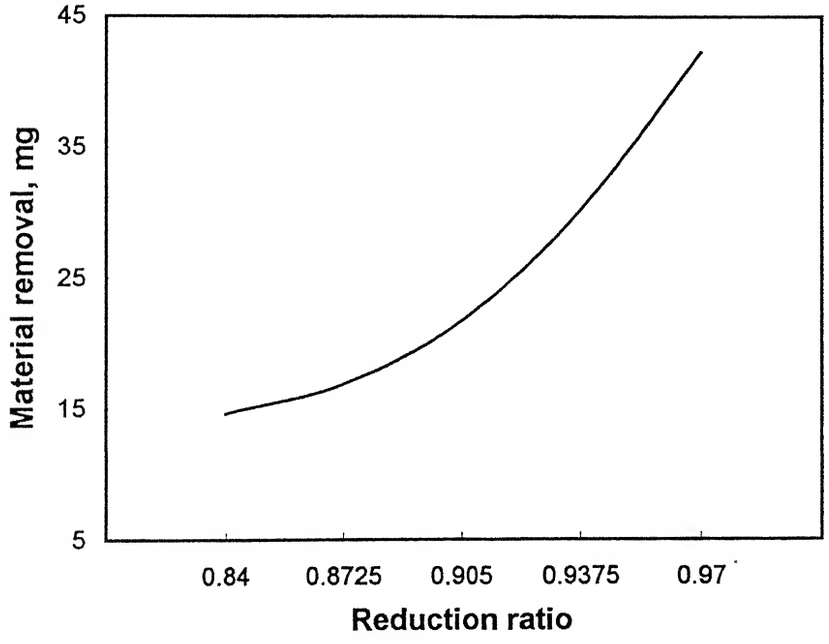


**Fig. 2.9 Variation of material removal with reduction ratio**

**($p_e$ = 50 bar, $N$ =15 cycles, $C$ = 66%)**

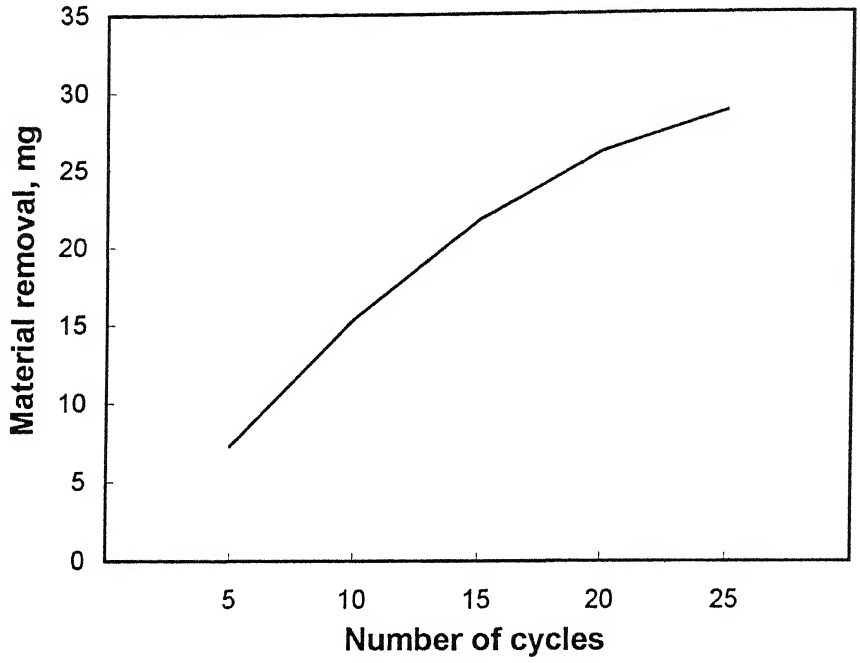


**Fig. 2.10 Variation of material removal with number of cycles**
**($p_e$ = 50 bar, $R_e$ = 0.905, $C$ = 66%)**

## 2.8.2 Surface roughness

The effect of percentage concentration of abrasives on the change in surface roughness indicates the increase in change in surface roughness with increase in percentage concentration of abrasives (Fig. 2.11). With higher concentration of abrasives, the number of abrasives taking part in machining will be more, resulting in more abrasion, and hence surface finish obtained for a specified number of cycles will be better. It is also observed that with increase in percentage concentration of abrasives, the improvement in surface roughness value is more rapid.

Figure 2.12 exhibits the role of extrusion pressure on surface roughness value obtained after the specified number of machining cycles It is observed that change in surface roughness value increases with increase in extrusion pressure but its rate decreases.

Figure 2.13 shows the effect of number of cycles on change in surface roughness value of the workpiece surface. As the number of cycles increases, the roughness value decreases. In other words, change in surface roughness value increases with number of

cycles (Fig 2 13) Initially, rate of improvement in surface roughness value is higher because of availability of peaks in early stages, but as these peaks get machined, the rate of improvement in surface roughness value slowly decreases

Figure 2 14 illustrates the effect of reduction ratio on change in surface roughness value of workpiece surface It is observed that change in surface roughness value increases with increase in reduction ratio, at specified number of cycles At higher reduction ratio, the material removal is higher due to higher slug length of flow and higher normal forces As a consequence, peaks get abraded more in specified number of cycles, and hence, surface roughness value is lowered

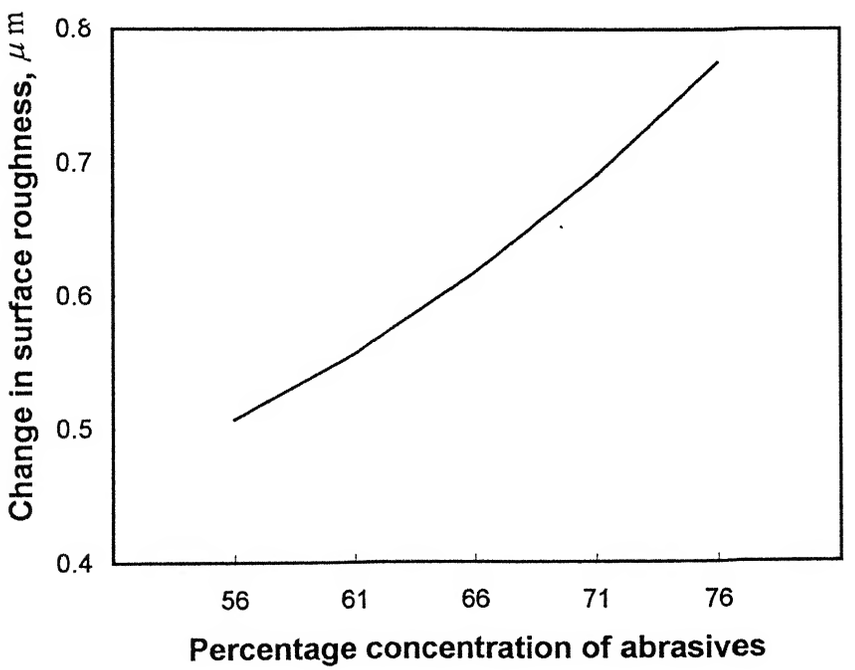


**Fig. 2.11 Variation of change in surface roughness with percentage concentration of abrasives**

**($p_e$ = 50 bar, $R_e$ = 0.905, $N$ =15 cycles)**

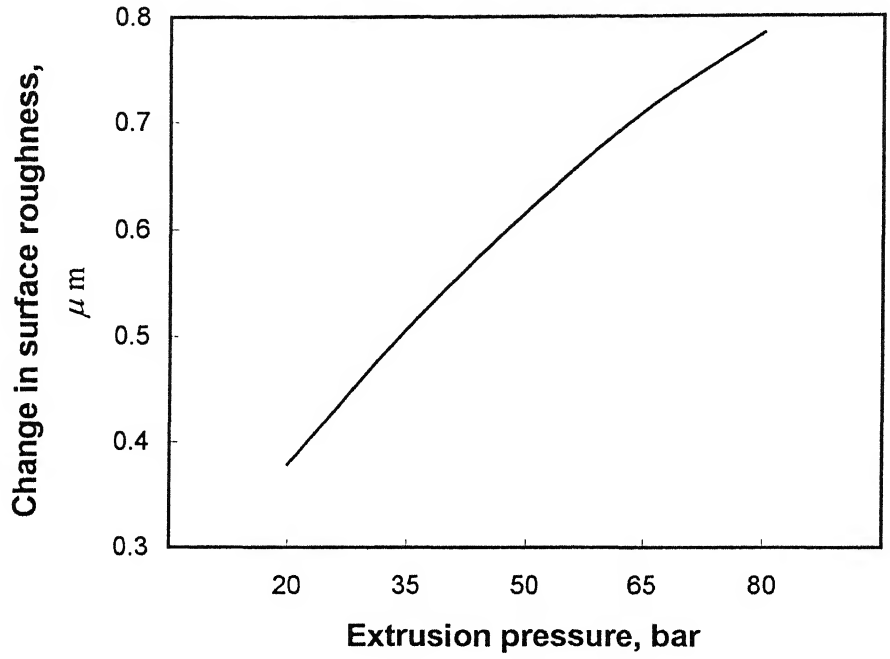


**Fig. 2.12 Variation of change in surface roughness with extrusion pressure ($R_e$ = 0.905, $N$ =15 cycles, $C$ = 66%)**

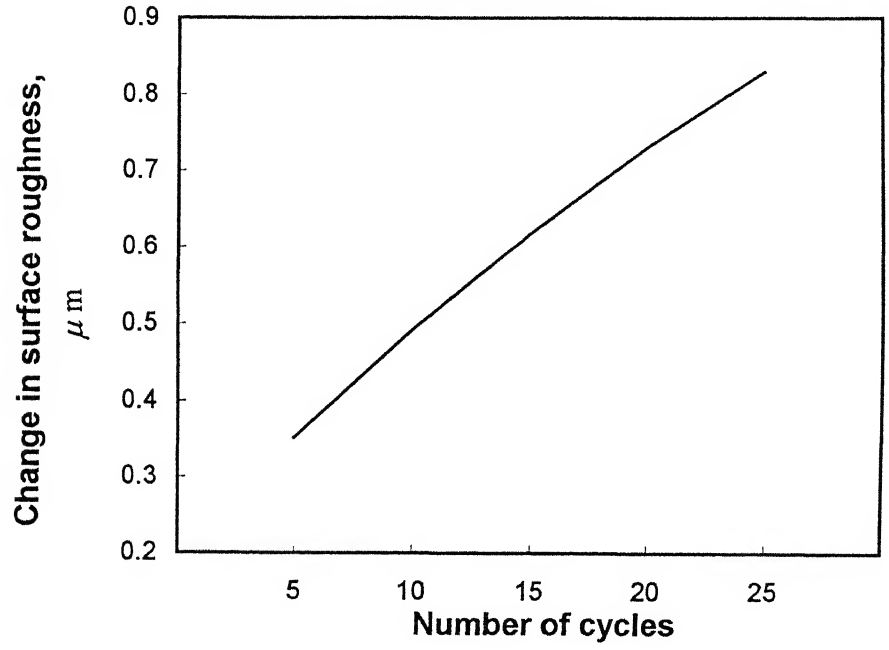


**Fig. 2.13 Variation of change in surface roughness with number of cycles ($p_e$ = 50 bar, $R_e$ = 0.905, $C$ = 66%)**

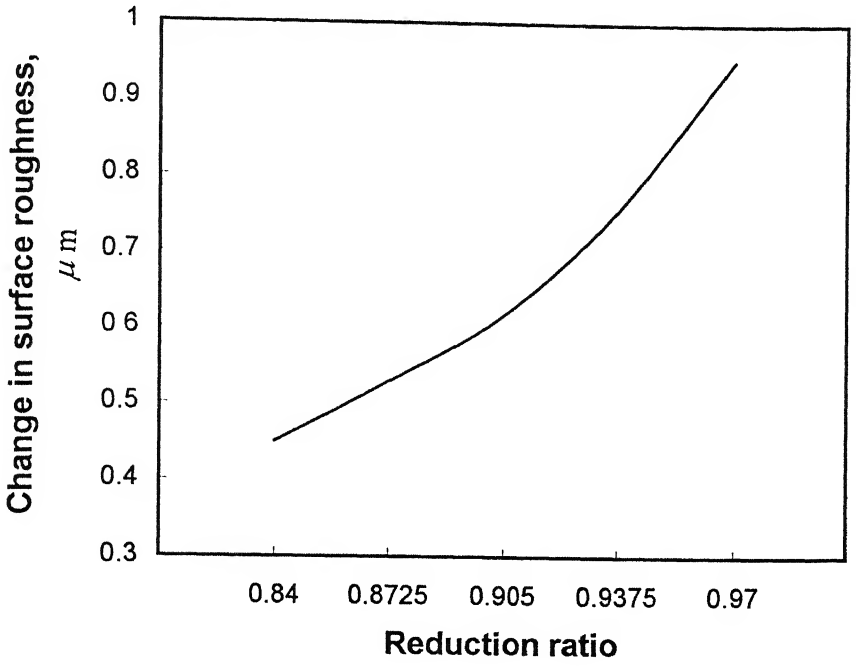


**Fig. 2.14 Variation of change in surface roughness with reduction ratio ($p_e$ = 50 bar, $N$ =15 cycles, $C$ = 66%)**

## 2.9 Conclusions

AFM experiments on mild steel workpieces using SiC abrasives mixed with polyborosiloxane carrier indicate that required surface finish of workpiece surface could be achieved by controlling the AFM process parameters. Central composite rotatable design made possible to study the effect of four important process parameters on process performance by performing only 31 experiments. A comparison between RSA results (derived from equations (2 6) and (2.7)) and experimental data reveals that RSA results can be considered as representative of experimental results. An increase in extrusion pressure increases the depth of indentation of abrasive and increase in percentage concentration of abrasives increases active grain density and media viscosity, hence material removal and change in surface roughness are higher at higher extrusion pressure and concentration of abrasives in media. Material removal and change in surface roughness also increase with increase in reduction ratio and number of cycles.

# Chapter 3

## Modeling of Material Removal and Surface Roughness in AFM

### 3.1. Introduction

Not much information is available in the **literature**, which deals with the theoretical analysis of material removal mechanism in AFM. The relationship between process parameters and performance characteristics of the process is not known completely. The exact mechanism by which the individual abrasive particle accomplishes material removal is only partially understood. There is a need to carry out systematic theoretical analysis of the media flow to determine the stresses and machining forces acting on the workpiece. This will help in the modeling and proper understanding of the machining action during AFM. Once machining forces acting on the workpiece surface, developed due to media flow, are known, an expression can be established for material removal and surface roughness in terms of extrusion pressure and other process variables. The numerical simulation of viscous flow has been the topic of many researchers [26 -30]. Early numerical formulation of viscous materials involved finite element technique based on the Galerkin models, and finite difference technique based on the stream-function vorticity formulations. Zienkiewicz et al. [26] have presented the flow-formulation approach in forming and extrusion, investigating two techniques, viz. the pressure-velocity formulation with Lagrangian constraints and the penalty-function approach. Dixit et al. [27] carried out deformation analysis of the steady-state wire drawing process and Reddy et al. [28] carried out analysis of tube extrusion by FEM using the mixed pressure-velocity formulation. The initial developments of finite difference and finite element methods used for solving non-Newtonian flow have been reviewed by Crochet et al. [29]. Rajeshwar et al. [23] presented a simulation model to determine the characteristics of media flow during machining. The finite difference method was chosen for obtaining the solution. Lim and Dunne [31] have performed finite element modeling of the axisymmetric extrusion

of an aluminum matrix composite containing silicon carbide particles using continuum level constitutive equations In their analysis for making the problem mathematically tractable, they considered metal matrix composite material containing high volume fraction of reinforcement as isotropic and homogeneous. Wilson et al [32] reported that if the settling velocity of discrete solid particles transported by a carrier liquid is very small, then the slurry can be considered as single phase. If the mixture can be transported with a uniform solid concentration across the pipe, then during such transport the mixture can be viewed as homogeneous. The mixture behaves as Newtonian at low solid concentrations and non-Newtonian at higher concentrations.

In the present case of AFM, the physical state of the media is that of a very viscous fluid, and able to adopt the shape of any container. The state of abrasives in the carrier is very similar to what has been stated in the preceeding paragraph through diversified examples. Hence, for simplification of the analysis, it is assumed that the abrasives are uniformly distributed in the carrier (polyborosiloxane), so that the media acts as a homogeneous mixture (continuous phase) [20]. Others [23] also have analysed the deformation of media in AFM process considering it as homogeneous and isotropic.

The **objective** of the present chapter is to establish a model for media flow in AFM, and hence to determine the stresses developed during the flow. These computed stresses can be used to evaluate the machining force and hence, material removal and surface roughness can be obtained in AFM for the given machining conditions. This chapter also describes the simulation of flow of media as a viscoelastic material in AFM process. Solving this problem using available classical methods would be very difficult and tedious. It is also not possible to apply the classical methods to complex shapes like turbine blades which are finished by AFM process. Hence, finite element method has been used to solve such complex geometry problems. Finite element technique is used to solve the governing equations in terms of primary variables (velocity and pressure). Further, theoretical approach to the estimation of material removal and surface finish during abrasive flow machining process has also been presented.

## 3.2 Analysis of Media Flow in AFM Process

The mathematical representation of the flow of media in AFM process involves the equations of continuity and momentum, and the constitutive equations The following assumptions are made to simplify the analysis:

1 The media characteristics are similar to a Maxwell fluid [33]

2. The media is isotropic and homogeneous. The media properties are independent of temperature, and constant with time and space.

3 For cylindrical workpiece, media flow is taken to be axi-symmetric.

4. The media flow is assumed to be steady and fully developed

Steady state, incompressible and axi-symmetric form of the continuity, momentum and constitutive equations is given below.

### 3.2.1. Basic equations

**(A) Continuity equation** (conservation of mass)

For steady state, incompressible and axi-symmetric flow of media, neglecting the volume of material removed* from work surface, the condition of volume constancy can be expressed as,

$$\dot{\varepsilon}_{rr} + \dot{\varepsilon}_{\theta\theta} + \dot{\varepsilon}_{zz} = 0 \tag{3.1}$$

where, $\dot{\varepsilon}_{rr}$, $\dot{\varepsilon}_{\theta\theta}$ and $\dot{\varepsilon}_{zz}$ are the components of strain rate tensor in $r$, $\theta$, and $z$ directions, respectively and can be expressed in terms of the velocity $v_i$ as

$$\dot{\varepsilon}_{ij} = \frac{1}{2}\left\{\frac{\partial v_j}{\partial x_k} + \frac{\partial v_k}{\partial x_j}\right\} \tag{3.2}$$

**(B) Momentum equations** (balance of momentum)

The momentum equations for a steady-state axisymmetric flow of media (neglecting the body forces) have the following form:

$$\rho\left[v_r \frac{\partial v_r}{\partial r} + v_z \frac{\partial v_r}{\partial z}\right] + \frac{\partial p}{\partial r} - \left[\frac{1}{r}\frac{\partial (r\tau_{rr})}{\partial r} - \frac{\tau_{\theta\theta}}{r} + \frac{\partial \tau_{rz}}{\partial z}\right] = 0 \tag{3.3}$$

and

* The total volume of material removed during AFM is extremely small, because it is a finishing process and not a bulk material removal process

$$\rho\left[v_r\frac{\partial v_z}{\partial r}+v_z\frac{\partial v_z}{\partial z}\right]+\frac{\partial p}{\partial z}-\left[\frac{1}{r}\frac{\partial(r\tau_{rz})}{\partial r}+\frac{\partial\tau_{zz}}{\partial z}\right]=0 \tag{3.4}$$

where, $\rho$ is density of media, $p$ is pressure (hydrostatic part of stress tensor), and $\tau_{ij}$ is the extra-stress (deviatoric part of stress tensor)

**(C ) Constitutive equations**

The media exhibits both viscous and elastic properties [33]. In the present analysis, simple constitutive equation which contains a minimum number of material parameters such as model of Maxwell is selected According to Maxwell's model, the constitutive equation is given as follows·

$$\tau_{ij}+\lambda\frac{d\tau_{ij}}{dt}=\mu\,\dot{\varepsilon}_{ij} \tag{3.5}$$

where, $\lambda$ is the relaxation time and $\mu$ is viscosity coefficient.

$\frac{d}{dt}$ is material time derivative For steady state viscoelastic flow, the material derivative of the stress deviator is defined as

$$\frac{d\tau_{ij}}{dt}=v_k\frac{\partial\tau_{ij}}{\partial x_k} \tag{3.6}$$

where $v_k$ are components of velocity tensor.

The expanded form of the eqn (3 5) is given by the following equations.

$$\tau_{rr}+\lambda\left(v_r\frac{\partial\tau_{rr}}{\partial r}+v_z\frac{\partial\tau_{rr}}{\partial z}\right)=\mu\,\dot{\varepsilon}_{rr} \tag{3.7}$$

$$\tau_{zz}+\lambda\left(v_r\frac{\partial\tau_{zz}}{\partial r}+v_z\frac{\partial\tau_{zz}}{\partial z}\right)=\mu\,\dot{\varepsilon}_{zz} \tag{3.8}$$

$$\tau_{rz}+\lambda\left(v_r\frac{\partial\tau_{rz}}{\partial r}+v_z\frac{\partial\tau_{rz}}{\partial z}\right)=\mu\,\dot{\varepsilon}_{rz} \tag{3.9}$$

$$\tau_{\theta\theta}+\lambda\left(v_r\frac{\partial\tau_{\theta\theta}}{\partial r}+v_z\frac{\partial\tau_{\theta\theta}}{\partial z}\right)=\mu\,\dot{\varepsilon}_{\theta\theta} \tag{3.10}$$

For an incompressible fluid, the total stress tensor $\sigma_{ij}$ is given by

$$\sigma_{ij} = - p \delta_{ij} + \tau_{ij} \qquad (3\ 11)$$

where, $\delta_{ij}$ are components of the identity tensor ( or Kronecker delta)

### 3.2.2 Non-dimensionalization

Non-dimensionalization is usually required to avoid ill-conditioning and numerical difficulties. The non-dimensionalization of all physical quantities used above has been done using characteristic dimensional quantities as given below

$$\bar{r} = \frac{r}{r_w} ; \qquad \bar{z} = \frac{z}{r_w} , \qquad \bar{v}_r = \frac{v_r}{v_p} ; \qquad \bar{v}_z = \frac{v_z}{v_p}$$

$$\bar{\dot{\varepsilon}}_{ij} = \frac{\dot{\varepsilon}_{ij}}{(v_p / r_w)} \qquad \bar{p} = \frac{p}{\sigma_o} ; \qquad \bar{\tau}_{ij} = \frac{\tau_{ij}}{\sigma_o} , \qquad \bar{\mu} = \frac{\mu}{\mu_o}$$

$$\text{and} \quad W = \lambda \frac{v_p}{r_w} \qquad (3\ 12)$$

where, W is non-dimensional parameter which is sometimes called Weissenberg number, and $\mu_o = \frac{\sigma_o}{(v_p / r_w)}$; $\sigma_o$ is the flow stress of material; $r_w$ is the radius of workpiece, and $v_p$ is velocity of media flow at inlet

Substituting non-dimensional parameters in continuity, momentum and constitutive equations (3.1, 3.3, 3 4 and 3.5), we obtain

$$\bar{\dot{\varepsilon}}_{rr} + \bar{\dot{\varepsilon}}_{\theta\theta} + \bar{\dot{\varepsilon}}_{zz} = 0 \qquad (3.13)$$

$$\frac{(\rho v_p r_w)}{\mu_o} [ \bar{v}_r \frac{\partial \bar{v}_r}{\partial \bar{r}} + \bar{v}_z \frac{\partial \bar{v}_r}{\partial \bar{z}} ] + [ \frac{\partial \bar{p}}{\partial \bar{r}} - \frac{1}{\bar{r}} \frac{\partial (\bar{r} \bar{\tau}_{rr})}{\partial \bar{r}} + \frac{\bar{\tau}_{\theta\theta}}{\bar{r}} - \frac{\partial \bar{\tau}_{rz}}{\partial \bar{z}} ] = 0 \qquad (3.14)$$

$$\frac{(\rho v_p r_w)}{\mu_o} [ \bar{v}_r \frac{\partial \bar{v}_z}{\partial \bar{r}} + \bar{v}_z \frac{\partial \bar{v}_z}{\partial \bar{z}} ] + [ \frac{\partial \bar{p}}{\partial \bar{z}} - \frac{1}{\bar{r}} \frac{\partial \bar{r} \bar{\tau}_{rz}}{\partial \bar{r}} - \frac{\partial \bar{\tau}_{zz}}{\partial \bar{z}} ] = 0 \qquad (3.15)$$

$$\bar{\tau}_{ij} + W \frac{d\tau_{ij}}{dt} = \bar{\mu}\ \bar{\dot{\varepsilon}}_{ij} \tag{3.16}$$

For convenience in writing, the overbar (-) from non-dimensional parameters is dropped in the succeeding description. Since Reynolds number $\frac{(\rho\, v_p\, r_w)}{\mu_o}$ is found to be typically of the order of $10^{-8}$ for all the cases considered here, the inertial terms of eqns (3 14 and 3.15) are ignored in the next section.

### 3.2.3 Galerkin or weak formulation

The finite element formulation of flow of the rigid plastic material in terms of primary variables (pressure and velocity) has been presented by Dixit et al. [27]. Similar formulations with some modifications are possible for the flow of AFM media, which is a viscoelastic incompressible material

In the present analysis, the Galerkin weighted residual method [34] is employed to reduce the governing differential equations by using appropriate weighting functions for the momentum and continuity equations. Let $v_r$, $v_z$, and $p$ constitute the functions that satisfy all the essential boundary conditions. Then $v_r$, $v_z$, and $p$ constitute a weak solution if the following integral equation is satisfied.

$$\int_{\Omega} [\{\dot{\varepsilon}_{rr} + \dot{\varepsilon}_{\theta\theta} + \dot{\varepsilon}_{zz}\}\ w_p + \{\frac{\partial p}{\partial r} - \frac{1}{r}\frac{\partial(r\,\tau_{rr})}{\partial r} + \frac{\tau_{\theta\theta}}{r} - \frac{\partial \tau_{rz}}{\partial z}\} w_r$$

$$+ \{\frac{\partial p}{\partial z} - \frac{1}{r}\frac{\partial(r\tau_{rz})}{\partial r} - \frac{\partial \tau_{zz}}{\partial z}\} w_z\ ]\, 2\pi r\, dr\, dz = 0 \tag{3.17}$$

where, $w_p$, $w_r$ and $w_z$ are the weight functions which satisfy the homogeneous versions of the boundary conditions and $\Omega$ represents the area of the domain.

Performing the integration by parts on second and third segments of the above equation, the following weak form is obtained:

$$\int_{\Omega} [I_1 + I_2]\, 2\,\pi\, r\, dr\, dz - \int_{\Gamma_1} I_3\, d\Gamma_1 - \int_{\Gamma_2} I_4\, d\Gamma_2 = 0 \tag{3.18}$$

where, $I_1 = \{ \dot{\varepsilon}_{rr} + \dot{\varepsilon}_{\theta\theta} + \dot{\varepsilon}_{zz} \} w_p$ (3 19)

$$I_2 = -p \{ \dot{\varepsilon}_{rr}(w) + \dot{\varepsilon}_{\theta\theta}(w) + \dot{\varepsilon}_{zz}(w) \} + \{ \tau_{zz} \frac{\partial w_z}{\partial z} + \tau_{rr} \frac{\partial w_r}{\partial r} + \tau_{\theta\theta} \frac{w_r}{r} + \tau_{rz} (\frac{\partial w_z}{\partial r} + \frac{\partial w_r}{\partial z}) \}$$

(3 20)

$$I_3 = t_z w_z \quad (3\ 21)$$

$$I_4 = t_r w_r \quad (3\ 22)$$

and $\Gamma_1$ and $\Gamma_2$ are the boundaries where the traction components $t_r$ and $t_z$ are specified

The term $\dot{\varepsilon}_{rr}(w)$, $\dot{\varepsilon}_{\theta\theta}(w)$, $\dot{\varepsilon}_{zz}(w)$ and $\dot{\varepsilon}_{rz}(w)$ are defined as

$$\dot{\varepsilon}_{rr}(w) = \frac{\partial w_r}{\partial r}, \quad \dot{\varepsilon}_{zz}(w) = \frac{\partial w_z}{\partial z}, \quad \dot{\varepsilon}_{\theta\theta}(w) = \frac{w_r}{r}; \quad \text{and } \dot{\varepsilon}_{rz}(w) = \frac{1}{2}\left( \frac{\partial w_r}{\partial r} + \frac{\partial w_z}{\partial z} \right)$$

(3 23)

### 3.2.4 Finite element approximations

In the present analysis, Langrangian biquadratic shape function for $v_r$ and $v_z$, and bilinear shape function for $p$ over a 9 noded quadrilateral element are used The approximations for $v_r$ and $v_z$ are as follows :

$$\begin{Bmatrix} v_r \\ v_z \end{Bmatrix} = \begin{bmatrix} N_1 & 0 & N_2 & 0 & \text{----} & N_9 & 0 \\ 0 & N_1 & 0 & N_2 & \text{----} & 0 & N_9 \end{bmatrix} \begin{Bmatrix} (v_{r_1})^e \\ (v_{z_1})^e \\ - \\ - \\ - \\ (v_{r_9})^e \\ (v_{z_9})^e \end{Bmatrix} = [N_v]\{v^e\} \quad (3\ 24)$$

In Galerkin formulation, the weight functions corresponding to velocities are approximated using the same shape functions as that for velocity. Therefore,

$$\{w_v\} = \begin{Bmatrix} w_r \\ w_z \end{Bmatrix} = [N_v]\{w_v^e\} \quad (3\ 25)$$

The vectors $\{v^e\}$ and $\{w_v^e\}$ contain the velocities at the nodes of elements and their corresponding weight functions respectively. The approximation for $p$ is as follows:

$$p = \begin{bmatrix} N_1^p & N_2^p & N_3^p & N_4^p \end{bmatrix} \begin{Bmatrix} p_1^e \\ p_2^e \\ p_3^e \\ p_4^e \end{Bmatrix} \tag{3.26}$$

i.e. $p = \{N_p\}^T \{p^e\}$ (3.27)

The weight function corresponding to pressure is approximated using the shape functions as that for pressure.

$$w_p = \{N_p\}^T \{w_p^e\} \tag{3.28}$$

The deviatoric stresses are approximated by the same shape functions as used for pressure. Therefore,

$$\{\tau\} = [N_\tau] \{\tau^e\} \tag{3.29}$$

$$[N_\tau] = \begin{bmatrix} N_1 & 0 & 0 & 0 & N_2 & 0 & 0 & 0 & . & . & N_4 & 0 & 0 & 0 \\ 0 & N_1 & 0 & 0 & 0 & N_2 & 0 & 0 & . & . & 0 & N_4 & 0 & 0 \\ 0 & 0 & \sqrt{2}N_1 & 0 & 0 & 0 & \sqrt{2}N_2 & 0 & . & . & 0 & 0 & \sqrt{2}N_4 & 0 \\ 0 & 0 & 0 & N_1 & 0 & 0 & 0 & N_2 & . & . & 0 & 0 & 0 & N_4 \end{bmatrix} \tag{3.30}$$

$$\{\tau^e\} = \begin{Bmatrix} (\tau_{rr})_1 \\ (\tau_{zz})_1 \\ (\tau_{rz})_1 \\ (\tau_{\theta\theta})_1 \\ . \\ . \\ . \\ (\tau_{rr})_4 \\ (\tau_{zz})_4 \\ (\tau_{rz})_4 \\ (\tau_{\theta\theta})_4 \end{Bmatrix} \tag{3.31}$$

### 3.2.5 Finite element equations

To facilitate derivation of the finite element equations, it is first necessary to express eqn (3 18) in vector form The following vectors are defined for that purpose The strain vector is given by

$$\dot{\varepsilon} = \begin{bmatrix} \dot{\varepsilon}_{rr} \\ \dot{\varepsilon}_{zz} \\ \sqrt{2}\,\varepsilon_{rz} \\ \dot{\varepsilon}_{\theta\theta} \end{bmatrix} = \begin{bmatrix} \dfrac{\partial v_r}{\partial r} \\ \dfrac{\partial v_z}{\partial z} \\ \dfrac{1}{\sqrt{2}}\left[\dfrac{\partial v_z}{\partial r} + \dfrac{\partial v_r}{\partial z}\right] \\ \dfrac{v_r}{r} \end{bmatrix} \tag{3 32}$$

Substitution of the approximating expressions in the above equation lead to

$$\{\dot{\varepsilon}\} = [B]\{v^e\} \quad \text{and} \quad \{\dot{\varepsilon}(w)\} = [B]\{w_v^e\} \tag{3.33}$$

where,

$$[B] = \begin{bmatrix} \dfrac{\partial N_1}{\partial r} & 0 & \dfrac{\partial N_2}{\partial r} & 0 & - - - & \dfrac{\partial N_9}{\partial r} & 0 \\ 0 & \dfrac{\partial N_1}{\partial z} & 0 & \dfrac{\partial N_2}{\partial z} & - - - & 0 & \dfrac{\partial N_9}{\partial z} \\ \dfrac{1}{\sqrt{2}}\dfrac{\partial N_1}{\partial z} & \dfrac{1}{\sqrt{2}}\dfrac{\partial N_1}{\partial r} & \dfrac{1}{\sqrt{2}}\dfrac{\partial N_2}{\partial z} & \dfrac{1}{\sqrt{2}}\dfrac{\partial N_2}{\partial r} & - - - & \dfrac{1}{\sqrt{2}}\dfrac{\partial N_9}{\partial z} & \dfrac{1}{\sqrt{2}}\dfrac{\partial N_9}{\partial r} \\ \dfrac{N_1}{r} & 0 & \dfrac{N_2}{r} & 0 & - - - & \dfrac{N_9}{r} & 0 \end{bmatrix} \tag{3.34}$$

$$\dot{\varepsilon}_{rr} + \dot{\varepsilon}_{\theta\theta} + \dot{\varepsilon}_{zz} = [1 \;\; 1 \;\; 0 \;\; 1]\{\dot{\varepsilon}\} = \{m\}^T [B]\{v^e\} \tag{3.35}$$

where, $$\{m\} = \begin{bmatrix} 1 \\ 1 \\ 0 \\ 1 \end{bmatrix}. \tag{3.36}$$

Similarly,

$$\dot{\varepsilon}_{rr}(w) + \dot{\varepsilon}_{\theta\theta}(w) + \dot{\varepsilon}_{zz}(w) = \{m\}^T [B]\{w_v^e\} \tag{3.37}$$

Substituting the above equations into the eqn (3.18) leads to the following finite element equation in the local variables ·

$$\sum_{e=1}^{NAE}\{w^e\}^T[k^e]\{\gamma^e\} = \sum_{b=1}^{NBE}\{w_r^b\}^T\{f_r^b\} + \sum_{b=1}^{NBE}\{w_z^b\}^T\{f_z^b\} + \sum_{e=1}^{NAE}\{w_v^e\}^T\{f\} \tag{3.38}$$

$$\text{where, } \{w^e\} = \begin{Bmatrix}\{w_p^e\}\\ \{w_v^e\}\end{Bmatrix} \tag{3.39}$$

$$\{\gamma^e\} = \begin{Bmatrix}\{p^e\}\\ \{v^e\}\end{Bmatrix} \tag{3.40}$$

$$[k^e] = \begin{bmatrix}0 & [k_{pv}^e]\\ [k_{pv}^e] & [k_{vv}^e]\end{bmatrix} \tag{3.41}$$

$$[k_{pv}^e] = -\int_{A^e}\{N_p\}\{m\}^T[B]\,2\pi r\,dr\,dz \tag{3.42}$$

$$\{m\}^T = \{1\ 1\ 0\ 1\} \tag{3.43}$$

$$[k_{vv}^e] = \int_{A^e}\mu\,[B]^T[B]\,2\pi r\,dr\,dz \tag{3.44}$$

$$[k_{vv}^e] = -\int_{A^e}[B]^T\{m\}\{N_p\}^T\,2\pi\,r\,dr\,dz \tag{3.45}$$

$$\{f_r^b\} = \int_{\Gamma^b}\{N_b\}\{N_b\}^T\{t_r^b\}\,2\pi\,r\,d\Gamma \tag{3.46}$$

$$\{f_z^b\} = \int_{\Gamma^b}\{N_b\}\{N_b\}^T\{t_z^b\}\,2\pi\,r\,d\Gamma \tag{3.47}$$

$$\{f\} = \int_{A^e}[B]^T W\left\{v_z\frac{\partial[N_\tau]}{\partial z}\{\tau^e\} + v_r\frac{\partial[N_\tau]}{\partial r}\{\tau^e\}\right\}2\pi r\,dr\,dz \tag{3.48}$$

where $NAE$ is the number of area elements and $NBE$ is the number of boundary elements.

The variables of the area integrals (3.46 to 3.47) are transformed to the natural coordinates $(\xi,\eta)$ using the following transformation:

$$\int_{A^e}(...)\,dr\,dz = \int_{-1}^{+1}\int_{-1}^{+1}(....)|J|\,d\xi\,d\eta \tag{3.49}$$

where $|J|$ is the determinant of the elemental Jacobian matrix and is given by

$$|J| = \begin{bmatrix} \frac{\partial z}{\partial \xi} & \frac{\partial z}{\partial \eta} \\ \frac{\partial r}{\partial \xi} & \frac{\partial r}{\partial \eta} \end{bmatrix} \tag{3 50}$$

The choice of local coordinate system is dictated by the Gauss quadrature rule [35] used in the numerical evaluation of integrals over the element.

Similarly the boundary integrals (eqns 3 46 and 3.47) are transformed to integrals over the interval (-1,1) by the relation

$$\int_{\Gamma} (...)\, d\Gamma = \int_{-1}^{+1} (....) |J_b|\, d\varsigma \tag{3.51}$$

where $|J_b|$ is the Jacobian for the boundary element and is given by

$$|J_b| = \sqrt{(\frac{\partial z}{\partial \varsigma})^2 + (\frac{\partial r}{\partial \varsigma})^2} \tag{3.52}$$

The final finite element equation is obtained by assembling the elemental area and boundary matrices into global area and boundary matrices respectively. The elemental area matrices $[k^e]$ are calculated by evaluating the integrals by Guass quadrature integration technique. The assembly of the elemental area matrices into global area matrices is done by transferring the elements corresponding to a local degree of freedom in each elemental area matrix to positions of corresponding global degree of freedom in the global area matrix. The assembled finite element equation may be written as

$$[K]\ \{Y\} = \{F\} + \{F_e\} \tag{3.53}$$

where [K] is the global coefficient matrix, Y is the global nodal primary variables (pressures and velocities) and $F$ and $F_e$ are the global right side vectors. Here, $F_e$ denotes the elastic force component.

After substitution of boundary conditions as discussed in the next section, the final equation (3.53) is solved by Householder Method [36].

### 3.2.6 Boundary conditions

In the present work, axi-symmetric abrasive media flow is considered for the analysis taking into consideration the schematic diagram of the AFM process shown in

Fig. 1.4. The domain along with the boundary conditions is shown in Fig. 3.1 and boundary conditions are described as given below:

(i) Entry (at AB)

$v_r = 0$ ; $v_z = v_p$

where $v_p$ is the velocity of piston or velocity of flow at inlet.

(ii) Exit ( at HG)

$v_r = 0$ ; $t_z = 0$

(iii) Surface of media cylinder (at BC and FG)

$v_r = 0$ ; $t_z = 0$

(iv) Media tooling interface (CD and EF)

The normal component of velocity ($v_n$) at any point on the boundary must be zero. Hence,

$v_r + v_z \tan\alpha = 0$ ; at CD

$v_r - v_z \tan\alpha = 0$ ; at EF

where $\alpha$ is the angle made by the outward unit normal at tool surface with the $r$-axis (Fig. 3.1). The secondary boundary conditions are specified in terms of a friction condition. The Coulomb friction relation is used here. Thus

$|t_s| = f\,|t_n|$

where $t_s$ and $t_n$ are the tangential and normal stress components along the boundary CD and EF (Fig. 3.1 and 3.2). $f$ is the coefficient of friction assumed to be constant along the interface.

(iv) Surface of workpiece (DE)

$v_r = 0$ ; $|t_z| = f\,|t_r|$

(vi) Axis of symmetry (AH)

$v_r = 0$ ; $t_z = 0$

The geometry of flowing media is discretized using a mesh of $5 \times 20$, 9 node elements in the r and z directions, respectively (Fig. 3.3). The mesh emphasizes radial and axial refinement near the singularity. The experience with inelastic flow [30] has shown

that radial and axial mesh refinement is very important to resolve adequately steep gradients Also it has been known in viscous calculations that elements near the singularity with large aspect ratios produce numerical instabilities. The fine mesh offers a compromise between these two concerns.

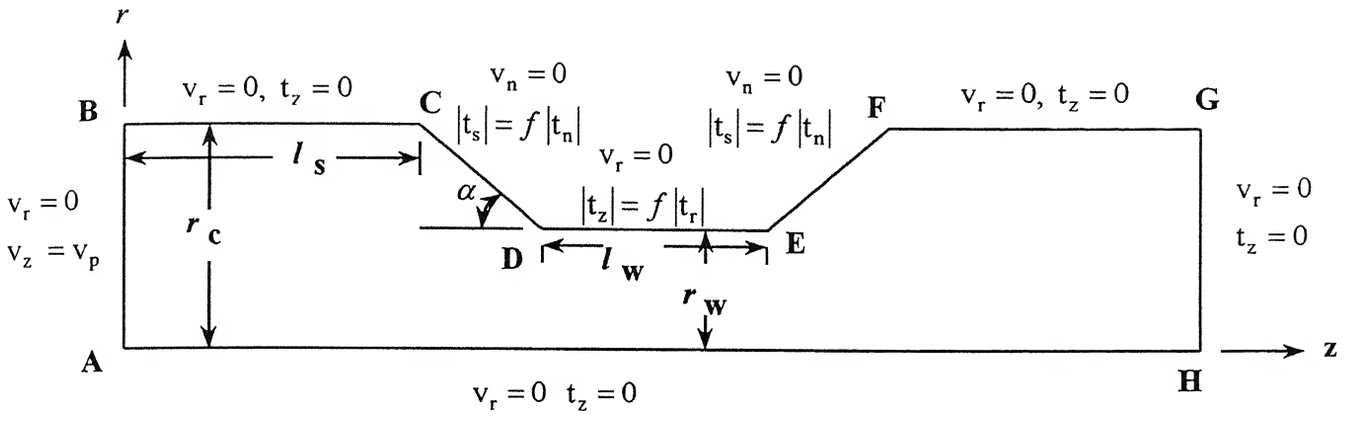


**Fig. 3.1 The domain and boundary conditions for axisymmetric flow of media in AFM process**

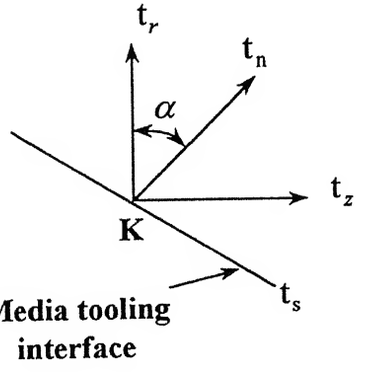


**Fig 3.2 The boundary tractions at typical boundary node K**

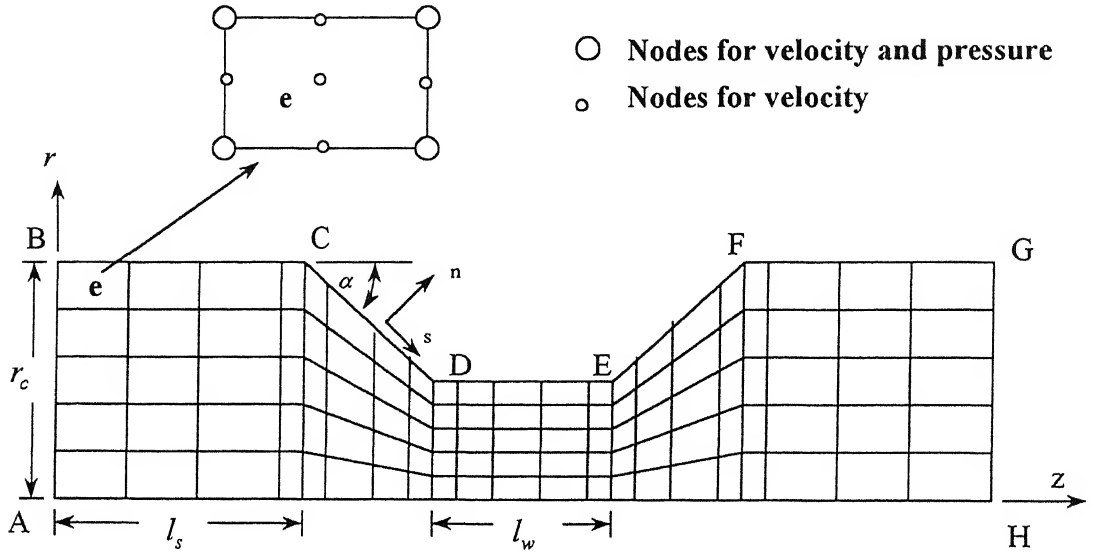


**Fig. 3.3 The finite element mesh and a typical element 'e'**

### 3.2.7 Solution procedure

The initial stress rate method described by Dawson and Thompson [37] is used to solve the present viscoelastic flow problem. A viscous approximation for steady state viscoplastic analysis is extended to include the effect of the elastic strains. The solution procedure follows with the subscript $i$ designating the $i$th iteration.

**Step 1**. The approximations for stress rate are initialized to zero within each element, ie $\left\{\frac{d\tau}{dt}\right\}_{i=0} = 0$. This in turn will require the elastic forces, $\{F_e\}_{i=0}$ for the system to be equal to zero.

**Step 2.** The following equation is solved for velocities and pressures.

$$[\mathrm{K}]\ \{\mathrm{Y}\}_{i+1} = \{F + \{F_e\}_i \qquad (3.54)$$

For $i = 0$ this will correspond to viscous solution.

**Step 3.** Using the velocities from step 2,

$\{\dot{\varepsilon}\}_{i+1} = [B]\ \{\mathrm{v}^e\}_{i+1}$ and $\tau_{i+1} = \mu\ \{\dot{\varepsilon}\}_{i+1}$ - W $\left\{\frac{d\tau}{dt}\right\}_i$ are determined for each element.

**Step 4.** The gradient of the stress found from step 3 is determined and with the velocity from step 2, the stress rate $\left\{\frac{d\tau}{dt}\right\}_{i+1}$ is evaluated according to eqn (3 6)

$$\left\{\frac{d\tau}{dt}\right\}_{i+1} = \left\{ v_z \frac{\partial[N_\tau]}{\partial z}\{\tau^e\} + v_r \frac{\partial[N_\tau]}{\partial r}\{\tau^e\}\right\}_{i+1} \qquad (3\ 55)$$

**Step 5.** A new elastic force matrix is computed

$$\{F_e\}_{i+1} = \int_{A^e} [B]^T \; W \left\{\frac{d\tau}{dt}\right\}_{i+1} 2\,\pi\, r\, dr\, dz \qquad (3\ 56)$$

**Step 6.** If there is significant change in $\{F_e\}$ between the $i$th and $(i+1)$th iterations, return to step 2 If change is less than $10^{-3}$, convergence is obtained.

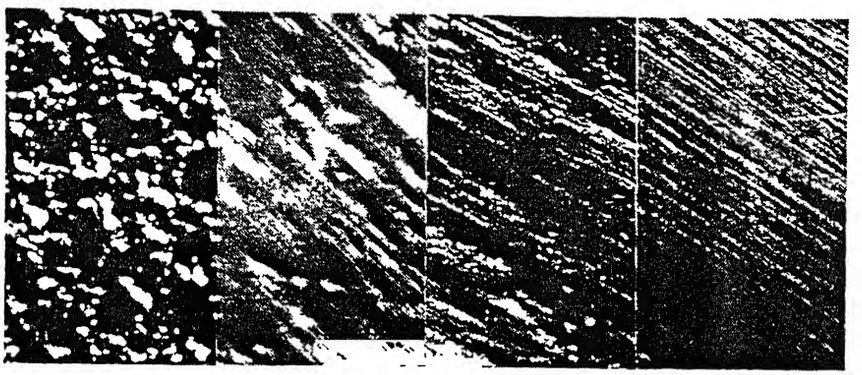

**Fig. 3.4 AFM process removes high spots of the surface [10]**

## 3.3 Mechanism of Material Removal in AFM

The abrasion in AFM referred here is defined as the removal of solid material from a surface by the unidirectional sliding action of discrete particles of another material. AFM process grinds away the high spots of the area, yielding a more uniform and unidirectional surface [10]. Fig 3.4 shows the progressive AFM action of abrasive media on the extrusion die [10]. The basic mechanism of abrasion in general has been the subject of many investigators. Khrushchov and Bavichov [38] identified following two processes taking place when abrasive grains make contact with the wearing surface : (1) The formation of plastically impressed grooves which did not involve material removal, and (2) the

separation of material particles in the form of micro chips. It is found [39,40] that the chip cutting and rubbing depend upon the shape of indenting particles In particular, spherical indentors have been found to show a change over from rubbing to at least partial chip formation when the indentation strain (defined as the depth of indentation divided by the diameter of the indentor) exceeds a certain value. Pure microcutting results in a volume loss in the form of chips and equal to the volume of the grooves produced.

## 3.4 Modeling for Material Removal and Surface Roughness

Abrasive flow machining is considered to be a scratching action performed by abrasive grains in the AFM media The normal force applied to a spherical grain will lead it to penetrate in the surface (Fig 3.5) [41]. The grain produces a groove on the workpiece surface whose section corresponds to the profile of the grain. As the grain is translated horizontally, it removes material from the workpiece surface The amount of stock removal is then equal to the total volume of the grooves produced on the workpiece surface by each grain in the media. The idealized classical model of abrasive wear [42] provides a theoretical basis for the determination of material removal by AFM process. If the number of active grains, their shape and depth of the groove produced are known, the volume of stock removal can be calculated

### 3.4.1 Assumptions

The following assumptions are adopted for the analysis of material removal by AFM process:

1. Most of the abrasive grains are blocky crystals that may be approximated to be spherical in shape [41] This is also reasonable considering the large negative rake angles presented by the grains. Observation of abrasive particles also shows that for the most part, they are generally rounded, though irregular in shape and are not composed of acute cutting edges .
2. It is assumed that each grain consists of a single active cutting edge. If there are more than one cutting edge on one grain, there is no space to store the chip between the cutting edges. So that cutting edge can not be active any more. As a result, the grain acts as one cutting edge [43].

3 To render the mathematics tractable it is necessary to assume that the load on each particle is constant and equal to the average load

4 All active grains are assumed to be of the same size, which is equal to the average of given range of mesh size.

5 Every abrasive grain is assumed to achieve the same penetration depth depending upon the applied force for a given workpiece material..

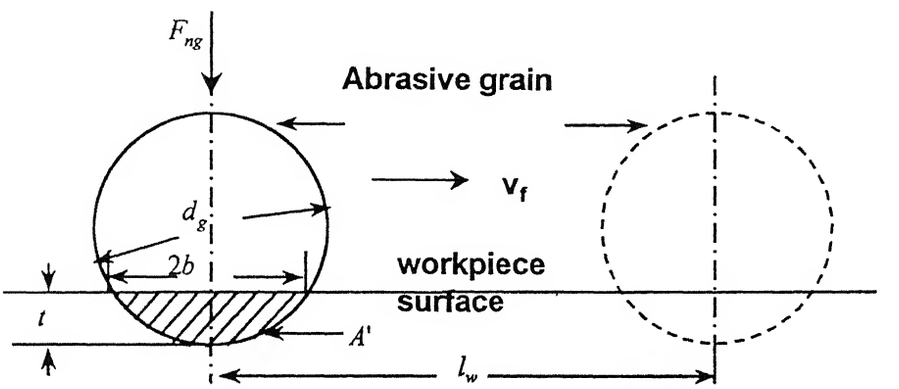


**Fig. 3.5 Schematic diagram of a spherical abrasive grain removing material from the workpiece surface.**

## 3.4.2 Material removal

The normal force acting on a spherical grain will cause it to penetrate the surface of the workpiece When this grain is translated horizontally, the plastically deformed zone beneath the surface will be inclined and give rise to upward flow thus forming a chip which is subsequently sheared from the surface.

The indenting force $F_{ng}$ (normal force) on a spherical grain of diameter $d_g$ is given as

$$F_{ng} = \sigma_n \frac{\pi d_g^2}{4} \tag{3.57}$$

where, $\sigma_n$ is normal stress acting on the grain.

If $b$ is the radius of the projected area of indentation $\nabla A$, $t$ is depth of indentation, and $H_w$ is hardness of workpiece material. Then,

$$F_{ng} = H_w \nabla A$$

$$= H_w \pi b^2 \tag{3.58}$$

From the geometry of Fig 3.5, radius of the projected area '$b$' of the indent made and depth of indentation $t$ can be obtained as given below.

$$b = \sqrt{t(d_g - t)} \tag{3.59}$$

$$t = \frac{d_g}{2} - \sqrt{(\frac{d_g^2}{4} - b^2)} \tag{3.60}$$

Substituting the value of $b$ from eqn (3.58), into eqn. (3.60), we obtain

$$t = \frac{d_g}{2} - \sqrt{\frac{d_g^2}{4} - \frac{F_{ng}}{H_w \pi}} \tag{3.61}$$

The cross sectional area $A'$ of the groove generated (shaded portion of the grain, as shown in Fig. 3.5) can be derived from the geometry of the figure.

$$A' = \frac{d_g^2}{4} \sin^{-1} \frac{2\sqrt{t(d_g - t)}}{d_g} - \sqrt{t(d_g - t)}(\frac{d_g}{2} - t) \tag{3.62}$$

Therefore, volume of the material removed ($V_g$) by an abrasive grain is equal to the product of area $A'$ and length of contact $L_l$ of grain with workpiece surface.

$$V_g = [\frac{d_g^2}{4} \sin^{-1} \frac{2\sqrt{t(d_g - t)}}{d_g} - \sqrt{t(d_g - t)}(\frac{d_g}{2} - t)] L_l \tag{3.63}$$

In practice, the total material removal is made up of a number of similar processes. Let $n$ be the number of abrasive grains simultaneously acting per unit area of contact. Then, total no. of abrasive grains ($n_s$) indenting in the workpiece surface per stroke are given by

$$n_s = 2 \pi r_w n v_f \frac{l_s}{v_p} \tag{3.64}$$

where, $l_s$ is stroke length, $v_p$ is velocity of piston, $v_f$ is velocity of flow across workpiece surface, and $r_w$ is radius of cylindrical workpiece (Fig. 3.1)

From continuity equation

$$\frac{V_f}{V_p} = \frac{r_c^2}{r_w^2} \tag{3.65}$$

where, $r_c$ is radius of media cylinder.

By substituting the value of $\frac{V_f}{V_p}$ from eqn. (3.65) into eqn. (3 64), $n_s$ can be calculated as given below

$$n_s = 2\ \pi\ r_w n l_s \frac{r_c^2}{r_w^2} \tag{3.66}$$

Hence, volumetric material removal in $i$th stroke ($V_i$ ) in AFM is given as

$$V_i = 2\ \pi\ n l_s \frac{r_c^2}{r_w} \left[\frac{d_g^2}{4}\sin^{-1}\frac{2\sqrt{t(d_g - t)}}{d_g} - \sqrt{t(d_g - t)}\left(\frac{d_g}{2} - t\right)\right] L_i \tag{3.67}$$

This simple model (eqn 3.67) suggests that material removal per unit length of sliding depends on depth of indentation (given by eqn.3.61), size of abrasive grain and active grain density for given size of workpiece and media cylinder.

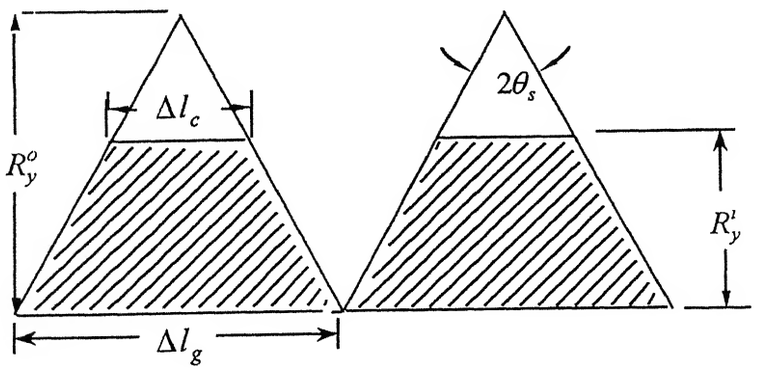


**Fig. 3.6 Simplified surface geometry**

### 3.4.3 Surface roughness

AFM removes the high spots of the surface profile of workpiece, yielding a more uniform surface [10]. It is assumed that the surfaces of the workpiece have uniform profile without statistical distribution, that they have an initial surface roughness $R_a^o$, and that the abrasives move in the length direction of the scratches [44]. There is a constant ratio between the peak to valley surface roughness ($R_y$) and average roughness ($R_a$) Let $R_a^i$ be the surface roughness obtained after $i$th stroke during AFM From Fig. 3.6, the actual contact length ($L_i$) between the workpiece and a spherical abrasive grain is given as

$$L_i = (\frac{\nabla l_c}{\nabla l_g}) l_w$$

$$= [\frac{(R_a^o - R_a^i)\tan\theta_s}{R_a^o \tan\theta_s}] l_w = [1- \frac{R_a^i}{R_a^o}] l_w \qquad (3.68)$$

where, $\nabla l_c$ and $\nabla l_g$ are shown in Fig. 3.6 and $2\theta_s$ is mean angle of surface asperity.

Substituting the value of $L_i$ from eqn (3.68) into eqn.(3.67), the volumetric material removal in $i$th stroke $V_i$ is given as

$$V_i = 2\ \pi\ n l_s \frac{r_c^2}{r_w} [\frac{d_g^2}{4}\sin^{-1}\frac{2\sqrt{t(d_g - t)}}{d_g} - \sqrt{t(d_g - t)}(\frac{d_g}{2} - t)]\ [1- \frac{R_a^i}{R_a^o}]\ l_w \qquad (3.69)$$

$$\text{Let } D = 2\ \pi\ n l_s \frac{r_c^2}{r_w} l_w [\frac{d_g^2}{4}\sin^{-1}\frac{2\sqrt{t(d_g - t)}}{d_g} - \sqrt{t(d_g - t)}(\frac{d_g}{2} - t)] \qquad (3.70)$$

$$\text{Hence, } V_i = D\ [1- \frac{R_a^i}{R_a^o}] \qquad (3\ 71)$$

Total volumetric material removal in $N$ number of cycles is evaluated as

$$V = \sum_{i=1}^{2N} V_i$$

$$V = 2\ \pi\ n l_s \frac{r_c^2}{r_w} l_w [\frac{d_g^2}{4}\sin^{-1}\frac{2\sqrt{t(d_g - t)}}{d_g} - \sqrt{t(d_g - t)}(\frac{d_g}{2} - t)] \sum_{i=1}^{2N} [1- \frac{R_a^i}{R_a^o}] \qquad (3.72)$$

Weight of matrial removed $W_m$ in $N$ number of cycles is given as

$$W_m = 2\ \pi\ \rho_w\ n l_s \frac{r_c^2}{r_w} l_w \left[\frac{d_g^2}{4}\sin^{-1}\frac{2\sqrt{t(d_g - t)}}{d_g} - \sqrt{t(d_g - t)}\left(\frac{d_g}{2} - t\right)\right]\sum_{i=1}^{2N}\left[1 - \frac{R_a^i}{R_a^o}\right] \quad (3.73)$$

where, $\rho_w$ is the density of workpiece material.

For a machined surface, the ratio of peak-to-valley roughness ($R_y$) and arithmetic average roughness ($R_a$) is closer to 5 for ground surfaces and is about 10 for honed surfaces [45]. This ratio is assumed to be 7 for the workpiece surface used for AFM in the present case. The value of this ratio obtained during experimentation is also very close to 7. Some representative values of $R_y$ and $R_a$ are given in Table 3.1 extracted from the Table A.3 given in Appendix A.

**Table 3.1 Representative values of $R_a$ and $R_y$ of workpieces**

| S.No. | $R_a$ | $R_y$ |
|---|---|---|
| 1 | 2.08 | 14.49 |
| 2 | 1.60 | 11.99 |
| 3 | 1.85 | 17.18 |
| 4 | 2.08 | 15.11 |
| 5 | 2.15 | 17.60 |
| 6 | 1.93 | 13.98 |
| 7 | 2.31 | 13.93 |
| 8 | 1.82 | 14.01 |
| 9 | 2.12 | 14.98 |
| 10 | 2.01 | 15.18 |

The sum of volumes of all the grooves produced during AFM process is equal to the volumetric material removed from the workpiece surface. Hence

Volume of the material removed in *i*th stroke = actual contact length × width of workpiece ×total height of material removed

$$V_t = [1- \frac{R_a^t}{R_a^o}] l_w * 2 \pi r_w * 7 (R_a^{t-1} - R_a^t) \quad (3.74)$$

Substituting value of $V_t$ from eqn. (3.71) into eqn. (3 74), and simplifying , we find,

$$R_a^t = R_a^{t-1} - \frac{D}{14 \pi r_w l_w} \quad (3\ 75)$$

Substituting value of $D$ from eqn.(3.70) into eqn.(3.75),

$$R_a^t = R_a^{t-1} - \frac{1}{7} n l_s \frac{r_c^2}{r_w^2} [\frac{d_g^2}{4} \sin^{-1} \frac{2\sqrt{t(d_g - t)}}{d_g} - \sqrt{t(d_g - t)}(\frac{d_g}{2} - t)] \quad (3.76)$$

A critical surface roughness ($R_{cr}$) may exist at the given machining conditions, such that the surface roughness will no longer improve beyond that. The critical surface roughness is equal to the depth of indentation of spherical abrasive grains in the machined surface.

$$R_{cr} = \frac{d_g}{2} - \sqrt{\frac{d_g^2}{4} - \frac{F_{ng}}{H_w \pi}} \quad (3.77)$$

It should be noted that when the value of $R_a^o$ is comparatively small, and normal pressure and grain size are large enough, the value of final surface roughness may be greater than initial surface roughness. Such experimental observations have been reported by Jha [24]. Hence, selection of the process parameters should be done with due consideration to the initial surface roughness of workpiece.

## 3.5 Results and Discussion

The simulation procedure involves the determination of stresses on the workpiece surface by finite element technique as described in section 3.2 of this chapter. The normal stress, so obtained from the flow model, is used for the estimation of material removal and surface finish as mentioned in section 3.4 of the chapter. The flow chart of the procedure followed for determination of material removal and surface roughness in AFM is shown in Fig. 3.7. The viscosity of media is determined experimentally and its value at various abrasives concentration is reported in Appendix B. The other numerical values used in the simulation are given in Appendix C.

Figure 3 8 shows a comparison of the experimental and theoretical average velocity of piston and the average extrusion pressure acting on the piston during its stroke A good agreement exists between the results from the theoretical model and the experimental results It clearly indicates that the proposed flow model provides a reasonably good estimate of the flow characteristics involved in AFM process In Figure 3 9, the extrusion pressures are plotted against the piston velocity for various angles of tooling ($\alpha$) (tooling directs the media to the areas of the workpiece to be abraded Fig 1.4). It is observed that the present FEM analysis gives a linear relationship between the extrusion pressure and the velocity of the piston. The piston pressure increases linearly with piston velocity and its value is more for higher angle of tooling. Further to achieve the same flow velocity of media, tooling angle should be low at low pressure Thus, for a given piston velocity, it requires highest pressure at 90° tooling angle which is a commonly used configuration. Hence, the tooling should be designed to achieve the desired results. Normal stress also varies linearly with piston velocity (Fig. 3.10) and its value is higher for higher value of angle of tooling. At lower radial pressure, the penetration depth expected is lower. If radial pressure is very high and the abrasive grain size is also high, then in some cases, it may lead to the final surface finish worse than the initial surface finish Hence, grain size selection and design of tooling to achieve the appropriate radial pressure is important so that the desired surface finish can be achieved

Figure 3.11 shows the variation in extrusion pressure values obtained for media subjected to various reductions. Reduction ratio expresses the reduction in cross sectional area of flow. It is seen that the piston pressure increases with increase in reduction ratio (Fig. 3.10). With higher value of reduction ratio, the rate of increase in piston pressures is also higher. Figure 3.12 shows the effect of reduction ratio on normal stresses on the workpiece surfaces for various angles of tooling. For higher value of reduction ratio, the normal stress at the workpiece surface is higher. This fact can explain the experimental observations [12] that high abrading action occurs at the cross section of high restriction and less abrading action in the region of less restriction (because abrasion is directly proportional to normal stress). The computed stresses have been used to evaluate the machining forces acting in abrasive flow machining. The machining force so evaluated from the analysis has been employed to carry out theoretical analysis of material removal

and surface roughness in AFM Thus, analysis of media flow is an important step in the direction of modeling of AFM process

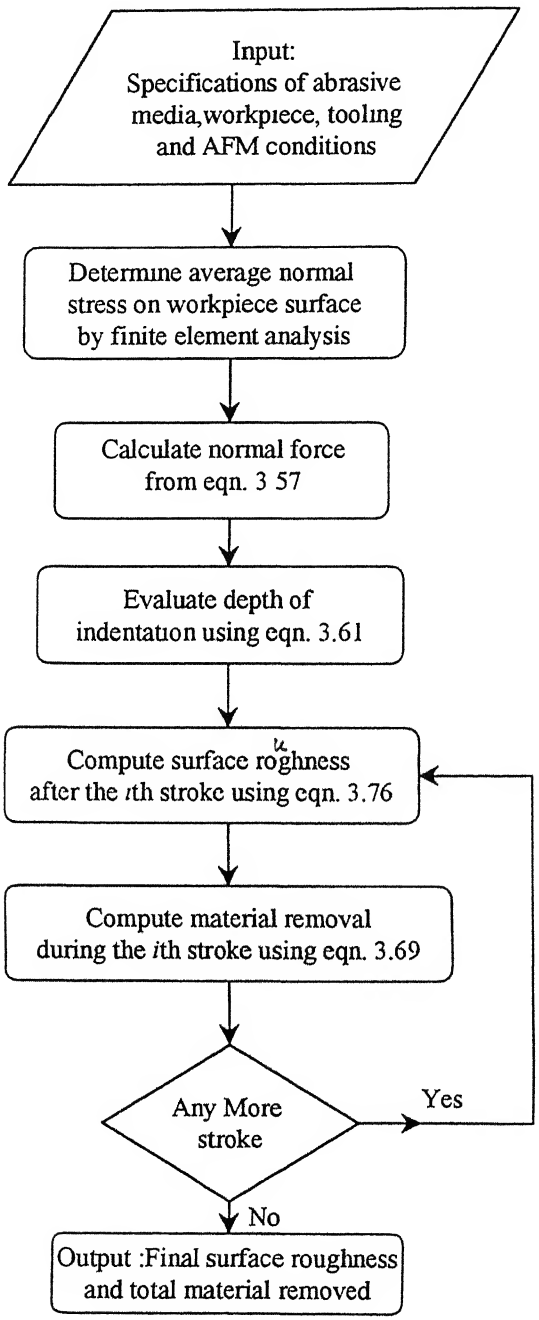


**Fig. 3.7 Flow chart for determination of material removal and surface roughness by theoretical model**

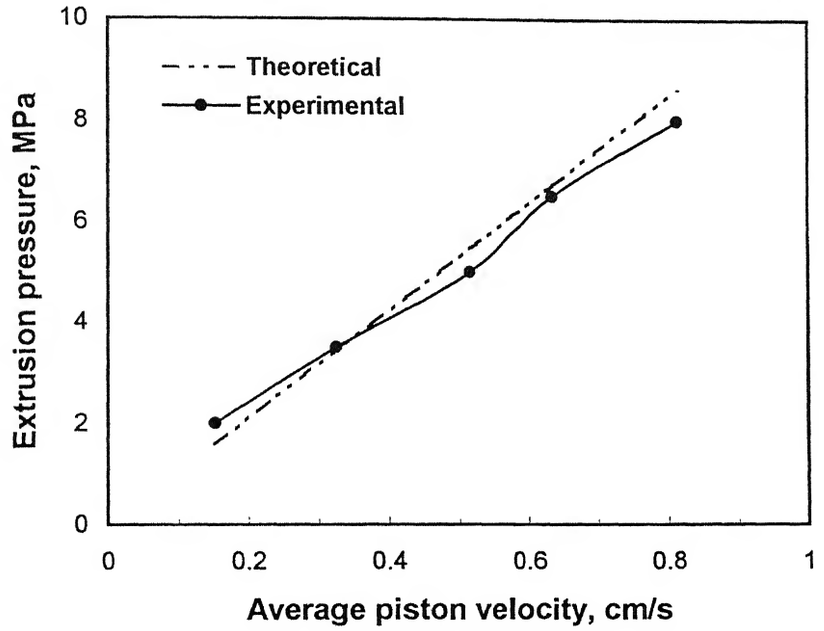


**Fig. 3.8 Variation in extrusion pressure with average piston velocity ($\alpha$=30$^0$, $C$=66%, $R_e$ = 90.50%)**

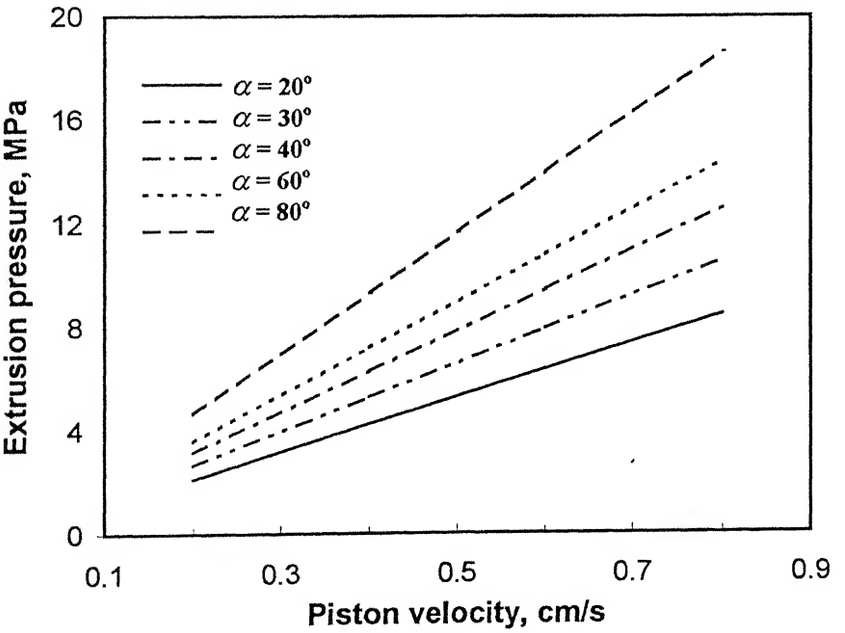


**Fig. 3.9 Variation in extrusion pressure with piston velocity for various tooling angles ($\alpha$)**

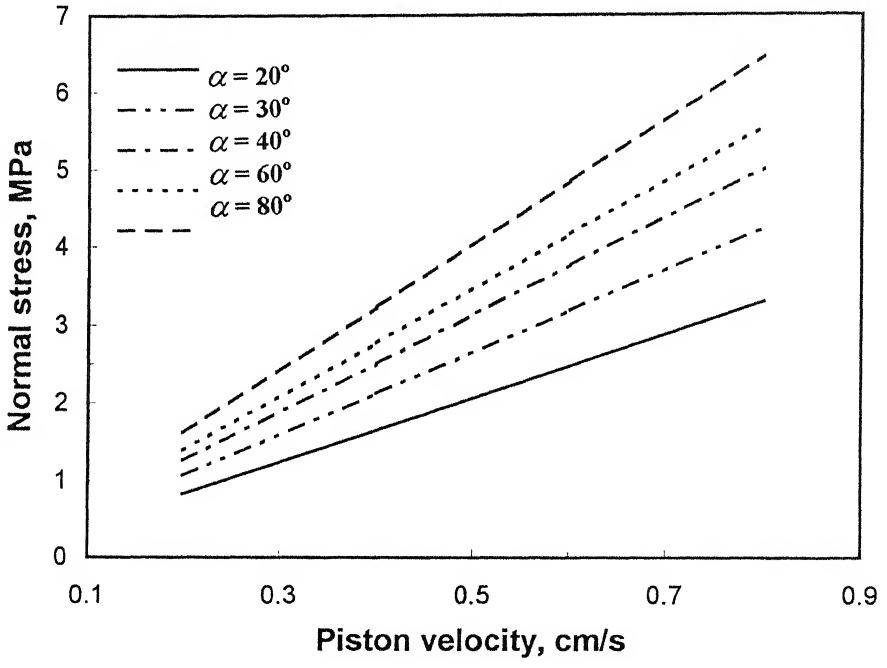


**Fig. 3.10 Variation in normal stress on workpiece surface with piston velocity for various tooling angles ($\alpha$)**

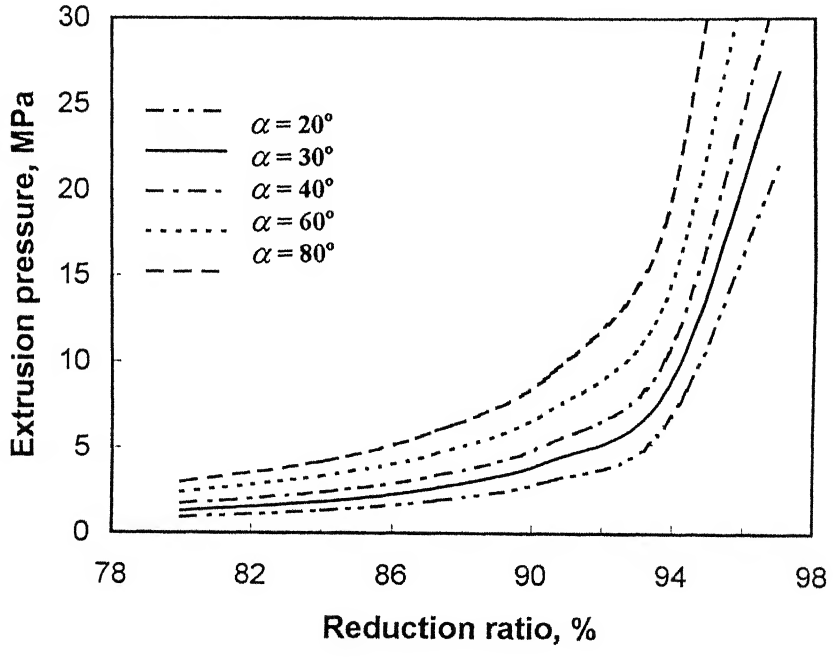


**Fig. 3.11 Variation in extrusion pressure with reduction ratio for various tooling angles ($\alpha$)**

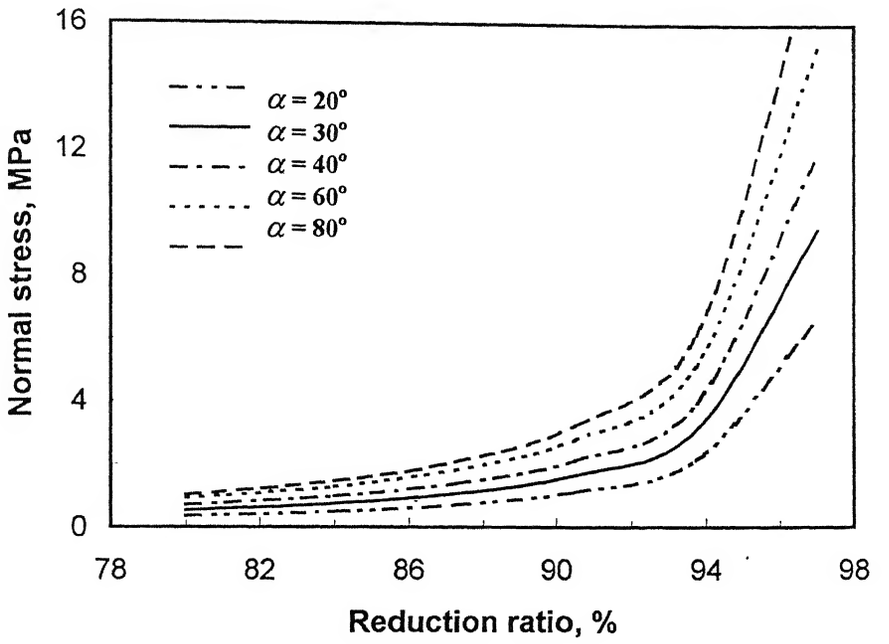


**Fig. 3.12 Variation of normal stress with reduction ratio for various tooling angles ($\alpha$)**

### 3.5.1 Material removal

The values of number of active abrasive grains per unit area of contact under static conditions at various concentrations and mesh sizes have been reported in chapter 4. The same values have been used in the present computations of material removal and surface roughness. An estimate of the depth of indentation of abrasive in the workpiece material reveals that its value decreases with increase in the hardness of workpiece material (Fig. 3.13) and mesh size of grains (Fig. 3.14). Figure 3.15 compares the response surface analysis (RSA) and theoretical results between the extrusion pressure and material removal. It is found that material removal increases with increase in extrusion pressure. The simulation results for material removal agree well with the RSA results at low extrusion pressures. But at higher extrusion pressures, number of abrasive grains taking part in actual cutting may be less due to rolling action of grains at higher velocity.

Hence, RSA material removal is less than theoretical (Fig. 3.15). Due to higher pressure, penetration depth increases. Now, if the viscosity of media is not high enough to keep the grain intact with the media, due to larger tangential force it may rotate and reenter inside the media resulting in lower depth of indentation. Another possibility is that increased force may not result in increased depth of indentation. Because of low viscosity of media, it may not be able to withstand the acting high force, and ultimately the grain may penetrate inside the media resulting in the reduced depth of indentation in the workpiece material. Hence, lower material removal is achieved compared to the theoretical value. This phenomenon of rolling and/or reentry inside the media has not been accounted in the theoretical analysis. Hence, the increasing difference between theoretical and RSA results at higher extrusion pressure is seen in Fig. 3.15 Material removal also increases with increase in reduction ratio (Fig. 3.16). It is due to increase in depth of indentation at higher reduction ratio. At higher reduction ratio, the normal stress acting on the workpiece surface is higher (Fig. 3.12), leading to higher material removal.

Figure 3.17 shows the effect of percentage concentration of abrasives by weight on material removal. As the percentage concentration of abrasives in media increases, the material removal increases because higher concentration results in higher viscosity of media (Fig. B.3 in Appendix B). Hence, abrasive grains (or media) can sustain higher normal and tangential forces. As a result, higher depth of indentation (or higher material removal) can be achieved. With higher percentage concentration of abrasives, more number of abrasive grains come in contact with the surface to be machined (Fig. 4.7 in chapter 4). All these factors lead to an increase in material removal. However, the difference between RSA results and theoretical ones increases with increase in the percentage concentration of abrasives. It can be explained on the basis of comparatively low viscosity of the carrier and non-linear relationship between percentage concentration of abrasives and number of active grains (as discussed in chapter 4). Material removal also increases with number of cycles (Fig. 3.18). However, in this case also, the deviation between the two curves increases with the increase in number of cycles.

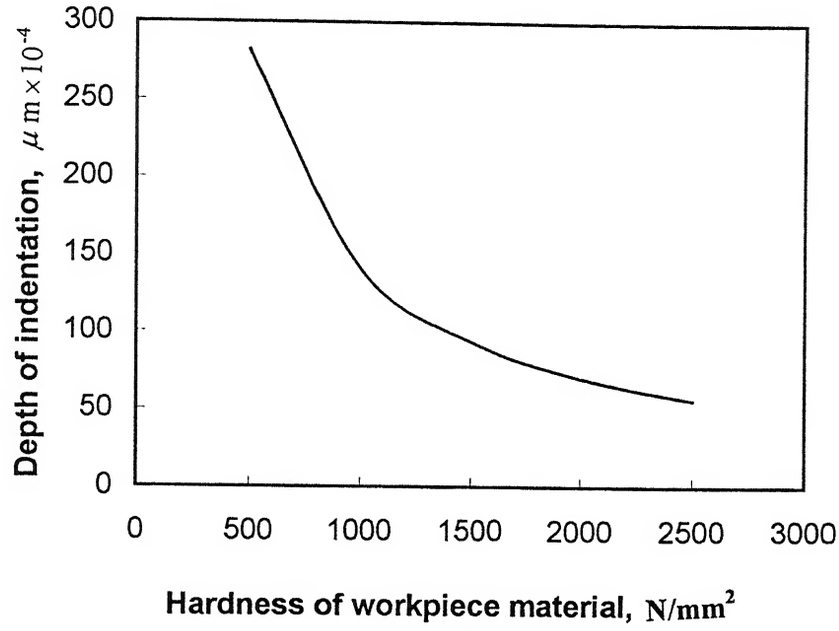


**Fig. 3.13 Effect of hardness of workpiece material on depth of indentation ($p_e$ = 50 bar, $M$ = 55)**

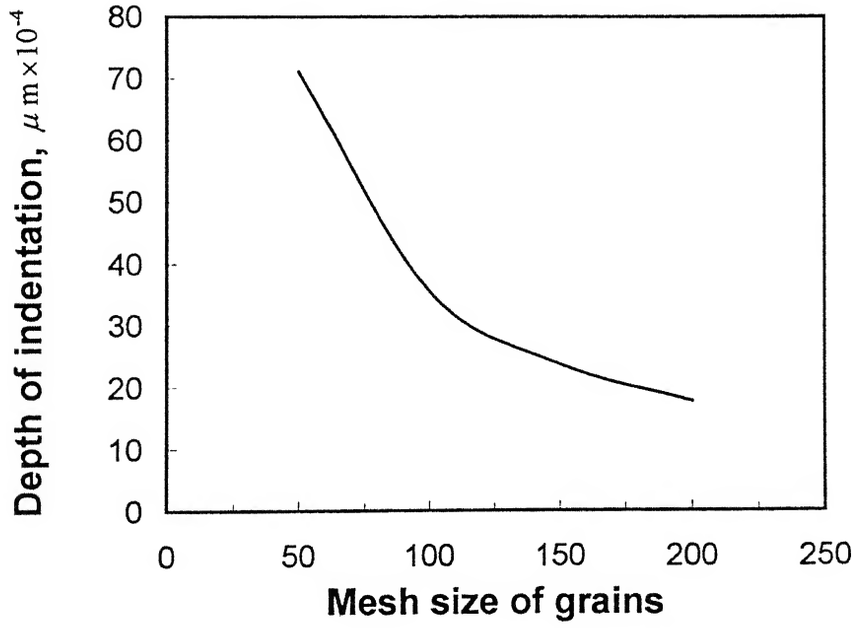


**Fig. 3.14 Effect of average mesh size of grains on depth of indentation ($p_e$ = 50 bar, $H_w$ = 2177.80 N/mm$^2$)**

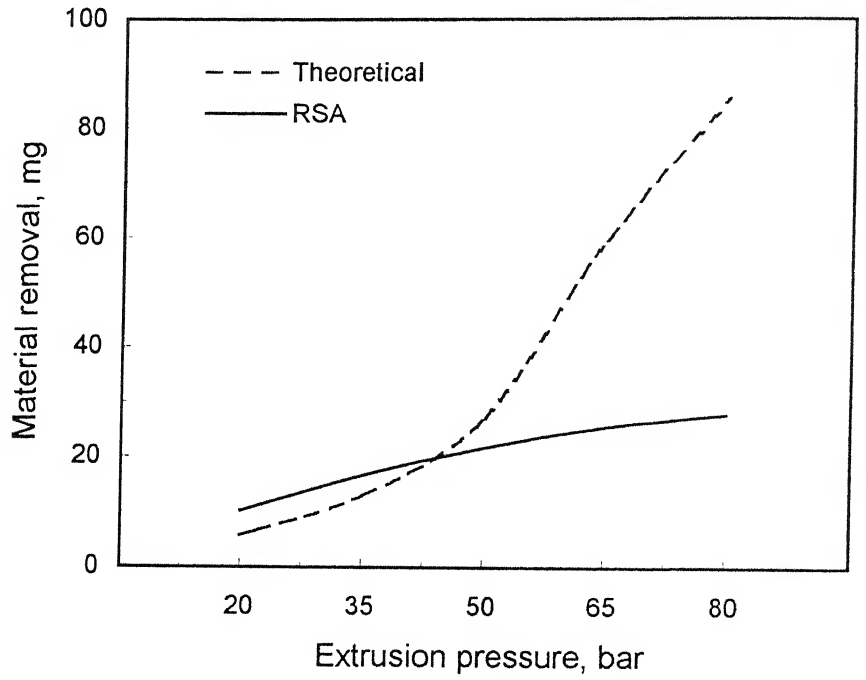


**Fig. 3.15 Variation of material removal with extrusion pressure ($R_e$ = 0.805, $N$ = 15, $C$ = 66 %)**

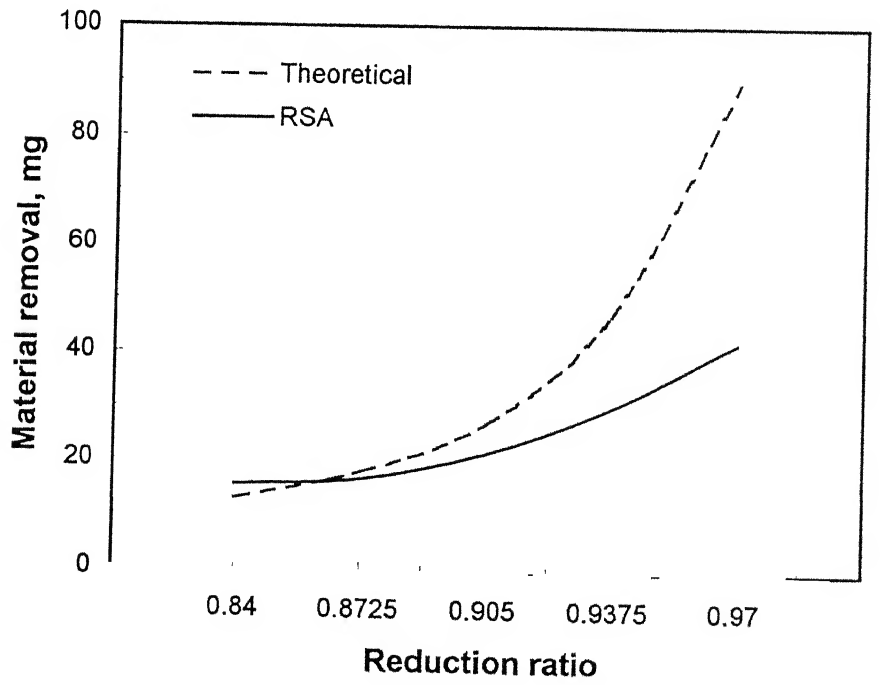


**Fig. 3.16 Variation of material removal with reduction ratio ($p_e$ = 50 bar, $N$ = 15, $C$ = 66 %)**

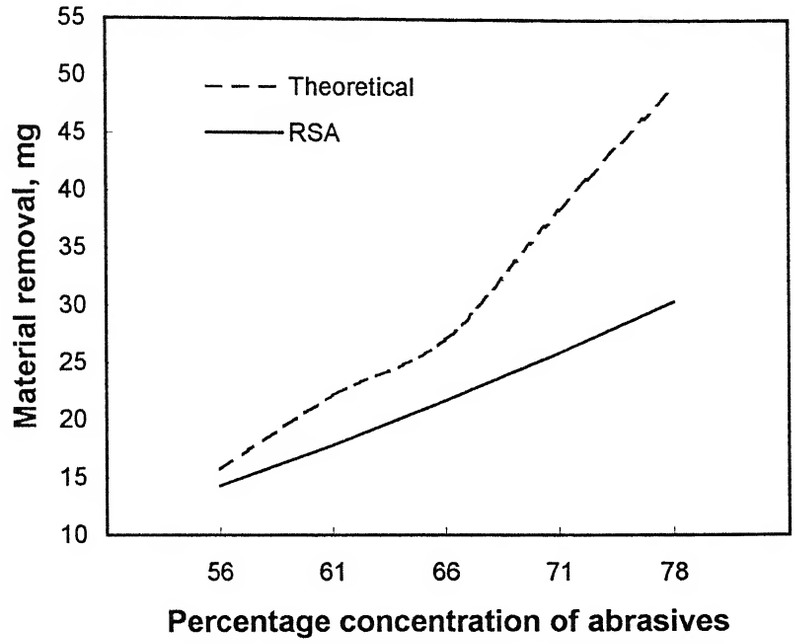


**3.17 Variation of material removal with percentage concentration of abrasives**
**($p_e$ = 50 bar, $R_e$ = 0.905 $N$ = 15)**

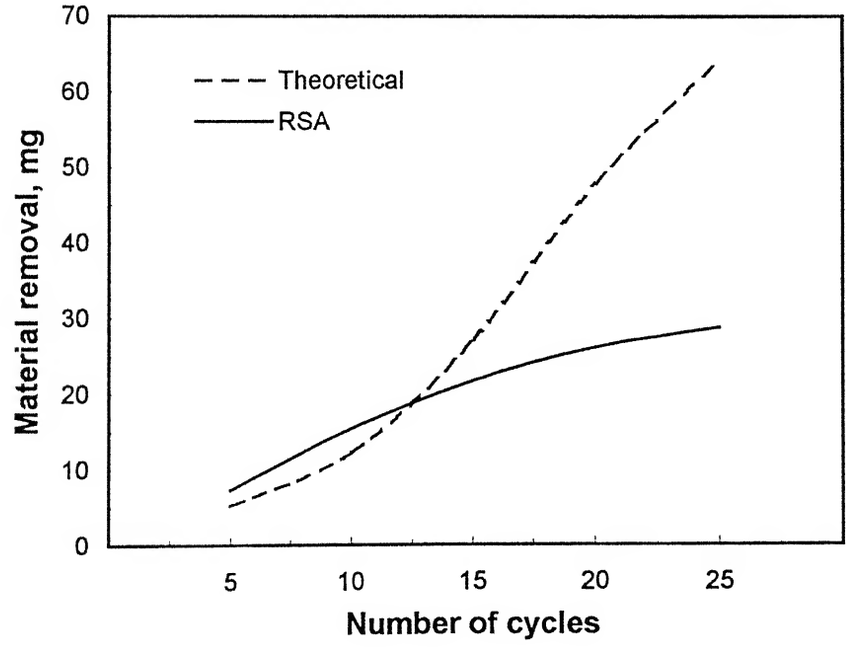


**Fig. 3.18 Variation of material removal with number of cycles**
**($p_e$ = 50 bar, $R_e$ = 0.905, $C$ = 66 %)**

### 3.5.2 Surface roughness

Figure 3 19 exhibits the role of extrusion pressure on surface roughness value obtained after the specified number of machining cycles. It is observed that change in surface roughness value ($\Delta R_a = R_a^o - R_a^i$) increases with increase in extrusion pressure In response surface analysis (RSA) results, increase in change in surface roughness at higher pressure is less than theoretical value. It may be due to rolling action of grains at high pressure Change in surface roughness increases with increase in percentage concentration of abrasives (Fig 3.20) With higher percentage concentration of abrasives, the number of abrasives taking part in machining will be more, and hence surface roughness obtained for a specified number of cycles will be better. Change in surface roughness also increases with reduction ratio (Fig 3 21) and number of cycles (Fig 3.22), due to increase in length of slug of media passed across the workpiece surface. It has been found theoretically that for workpiece of low hardness material, the surface roughness value decreases upto a certain value of extrusion pressure for specified number of cycles (Fig. 3.23). Beyond this value of extrusion pressure, the surface value can not be further improved. If the pressure is large enough, then it may lead the surface roughness worse than the initial one due to increase in depth of indentation

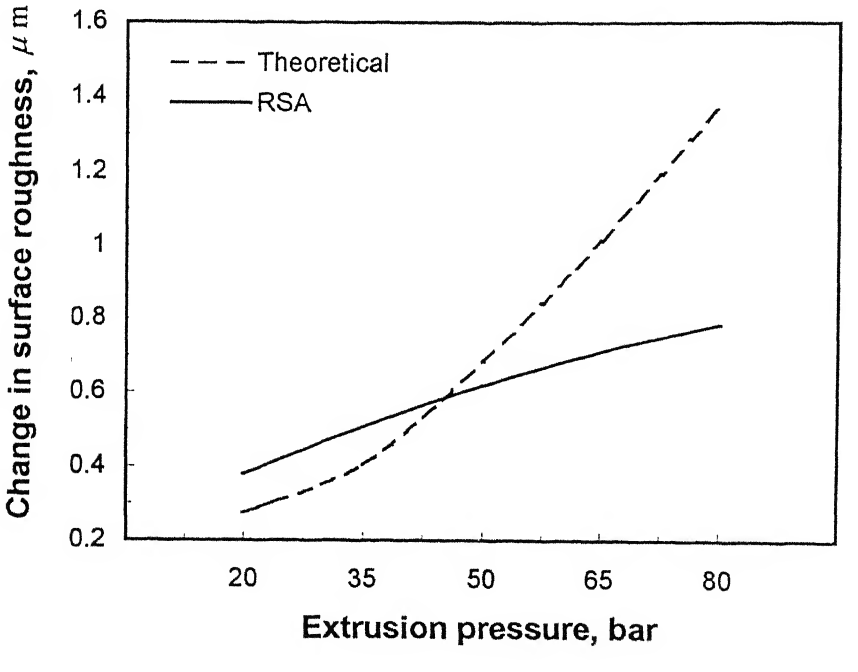


**Fig. 3.19 Variation of change in surface roughness with extrusion pressure ($R_e$ = 0.805, $N$ = 15, $C$ = 66 %)**

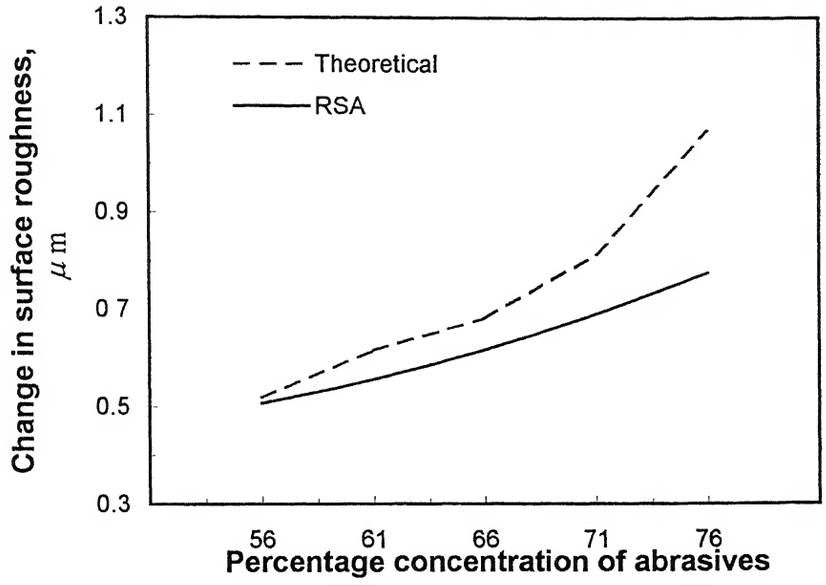


**Fig. 3.20 Variation of change in surface roughness with percentage concentration of abrasives ($p_e$ = 50 bar, $R_e$ = 0.905 $N$ = 15)**

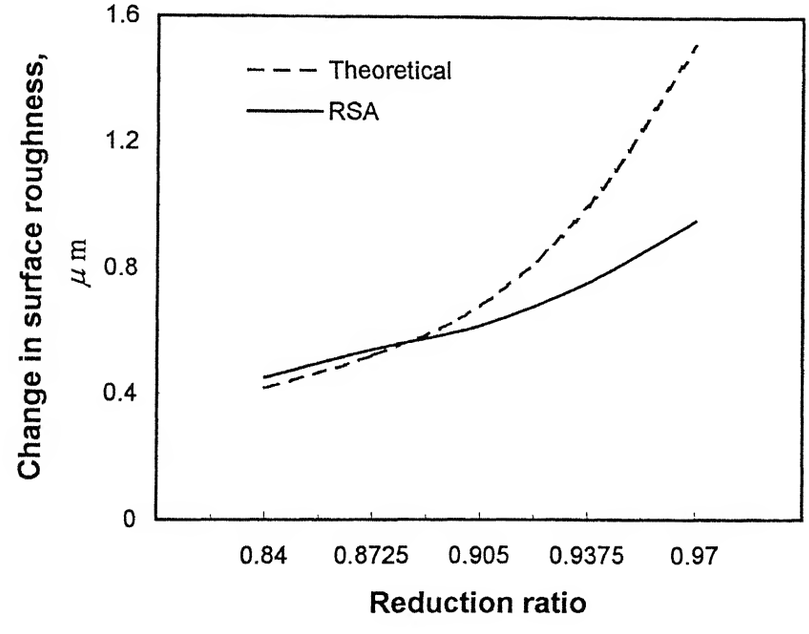


**Fig. 3.21 Variation of change in surface roughness with reduction ratio ($p_e$ = 50 bar, $N$ = 15, $C$ = 66 %)**

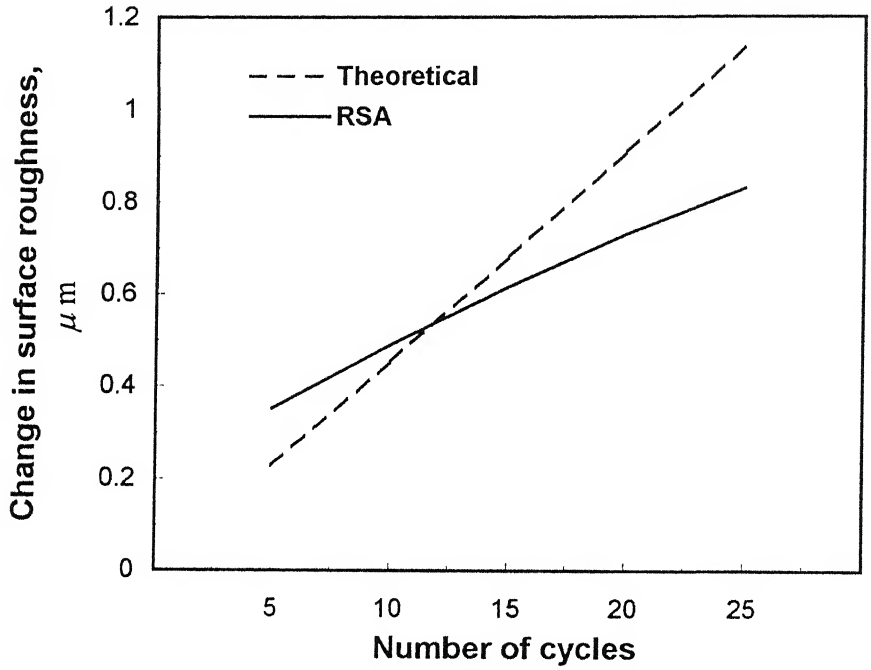


**Fig. 3.22 Variation of change in surface roughness with number of cycles**
**[$p_e$ = 50 bar, $R_e$ = 0.905, $C$ = 66 %]**

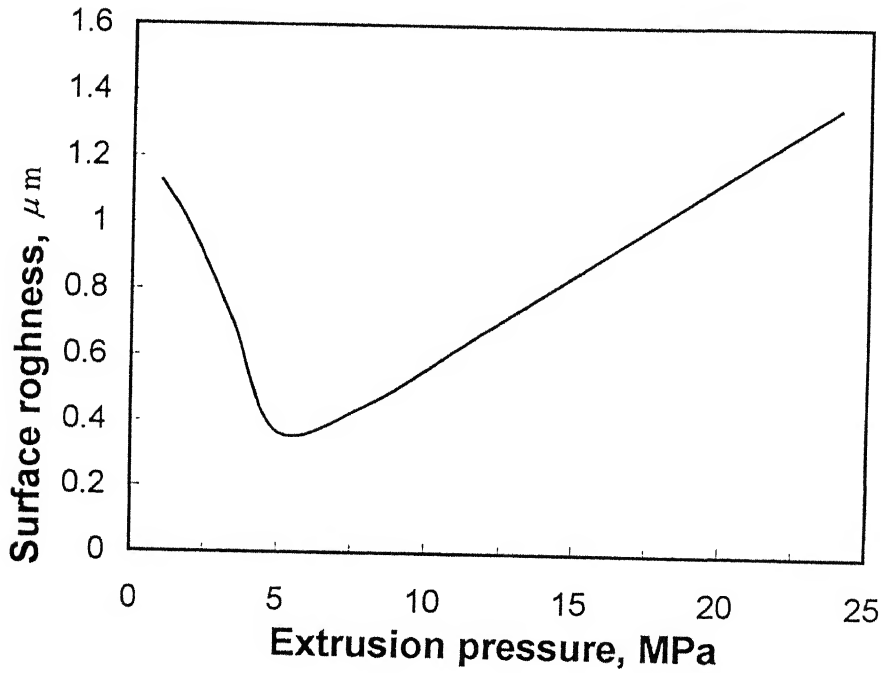


**Fig. 3.23 Variation of surface roughness value with extrusion pressure**
**($H_w$ = 500 N/mm$^2$, $N$ = 10, $R_e$ = 0.905, $C$ = 66 %, $M$ = 50 – 60)**

## 3.6 Conclusions

In the present chapter, a model for the flow of AFM media through cylindrical workpiece has been developed and solved by finite element method It predicts the normal stresses at the workpiece surface A model for estimation of the material removal and change in surface roughness has also been presented The analysis includes the operating conditions of the process, viz abrasive size, number of contacting abrasive particles, extrusion pressure, workpiece material hardness, and size of workpiece to be machined Good agreement is found between the RSA results (which are derived from experimetal data) and theoretical predictions. The following conclusions have been derived from the present analysis

1. A good agreement exists between the theoretical and experimental results for extrusion pressure and average piston velocity It clearly indicates that the proposed flow model provides a reasonably good estimate of the flow characteristics involved in AFM process
2 The piston velocity increases linearly with extrusion pressure and its value is higher for larger angle of tooling.
3 At higher value of reduction ratio, the rate of increase in extrusion pressure is higher The normal stresses on the workpiece surface increase with increase in reduction ratio
4 Material removal increases with extrusion pressure and percentage concentration of abrasives in media.
5. Change in surface roughness value increases with increase in extrusion pressure, percentage concentration of abrasives and reduction ratio for a specified number of cycles
6. Beyond a certain value of extrusion pressure, surface roughness deteriorates due to increase in depth of indentation. The minimum surface roughness value is equal to the critical surface roughness.

# Chapter 4

# Simulation of Surface Generation in AFM

## 4.1 Introduction

The theoretical model discussed in the previous chapter has been derived, assuming constant depth of indentation of every grain and uniform surface profile without statistical distribution. Stochastic simulation methodology has been discussed in this chapter to generate surface profile which is more close to actual AFM results. The process of finishing in AFM is random removal of material by individual abrasive grains in the form of microscopic chips. The shape of removed material is determined by the kinematics and the shape of abrasive grains. It is easier to calculate the shape of cut groove from the relative motion between the workpiece material and single grain under consideration. However, it is difficult to estimate the roughness of the machined surface. This difficulty is due to the complicated and random distribution of grains in the media. Abrasive flow machining is viewed as a stochastic process whose events are generated by the interactions between the abrasive grains and workpiece. By simulating these individual events, it is possible to predict the characteristics of surface likely to be generated in AFM. Simulation techniques can help in understanding the mechanics of AFM process by predicting the effects of various parameters on the responses and comparing them with RSA results.

Not much information is available in the literature which deals with the simulation of surface generation and material removal in AFM process. In case of grinding, there have been many attempts in the past to model the surface generated using statistical approach [46]. Yoshikawa and Sata [47] simulated the grinding process by the Monte Carlo method. Random numbers were used to give the coordinates of the position of a grain on the grinding wheel. By this method, the distribution of the grains spacing and of the undeformed chip geometry, together with the generated surface profile are obtainable from the structure of the grinding wheel which has random character. The assumption of the grains existing independent of each other on the wheel surface is the major drawback of this

model. A grinding model is postulated by Law and Wu [48], in terms of grain distribution on the abrasive wheel and kinematic grinding conditions. Transverse workpiece profiles have been conjectured as sample realizations of the stochastic grinding process. Hamed et al. [49] applied an approach to generate random surfaces by computer simulation which involves the use of a series of 'unit events' to produce a surface profile. The work confirmed that the random engineering surfaces can be described statistically by a profile having ordinate heights with a Gaussian distribution together with a form of exponential autocorrelation function Bhateja [50] evolved a hypothesis that the ground surface texture is complementary to the envelope of a large number of active transverse wheel profiles that traverse the grinding zone. Based on this approach, the relationship between the roughness of the wheel and the workpiece could be established. Classical two body abrasion theories have been applied in a statistical simulation model by Staffan et al. [51]. A unique feature of the model is that the abrasive simulation is performed on a surface of realistic topography, developed during the simulation process. Koshy et al [46] presented a stochastic simulation of the diamond grinding wheel which entails a random sampling technique. The indices that characterize the topography of a diamond wheel viz. the static grain count, the protrusion height distribution, the distribution of inter grains spacing, and the projected area due to exposed abrasives are estimated by this model.

The approaches discussed above, to model surface generation can be applied to AFM process with certain modifications depending upon the AFM conditions. As the distribution of grain cutting edges in the media are random and grains which contribute to generate a measurable profile on the workpiece are numerous, it is very difficult to describe the necessary configuration of media surface in a deterministic way. On the other hand, it is possible to obtain a complete profile of workpiece surface generated by motion of the grains, by simulation. The surface generated in AFM is the cumulative outcome of numerous abrasive-workpiece interaction events. By simulating these individual events, it is hence possible to predict the characteristics of machined surface. Implementation of the same, requires information on the topography of the AFM media and the kinematics of the AFM process.

The present chapter describes the concepts of a proposed versatile simulation model, which generates and statistically evaluates the interaction between spherical abrasive

grains and a workpiece surface The simulation enables prediction of the roughness of the machined surface and material removal with reference to the abrasive grit size and percentage concentration, in addition to obtaining the statistical characteristics of machined surface. Active grain density has also been estimated from the present stochastic simulation.

## 4.2 Simulation of Surface Generation

The method applied here to explore the nature of the generated profile is simulation by employing mechanics of AFM process. The model used for material removal in AFM process is restricted to pure microcutting without material displacement. All considerations are geometrical in nature. During AFM process, media is passed across the workpiece surface. AFM is considered to be a scratching action performed by abrasive grains in the media. The force applied to the media will cause an active grain to indent in the workpiece surface. The grain produces a groove on the workpiece surface and the groove section corresponds to the profile of the grain. As the grain is translated horizontally, it removes material from the workpiece surface.

The simulation of surface generation in AFM is carried out based upon the following assumptions:

1. The path traced by an individual grain is straight line.
2. The material is removed in the form of chips without side pile up, whenever grain workpiece interference occurs.
3. Abrasive grain is approximated by a sphere. This is also reasonable considering the large negative rake angles presented by the grains [41]. Observation of abrasive particles also shows that they are generally rounded in shape, and are not composed of acute cutting edges [52].
4. During the manufacturing of particles, a large number of chance factors are at work. This leads to the emergence of a normal distribution of particle size, which has been observed to hold for narrow range [46]. Hence, the distribution of abrasives' radii is assumed to be normal, and symmetric about the mean grain radius.

Since each nominal grit size includes a range of abrasive particle size (Fig. 4.1), two grit numbers $M_a$ and $M_b$ are used to denote the abrasive mesh size. $M_a$ refers to the sieve that would let the abrasive grains pass through and $M_b$ refers to the sieve that would detain most of them The grit radius $r_g$ is related to the sieve number [3] as

$$r_g \text{ (mm)} = 7\ 62\ \ M^{-1} \tag{4.1}$$

As the distribution of abrasives radii is assumed to be normal and symmetric about its mean, the mean grain radius $r_{gm}$ is given as follows.

$$r_{gm} = \frac{r_{ga} + r_{gb}}{2} = 3\ 81\ \frac{(M_a + M_b)}{M_a M_b} \tag{4 2}$$

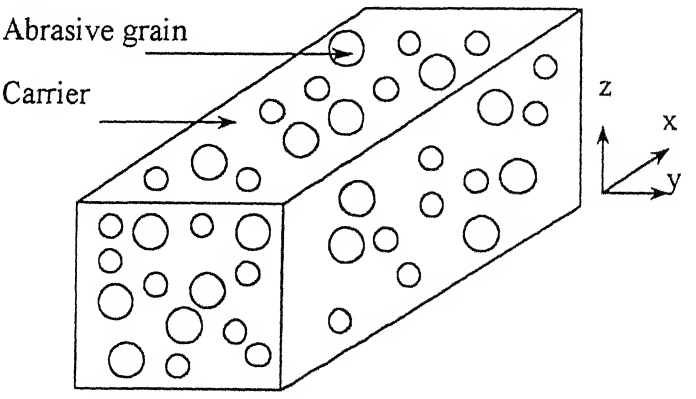


**Fig. 4.1 Schematic representation of distribution of grains in abrasive media**

Since, the range of normally distributed random variables, in general, is six times the standard deviation, the standard deviation of the grain radius $S_r$ is evaluated as

$$S_r = 1.27\ \frac{(M_a - M_b)}{M_a M_b} \tag{4.3}$$

For AFM media having $C$% concentration of abrasives by weight, the total volume of abrasive grains ($V_a$) in the $V_m$ volume of media is given by

$$V_a = \frac{C\rho_m V_m}{100\rho_a} \tag{4 4}$$

where density of media $\rho_m$ in terms of abrasive density $\rho_a$ and carrier density $\rho_c$ is given by the relation,

$$\rho_m = \frac{100\rho_a\rho_c}{[C\rho_c + (100 - C)\rho_a]} \tag{4 5}$$

Length of media $l_m$ passed through workpiece in one stroke (i e. slug length),

$$l_m = \frac{r_c^2 l_s}{r_w^2} = \frac{l_s}{(1 - R_e)} \tag{4.6}$$

where $R_e$ is the reduction ratio given by, $R_e = 1 - \left(\frac{r_w^2}{r_c^2}\right)$. $r_c$ and $r_w$ are the radii of media cylinder and workpiece respectively. Reduction ratio expresses the reduction in cross sectional area of flow

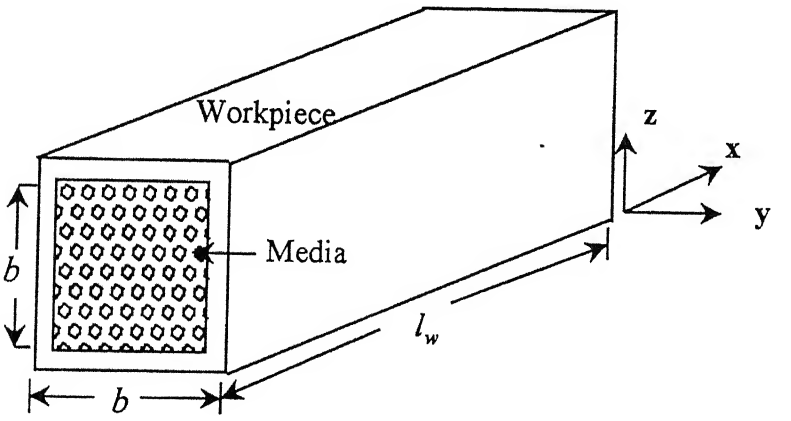


**Fig. 4.2 (a) Schematic representation of simulated AFM media**

To simplify the analysis, total periphery of circular cross section of the workpiece is converted to equivalent periphery of square cross section (Fig. 4.2 (a)); keeping total length of media passed through the workpiece as constant.

Side of square cross section, $w = \frac{\pi r_w}{2}$ (4.7)

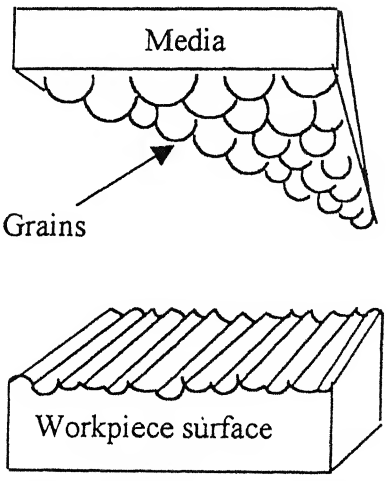


**Fig. 4.2 (b) Cross sectional representation of workpiece surface and media**

Let a square cross section of side $w$ and length $l_m$ (Fig.4 2) of the AFM media is considered for simulation. Then, volume of abrasive grain in the volume of abrasive media ($V_m = w^2\ l_m$) passed in one stroke across workpiece surface is related as

$$V_a = \frac{C\, w^2 l_m \rho_m}{100 \rho_a} \qquad (4.8\ a)$$

$$V_a = \frac{C\, w^2\, l_m \rho_c}{C\rho_c + (100 - C)\rho_a} \qquad (4.8\ b)$$

Only one side out of the four sides of a square cross section has been considered for simulation It is assumed that there is same surface pattern and amount of material removal obtained for the remaining three sides of workpiece. This saved the computational time with a small difference in the results obtained. During computation, it is found that total number of grains in the media passed in one stroke across the workpiece surfaces are of the order of $10^{10}$ for the conditions taken in the AFM simulation. It creates computational and memory problems. Hence, a thickness of 5 mm of abrasive media has been considered to be flowing over workpiece surface, keeping the length and width of flowing media constant. This reduction in simulated thickness of media does not affect the number of grains interacting with surface profile and distribution of grains in the media near the workpiece surface. On the other hand, this modification reduced the computational time and memory requirements drastically

The first step in the simulation is to generate '$N_a$' normally distributed random numbers with mean radius $r_{gm}$ and standard deviation $S_r$ which correspond to the grain radius $r_g$ such that

$$\frac{4}{3}\pi \sum_{i=1}^{Na} r_{gi}^3 \approx V_a \qquad (4\,9)$$

where $r_{gi}$ is the radius of the $i$th grain and $N_a$ is the total number of grains in the simulated volume

For a spherical grain of diameter $d_g$, the maximum depth of indentation $t$ of a grain in workpiece material has been derived in chapter 3 and can be given by eqn (4.10).

$$t = \frac{d_g}{2} - \frac{d_g}{2}\sqrt{1 - \frac{\sigma_n}{H_w}} \qquad (4.10)$$

where $\sigma_n$ is the normal stress acting on the grain and $H_w$ is the hardness of workpiece material.

The distribution of grains in the media is represented by giving their coordinates (x, y, z), the components of which give the position of a grain in axial, transverse and perpendicular to surface directions. Grains are randomly positioned in the AFM media so that x, y, and z generally have a uniform distribution. Thus, the position of the grains with respect to the surface is decided by a random number generator. A subroutine from NAG software is used for the generation of random numbers.

Now, a set of these uniformly distributed random numbers $N_a$ ($x_i$ , $y_i$ , $z_i$ ), is generated to represent the x,y,z coordinates of the center of each of $N_a$ grains.

Only grains which do not overlap are considered. For this purpose, the grains are assumed to occupy a region of influence equivalent to nominal grain diameter. Generation of the coordinates of the $i$th grain is therefore subject to the condition, that distance between two adjacent grains is equal to or more than the sum of their radii.

$$[\,(x_i - x_j)^2 + (y_i - y_j)^2 + (z_i - z_j)^2\,]^{1/2} \geq (r_{gi} + r_{gj}) \;;\quad j = 1 \text{ to } i-1 \qquad (4.11)$$

The profile of the workpiece surface can be displayed in the form of a two dimensional cross-section perpendicular to the grooving direction. In the manufacturing processes involving the random removal of material, the roughness is effectively produced

by many independent particles' hits Hence, the amplitude distribution of the roughness waveform could be justifiably expected to be Gaussian no matter how much of the individual hits have affected the surface profile [48]. The original profile of the workpiece is taken to be Gaussian, represented in digital form and coordinates (x',z') of the profile are stored in the computer at 0 1 $\mu$m spatial resolution.

The centers of the abrasive grains $(x_i, z_i)$ are defined with respect to the coordinate system fixed to the workpiece. Active grains are only those grains, which actually take part in the material removal In Fig 4.3, grain G1 is interacting with workpiece profile, hence it is an active grain Whereas, grain G2 is passing over the workpiece surface profile without removing any material It is considered as an inactive grain. During the simulation process, if the active grain interacts with the workpiece profile at the appropriate location, then a hit is recorded. The grain indenting the workpiece surface would have the z coordinates of its surface below the corresponding z coordinates of surface profile of the workpiece. These grains can be identified by segregating grains which satisfy the following condition.

$$z' - (z_i - r_{gi}) \geq 0.0 \qquad (4.12)$$

The machining process is simulated by comparing the coordinates of a grain with the corresponding surface points on the workpiece. The coordinates of the cutting surface of a grain are generated by solving the equation of a circle for discrete values of x. An active grain such as G1 of radius $r_i$ (Fig.4.3) would modify the work profile only within the interval $(x_i - r_i)$ to $(x_i + r_i)$. It is assumed that the cross-sectional shape of the groove formed by the sliding abrasives on the workpiece surface is truncated circular profile. In other words, material removal is by ideal ductile microcutting with no pile-up of material on the sides of the groove.

Material removal in AFM process is simulated by successive abrasive grain grooving in the workpiece. The height of the profile at the location is then modified to correspond to this interaction. The modification of the profile of the work surface as each active grain slides past the work surface is modeled by transforming the coordinates of the profile of individual active abrasive grain to the workpiece, based on geometrical considerations alone. When a grain passes across the material, the computer calculates the

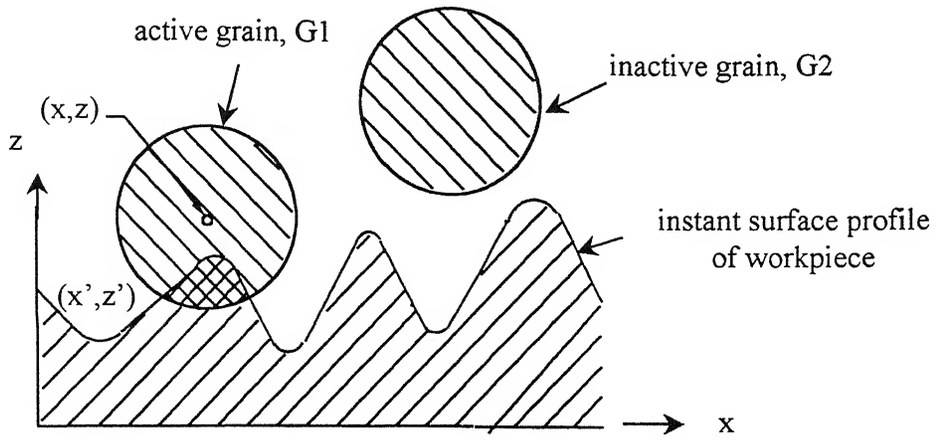


**Fig. 4.3 Schematic diagram of interaction of an abrasive grain with workpiece surface**

successive new heights of surface profile from the reference surface, thus generating new surface profiles. After each grooving event the groove width and volume of material removed are calculated and stored. After completion of simulation of abrasion by each abrasive grain, the resulting surface profile is calculated. Thus, a simulated sample profile of the machined surface, and volume of material removed after each stroke are obtained. The whole process of simulation from generation of random numbers to modification of workpiece surface profile is continued until the required number of cycles of AFM process is completed. The flow chart of AFM simulation is shown in Fig. 4 4

For studying the characteristics of the machined surface, a projected profile length of 12 mm was considered at a resolution of 1 $\mu$m. For sampling length, the mean line was computed such as the area of the solids above the line is equal to the area of the voids below it The roughness parameter $R_a$ is the average height from a mean line of all ordinates of the surface, and is calculated as follows:

$$R_a = \frac{1}{L} \int_0^L |z(x)| dx \qquad (4.13)$$

where z(x) is the height of the profile from the mean line and $L$ is the sampling length used to compute the average roughness of the profile. Since the initial surface roughness of all the workpieces was not exactly same, the change in surface roughness of the machined surface has been plotted for comparison purposes.

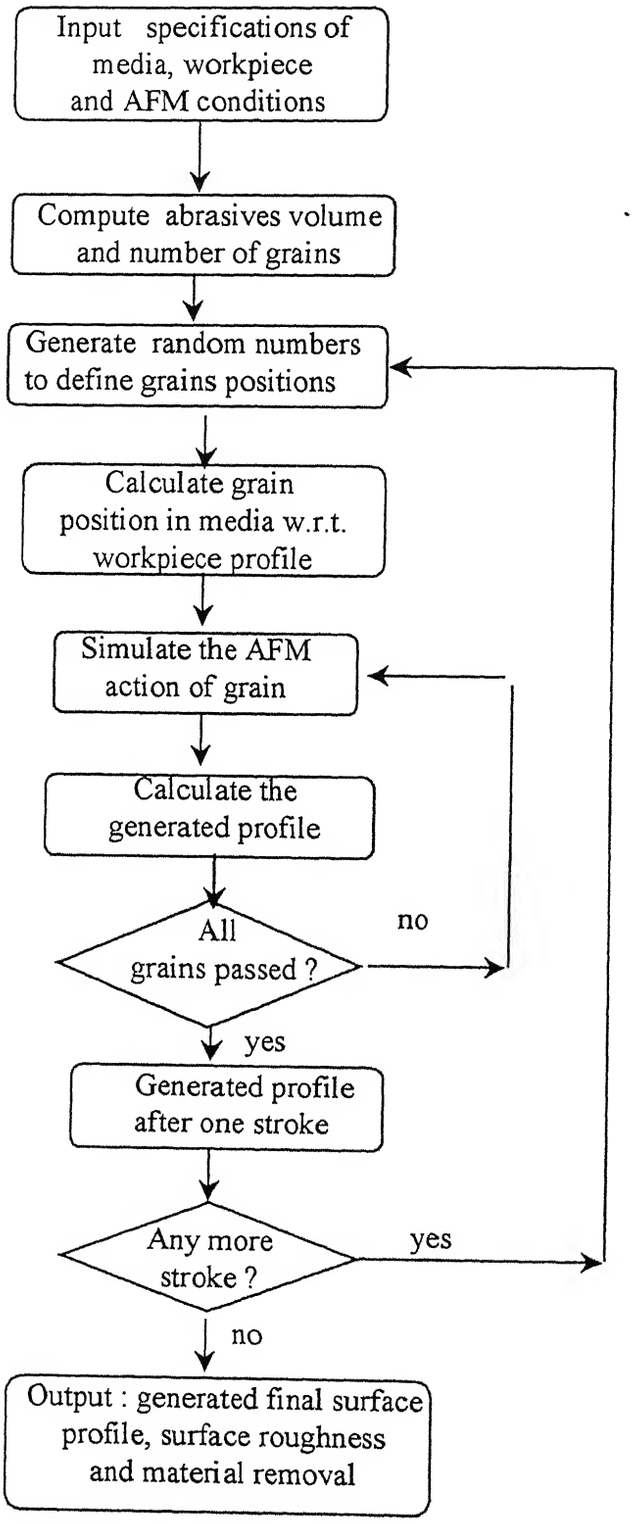


**Fig. 4.4 Flow chart of AFM simulation**

## 4.3 Active Grain Density in AFM Media

The spatial distribution of abrasive grains over the media surface in contact with the workpiece and their morphology comprise the AFM media topography The AFM media topography is characterized microscopically by nominal grain size, the static grain density and a three dimensional distribution of grain positions.

The cutting edges in media are geometrically undefined in location and shape As a result, estimations are difficult to make with any degree of accuracy It has, therefore, been necessary to develop techniques for examining details of the media topography in order to ascertain quantitative measurements of cutting edges.

A method has been proposed by Rajurkar [17] to estimate the number of abrasive grains by using the frequency associated with the primary root from the data dependent system (DDS) models of the AFM generated surface profiles. The range of values of number of dynamic active grains (for 70 mesh size with 66 % concentration of abrasives in medium viscosity media) over a unit area of extrusion passage ($in^2$) was found to be in the range of 98 to 312 Values of active grains in media at other concentrations and mesh sizes have not been reported. No systematic effort has been made to estimate the topography of media and simulate the generated profile theoretically.

But characterization of the topography of conventional grinding wheels has introduced considerable interest among researchers in the past Reference [46] presented a survey of models available for the topography of conventional grinding wheel. Nakayama and Shaw [53] proposed the distribution of effective grain density versus the radial distance from the outermost grains by a dynamic method. In these studies, the roughness equations derived or grain distribution employed contain parameters which are difficult to determine by experiments.

The objective of this section is to present a method, utilizing microscope techniques for quantitatively characterizing the topography of AFM media. The stochastic simulation method described in the previous section is also used to evaluate the active grain density.

Scanning electron microscope (SEM) has been tried for the analysis of topography of media. It is observed that the shape of a sample surface of polyborosiloxane media keeps

changing under vacuum which is applied in SEM It is due to the flexible and semisolid nature of polyborosiloxane media Hence, it is not possible to analyze correctly the topography of media by SEM. As a solution to this, optical microscope is used for determining the active grain density of media

### 4.3.1 Active grain density measurement by optical microscope

The undefined cutting area and the extremely small dimensions of the abrasive grains under observation present barriers in the assessment of the cutting surface of media. It is therefore suggested to use a microscope for the analysis of the cutting surface of the media

During AFM only a small number of grains come in contact with the work material. Whether a grain will be active or not, depends on the kinematics and geometric properties of the process. Hence, active grains are those which are supposed to take part in material removal process or those particles contacting the workpiece surface during machining. The static grain count is the number of all protruding grains on the media surface per unit area.

Microscopic method involves the use of an optical microscope or scanning electron microscope to observe and measure topographic features of the media surface. When viewing normal to the media surface, flattened areas on the grain tips reflect light and appear shiny against a dark background [3]. Such areas are often referred to as wear flats since during movement of media across the surface to be machined, wear of grains by rubbing takes place.

The media with different grit sizes and concentration of abrasives have been employed to determine the number of cutting edges on the media surface. The media leaving the workpiece surface after machining is taken out of the AFM set-up without disturbing the cross sectional shape and position of grains, and then the value of grain density is measured by means of an optical microscope sighting on the distinct grains. Since the microscopic measurements are made on media surface after machining, the concentration of the cutting points (or grain densities) and their spacings represent dynamic values for the AFM conditions.

For the purpose of measurement and analysis, a number of viewing areas is randomly selected. The number of distinct grains counted per unit area of viewing on the media surface is interpreted as "active grain density". The average number of cutting points per unit length can be estimated as the number of grains per unit length intersecting a straight line superimposed in the viewing area

The values of active grain density for various concentration and mesh size, for two different carriers (putty and polyborosiloxane), are given in Table A 5 (Appendix A) The abrasive used with both carriers is silicon carbide

### 4.3.2 Results and comparison with stochastic simulation

Fig 4.5 represents the variation in active grain density as a function of abrasive concentration for different grit sizes with putty as carrier. The active grain density increases with an increase in abrasive concentration, and for a particular concentration, it is higher for a larger mesh number (or smaller grain diameter) (Fig. 4.6). Fig. 4 7 shows the variation of active grain density with concentration when polyborosiloxane is used as a carrier. Only mesh size of 50-60 is used with polyborosiloxane due to limited availability of abrasive media with polyborosiloxane which is procured from Exrtrude Hone, USA. The active grain density at a particular percentage concentration of abrasives by weight is higher for putty as carrier than for polyborosiloxane (Table A.5, Appendix A). As density of putty (2240.0 kg/m$^3$) is higher than polyborosiloxane (985.0 kg/m$^3$), for the same weight of media, the volume of polyborosiloxane carrier is higher than putty. As a result, the number of abrasive grains per unit area will be lower in polyborosiloxane abrasive mixture than putty abrasive mixture at a particular percentage concentration of abrasives by weight. As seen from the Figs. 4.5-4.7, the experimental values are generally lower than the calculated values of active grain density. One reason for this may be experimental difficulties in detecting all contacts and an unintentional tendency to overlook small contact areas when scanning large abrasives. However, the simulated results and the results obtained from the microscopic measurement method are close to each other, and hence validate the simulated results.

In actual practice, the value of active grains should remain relatively stable for low number of strokes. There may be slight increase in the active grain density, as grains fracture produces more smaller grains Once the number of strokes reaches a critical value and the media has absorbed too much of chips, the value of active grain density may take a drastic downturn. Hence, media must be replaced after a certain number of cycles to maintain the performance of the process Further work is required to determine the grain wear and critical number of cycles for media replacement.

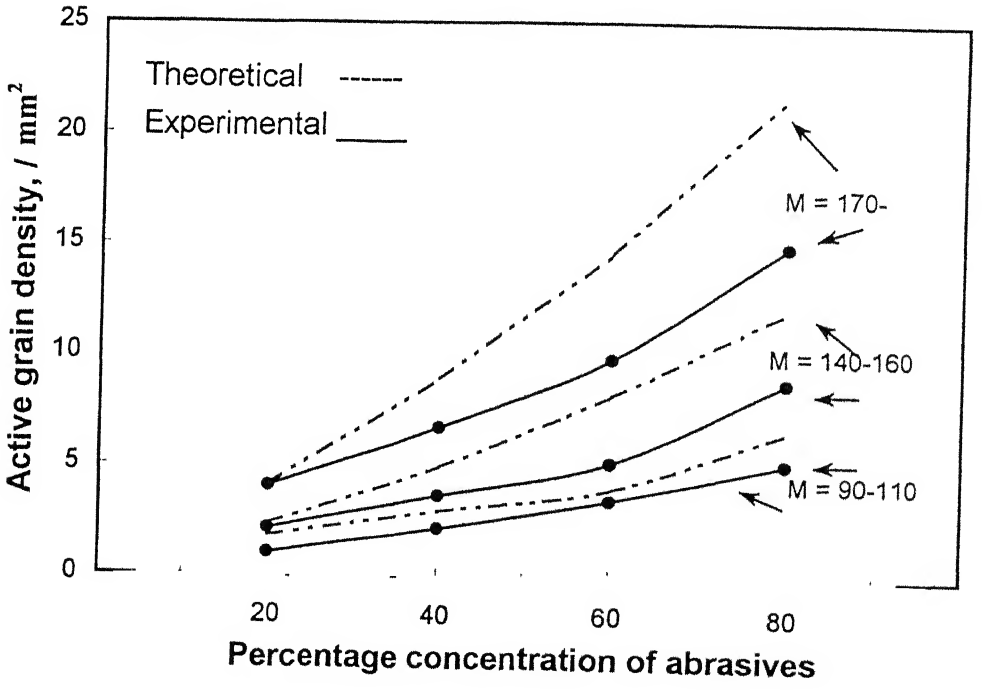


**Fig. 4.5 Variation of active grain density with percentage concentration and mesh size for putty as carrier**

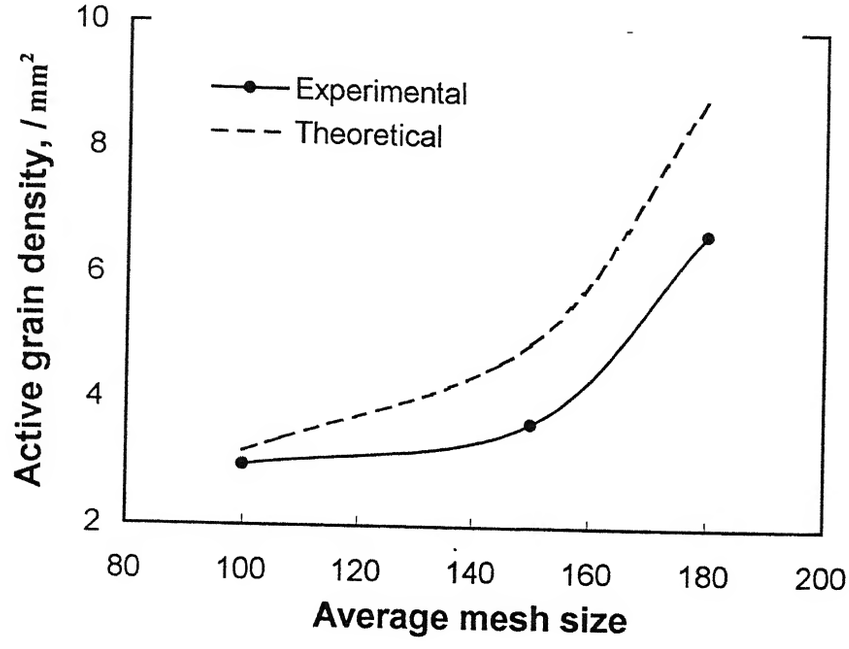


**Fig. 4.6 Variation of active grain density with average mesh size for putty as carrier (C=40%)**

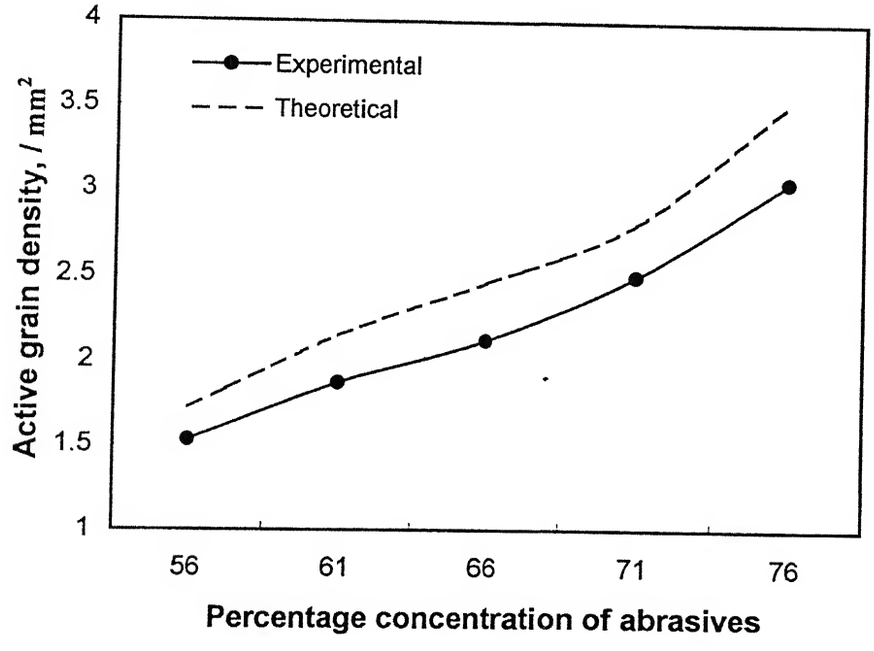


**Fig.4.7 Variation of active grain density with percentage concentration of abrasives for polyborosiloxane as carrier**

## 4.4 Results and Discussion

The conditions, under which the present simulation has been carried out, are given in Appendix C. The assumed initial Guassian surface profile of the workpiece is shown in Fig 4.8(a) The surface profile obtained after simulation for the specified machining conditions is illustrated in Fig 4 8(b). The sampling length is 1 mm with coordinates at 1 $\mu$m resolution This profile resembles with the actual surface profile obtained from AFM experiments. Considerations of real shape of grains, effect of wear of grain, effect of elasticity, pile up of material and actual initial surface profile of the work can provide more realistic results in the simulation In the succeeding sections, the results for material removal and surface roughness, predicted by simulation, are discussed and compared with the response surface analysis (RSA) results and theoretical results (discussed in chapter 3)

### 4.4.1 Material removal

Figure 4.9 shows the effect of percentage concentration of abrasives by weight on material removal As the percentage concentration of abrasives in media increases material removal also increases, because higher concentration of abrasives results in higher number of active grains and hence higher material removal The difference between the RSA results and results due to theoretical model and simulation may be due to inaccuracy in measurement of active grain density specially at higher value of concentration Also generally, the measured value and stochastically determined value of active grain density is higher than the effective active grain density during the AFM process Hence, the predicted values of material removal at higher concentration are generally higher than the RSA data.

Figure 4.10 shows the effect of mesh size on material removal for mild steel workpieces. From the figure, it is evident that as the mesh size increases, the material removal increases. The reason for increase of material removal is that with increase in mesh size, area of the indented grooves and depth of indentation decrease but total number of interferences between grains and workpiece increases due to increase in active grain density (Table A.5 Appendix A and Fig 4.6). The overall effect is an increase in material removal with increase in abrasive mesh size.

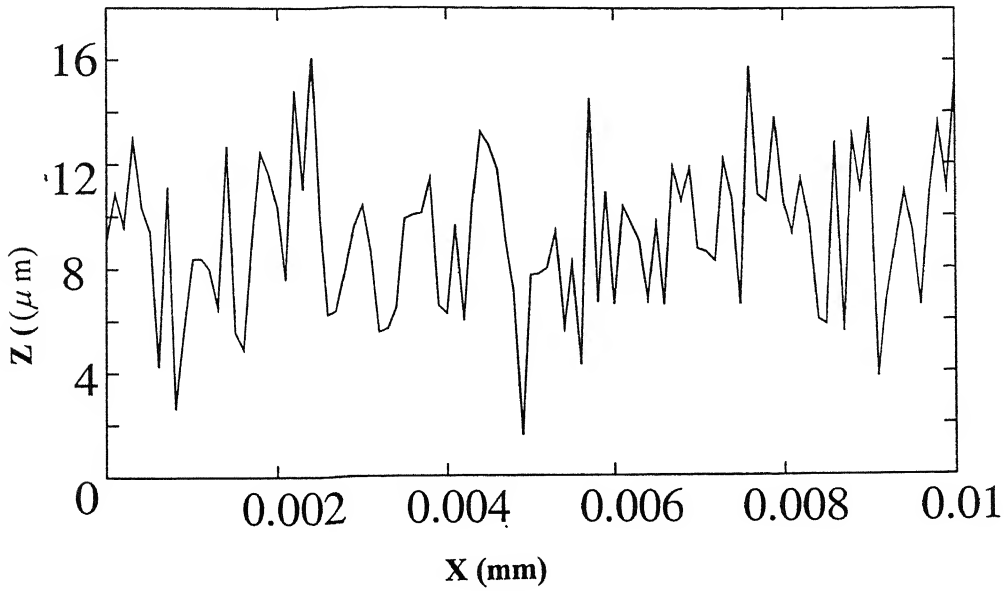


**(a) Assumed initial surface profile of the workpiece**

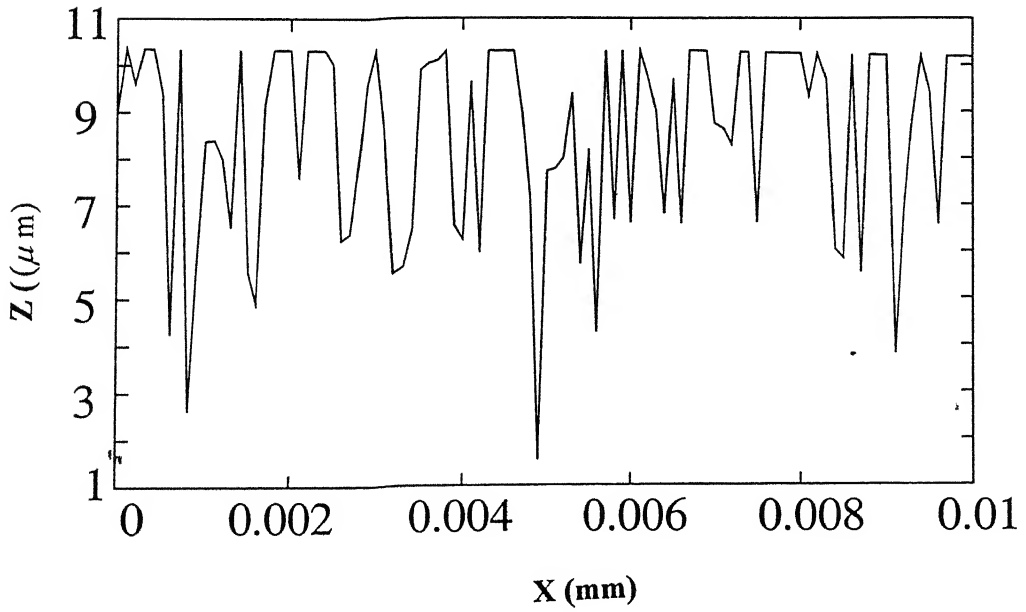


**(b) Final surface profile of the workpiece**

**Fig 4.8 (a) Initial surface profile and (b) profile obtained after simulation ($p_e$ = 50 bar, $M$ =50-60, $R_e$ = 0.905, $N$ =15, $C$ = 66%)**

It is found that material removal increases with increase in extrusion pressure (Fig. 4 11) The simulation results for material removal agree well with the RSA data. But at higher pressure, the number of abrasive grains taking part in actual cutting may be less due to rolling of grains at higher velocity. Hence, actual material removal will be less than theoretical one which can also be seen from Fig 4.11 also. This deviation would increase with increase in extrusion pressure Material removal also increases with increase in reduction ratio (Fig 4 12), due to increase in the slug length of media passed per unit time. At higher reduction ratio, the stresses acting on the workpiece surface are higher, leading to higher material removal. At lower value of reduction ratio, the predicted material removal can be observed to be in good agreement with the RSA results. At higher end of reduction ratio, a difference between the results exists. At higher reduction ratio, more grains come in contact with the workpiece surface in a cycle, due to increase in slug length Secondly, normal stresses at workpiece surface are higher at higher reduction ratio for a specified extrusion pressure. As a result, material removal is higher due to higher depth of indentation at higher normal stress. The same is also true with higher extrusion pressure. Material removal value increases with the number of cycles (Fig.4 13) and also the difference between the simulated and RSA results increases with increase in number of cycles. The difference in RSA values and theoretical results is more at higher number of cycles. Material removal in a specified number of cycles decreases with increase in hardness of workpiece material due to decrease in depth of indentation (Fig. 4.14).

### 4.4.2 Surface roughness

The effect of percentage concentration of abrasives on the change in surface roughness indicates increase of change in surface roughness ($\Delta R_a$) with increase in percentage concentration of abrasives (Fig. 4.15). With higher concentration of abrasives, the number of abrasives taking part in machining will be more, and hence surface roughness obtained for a specified number of cycles will be better. The values due to theoretical model are higher than that predicted by simulation for all concentrations. The predicted $\Delta R_a$ can be observed to be in better agreement at low percentage concentrations. At higher percentage of abrasives concentration, the $\Delta R_a$ is higher. This may be due to higher value

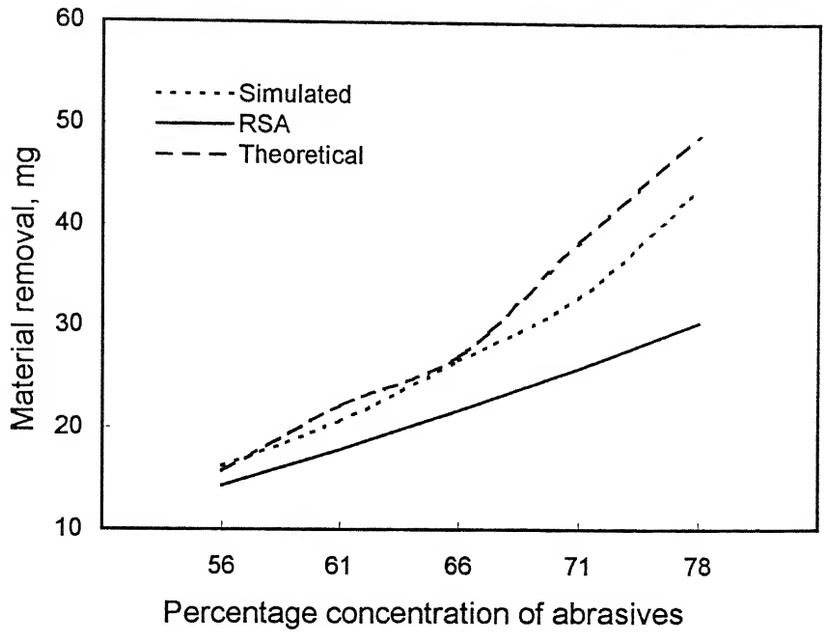


**Fig. 4.9 Variation of material removal with percentage concentration of abrasives ($p_e$ = 50 bar, $M$ =50-60, $R_e$ = 0.905, $N$ =15)**

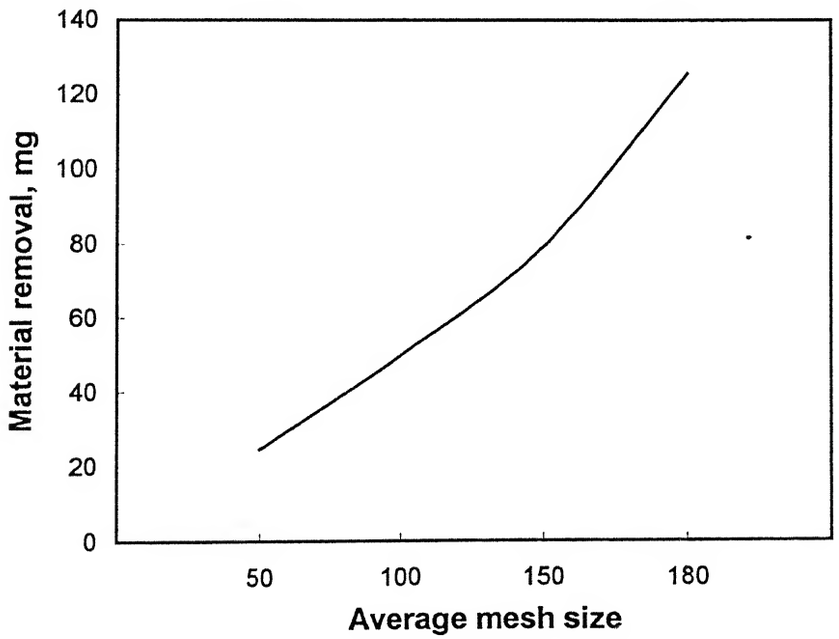


**Fig. 4.10 Simulated variation of material removal with mesh size of grains ($p_e$ = 50 bar, $R_e$ = 0.905, $N$ =15, $C$ = 66%)**

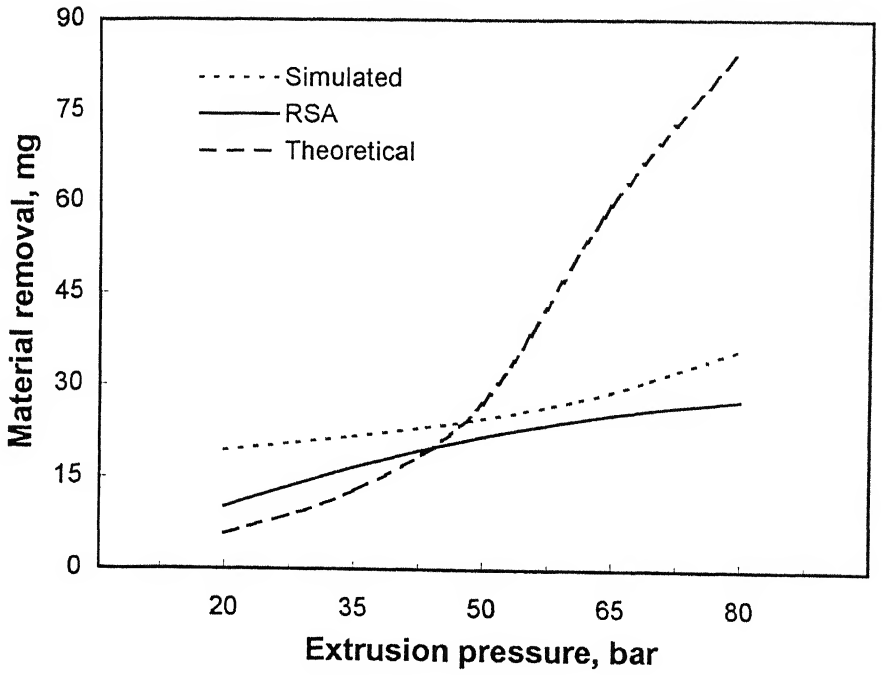


**Fig. 4.11 Variation of material removal with extrusion pressure**

**($M$ =50-60, $R_e$ = 0.905, $N$ =15, $C$ = 66%)**

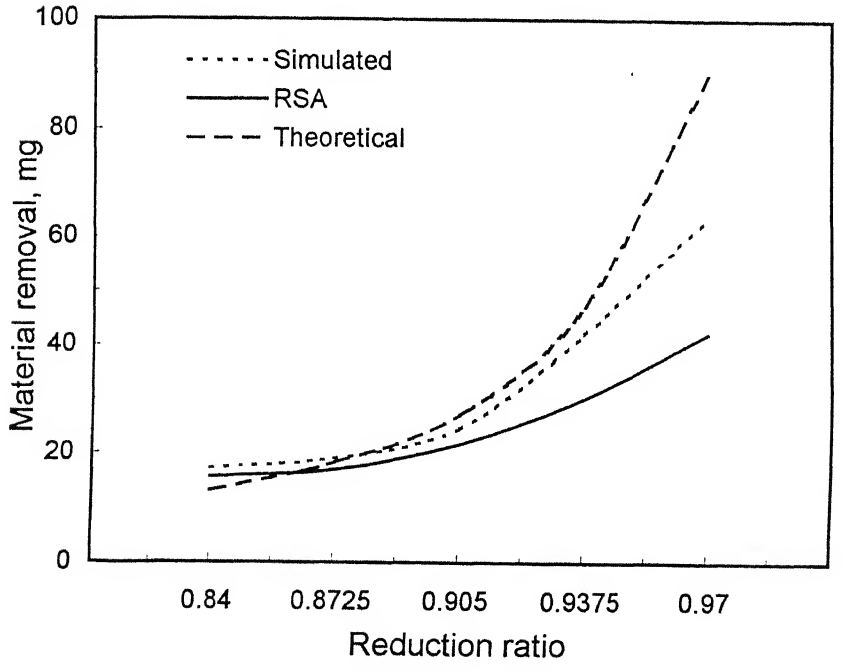


**Fig. 4.12 Variation of material removal with reduction ratio**

**($p_e$ = 50 bar, $M$ =50-60, $N$ =15, $C$ = 66%)**

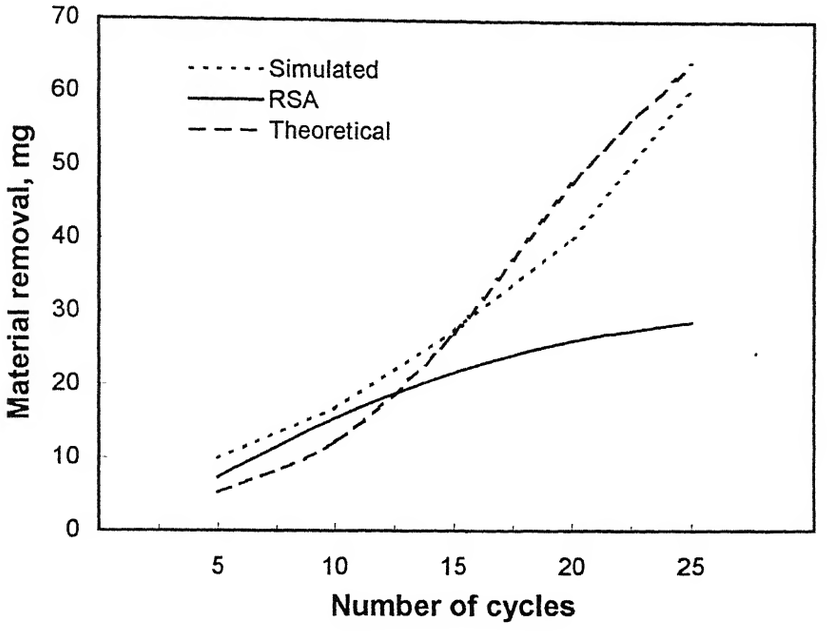


**Fig. 4.13 Variation of material removal with number of cycles**

**($p_e$ = 50 bar, $M$ =50-60, $R_e$ = 0.905, $C$ = 66%)**

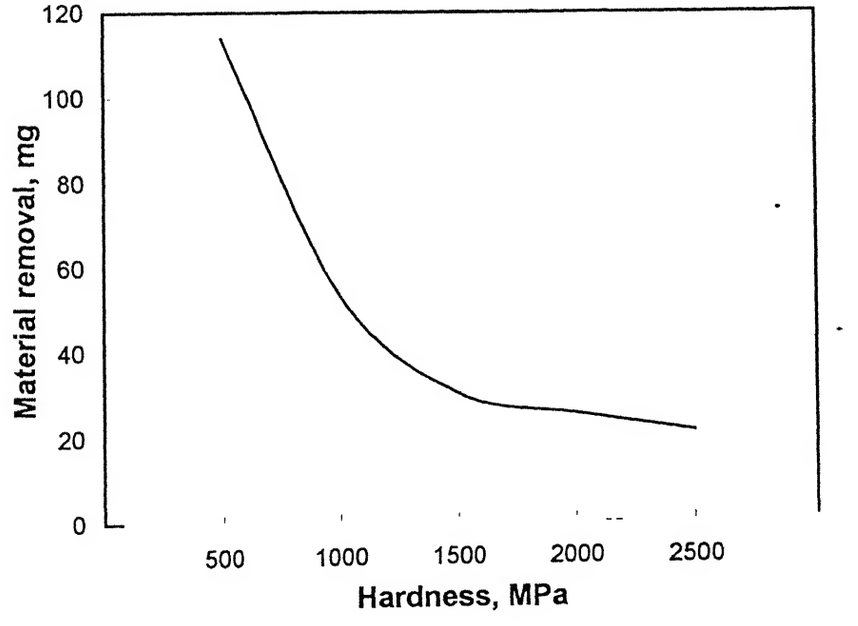


**Fig. 4.14 Simulated variation of material removal with hardness of workpiece material**

**($p_e$ = 50 bar, $M$ =50-60, $R_e$ = 0.905, $N$ =15, $C$ = 66%)**

of active grain density predicted by stochastic simulation and those measured by microscopic method, at higher percentage concentration.

$\Delta R_a$ value is higher for increased mesh size (Fig 4 16) If the grain size is large enough, then it may lead to the surface roughness worse than the initial one due to large depth of indentation. This can be explained with the help of simulation model also

Figure 4 17 exhibits the role of extrusion pressure on change in surface roughness value obtained after the specified number of machining cycles. It is observed that $\Delta R_a$ value increases with increase in extrusion pressure Figure 4.17 also presents a comparison of the change in surface roughness as a function of extrusion pressure, computed by theoretical model, simulation and due to experiments. The simulated results are in agreement with those of the RSA results. However, difference is more in case of the theoretical model This may be due to the assumption taken in modeling that only surface peaks are removed during AFM, but at higher pressure, in some sections of peaks, there may not be uniform material removal due to higher depth of indentation. As a result there is less change in surface roughness than those obtained by theoretical model. $\Delta R_a$ value also increases with number of cycles (Fig 4.18) and reduction ratio (Fig. 4.19). Comparison of results indicates that results due to theoretical model, simulation and RSA are in good agreement as far as lower numbers of cycles are concerned At higher value of number of cycles, difference between the RSA results and results obtained from the theoretical model and simulation increases. In practice, there may be more rolling of grains than sliding with reduction in surface roughness value at higher number of cycles. As a result, there will be less change in surface roughness at higher number of AFM cycles. Change in surface roughness decreases with increase in the hardness of workpiece material due to decrease in depth of indentation (Fig. 4.20).

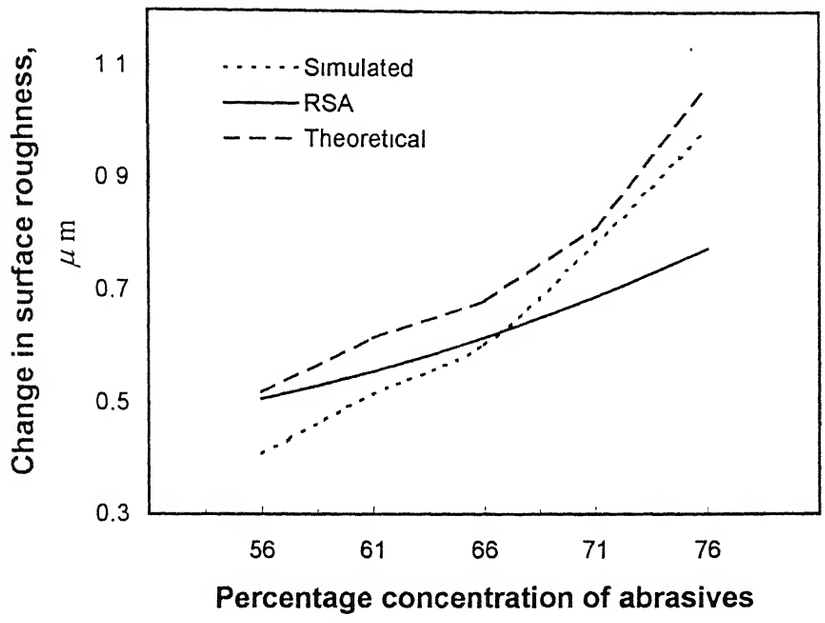


**Fig. 4.15 Variation of change in surface roughness with percentage concentration of abrasives ( $p_e$ = 50 bar, $M$ =50-60, $R_e$ = 0.905, $N$ =15)**

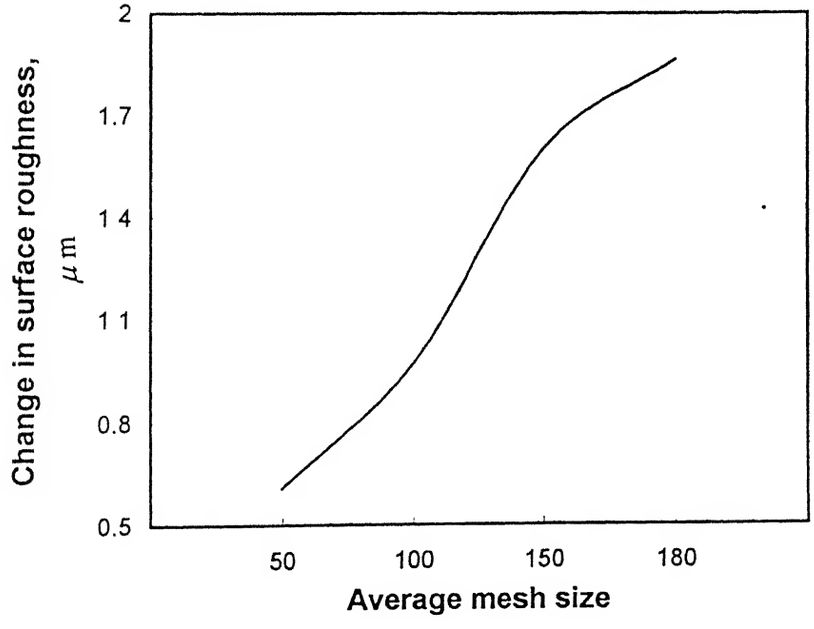


**Fig. 4.16 Simulated variation of change in surface roughness with mesh size of grains**

**( $p_e$ = 50 bar, $R_e$ = 0.905, $N$ =15, $C$ = 66%)**

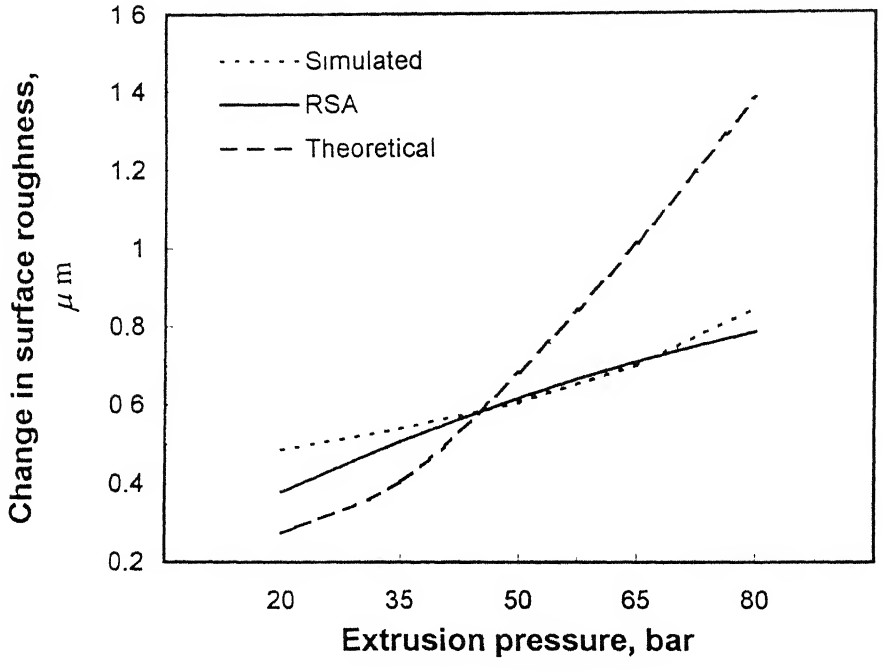


**Fig. 4.17 Variation of change in surface roughness with extrusion pressure**

**($M$ =50-60, $R_e$ = 0.905, $N$ =15, $C$ = 66%)**

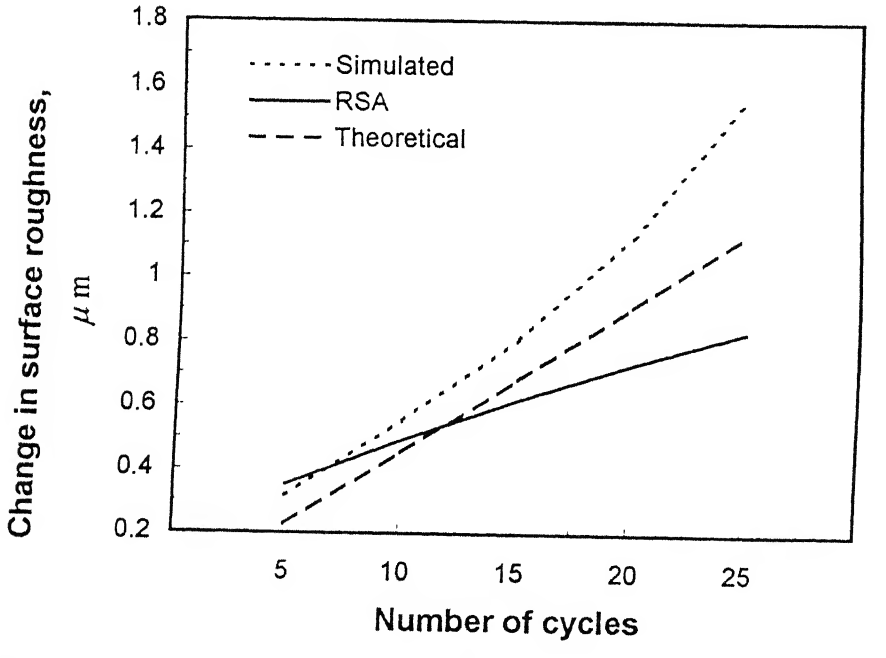


**Fig. 4.18 Variation of change in surface roughness with number of cycles**

**($p_e$ = 50 bar, $M$ =50-60, $R_e$ = 0.905, $C$ = 66%)**

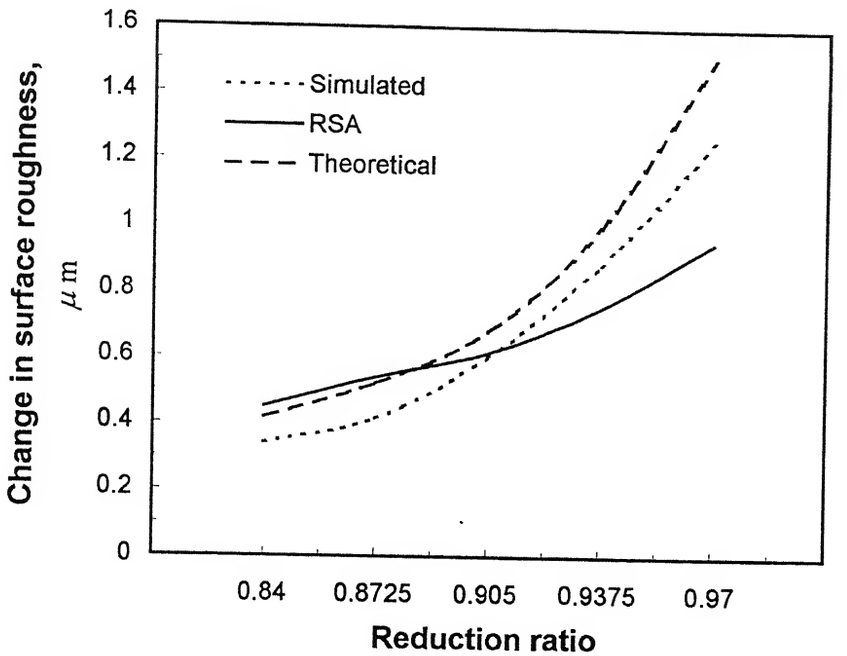


**Fig. 4.19 Variation of change in surface roughness with reduction ratio ($p_e$ = 50 bar, $M$ =50-60, $N$ = 15, $C$ = 66%)**

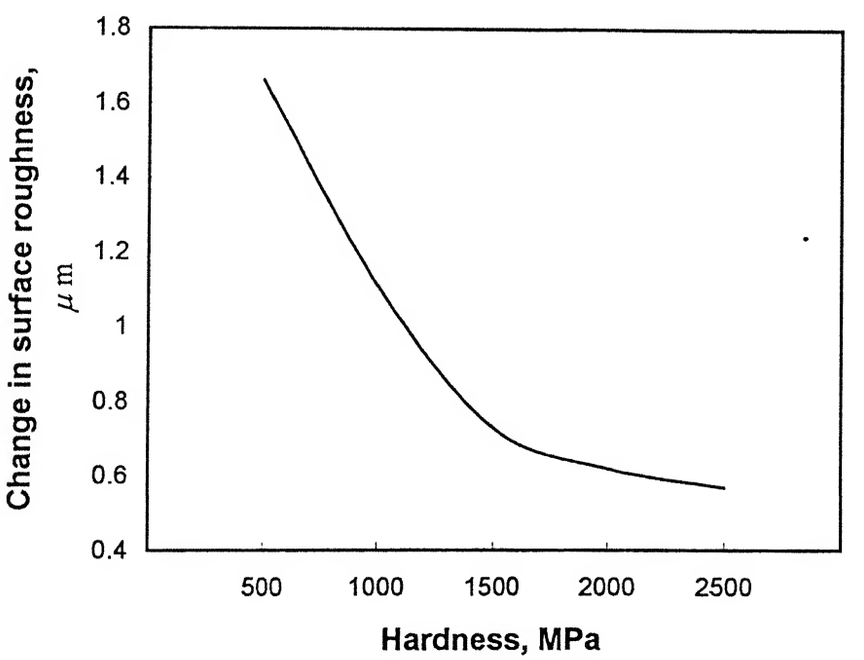


**Fig. 4.20 Simulated variation of change in surface roughness with hardness of workpiece material ($p_e$ = 50 bar, $M$ =50-60, $R_e$ = 0.905, $C$ = 66%, $N$ = 15)**

## 4.5 Conclusions

The generation of surface profile and material removal in AFM are simulated considering random distribution of abrasive grains in media and their interaction with workpiece profile during the process. The results of the proposed simulation and RSA are in good agreement, which justifies the use of this approach for generating the surface in AFM The simulation enables the prediction of surface roughness and material removal with reference to percentage concentration and mesh size of abrasives, extrusion pressure, number of cycles and reduction ratio The active number of abrasive grains per unit volume of media flow increases with percentage concentration of abrasives and reduction ratio, hence higher material removal and change in surface roughness is achieved Extrusion pressure, grain mesh size and hardness of workpiece affect the depth of indentation of a grain in workpiece material The significance of these parameters on final surface profile is discussed with reference to AFM process Change in surface roughness value and material removal increases with extrusion pressure, number of cycles, reduction ratio and percentage concentration of abrasives

# Chapter 5

# Thermal Aspects of AFM Process

## 5.1 Introduction

The AFM process modeling is complex due to little understood behaviour of the media and the complicated and random nature of material removal Both theoretical and empirical studies of abrasive flow machining are greatly hampered due to the inherent random nature and multiplicity of variables. To date it appears that there are no theoretical modeling for determination of tangential forces, specific energy and thermal aspects of AFM process. There are no systematic experimental measurement of forces and temperature distribution during AFM and its dependence on the relevant process parameters Thus, studies aimed at predicting the AFM performance are greatly hampered.

Inspite of the process being a critical one for the industries, the mechanics of the AFM process has not been studied in any great detail. In this study, an expression has been derived for the determination of tangential forces and specific energy. The tangential force acting during AFM is explained in terms of an equation which takes into account the forces arising from material removal and from rubbing between the workpiece and abrasives. The understanding of the forces provides a basis for the investigation of the AFM process. Preliminary results are also presented for the effect of process parameters on force ratio and specific energy. These results will allow the mechanics of AFM to be compared to the mechanics of other abrasive processes such as grinding.

An investigation on the theoretical and experimental determination of thermal properties of media has been carried out by Fletcher [22]. Davies and Fletcher [20] found experimentally that viscosity of media is significantly affected by temperature. Viscosity of high viscosity media reduces drastically even with a small increase in temperature (2-10 °C). The results [20] have shown that progression from low to high viscosity base media produces a reduction in the temperature rise. Hence, it is of great practical and theoretical interest to study the temperature rise during the AFM process. In the case of AFM, the complex nature of the process precludes a precise thermal analysis, and consideration of simplified models is required. The purpose of this chapter is to present a simple theoretical

thermal analysis and to provide a means for predicting approximate temperatures during the AFM process.

## 5.2 Forces and Specific Energy in AFM

In this section the mechanics of AFM process is analyzed from the consideration of the forces acting on a single grain in machining. A simple analysis based on abrasion theory for calculating the cutting forces due to a single abrasive grain can be expanded to predict the forces arising in AFM The machining action during AFM compares to a grinding operation as media uniformly removes material from the workpiece surface. When media is forced through a restricted passage, the media behaves as a deformable grinding stone [16]. Shaw [41] proposed a new theory of microchip formation for fine finish grinding assuming spherical abrasive grain. Brian Rowe and Xun Chen [54] also applied this theory for analysis and simulation of grinding process. In abrasive flow machining process, the normal force ($F_{ng}$) applied to such a spherical grain will cause it to penetrate the surface (Fig. 5 1). As the grain is translated horizontally, the plastically deformed zone beneath the surface will be inclined and will give rise to upward flow, thus forming a microchip which is subsequently sheared from the surface The following assumptions are made for determining the specific energy in AFM:

1. The path traced by an individual grain is straight line
2 The material is removed through plastic deformation in the form of chips without the side pile up, whenever grain workpiece interference occurs
3. Abrasive grain is approximated by a sphere [41,54]. This is also reasonable, considering the large negative rake angles presented by the grains.

Fig. 5.1 represents a grain indenting in workpiece material and producing a groove of depth $t$. In the absence of friction at the surface between the spherical grain and the workpiece, the magnitude of the force required to indent the workpiece is constant and independent of the direction in which it is loaded [41,54]. Therefore, radius $b$ of the projected area of indentation is given by,

$$F_{rg} = \pi b^2 H_w \qquad (5.1)$$

where, $H_w$ is hardness of workpiece material and $b$ is the radius of the projected area of indentation

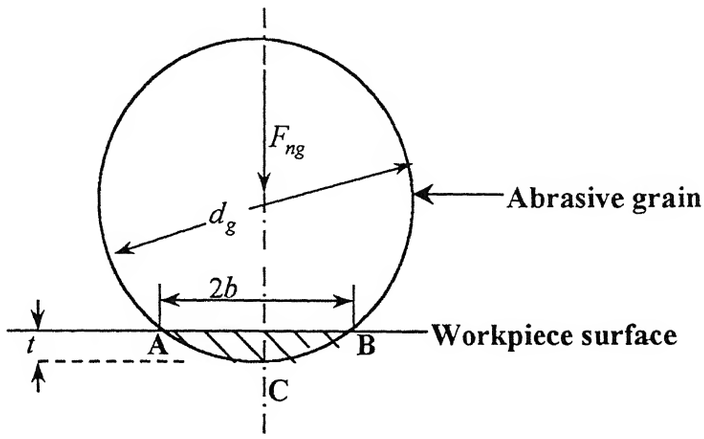


**Fig. 5.1 Schematic diagram of indenting spherical abrasive grain**

From geometry of Fig 5 2

$$\sin\theta = \frac{2b}{d_g} = \frac{2\sqrt{t\,(d_g - t)}}{d_g} \qquad (5\,2)$$

$$\cos\theta = \frac{d_g - 2t}{d_g} \qquad (5.3)$$

where, $\theta$ defines the line of action of the indentating force. Depth of indentation '$t$' has been derived in chapter 3 and is given by following equation.

$$t = \frac{d_g}{2} - \sqrt{\frac{d_g^2}{4} - \frac{F_{ng}}{H_w \pi}} \qquad (5.4)$$

Tangential component of the chip formating force $F_{tg}$ (Fig.5.2) can be written in terms of force $F_{rg}$ as given below

$$F_{tg} = F_{rg} \sin\theta \qquad (5\,5)$$

Substituting values of $F_{rg}$ and $\sin\theta$ from eqns (5.1) and (5.2) respectively in eqn. (5.5),

$$F_{tg} = \pi b^2 H_w \quad \frac{2\sqrt{t\,(d_g - t)}}{d_g}$$

$$= (\pi\ H_w)\ (\sqrt{t(d_g - t)}\,)^2\ \ \frac{2\sqrt{t(d_g - t)}}{d_g} \quad \text{(using eqn 3.59)}$$

$$= (2\pi\ H_w)\, t^{\frac{3}{2}}\, (d_g - t)^{\frac{3}{2}} / d_g \qquad (5.6)$$

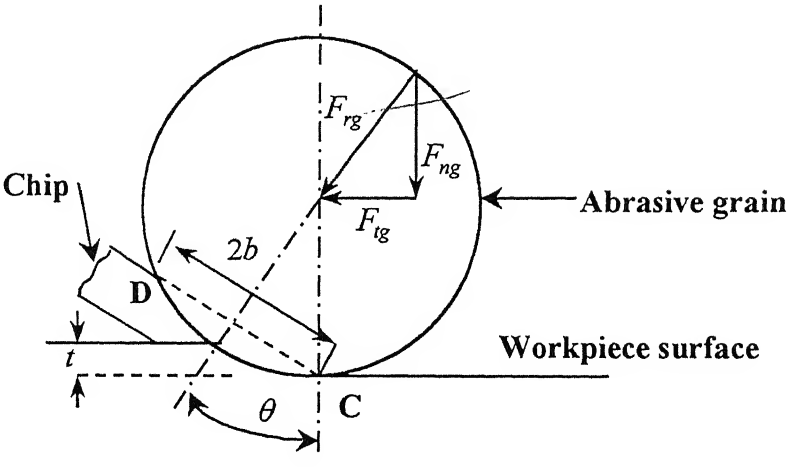


**Fig. 5.2 Abrasive grain producing a chip**

In practice, there will be friction along surface DC (Fig. 5.2). Assuming the mean coefficient of friction between grain and workpiece material to be $f$, the friction force will be $f\ F_{rg}$.

Hence, tangential component of friction force per active grit, $F_{tgf} = f\ F_{rg}\ \cos\theta$

$$= f\ \pi\ b^2 H_w\, (\frac{d_g}{2} - t) / (\frac{d_g}{2})$$

$$= f\ \pi\ H_w\ (\sqrt{t(d_g - t)}\,)^2\ \frac{(d_g - 2t)}{d_g} \quad \text{(using eqn. 3.59)}$$

$$= f\ \pi\ \ H_w\, t\, (d_g - t)\, \frac{(d_g - 2t)}{d_g} \qquad (5.7)$$

Total tangential force per active grain ($F_{tg}$) is equal to the sum of chip formation force and frictional force per active grain. Hence,

$$F_{tg} = (2\pi\ H_w)\, t^{\frac{3}{2}}\, (d_g - t)^{\frac{3}{2}} / d_g + f\ \pi\ \ H_w\, t\, (d_g - t)\, \frac{(d_g - 2t)}{d_g} \qquad (5.8)$$

The specific energy in machining and abrasive processes is defined as the energy expanded per unit volume of material removal

Specific energy, $u = F_{tg}\, v_f /(A' v_f)$ (5.9)

where, $v_f$ is velocity of flow of media along workpiece surface. It is also assumed to be equal to chip flow velocity. The area $A'$ of groove generated, which corresponds to the cross hatched area in Fig 5 1, is given by the following equation

$$A' = \frac{d_g^2}{4} sin^{-1} \frac{2\sqrt{t(d_g - t)}}{d_g} - \sqrt{t(d-t)}\left(\frac{d_g}{2} - t\right) \quad \text{(from eqn 3.62)} \quad (5\ 10)$$

Total contact area between workpiece and media = $\pi\ d_w l_w$ (5.11)

where, $d_w$ is diameter of cylindrical workpiece and $l_w$ is length of workpiece

Let $n$ is the number of all simultaneously acting grits per unit contact area (active grain density) of media and workpiece. Then, total no. of grains simultaneously acting on workpiece surface = $\pi\ n d_w l_w$ (5 12)

The tangential force acting between the workpiece surface and media is equal to the total of the tangential forces of all active grains within the contact area between the media and workpiece.

Therefore, total tangential force = tangential component of cutting force + tangential component of friction force

$$F_t = (\pi n d_w l_w)\ [(2\pi\ H_w)\, t^{\frac{3}{2}} (d_g - t)^{\frac{3}{2}}/d_g + f\,\pi\ H_w t (d_g - t)\frac{(d_g - 2t)}{d_g}]$$

$$= (\pi^2 n d_w l_w H_w)\,[2 t^{\frac{3}{2}} (d_g - t)^{\frac{3}{2}}/d_g + f\ t(d_g - t)\frac{(d_g - 2t)}{d_g}] \quad (5.13)$$

In the above eqn. (5 13), $H_w$, $d_g$, $d_w$, and $l_w$ are the parameters that can be determined in advance.

Total number of grains passed per stroke $= 2\,\pi\, r_w\, n\, l_s \frac{r_c^2}{r_w^2}$, (5.14)

where, $r_c$ and $r_w$ are inner radii of media cylinder and workpiece respectively, and $l_s$ is stroke length.

As it is assumed that the path traced by an individual grain is straight line, volume of material removed by a grain is equal to cross sectional area of groove produced

multiplied by length of contact along the workpiece surface To simplify the analysis, length of contact is assumed to be equal to the length of workpiece surface. Therefore,

$$\text{Volume of material removed per unit time} = (2\pi r_w n l_s \frac{r_c^2}{r_w^2})(A' l_w) / (l_s / v_p) \qquad (5.15)$$

where $v_p$ is the piston velocity.

Energy required per unit time = specific energy × volume of material removed per unit time

$$= u\ (2\pi r_w n l_s \frac{r_c^2}{r_w^2})(A' l_w) / (l_s / v_p) \qquad (5.16)$$

From continuity equation,

$$\frac{v_f}{v_p} = \frac{r_c^2}{r_w^2} \qquad (5.17)$$

For the situation, where energy is dispersed uniformly over the workpiece contact area ($2\pi r_w l_w$), the thermal flux [energy $(\text{time})^{-1}(\text{area})^{-1}$] will be

$$q = [\ u\ (2\pi r_w n l_s \frac{r_c^2}{r_w^2})(A' l_w) / (l_s / v_p)\ ] / (2\pi r_w l_w)$$

$$= [\ u n A'\ v_p \frac{r_c^2}{r_w^2}\ ] \qquad (5.18)$$

For AFM, the specific energy is generally much larger than for other metal cutting operations. In practice, the specific energy can be used for the calculation of surface temperatures. From a more fundamental view point, an understanding of the origin of AFM energy can provide the basis for physical description of the mechanics of the process.

## 5.3 Thermal Analysis of AFM Process

The thermal behavior of workpiece is analyzed by one dimensional unsteady state heat transfer theory. Following **assumptions** are made to simplify the thermal analysis of AFM process·

1. The quantity of the heat flowing into the workpiece and media is constant during a machining stroke.

2 The heat flows along the thickness direction of workpiece and media. The unsteady temperature distribution in the thin workpiece, which is heated on one side by machining action can be approximated as one dimensional. Conduction in the direction of motion is neglected. The value of Peclet number obtained is of the order of $10^4$ for all the cases considered. Hence, the conduction in the direction of motion can be neglected [55]

3 The composite properties of media are considered in the evaluation of temperature distribution

4. Thermal properties of media and workpiece are constant with time and space.

5 Media is cooled to initial temperature in media cylinder after each stroke.

The energy expanded in AFM is almost entirely dissipated as heat in the media-workpiece contact area, and causes the abrasive media and wokpiece temperature to rise. The heat generated in the AFM zone (Fig. 5.3) is removed from the region in the variety of ways

1. It may conduct into the workpiece, where it is finally convected away by surrounding air.

2 It may conduct into the media, where it is carried away by the motion of media.

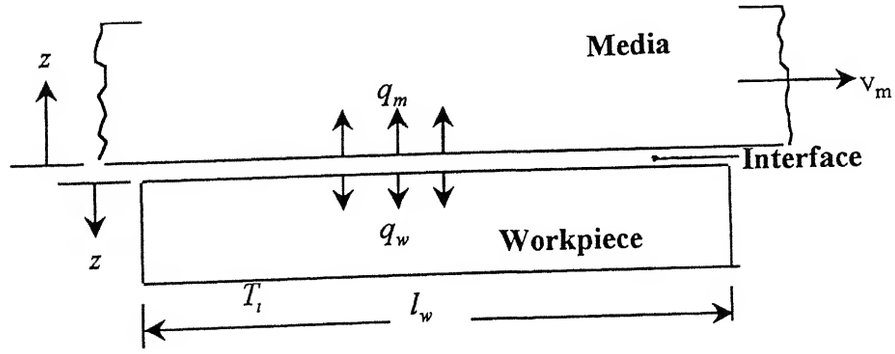


**Fig. 5.3 Model of abrasive flow machining zone**

**Workpiece** is assumed as one dimensional semi-infinite plate for the heat transfer analysis. For the same uniform initial temperature distribution, the surface of the workpiece is suddenly exposed to a constant heat flux $q_w$.

For constant properties of workpiece, the differential equation for the temperature ($T$) distribution in workpiece as a function of time $T(z,\tau)$ is given by the following equation:

$$\frac{\partial^2 T}{\partial z^2} = \frac{1}{\alpha_w}\frac{\partial T}{\partial \tau} \tag{5.19}$$

where $\alpha_w$ is the thermal diffusivity of the workpiece material and $\tau$ is time.

The initial and boundary conditions are

$$T(z,0) = T_i$$

$$q_w = k_w \frac{\partial T}{\partial z}\Big|_{z=0} \quad \text{for } \tau > 0$$

$$T(\infty, \tau) = T_i \tag{5.20}$$

where $T_i$ is the ambient temperature and $k_w$ the is thermal conductivity of workpiece material.

This problem has been solved by the Laplace transform technique [56].

The solution for this case is

$$T - T_i = \frac{2q_w}{k_w}\left[\sqrt{\frac{\alpha_w \tau}{\pi}}\, exp\left(\frac{-z^2}{4\alpha_w \tau}\right) - z\left(1 - erf\frac{z}{2\sqrt{\alpha_w \tau}}\right)\right] \tag{5.21}$$

where $q_w$ is the heat flow to the workpiece per unit time and per unit area. $z$ is the distance from the surface along the thickness, and $k_w$ is the thermal conductivity of workpiece material.

The Gauss error function is defined as

$$erf\frac{x}{2\sqrt{\alpha\tau}} = \frac{2}{\sqrt{\pi}}\int_0^{x/2(\sqrt{\alpha\tau})} e^{\eta^2} d\eta \tag{5.22}$$

The energy equation for the moving **media** is considered at steady state to avoid the complication of the numerical part. It is also reasonable since in AFM time required for moving media to complete one stroke is very less in comparison to total time required for machining a workpiece. As workpiece is fixed, the temperature distribution in the workpiece is analyzed with respect to time.

The energy equation for media can be written as

$$(\rho c_p)_m \, v_m \frac{\partial T}{\partial x} = k_m \frac{\partial^2 T}{\partial^2 z} \tag{5.23}$$

where, $v_m$ is the velocity of media, $\rho_m$, $k_m$, $c_{pm}$ are the density, thermal conductivity and specific heat of media, respectively.

The boundary conditions for $T(x,z)$ are

$$T(o,z) = T_i$$

$$- k_m \frac{\partial T}{\partial z} \Big|_{z=0} = q_m$$

$$T(x,\infty) = T_i \tag{5.24}$$

The solution to the differential equation (5.23) and boundary conditions, in non-dimensional form are

$$\bar{T} = 2 \left(\left(\frac{X}{\pi}\right)^{\frac{1}{2}} \exp\left(\frac{-X^2}{4X}\right) - Z \operatorname{erfc}\left(\frac{Z}{2X^{1/2}}\right)\right) \tag{5.25}$$

$\bar{T}$ is non-dimensional temperature, and it is given by

$$\bar{T} = \frac{(T - T_i)}{[q_m / (\rho c_p v)_m]} \tag{5.26}$$

Other non-dimensional parameters are given by

$$Z = \frac{z v_m}{\alpha_c} \qquad X = \frac{x v_m}{\alpha_c} \qquad L = \frac{l v_m}{\alpha_c}$$

The dimensional form of eqn (5.25) is

$$T - T_i = \frac{q_m}{(\rho c_p v)_m} \left[ 2 \left(\frac{x v_m}{\alpha_m \pi}\right)^{\frac{1}{2}} \exp\left(\frac{z^2 v_m}{4\alpha_m x}\right) - \left(\frac{z v_m}{\alpha_m}\right) \operatorname{erfc}\left(\frac{z}{2}\left(\frac{v_m}{x \alpha_m}\right)^{\frac{1}{2}}\right)\right] \tag{5.27}$$

Let $T_s$ be surface temperature at $T(x,0)$. From the eqn (5.27), the surface temperature is evaluated and is given by following expression.

$$T_s - T_i = 2 \, q_m \left(\frac{x}{\pi (k \rho c_p v)_m}\right)^{\frac{1}{2}} \tag{5.28}$$

The average surface temperature on the workpiece surface can be expressed as follow.

$$T_{sav} - T_i = 2\, q_m \left( \frac{l_w}{\pi (k\, \rho\, c_p\, \mathrm{v})_m} \right)^{\frac{1}{2}} \tag{5.29}$$

The surface temperature of workpiece obtained by the eqn. (5.21) can be written as follow

$$T_s - T_i = \frac{2 q_w}{k_w} \sqrt{\frac{\alpha_w\, \tau}{\pi}} \tag{5.30}$$

For the common average surface temperature $T_s$ (equating eqns (5.29) and (5.30)),

$$2\, q_m \left( \frac{l_w}{\pi (k\, \rho\, c_p\, \mathrm{v})_m} \right)^{\frac{1}{2}} = \frac{2 q_w}{k_w} \sqrt{\frac{\alpha_w\, \tau}{\pi}} \tag{5.31}$$

Let R be the fraction of the total heat flux $q$ entering into the workpiece, that is generated along the workpiece and media interface.

$$q = q_w + q_m = \mathrm{R}\, q + (1 - \mathrm{R})\, q \tag{5.32}$$

Then, after simplification of the eqn. (5 32) the fraction of heat entering the workpeice can be obtained by the following expression.

$$\mathrm{R} = \frac{\frac{2}{3} \left( \frac{l_w}{(\rho\, \mathrm{c_p}\, k\, \mathrm{v})_m} \right)^{\frac{1}{2}}}{\left( \frac{\tau}{(\rho\, c_p\, k)_w} \right)^{\frac{1}{2}} + \frac{2}{3} \left( \frac{l_w}{(\rho\, \mathrm{c_p}\, k\, \mathrm{v})_m} \right)^{\frac{1}{2}}} \tag{5.33}$$

## 5.4 Evaluation of Properties of Media

In order to evaluate temperature distribution, the properties of media must be known. A simple weighted mean model for specific heat capacity based on the relative properties (by mass) of each constituent in media, is used to determine the variation of this property in the mixture.

$$c_{pm} = (1 - C/100)\, c_{pc} + (C/100)\, c_{pa} \tag{5.34}$$

where, $C$ is the percentage concentration of abrasives in the media. $c_{pc}$ and $c_{pa}$ are the specific heat of carrier (polyborosilixane) and abrasives respectively.

The density of media $\rho_m$ in terms of abrasive density $\rho_a$ and carrier density $\rho_c$ is given by the relation,

$$\rho_m = \frac{100\rho_a\rho_c}{[C\rho_c + (100-C)\rho_a]} \tag{5.35}$$

The thermal conductivity of media [22] can be obtained by the following expression

$$k_m = \frac{1}{s_2}\left[\frac{k_c\, k_a s_1}{k_c\, d_g + k_a\, s_3} + k_c\, s_3 (1 + \frac{s_1}{s_2})\right] \tag{5.36}$$

$$s_1 = 0.8061\ d_g$$

$$s_2 = s_1\left[\frac{(100-C)}{C}\frac{\rho_a}{\rho_c} + 1\right]$$

$$s_3 = s_2 - s_1$$

where, $k_c$ and $k_a$ are thermal conductivity of carrier and abrasives, respectively.

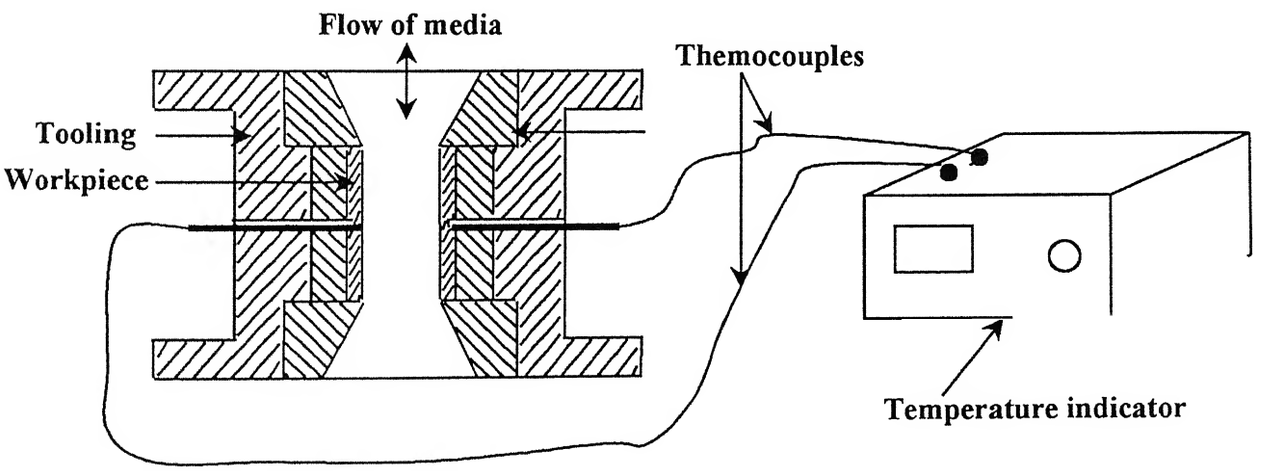


**Fig. 5.4 Experimental arrangement for temperature measurement**

## 5.5 Experimentation

Experiments have been conducted on the AFM set-up designed and fabricated in house Internal surfaces of mild steel workpieces have been finished using media (polyborosiloxane carrier mixed with SiC abrasives). The experimental arrangement for

measurement of temperature is shown in Fig. 5.4. Temperature at the workpiece surface during AFM has been measured using copper-constantan thermocouples. A multi-channel digital temperature indicator having resolution of 0.1 $^0$C was used for recording the temperature. The conditions, under which AFM experiments have been carried out, are given in Appendix C Details of experiments are discussed in chapter 2

## 5.6 Results and Discussion

The conditions of machining and values of various parameters, given in Appendix C, have been considered for the evaluation of forces, specific energy and heat flux The values of active grain density $n$, reported in chapter 4, have been used in the calculations. As machining action in AFM compares to grinding, the coefficient of friction between workpiece surface and abrasives is assumed to be 0.2 This is also cited in the literature [41] for calculation of specific energy in grinding. It is obvious that specific energy is a function of the average cross sectional area of a cut. The average cross sectional area of a cut seems to be smaller in AFM than grinding With work material of low hardness the cross sectional area of cut is larger with the same normal force. The specific energy in AFM (Fig. 5.5) is near to the range of specific energy in grinding (5-60 J/mm$^3$) [41] for mild steel workpiece. Generally it is higher in AFM due to lower depth of indentation. Fig. 5.6 indicates that specific energy decreases with increase in normal pressure due to higher depth of indentation. The normal pressure of indentation have been determined from the extrusion pressure applied in AFM, as explained in chapter 3 It is interesting to note that specific energy remains almost constant with change in abrasive mesh size (Fig. 5.7). The similar results have also been reported in case of grinding by Kannappan and Malkin [57].

A fraction of generated total heat initially going to the workpiece is 96.5% Its value reduces with the time of machining (Fig. 5.8). As a major portion of the heat enters into the workpiece, rise in temperature of the workpiece is much higher than rise in temperature of the media. It is due to much higher thermal conductivity of workpiece ($k_w$ = 60.5 W/m-K) as compared to the media. The thermal conductivity of media is 0.38 W/m-K for 66 % concentration of abrasives with average mesh size of 55. Temperature of workpiece increases with number of cycles (Fig. 5.9). Initially rate of rise in temperature is more, and it decreases with number of cycles. Measured values of rise in temperature are

lower than calculated ones due to simplification of analysis to one dimensional heat flow It is also observed (Fig 5 10) that rise in temperature increases with extrusion pressure, as higher energy at higher pressure results into increase in heat flux at workpiece surface

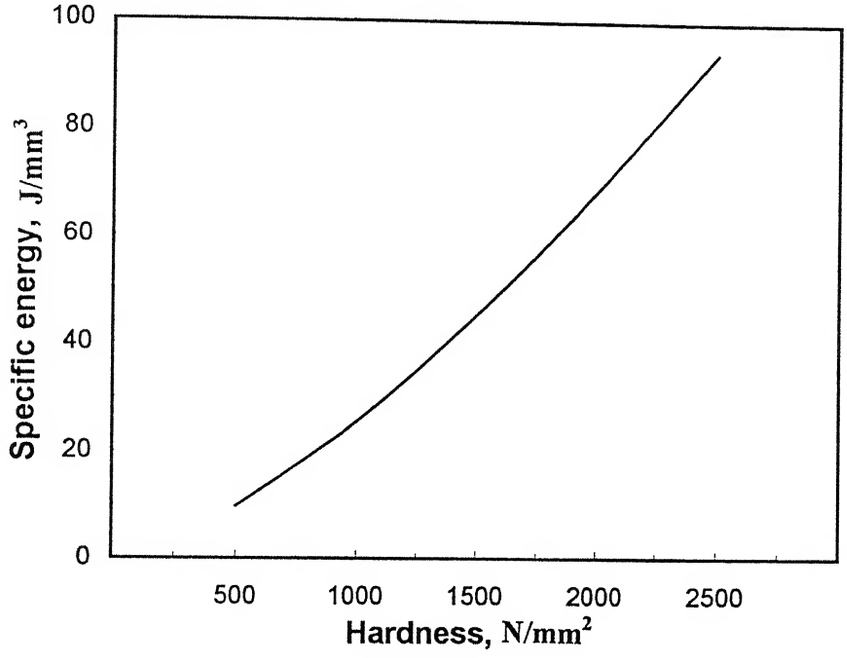


**Fig. 5.5 Variation of specific energy with hardness of workpiece material.**

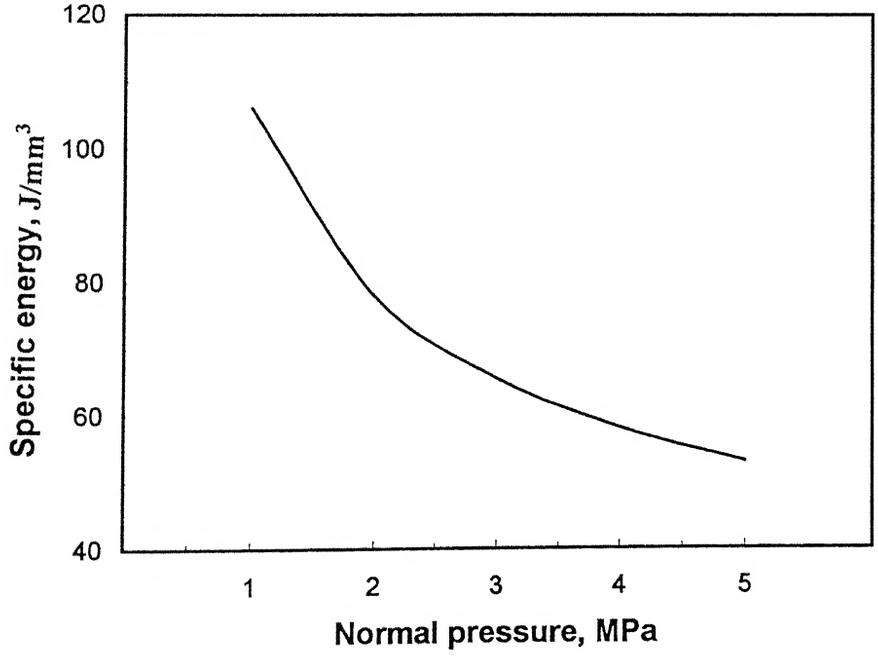


**Fig. 5.6 Variation of specific energy with normal pressure of indentation**

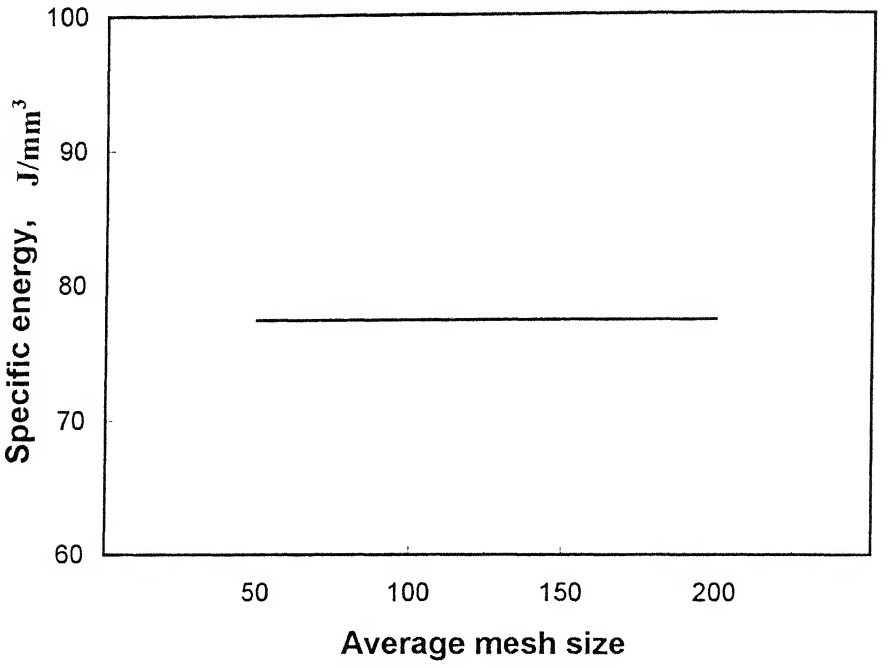


**Fig. 5.7 Variation of specific energy with mesh size of abrasive grains**

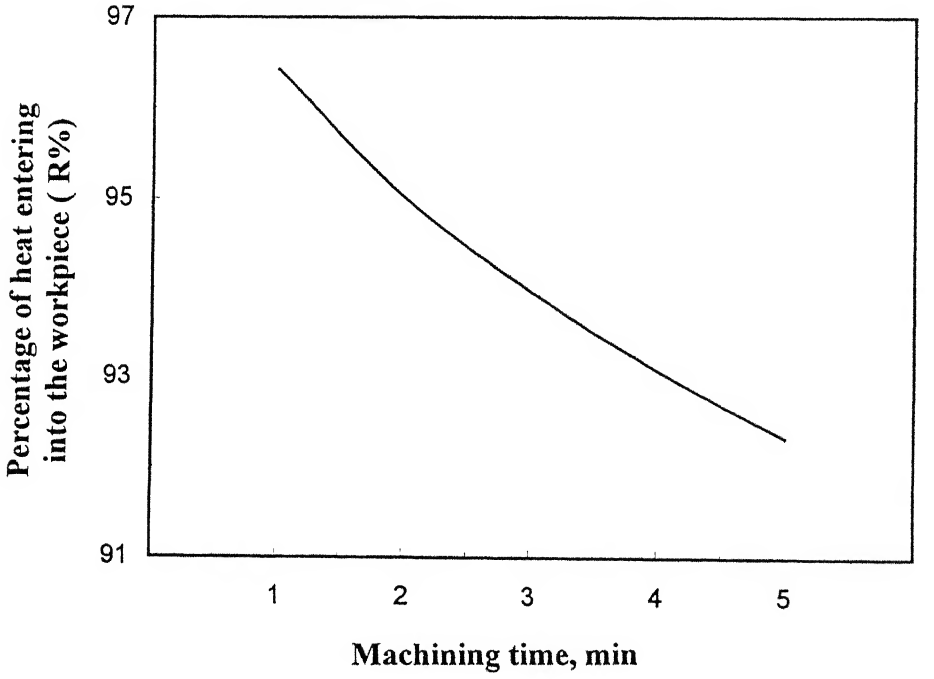


**Fig. 5.8 Variation of percentage of heat entering the workpiece with machining time**

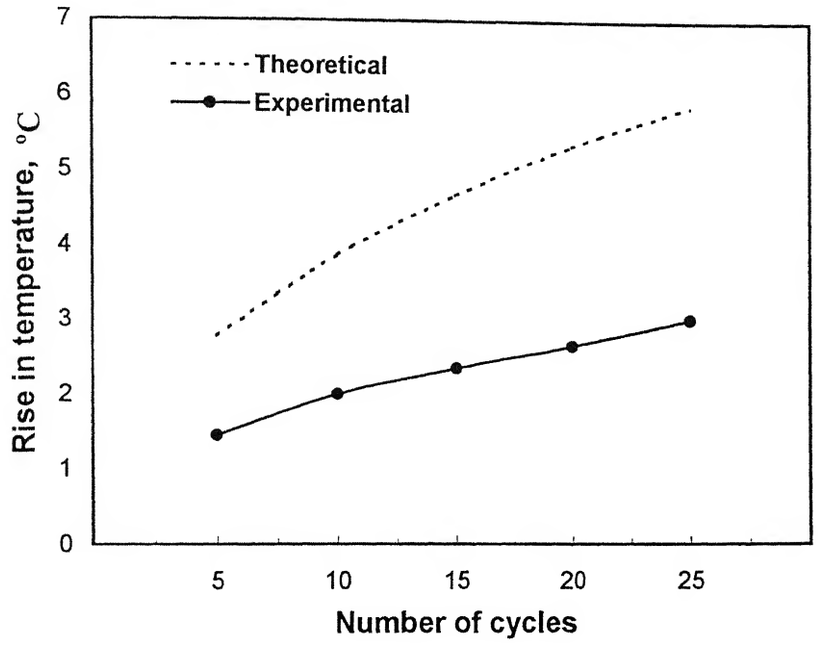


**Fig. 5.9 Change in temperature of workpiece with number of cycles**
**($C = 66$ %, $p_e = 50$ bar, $R_e = 0.905$)**

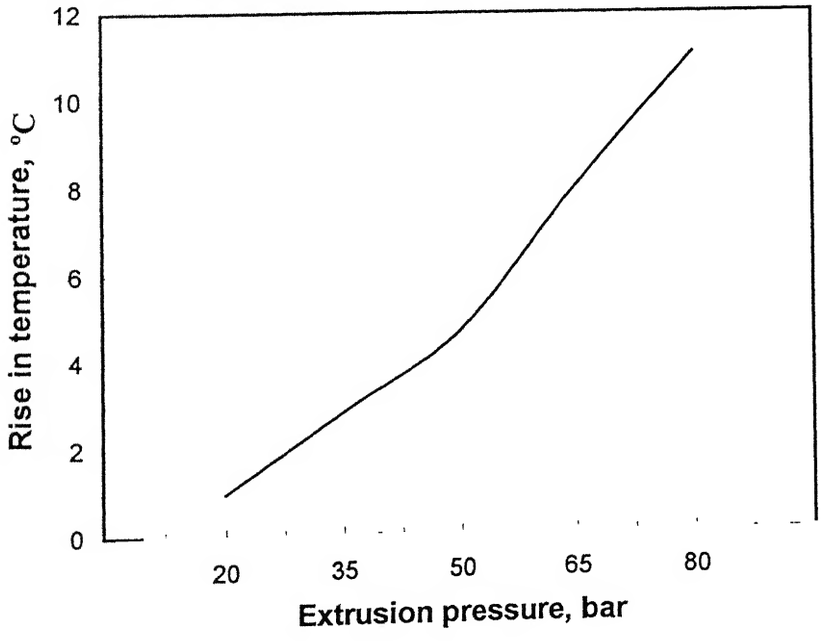


**Fig. 5.10 Change in temperature of workpiece surface with extrusion pressure**
**($C = 66$ %, $N = 15$, $R_e = 0.905$)**

## 5.7 Conclusions

The present analysis for specific energy and tangential force is a step forward in understanding the mechanism of AFM process. The specific energy for AFM (10-110 J/mm$^3$) process is partially overlapping the range of specific energy for grinding (5-60 J/mm$^3$). This justifies the inference of researchers that machining action in AFM compares to grinding It is interesting to note that specific energy remains constant with abrasive mesh size, but its value is higher for higher hardness of workpiece material

A simple model has been developed for the heat transfer in AFM process considering the heat flow to the workpiece and media A fraction of the heat entering the workpiece and media can be determined. The model predicted the workpiece temperature with reasonable accuracy However, The present analysis can be improved upon to give more realistic temperature distribution, by modeling the problem as a three dimensional unsteady state heat transfer problem

# Chapter -6

# Application of Neural Networks and Genetic Algorithms to AFM Process

## 6.1 Neural Networks in Manufacturing

The success of automated manufacturing relies to a large extent on the development of computer-based learning schemes that are able to code operational knowledge. The complex requirements of many modern applications demand for flexible/adaptable devices that can quickly react to changing circumstances as solution. Today's complicated machine tools, manufacturing cells and systems require systematic methods of monitoring, control and fault diagnostics. Neural network systems promise this capability. Process modeling and optimization are very important issues in manufacturing engineering. Abrasive flow machining process is too complicated to warrant appropriate analytical models and most of the time, analytical models are developed based on many simplified assumptions, which contradict reality. More importantly, it is sometimes difficult to adjust the parameters of the above mentioned models according to the actual situation of the machining process [58]. Because of the complexity of AFM process, the optimization as well as the optimal control is difficult to perform. Neural networks provide significant advantages in solving machining problems that require real-time encoding and interpretation of relationships among variables of high dimensional space. Neural networks have been shown to be effective for modeling complex non-linear processes. Unlike techniques such as non-linear regression, neural networks do not require a priori assumption of the functional form of the model (linear, polynomial and so on). Therefore, neural networks which can map the input/output relationships and possess massive parallel computing capability, have attracted attention in research.

Recently, neural networks have been applied in precision manufacturing to predict some machining phenomenon as well as machining quality. Chryssolouris and Guillot [59] modeled the machining processes by a multiple regression method and neural networks, and concluded that neural networks are superior to conventional multiple regression methods Rangwala and Dornfeld [60] presented a scheme that used a multilayered perceptron neural network to model the turning process and an augmented Lagrange multiplier method to optimize the material removal rate (MRR). A simple neural network model for grinding mode identification and surface quality prediction in grinding of silicon nitride is also established by Zouaghi and Ichida [61]. Sathyanarayan et al [62] used a neural network model to study creep feed grinding of super alloys, but the optimization was done analytically using an off -line multi-objective programming technique Liao and Chen [58] showed how multi-layer perceptron (MLP) networks can be used to model and optimize grinding processes. In their work, a generalized four-layer perceptron network was trained with the standard back propagation (BP) algorithm to model the process and a Boltzman factor was integrated with the BP algorithm for process optimization

It is the intent of this chapter to realize ways to evaluate accomplishment and performance of neural network in modeling and optimization of AFM process. In this chapter, architecture of neural network for prediction of material removal rate and surface roughness in AFM process is presented. First, a generalized back-propagation neural network is used to establish the process.model. The modeling phase is followed by an optimization phase, during which the network predicts the input conditions to be used by AFM process to maximize material removal rate subject to appropriate operating constraints on surface roughness and process parameters. The optimization of the AFM process is also done using genetic algorithm.

## 6.2 Overview of Neural Networks

Neural networks are developed to model the way in which the human brain performs a particular task, or process information. A neural network is a massively parallel distributed processor that has a natural propensity for storing experiential knowledge and making it available for use. The central motivation underlying the development of artificial

acquired and stored over time through the use of adaptive learning algorithms [63]. It resembles the brain in two respects :

1 Knowledge is acquired by the network through a learning process.

2 Interneuron connection strengths known as synaptic weights are used to store the knowledge.

A neural network is defined by three features. topology, functionality, and learning Topology refers to the number of layers, number of nodes in each layer, and the way nodes are connected. Functionality refers to the transfer function and discriminatory function (if any) of each node, and the cost function of the network outputs Learning refers to the learning algorithm and the values of learning parameters (e.g. learning rates, and momentum). Learning rules specify an initial set of weights and indicate how weights should be adapted during use to improve performance of the neural network system

Neural networks can be classified differently according to different criteria : the type of learning (supervised, unsupervised, self supervised), the mode of operation (on-line, off-line), the network interconnection architecture (feedforward, feedback, recurrent), the number of layers, the learning algorithm (Hebbbian, back-propagation, resonant, Widrow-Hoff, simulated annealing), and the type of data processed (binary, discrete, continuous, fuzzy).

The most popular neural network topology is feedforward networks, viz. multilayer perceptron (MLP). The back-propagation (BP) network is the most commonly used neural network because there exists a mathematically strict learning scheme to train the network and guarantee mapping between inputs and outputs. Therefore, MLP neural network with back-propagation algorithm is used in the present study for modeling and optimization of AFM process.

## 6.3 Back-Propagation Neural Network Model for AFM Process

Recently, it has been shown that multilayer perceptrons (MLP) neural networks are suitable for the modeling of manufacturing processes [58]. Multilayer perceptrons have been applied successfully to solve some difficult and diverse problems by training them in a supervised manner with a highly popular algorithm known as the error **back-propagation algorithm**. A multilayer perceptron has three distinctive characteristics [64].

1 The model of each neuron in the network includes a non-linearity at output end. The important point to emphasize here is that the non-linearity is smooth (i e , differentiable everywhere).

2 The network contains one or more layers of hidden neurons. These hidden neurons enable the network to learn complex tasks by extracting progressively more meaningful features from the input patterns.

3 The network exhibits a high degree of connectivity determined by the synapses of the network.

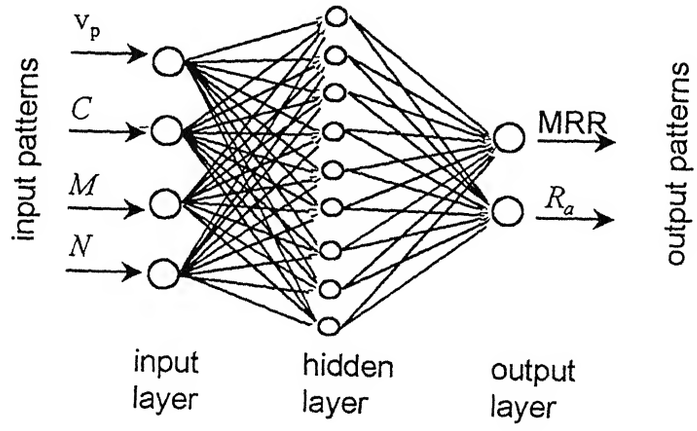


**Fig. 6.1 Structure of three layered neural network**

Back-propagation neural network [64] is usually referred to as feed forwarded, multilayered network with number of hidden layers (Fig. 6.1) trained with a gradient descent technique. This algorithm is based on the error correction learning rule. Basically, the error back-propagation process consists of two passes through the different layers of the network · a forward pass and a backward pass. In the forward pass, an activity pattern (input vector) is applied to the sensory nodes of the network, and its effect propagates through the network layer by layer Finally, a set of outputs is produced as the actual

response of the network During the backward pass, all synaptic weights are adjusted in accordance with the error correction rule Specifically, the actual response of the network is subtracted from the desired (target) response to produce an error signal. The synaptic weights are adjusted so as to make the actual response of the network move closer to the desired network

Let, $i$ and $j$ = Different neurons of the network

$w_{j,i,k}$ = Synaptic weight vector between neuron $j$ in layer ($k$-1) to neuron $i$ in layer $k$.

$v_{j,k}$ = Net internal activity levels of neuron $j$ in layer $k$.

$y_{j,k}$ = Function signals of the neuron $j$ in layer $k$.

The internal activity level $v_{j,k}$ is

$$v_{j,k} = \sum_{i=1}^{p} w_{j,i,k}\, y_{i,(k-1)} \tag{6.1}$$

where, $p$ is the total number of inputs applied to neuron $j$.

Assuming use of a logistic function for the sigmoidal nonlinearity, the function (output) signal of neuron $j$ in layer $k$ is

$$y_{j,k} = \phi_j(v_{j,k}) = \frac{1}{[1+\exp(-v_{j,k})]} \tag{6.2}$$

If neuron $j$ is in the first layer, $y_{j,1} = x_j$

and if neuron $j$ is in the output layer, $y_{j,k} = o_j$

where $x_j$ is the $j$th element of the input vector $x$ and $o_j$ is a function signal of the neuron j in the output layer.

The average of the instantaneous sum of the squared errors of the network

$$\varepsilon = \frac{1}{2}\sum_{j=1}^{q} e_j^2 = \frac{1}{2}\sum_{j=1}^{q}[d_j - o_j]^2 \tag{6.3}$$

where $q$ is the total number of output nodes. $d_j$ is the $j$th element of the desired response, $d$.

The back-propagation algorithm applies a correction $\Delta w_{i,j}$ to synaptic weights $w_{i,j}$, as given below.

$$\Delta w_{i,j} = \eta \delta_j y_i \tag{6.4}$$

where $\eta$ is a constant and it is called learning rate parameter of the back propagation algorithm.

The local gradient $\delta$ of the network, obtained by proceeding backward layer by layer, is given as

$$\delta_{j,k} = e_j o_j (1-o_j) \tag{6.5}$$

for neuron $j$ in the output layer.

$$\delta_{j,k} = y_{j,k}(1-y_{j,k})\sum_j \delta_{j,k+1} w_{j,i,k+1} \tag{6.6}$$

for neuron $j$ in the hidden layer $k$.

A simple method of increasing the rate of learning and yet avoiding the danger of instability is to modify the delta rule by including a momentum term [65]. Then,

$$\Delta w_{i,j}(n) = \alpha\, w_{i,j}(n-1) + \eta \delta_j y_j(n) \tag{6.7}$$

where $\alpha$ is usually a positive number called 'momentum constant'. n is the number of training pattern presented to the network.

The computation is iterated by presenting the new set of training examples to the network until the free parameters of the network stabilize their values and the average squared error computed over the entire training set is at a minimum or acceptably small value.

## 6.4 Optimization Using Neural Network

Nonlinear constrained programming is a basic tool in the systems where a set of design parameters is optimized subject to inequality constraints. The goal of this section is to propose a parallel structure, one that parallels the conventional optimization algorithm to solve this problem The key point in the optimization phase is to find the partial derivatives of the cost function with respect to the input data, not the partial derivatives of error with respect to the parameters of the network as in the modeling phase. Further, the process optimization is assured by minimizing a cost function L subject to the given constraints.

The constraints on input variables are

$$x_i(\min) \le x_i \le x_i(\max) \qquad (i = 1, p) \tag{6.8}$$

and the constraints on the output variables are

$$g_j(x) = (d_j - y_j) \le 0 \qquad (j = 1, q) \tag{6.9}$$

where $x_i$ (min) and $x_i$ (max) are the minimum and maximum values of the input variables $x_i$, respectively In AFM process, the constraint is on surface roughness.

In the simulation model presented below, the augmented Lagrange multiplier (ALM) method [66] is adapted to solve the above problem.

According to ALM method, the pseudo-objective function is given as

$$A(x, \lambda, r_p) = L(x) + \sum_j \lambda_j \{g_j(x) + s_j^2\} + r_p \{g_j(x) + s_j^2\}^2] \tag{6.10}$$

where $s_j$ are slack variables added to inequality constraints; $\lambda$ is the Lagrange multiplier; and $r_p$ is a penalty parameter.

$$A(x, \lambda, r_p) = L(x) + \sum_j \lambda_j \phi_j + r_p \phi_j^2] \tag{6.11}$$

where, $\phi_j = \max \{ g_j(x), -\frac{\lambda_j}{2 r_p} \}$.

The upgrade formula for $\lambda_j$ is

$$\lambda_j^{p+1} = \lambda_j^p + 2 r_p \phi_j . \tag{6.12}$$

The differentiation of the pseudo-objective function (given above) is obtained as

$$\frac{\partial A}{\partial x_i} = \frac{\partial L}{\partial x_i} + \sum_j R_j (\lambda_j + 2 r_p \phi_j) \frac{\partial g_j}{\partial x_i} \tag{6.13}$$

where $R_j = 1$ if $g_j(x) > -\frac{\lambda_j}{2 r_p}$

$= 0$ otherwise

The partial derivatives of L and $g$ can be calculated by using back-propagation algorithm. The amount of change in initial input values is proportional to the derivative of the objective function

$$\frac{\partial A}{\partial y_i} = \beta \sigma_{i,k} \frac{\partial A}{\partial y_j} \tag{6.14}$$

where $\beta$ is a parameter, which decides the rate of change in initial input values. The gradient $\sigma_{i,k}$ of the network, obtained by proceeding backward layer by layer, is given as

$$\sigma_{i,k} = \sum[w_{i,j,k}\, y_{j,k}\ (1-y_{j,k})] \qquad \text{for } (k-1)\text{th layer} \tag{6.15}$$

$$\sigma_{i,k-1} = \sum[\sigma_{i,k}\, w_{i,j,k-1}]\, y_{j,k-1}(1-y_{j,k-1}) \text{ for lower layers.} \tag{6.16}$$

For the first layer, $\dfrac{\partial A}{\partial y_i} = \dfrac{\partial A}{\partial x_i}$ (6.17)

The backward pass starts at the output layer by passing the change in objective function signals leftward through the network, layer by layer, and the recursively computing gradient $\sigma$, for each neuron. The recursive process permits the input of the network to undergo change in accordance with the analysis. The process is continued, until the input of the network stabilizes their values and the change in objective function value is at a minimum or acceptably small value.

In AFM process, the cost function $L(x)$, which is to be minimized, is negative of the material removal rate and constraint $g(x)$ is on the surface roughness, which should be less than or equal to maximum allowable surface roughness.

The solution to the above problem is a locally optimal set of process input variables. The optimization by neural network is simply an optimization procedure with two important differences: no assumption of an input-output model is made, and the optimization procedure is made in parallel.

## 6.5 Optimization Using Genetic Algorithms

Optimization of AFM process has also been carried out by genetic algorithm **to compare the results of optimization by neural network.** Even though the traditional or classical optimization algorithms [66,67] have been extensively used in many engineering design and decision-making problems, there are a number of shortcomings. Most of the popular methods require the gradient information, which may not be easy to calculate (or not available at all) in many real-world problems. Moreover, most of the traditional methods may converge to a locally optimal solution which may be very different from the actual global optimal solution. Further, none of these methods can be applied to a wide variety of problems. In order to alleviate some of these problems, a couple of non-traditional search and optimization algorithms - genetic algorithms and simulated annealing - are finding wide spread applicability in engineering design and decision making problems.

These methods work according to the principles of natural phenomenon and found to have successfully solved many non-linear programming (NLP) problems to a global optimality [68] In the next section, we describe the introduction and working principles of genetic algorithms

### 6.5.1 Introduction to genetic algorithms

Genetic Algorithm (GA) can be understood as an "intelligent" probabilistic search algorithm which can be applied to a variety of combinatorial optimization problems. The theoretical foundations of GAs were originally developed by Holland [69]. GAs are based on the evolutionary process of biological organisms in nature [70]. During the course of evolution, natural populations evolve according to the principles of natural selection and "survival of the fittest" Individuals which are more successful in adapting to their environment will have better chance of surviving and reproducing, whilst individuals which are less fit will be eliminated. This means that the genes from the highly fit individuals will spread to an increasing number of individuals in each successive generation. The combination of good characteristics from highly adapted ancestors may produce even more fit offspring. In this way, species evolve to become more and more well adapted to their environment.

### 6.5.2 Genetic algorithms - working principle

As described in the preceeding section, Genetic Algorithms are search and optimization procedures that are motivated by the principles of natural genetics and natural selection. Some fundamental ideas of genetics are borrowed and used artificially to construct search algorithms that are robust and require minimal problem information. Consider a typical unconstrained single variable optimization problem, which can be stated as [70]:

Maximize: $f(x)$ (6.18)

Variable bounds: $x_{\min} \leq x \leq x_{\max}$

In order to use GAs to solve the above problem, the variable $x$ is typically encoded into a string or *chromosome* structure which represents a possible solution to the given

problem. Binary coding is mostly used and the length of the string is usually determined by the accuracy of the solution desired For example, if five bit binary strings are used to code the variable $x$ then the string (0 0 0 0 0) is decoded to the value $x_{min}$, the string (1 1 1 1 1) is decoded to the value $x_{max}$, and any other string is decoded to a value in the range ($x_{min}$, $x_{max}$) uniquely. Thus, with five bit strings used to code the variable $x$, there will be a total of $2^5$ or 32 different strings that are possible, and the accuracy between two consecutive strings will be ($x_{max}$ - $x_{min}$)/32. If more accuracy is desired longer strings can be used. With a known coding, any string can be decoded to a $x$ value, which can be used to find the objective function value. A string's objective function value ($f(x)$) is called as the string's *fitness*. A pseudo code for a simple genetic algorithm is given in Figure 6 2. GAs begin with a population of strings (individuals) created at random [70]. Fitness of each individual is evaluated with respect to the given objective function. Then this initial population is operated by three main operators - *reproduction*, *crossover*, and *mutation* - to create hopefully a better population Highly fit individuals or *solutions* are given opportunities to reproduce by exchanging pieces of their genetic information, in a crossover procedure, with other highly fit individuals. This produces a new "offspring" solutions (i.e. *children*), which share some characteristics taken from both the parents. Mutation is often applied after crossover by altering some *genes* (i.e. bits) in the strings. The offspring can either replace the whole population (*generational* approach) or replace less fit individuals (*steady-state* approach). This new population is further evaluated and tested for some termination criteria. If the termination criteria are not met, this reproduction-crossover-mutation-evaluation cycle is repeated until the termination criteria are met. One cycle of these three operators and evaluation procedure is called a *generation* in GA terminology. Before discussing the application of genetic algorithms to the present work, let us briefly discuss these three GA operators for a better understanding of the GAs.

Reproduction selects the good strings in a population and forms a mating pool for the subsequent crossover. There exist a number of reproduction operators in GA literature, but the essential idea is that above average individuals are picked from the current population and duplicates of them are inserted in the mating pool. The commonly used reproduction operators are proportionate selection with roulette-wheel and tournament selection.

```
Begin
    Initialize population;
    Evaluate population;
    repeat
        Reproduction;
        Crossover;
        Mutation;
        Evaluate population;
    until (termination criteria);
end.
```

**Fig. 6.2 A Pseudo-code for a Simple Genetic Algorithm (SGA)**

Crossover operator is applied next to the strings in the mating pool. Here, two strings are picked at random from the mating pool and some portion of the information is exchanged between the strings. For example, in a single point crossover operator, this is performed by randomly choosing a crossing site along the string and by exchanging all bits on the right side of the cross site. In order to preserve some good strings found in the mating pool, not all strings in the population are used in crossover. If a crossover probability of $p_c$ is used, then ($p_c$×100)% of strings are used for crossover and the rest of the strings are simply copied to the new population.

Mutation changes a 1 to a 0 and vice-versa with a small mutation probability $p_m$ The need for mutation is to keep diversity in the population. For example, if in a particular position along the string length all strings in the population have a value 0, and a 1 is needed in that position to obtain the optimum then neither reproduction nor crossover will be able to create this. But mutation introduces some probability of turning that 0 into a 1. Furthermore, mutation may be found useful for local improvement of a solution.

### 6.5.3 Optimization of AFM process

The problem of optimization of AFM process can be described as minimizing or maximizing an objective function subject to a certain set of constraints. In the present analysis, the objective function is maximization of material removal rate (MRR), which is defined in terms of process variables. The process variables in the present case are average piston velocity ($v_p$), percentage concentration of abrasives ($C$), mesh size of grains ($M$) and number of cycle ($N$) In order to limit the search space, constraints in the form of lower and upper bounds on the process variables are imposed.

The equations given by Adsul [19], for predictions of MRR and surface roughness, were used here for optimization of AFM process. These models have been developed by multi variable regression analysis (MVRA). To estimate the regression coefficients, the method of least squares has been employed. The material removal rate (MRR) in g/min can be expressed as [19]

$$MRR = 5.285 \times 10^{-10} (v_p)^{1.6469} (C)^{3.0776} (M)^{-0.9371} (N)^{-0\ 1893} \quad (6.19)$$

The surface roughness ($R_a$) in $\mu$m can be expressed as

$$R_a = 2.8275 \times 10^{5} (v_p)^{-1\ 8221} (C)^{-1.3222} (M)^{0.1368} (N)^{-0.2258} \quad (6.20)$$

The problem of optimization of AFM process can be described as maximizing MRR subject to a certain set of constraints on surface roughness and input variables.

In order to use GA, the constrained optimization problem is stated as follows:

Maximize: MRR (6.21)

Subject to: $R_a \le R_{a\max}$ (6.22)

$$x_i^l \le x_i \le x_i^u$$

where $x_i^l$ and $x_i^u$ are the lower and upper bounds on the process variable $x_i$.

A Simple Genetic Algorithm code was used in the present study. The steps involved in the optimization using GA of AFM process can be stated as follows:

**STEP 1:** The GA parameters are initialized. This involves specifying the population size, maximum number of generations, string length of each variable, crossover and mutation

probabilities etc Upper and lower limits on each of the process variables are also specified The generation number is initialized to 0

**STEP 2:** An initial feasible random population is generated

**STEP 3:** The fitness of each individual in the population is evaluated.

**STEP 4:** Once the fitness of all the individuals is available, GA operations are performed, e g. reproduction, crossover, and mutation. Now, a new set of process variables is created which possibly is better than that of the previous generation. This completes one generation.

**STEP 5:** The generation number is incremented. If the current generation number is greater than the maximum number of generations, then the process is terminated. Otherwise, process is repeated from step 3.

## 6.6 Experimentation

Machining experiments were carried out by Adsul [19] on a set-up of AFM machine using aluminum as workpiece material. The media was a mixture of putty and silicon carbide abrasive particles. Experiments were designed and conducted for various sets of process variables, i.e. average piston velocity, abrasive concentration, abrasive mesh size and number of cycles. For performing these experiment compositions of different abrasive mesh sizes (100 to 240) and having different abrasive concentrations (33 to 45 %) were prepared. Percentage concentration of abrasives is defined as the ratio of weight of abrasives and total weight of abrasive media (abrasives +carrier) multiplied by 100. The piston velocity range chosen was from 40 to 85 cm/min. Average material removal rate (MRR) over test duration was measured. In these experiments, the effect of various process parameters on surface roughness and material removal rate were studied. The data collected from these experiments have been used to train the neural network and to test the validity of the present model. The details of experimental results used in this paper are given in Appendix D.

## 6.7 Simulation Procedure

The objective of the simulation using neural network was to first have the system learn the appropriate mappings between input and output variables by observing the training samples. The trained system was then used to determine the input conditions that maximizes material removal rate (MRR) subject to certain constraints. The three layer back-propagation with four inputs, two outputs and nine hidden nodes was employed for neural network. The network was trained using 25 samples that span the allowable ranges of input variables. Due to limited number of data available in the work by Adsul on **AFM experiments** restricted us to take only 25 data points in this study. The inputs were average piston velocity ($v_p$), percentage concentration of the abrasives ($C$), abrasive mesh size ($M$) and number of cycles ($N$), and outputs were material removal rate (MRR) and surface roughness ($R_a$). A random generator was used to initialize the values of the learning parameter. In order to decide the structure of neural network, the rate of error convergence was checked by changing the number of hidden layers and also by adjusting the learning rate and momentum rate. As a result, a neural network with nine neurons in the hidden layer was adopted for storing knowledge in the form of weights between neurons. The simulation results for the initial training indicate (Fig. 6.3) that it takes about 4000 iterations for the root mean error to reduce to 2%.

A crucial problem in back-propagation is its generalization ability. There is no certainty that the network successfully trained on the given samples provides desired input/output associations for untrained pattern as well. Concerning this problem, some authors [71] showed experimentally and mathematically that the generalization capability could remarkably be enhanced by training the network with **noise injected inputs**. The addition of random noise allows the system to jump out of the local minima that may trap it in a high error state. In the present simulation, the network was trained by both noiseless data and noise injected data. Fig. 6.4 shows five different cases studied, and explanation of different abbreviations used. For example, abbreviation NioNi indicates that network was trained with noisy data (ie noise is added in both inputs and outputs), and prediction is also for noisy input. In the Fig. 6.4, information after first capital letter follows for training data

and that after second capital letter follows for prediction data It is seen that the root mean percentage error is almost the same for various cases for low percentage of noise However, it increases rapidly with the increase in percentage noise except for the case of NiNi which means training with noisy input variables and prediction for noisy input It is observed that for the same parameters of the network, the total error with 2.5 percentage random noise injected inputs is lesser than the error obtained with noiseless inputs It is also found that training with 2 5 % noise injected inputs provides enhanced learning compared to noiseless input (Fig. 6.4) Variations is observed in the response of the network during learning but the difference between the two is not significant after about 4000 iterations. The number of iterations required to achieve same amount of error in noise injected learning is less than the number of iterations required in noiseless learning. For example, for 2.0 % error, number of iterations required with noiseless input are 3710, while with 2.5% noise injected input, it is only 3390 (Fig 6.4). Thus, noise control method consistently produced faster learning than standard back-propagation

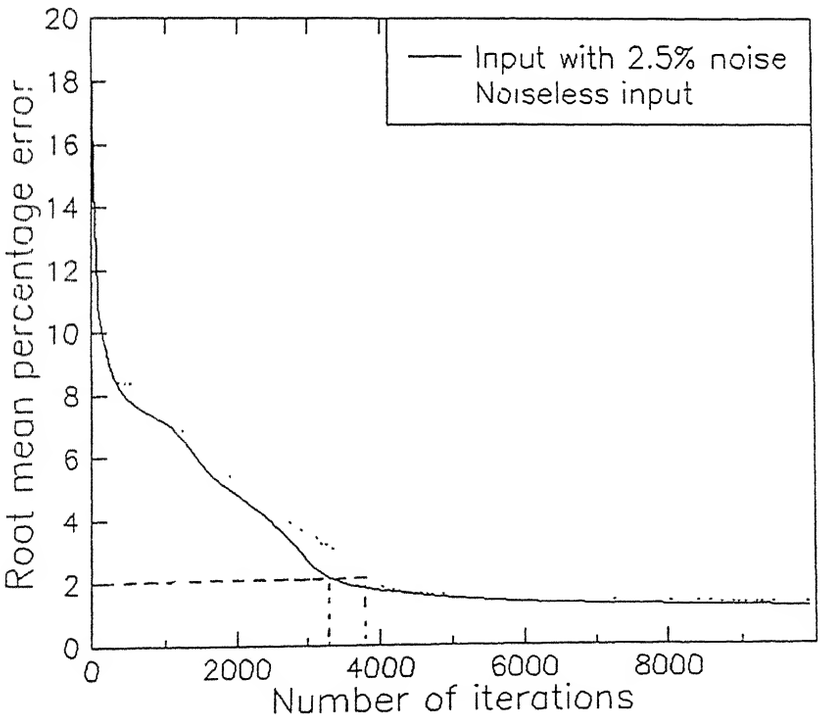


**Fig. 6.3 Variation of root mean percentage error with number of iterations**

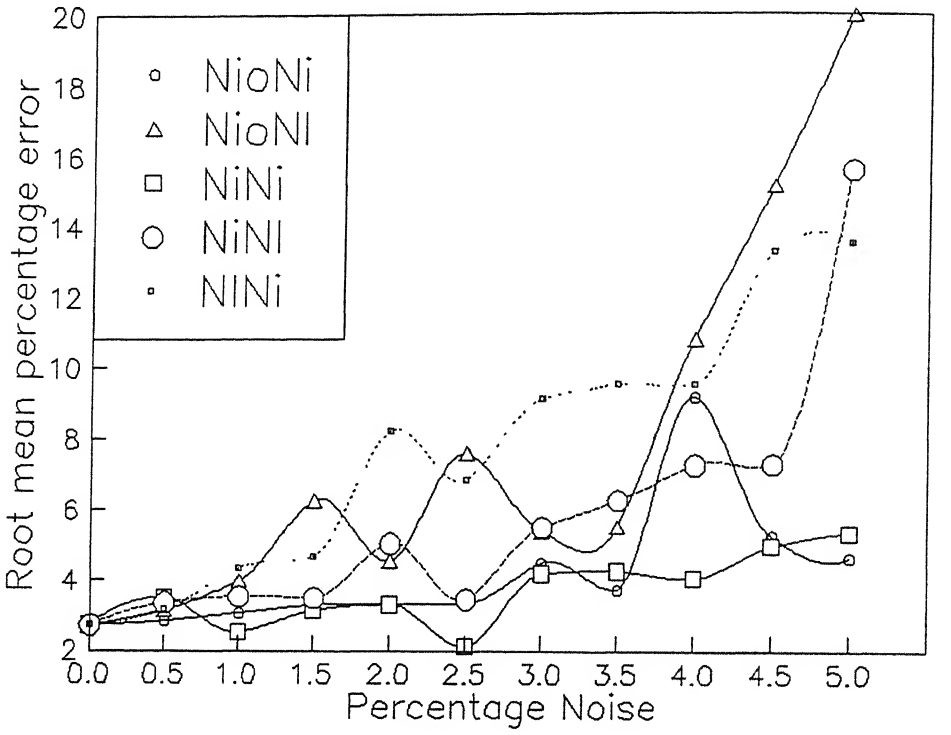


**Fig. 6.4 Effect of noise in back propagation learning.**

NioNi · Training with Noisy input and output, and prediction using Noisy input.

NioNI : Training with Noisy input and output, and prediction using Noiseless input

NiNi · Training with Noisy input, and prediction using Noisy input.

NiNI : Training with Noisy input and prediction using Noiseless input.

NINi . Training with Noiseless input and prediction using Noisy input.

## 6.8 Results and Discussion

The experimental results have been compared with the results computed using multi variable regression analysis (MVRA) (eqns. (6.19) and (6.20)), and those obtained by neural network discussed above. The MRR and surface roughness results predicted by simulation using neural network show a good agreement with the experimental results and the results obtained by the MVRA models (Fig. 6.5-6.11) for a wide range of operating conditions. Variation of surface roughness with number of cycles (Fig. 6.9) indicates that

error in prediction is higher at lower number of cycles At higher value of number of cycles, predictions by neural network are in good agreement with experimental values. A comparison of results predicted by the present neural network model and regression model also revealed that absolute percentage error in prediction of untrained data by neural network model was from 0.25 % to 8.95 %, whereas it was from 0.09 % to 25 % in results predicted by multi variable regression analysis

Next, the network has been used to determine a set of optimal inputs. In the present case of optimization of AFM process, the cost function, L(x) which is to be minimized, is the negative of material removal rate (MRR) and constraint $g(x)$ is on the surface roughness obtained, which should be less than or equal to the maximum allowable surface roughness, $R_{a\max}$ . The cost function is given as

$$L(x) = - MRR \tag{6.23}$$

subject to inequality constraints

$$g(x) = R_a \leq R_{a\max} \tag{6.24}$$

According to the experimental set-up and workpiece used, the limits on the input variables are as follows :

$40.0 \leq v_p \leq 85.0$

$33.0 \leq C \leq 45.0$

$100.0 \leq M \leq 240.0$

$20.0 \leq N \leq 120.0$

Table 6.1 shows the optimal inputs synthesized by the network for different values of constraint on surface roughness.

In order to optimize the present problem using GA, the following parameters has been specified by practice, to get optimal solutions with less computational effort.

Population size = 50

Max. number of generations = 200

Total string length = 40

Cross over probability = 0.8

Mutation probability = 0.01

The optimal inputs and corresponding values of outputs obtained by GA are presented in Table 6 2. The results obtained by neural network approach and genetic algorithm are very close. It indicates that the network possesses sufficient knowledge in order to perform optimization.

**Table 6.1 Optimization results of the network**

| No | $R_{a\max}$ | optimal inputs | | | | optimal outputs | |
|---|---|---|---|---|---|---|---|
| | $\mu$m | $v_p$ cm/min | $C$ | $M$ | $N$ | $R_a$ $\mu$m | MRR mg/min |
| 1 | 0 7 | 85.00 | 44.92 | 101.90 | 20.78 | 0.625 | 0 716 |
| 2. | 0 6 | 84 60 | 44 38 | 100.44 | 21.46 | 0 590 | 0 692 |
| 3 | 0 5 | 83.59 | 44 80 | 101.17 | 33.78 | 0.500 | 0.635 |
| 4. | 0 4 | 84 25 | 44.56 | 101.76 | 54.40 | 0.392 | 0 538 |
| 5 | 0.3 | 85.00 | 44.88 | 101.03 | 119.70 | 0.289 | 0.516 |

**Table 6.2 Optimization results of the genetic algorithm**

| No. | $R_{a\max}$ | optimal inputs | | | | optimal outputs | |
|---|---|---|---|---|---|---|---|
| | $\mu$m | $v_p$ cm/min | $C$ | $M$ | $N$ | $R_a$ $\mu$m | MRR mg/min |
| 1. | 0.7 | 84 69 | 44.45 | 100.88 | 21.09 | 0.607 | 0.697 |
| 2. | 0.6 | 84.82 | 44.97 | 101.02 | 25.47 | 0.553 | 0 695 |
| 3. | 0.5 | 84.95 | 45.00 | 102.05 | 33.00 | 0.490 | 0.669 |
| 4. | 0.4 | 85.00 | 44.74 | 100.43 | 63.4 | 0.370 | 0.580 |
| 5. | 0.3 | 84.95 | 44.96 | 101.02 | 111.13 | 0.288 | 0.525 |

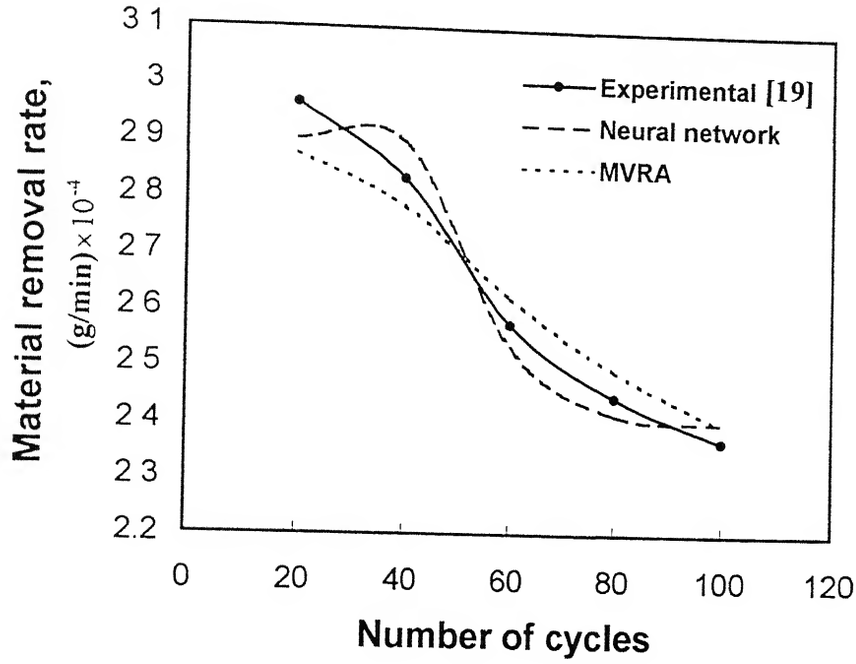


**Fig. 6.5 Effect of number of cycles on material removal rate**

**($C$ = 45%, $v_p$ = 51.5 cm/min, $M$ = 100)**

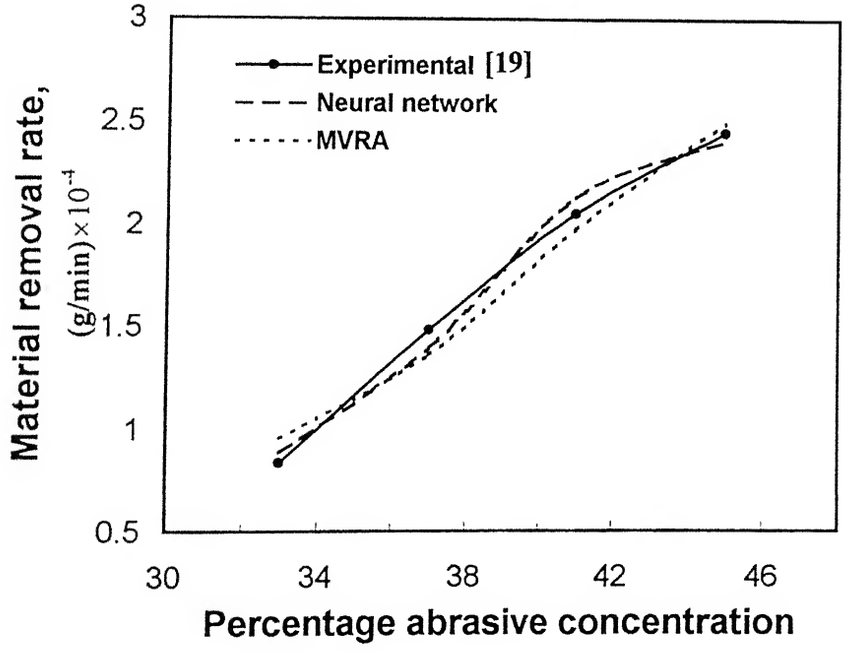


**Fig. 6.6 Effect of percentage abrasive concentration on material removal rate**

**( $v_p$ = 51.5 cm/min, $M$ = 100, $N$ = 80)**

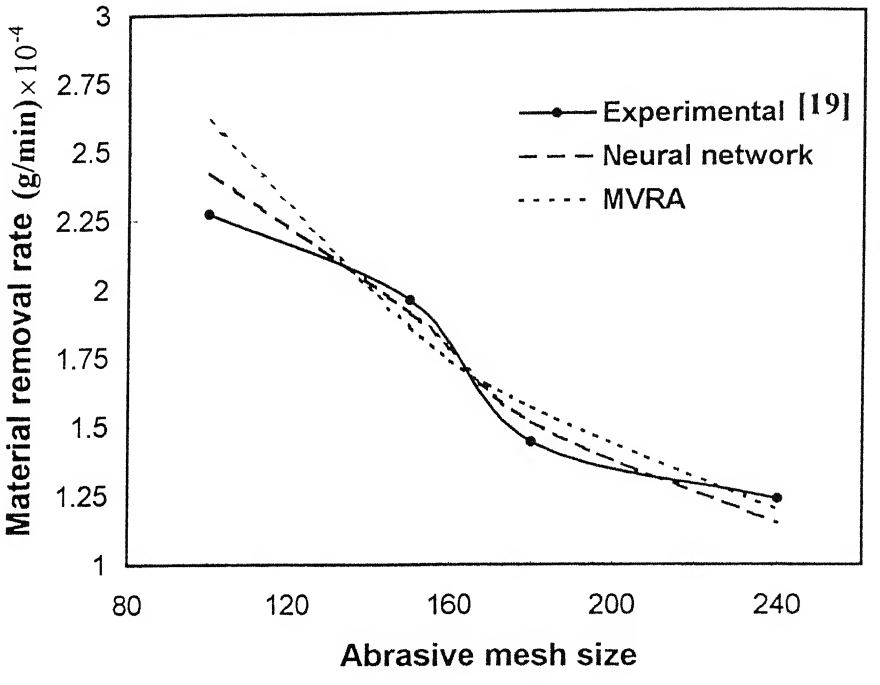


**Fig. 6.7 Effect of abrasive mesh size on material removal rate**

**($C$ = 45%, $v_p$ = 51.5 cm/min, $N$ = 50)**

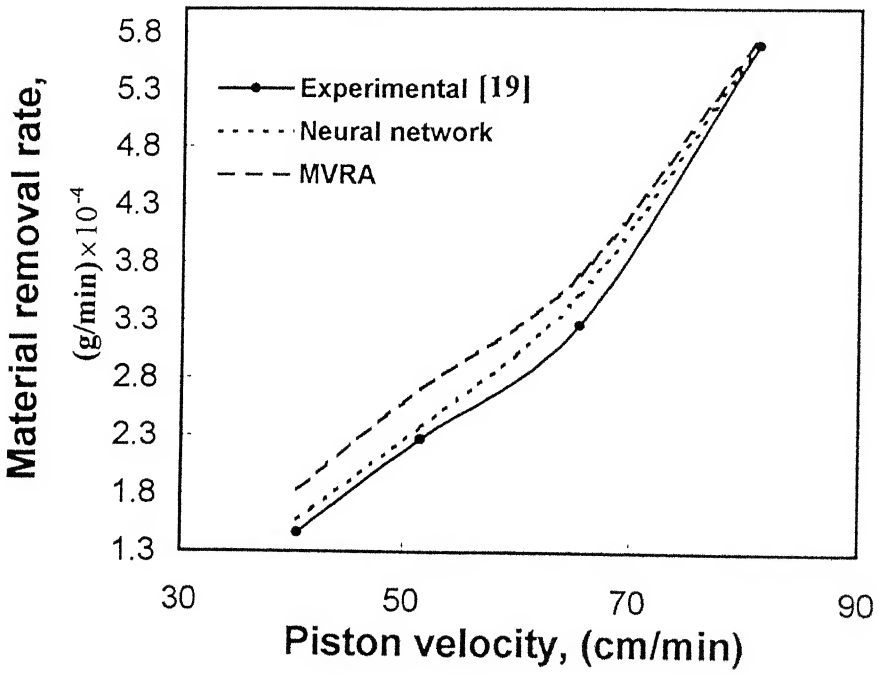


**Fig. 6.8 Effect of piston velocity on material removal rate**

**($C$ = 45%, $M$ = 100, $N$ = 50)**

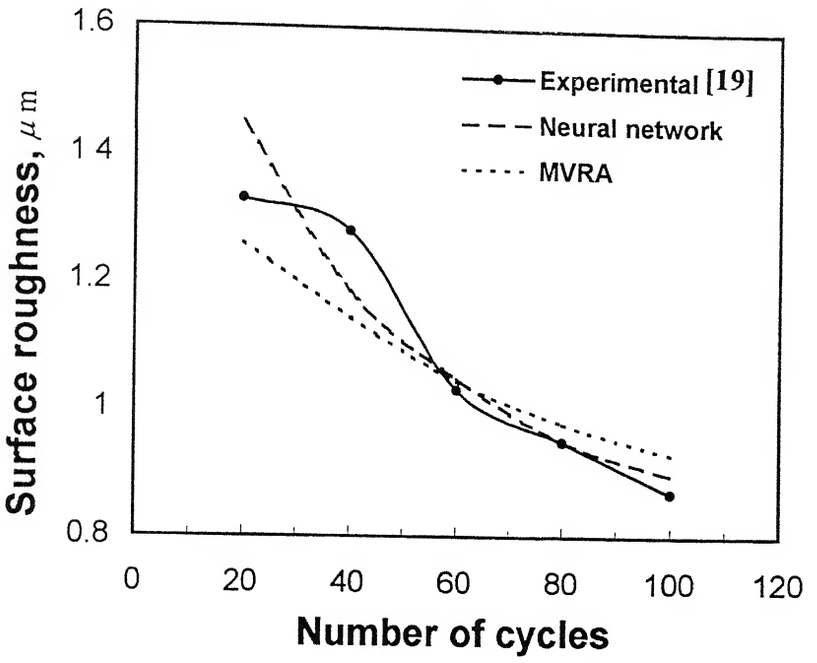


**Fig. 6.9 Effect of number of cycles on surface roughness**

**($C$ = 45%, $v_p$ = 51.5 cm/min, $M$ = 100)**

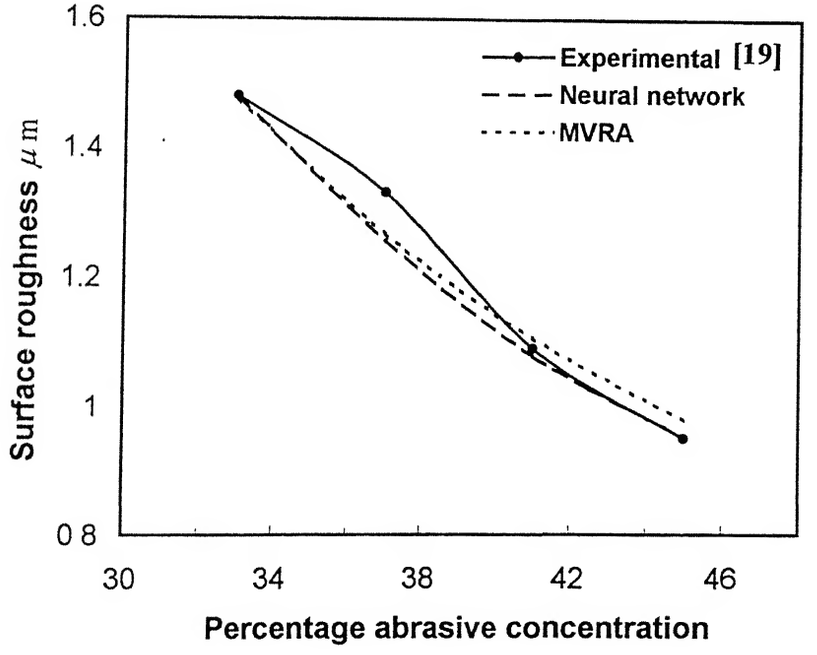


**Fig. 6.10 Effect of percentage concentration on surface roughness**

**($v_p$ = 51.5 cm/min, $M$ = 100, $N$ = 80)**

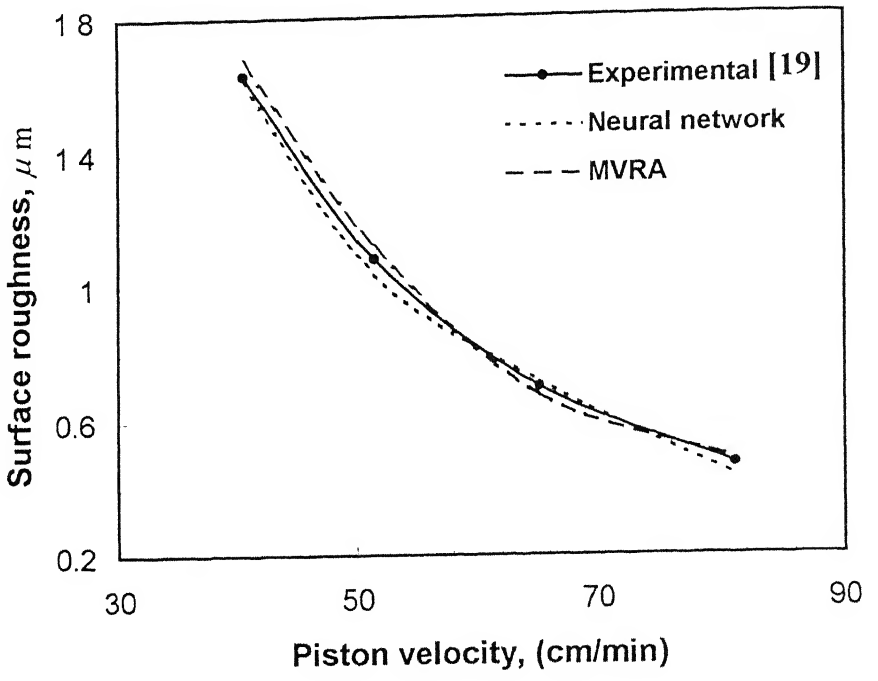


**Fig. 6.11 Effect of piston velocity on surface roughness**

**($C$ = 45%, $M$ = 100, $N$ = 50)**

## 6.9 Conclusions

In this chapter, the effectiveness of using back-propagation neural network for process modeling and optimization of abrasive flow machining process has been demonstrated. Simulation results show a good agreement with experimental results for a wide range of machining conditions. The optimization results of the neural network also coincide well with the results obtained by genetic algorithm. Based on the simulation and optimization results, the following conclusions can be drawn .

1 The possibility of using this neural network model for machined surface quality and material removal rate prediction for AFM process has been confirmed.

2. It is observed that learning could remarkably be enhanced by training the network with noise injected inputs

3 Appropriately trained neural network successfully synthesizes optimal input conditions for AFM process. The optimal input conditions maximize the material removal rate, subject to appropriate process constraints.

4 An important consideration is that process optimization can be performed in the absence of process models and purely by observations of experimental information.

5 The discussed neural network system is fairly general and can be extended to other abrasive processes to improve machining efficiency.

# Chapter 7

# Conclusions and Scope for Future Work

## 7.1 Conclusions

The present thesis work comprises both experimental and theoretical investigations. Experiments have been conducted to study the influence of the process parameters on the process performance. A model has been proposed for analysing the media flow in AFM process through media cylinder and workpiece, and solved by finite element method. A model for the prediction of material removal and surface roughness in AFM has also been presented. The generation of surface profile and material removal in AFM have been simulated considering random distribution of abrasive grains in media and their interaction with workpiece surface profile during the process. Specific energy and thermal aspects of AFM have also been analysed. Further, the effectiveness of using back-propagation neural network for process modeling and optimization of AFM process has been demonstrated On the basis of above mentioned experimental and theoretical investigations, the following conclusions have been drawn:

### Experimental investigations

- AFM experiments on mild steel workpiece using SiC abrasives mixed with polyborosiloxane carrier indicate that AFM successfully reduces the surface roughness of workpieces. AFM performance can be easily controlled by varying the process parameters.
- An increase in extrusion pressure increases the depth of indentation of abrasives, and increase in percentage concentration of abrasives increases active grain density and

media viscosity, hence material removal and change in surface roughness are higher at higher extrusion pressure and concentration of abrasives in media

- The slug length of media flow in a stroke increases with increase in reduction ratio. Hence, material removal and change in surface roughness increase with increase in reduction ratio.

## Analysis of material removal and surface roughness in AFM

- A good agreement exists between the theoretical and experimental values of extrusion pressures at various values of piston velocities. It clearly indicates that the proposed flow model provides a reasonably good estimate of the flow characteristics involved in AFM process
- At a particular extrusion pressure, piston velocity is higher at lower angle of tooling. But the length of tooling increases with decrease in angle of tooling, $\alpha$. Hence, there is a need to determine the optimum angle of tooling for minimum extrusion power and machining time.
- The piston velocity increases linearly with extrusion pressure for a specified reduction ratio. At higher value of reduction ratio, the rate of increase in extrusion pressure is also higher. The normal stresses on the workpiece surface increase with increase in reduction ratio Finite element analysis of media flow has been carried out to predict the normal stresses at the workpiece surface.
- A model has been developed for prediction of material removal and surface roughness by applying abrasion theory. The model is based on accumulated plastic flow of workpiece material by repeated indentation by moving abrasive particles. Good agreement is found between the response surface analysis (RSA) and theoretical results.
- Material removal increases with extrusion pressure, reduction ratio and percentage concentration of abrasives for a specified number of cycles.
- Change in surface roughness ($\Delta Ra$) value increases with increase in extrusion pressure, percentage concentration of abrasives, and reduction ratio for a specified number of cycles.

## Simulation of surface generation in AFM

- The generation of surface profile and material removal in AFM have been simulated considering random distribution of abrasive grains in the media and their interaction with workpiece profile during machining. The results of the proposed simulation and RSA are in good agreement, which justifies the use of this approach for predicting the expected surface characteristics in AFM
- Two approaches to determine active grain density in media – first, optical microscope technique and second, stochastic simulation method have been proposed. The results of stochastic simulation method are in agreement with the data obtained by microscopic technique.
- Active grain density increases with an increase in abrasive concentration, and for a particular concentration, it is higher for a larger mesh number.
- The number of active grains per unit volume of media flow increases with percentage concentration of abrasives and reduction ratio, hence higher material removal and higher change in surface roughness are achieved.
- Extrusion pressure, grain mesh size and hardness of workpiece material affect the depth of indentation of a grain in the workpiece material. Change in surface roughness value and material removal increase with extrusion pressure, number of cycles, reduction ratio and percentage concentration of abrasives.
- A comparison of results predicted by theoretical model and simulation with RSA results reveals that results obtained from simulation are more close to RSA results than those obtained from the theoretical model. The original profile of the workpiece is taken to be Guassian in simulation, which is more close to the actual profile, than the triangular profile assumed in the theoretical model.

## Thermal aspects of AFM process

- Specific energy for AFM process (10-110 J/mm$^3$) is overlapping the range of specific energy for grinding (5-60 J/mm$^3$). This justifies that machining action of AFM compares to grinding.

- Specific energy remains constant with abrasive mesh size. Its value increases with increase in hardness of the workpiece material and decreases with increase in applied normal pressure.
- A simple model has been developed for heat transfer analysis in AFM process
- It is found that the major portion of heat, developed at media-workpiece interface, enters into the workpiece. Hence, rise in temperature of workpiece is higher than rise in temperature of media. It is also observed that rise in temperature of workpiece increases with increase in extrusion pressure and number of cycles.

## Application of neural network and genetic algorithm to AFM

- AFM process is too complicated to warrant appropriate analytical model which are generally based on many assumptions. Hence, the possibility of using this neural network model for machined surface quality and material removal rate prediction for AFM process has been confirmed.
- Appropriately trained network successfully synthesizes optimal input conditions for AFM process.
- Genetic algorithm has been successfully applied for optimization of AFM process. The optimization results of the neural network coincide well with the results obtained by genetic algorithm.

## 7.2 Scope for Future Work

In the present study, an attempt has been made to understand the mechanism of AFM process and its performance to a certain extent. Following are the areas in which further work can be carried out·

1 As the present investigations are confined to cylindrical surfaces only, there is a need to study other shapes like flat and complex surfaces.

2 AFM process is flexible in handling different types and shapes of tooling. Various types of tooling can be designed and experiments can be conducted for different shapes of workpieces especially for finishing complicated external shapes.

3. There is a need to develop a mechanical device for efficient and uniform mixing of abrasive grains in the media.

4. An extension of the theoretical model of media flow to three dimensional shapes and consideration of change in machining conditions of the AFM process with time are important issues that need to be investigated. Although the method has been defined for, and applied to, axisymmetric problems, the technique is easily extendible to three dimensional cases.

5. Investigations in the area of media development are also required The other material as carrier can be tested and developed economically.

6. For better understanding of the process, investigations in the area of media viscosity and its flow characteristics are needed.

7. As initial finish of the part is significant in AFM process, detailed study on this aspect will be of considerable interest for better understanding of the process.

8. There is further scope to extend this work to finish workpieces of hard materials like ceramics and glass.

9. The discussed neural network system is fairly general and can be extended to other abrasive processes to improve machining efficiency. The proposed off-line model can be applied for the on-line control of abrasive flow machining process.

10. Systematic modeling and analysis, optimum selection of process parameters, topography and micro-structural analysis of generated surface, abrasive grain wear phenomenon, and development of process control strategy are the main issues which need to be further investigated for continued developments and expended use of AFM process.
11. The major constraint in the present work is the constant abrasive mesh size Experiments should be conducted in future, with different mesh sizes to understand its effect on the material removal and surface finish. The effect of back pressure on material removal and surface finish can also be studied

# References


1. Subramanian K., Finishing methods using multipoint or random cutting edges, *Surface Engineering, ASM International,* **5**, 1994, 91-109.

2. Inasaki I., Tonshoff H.K. and Howes T. D., et al., Abrasive machining in future, *Annals of the CIRP,* **42**, 1993, 723-732.

3. Malkin S., *Grinding Technology - Theory and Applications of Machining with Abrasives,* John Wiley & Sons, 1989.

4. Ghosh A. and Mallik A. K., *Manufacturing Science,* East-West Private Limited, New Delhi, 1985.

5. Jeong-Du Kim and Min-Seog Choi, Stochastic approach to experimental analysis of cylindrical lapping process, *Int. J. Machine Tools Manufact.,* **35**, 1995, 51-59.

6. Hams Fischer and Joseph Byrenes, The fundamentals of honing, Technical paper, *Society of Manufacturing Engineers,* Dear born, 1994.

7. Lee J. and Malkin S., Experimental investigations of bore honing process, *Trans. ASME, J. Engineering for Industry,* **115**, 1993, 406-414.

8. Shinmura T., Takazawa K. and Hatano E., Study on magnetic abrasive finishing, *Annals of the CIRP,* **39**, 1990, 325-328.

9. Rhoades L. J., Abrasive flow machining with not-so-silly putty, *Metal Finishing,* July 1987, 27-29.

10. Rhoades L. J., Abrasive flow machining, *Manufacturing Engineering,* 1988, 75-78.

11. Rhoades L. J., Abrasive Flow Machining A case study, *J. Materials Processing Technology*, **28**, 1991, 107-116.

12. Studley N., Abrasive flow machining, *Proc. Int. Gas Turbine Congress held at Yokohama*, 1991, 311-316.

13. Przyklenk K., AFM - A process for surface finishing and deburring of workpieces with a complicated shape by means of an abrasive laden medium, *ASME, NewYork, PED*, **22**, 1986, 101-110

14 Kohut Tom, Surface finishing with AFM, *SME technical paper*, 1989, 35-43

15. Perry W.B., Abrasive Flow Machining - principles and practices, *Non-traditional conference proceedings* (special report- personal communication), 1989, 121-127.

16. Williams R. E. and Rajurkar K. P., Metal removal and surface finish characteristics in abrasive flow machining, in : Mechanics of deburring and surface finishing process, *ASME, New York; PED*, **38**, New York, 1989, 93-106.

17. Williams R. E. and Rajurkar K. P., Stochastic modeling and analysis of abrasive flow machining, *Trans. ASME, J. Engineering for Industry*, **114**, 1992, 74-81.

18. Loveless T. R., Williams R. E. and Rajurkar K. P., A study of the effects of abrasive flow finishing on various machined surfaces, *J. Materials Processing Technology*, **47**, 1994, 133-151.

19. Adsul S. G., *Experimental investigations into abrasive flow machining*, M. Tech. Thesis, Indian Institute of Technology, Kanpur, 1996.

20. Davies P.J., Fletcher A. J., The assessment of the rheological characteristics of various polyborosilixane/grit mixtures as utilized in the abrasive flow machining, *Proceedings of Instn. Mech. Engrs.*, **209**, 1995, 409-418.

21. Ranganatha C., *Evaluation of properties of media used in abrasive flow machining*, M. Tech. Thesis, Indian Institute of Technology, Kanpur, 1997.

22. Fletcher A. J. and Fioravant A., Polishing and honing processes : an investigation of the thermal properties of mixtures of polyborosiloxane and silicon carbide abrasive, *Proceedings of Instn. Mech. Engrs.*, **210**, 1996, 255-266.

23. Rajeshwar G., Kozak J. and Rajurkar K. P., Modeling and computer simulation of media flow in abrasive flow machining process, *Proceedings of the International Mechanical Engineering Congress and Exposition, Chicago, PED,* **68,** 1994, 965-971.

24. Jha Sunil, *On the abrasive flow machining process performance*, M. Tech. Thesis, Indian Institute of Technology, Kanpur, 1998.

25. William G. C. and Gertrude M Cox, *Experimental Designs*, Asia Publishing House, Bombay, 1977.

26. Zienkiwicz O. C., Jain P. C. and Onate E., Flow of solids during forming and extrusion : some aspects of numerical solutions, *Int. J. Solids Structures,* **14,** 1978, 15-38.

27. Dixit U.S. and Dixit P.M., An analysis of the steady-state wire drawing of strain-hardening material, *J. Materials Processing Technology,* **47,** 1995, 201-229.

28. Reddy V.N., Dixit P.M. and Lal G.K., Analysis of axisymmetric tube extrusion, *Int. J. Machine Tools Manufact.*, **36,** 1996, 1253-1267.

29. Crochet M. J., Davies A. R. and Walters K., *Numerical Simulation of Non-Newtonian Flow*, Elesvier, New York , 1984.

30. Kim-E. M. E., Brown R. A. and Armstrong R. C., The role of inertia and shear thinning in flow of an inelastic liquid through an axisymmetric sudden contraction, *J. Non-Newtonian Fluid Mechanics,* **13,** 1983,341-363.

31. Lim L. M. and Dunne F.P.E., Modeling central bursting in the extrusion of particulaqte reinforced metal matrix composite materials, *Int. J. Machine Tools Manufact.*, **37**, 1997, 901-915.

32. Wilson K. C., Addie G. R., Sellgren A. and Clift R., *Slurry Transport Using Centrifugal Pumps*, Blackie Academic and Professional, London, 1997.

33. Darby Ronald, *Viscoelastic Fluids*, Marcel Dekker Inc., 1976.

34. Zienkiwiewicz O. C. and Morgan K., *Finite Elements and Approximation,* Wiley, New York, 1983.

35. Reddy, J. N., *An Introduction to the Finite Element method*, McGraw Hill, New York, 1985.

36. Bathe K. J., *Finite Element Procedures in Engineering Analysis*, Prentice Hall of India, 1990.

37. Dawson Paul R. and Thompson Erik G., Finite element analysis of steady state elasto-visco-plastic flow by the initial stress rate method, *Int. J. for Numerical Methods in Engineering,* **12**, 1978, 47-57.

38. Khrushchov M. M. and Bavichev M. A., *Research on wear of metals,* Ch.8, NEL Translation No.893, National Engineering Laboratory, East Kilbride , 1960.

39. Graham D. and Baul R. M., An investigation into the mode of material removal in the grinding process, *Wear,* **19,** 1972, 301-314 .

40. Aghan R. L. and Samuels L. E., Mechanism of abrasive polishing, *Wear,* **16,** 1970,

41. Shaw M. C., A new theory of grinding, *Proc. Of the Institution's Conference on Production Science in Industry*, Melbourne, 1971, 73-78.

42. Rabinowicz E., Dunn L. A.and Russell P. G., A study of abrasive wear under three body conditions, *Wear*, **4,** 1961, 345-355.

43. Verkerk J., Final report concerning CIRP co-operative work on the characterization of grinding wheel topography, *Annals of the CIRP*, **26,** 1977, 385-394.

44. Jeong-Du Kim and Min-seog Choi, Simulation for the prediction of surface accuracy in magnetic abrasive machining, *J. Materials Processing Technology,* **53,** 1995, 630-642.

45. Shaw M. C., *Principles of Abrasive Processing,* Clarendon Press, Oxford, 1996.

46. Koshy P., Jain V. K. and Lal G.K., Stochastic simulation approach to modeling diamond wheel topography, *Int. J. Machine Tools Manufact.*, **37 (6)**, 1997, 751-761.

47. Yoshikawa H. and Sata T., Simulated grinding process by Monte Carlo method, *Annals of the CIRP*, **16**, 1968, 297-302.

48. Law S. S., Wu S. M. and Jogelkar A. M., On building models for the grinding process, *Trans. ASME, J. Engineering for Industry,* **95,** 1973, 983-991.

49. Hamed M. S., Whitehouse D. J. and Buttery T. C., Random surface generation - integrated approach, *Annals of the CIRP*, **27**, 1978, 499-504.

50. Bhateja C. P., An enveloping profile approach for the generation of ground surface texture, *Annals of the CIRP*, **25**, 1971, 333-337.

51. Staffan Jacobson, Per Wallen and Sture Hogmark, Fundamental aspects of abrasive wear studied by a new numerical simulation model, *Wear,* **123,** 1988, 207-223..

52. Wang Y., An analysis of the influence of plastic indentation on three body abrasive wear of metals, *Wear,* **212,** 1988, 123-133.

53. Nakayama K. and Shaw M. C., Method of determining effective number of cutting points per unit area, *Proc. Inst. Mech. Engineers,* **68,** 1967, 182-191.

54. Chen Xun and Brian Rowe W., Analysis and simulation of the grinding process. Part II : Mechanics of grinding, *Int. J. Machine Tools Manufact.,* **36,** 1996, 883-896.

55. Adrienne S. Lavine, A simple model for convective cooling during the grinding process, *Trans. ASME, J. Engineering for Industry,* **110,** 1988, 1-68.

56. Sadick Kakac and Yaman Yener, *Heat Conduction,* Taylor and Francis, Washington, 1993.

57. Kannappan S. and Malkin S., Effect of grain mesh size and operating parameters on the mechanics of grinding, *Trans. ASME, J. Engineering for Industry,* **94,** 1972, 833-842.

58. Liao and Chen L. J., A neural network approach for grinding processes : modeling and optimization, *Int. J. Machine Tools Manufact.,* **34,** 1994, 919-928.

59. Chryssolouris G. and Guillot M., Modeling of machining processes using neural network, *Trans. ASME., J. Engineering for Industry,* **112,** 1990, 122-131.

60. Rangwala S. and Dornfeld D. A., Learning and optimization of machining operations using computing abilities of neural networks, *IEEE, Trans. on Systems, Man and Cybernetics,* **19,** 1990, 299-314.

61. Zouaghi N and Ichida Y., Grinding mode identification and surface quality prediction using neural networks in grinding of Silicon Nitride, *Int. J. Japan Soc. Prec. Eng.*, **30** 1996, 35-40.

62 Sathyanarayan G., Joseph L. I. and Ming-Kuen Chen, Neural networks modeling and multi-objective optimization of creep feed grinding of super alloys, *Int. J. Production Research*, **30**, 1992, 2421-2428

63. Lippman R., An introduction to computing with neural nets, *IEEE Trans., Acoust. Signal Processing, ASSP – 4*, 1987, 4-18.

64. Simon Haykin, *Neural Networks - A Comprehensive Foundation*, Macmillan Publishing Company, New York, 1984.

65. Ramelhart E., Hinton G. E. and Williams R. J., Learning representations by back-propagating errors, *Nature (London)*, **323**, 1986, 533-536.

66. Vanderplants, G. N., *Numerical Optimization Techniques for Engineering Design : with Applications*, McGraw Hill, New York, 1986.

67. Deb K., *Optimization Methods for Engineering Design: Algorithms and Examples*, Prentice-Hall, New Delhi, 1995.

68. Deb K., Genetic Algorithms for Engineering Design Optimization, A collection of papers prepared for the course ME 767 - *Evolutionary Algorithms in Search and Optimization*, Department of Mechanical Engineering, Indian Institute of Technology, Kanpur, 1996.

69. Holland J. H., *Adaptation in Natural and Artificial Systems*, University of Michigan Press, Ann Arbor, MI, 1975.

70. Goldberg D. E., *Genetic algorithms in search, Optimization and Machine Learning*, Addison Wesley, New York, 1989.

71. K. Matsuoka, Noise injection into inputs in back-propagation learning, *IEEE Trans. on Systems, Man, and Cybernetics*, **22**, 1992, 436-440.

72. Van Wazer, *Viscosity and Flow Measurements*, Interscience Publishers, 1963, 189-191.

# Appendix A

# Experimental Measurements

**Table A.1 Central composite rotatable design for 4 variables [25]**

| | Variables | | | | Values for calculation of coefficients | | | | | | | | | | Response |
|---|---|---|---|---|---|---|---|---|---|---|---|---|---|---|---|
| S N | $x_1$ | $x_2$ | $x_3$ | $x_4$ | $x_1^2$ | $x_2^2$ | $x_3^2$ | $x_4^2$ | $x_1x_2$ | $x_1x_3$ | $x_1x_4$ | $x_2x_3$ | $x_2x_4$ | $x_3x_4$ | y |
| 1 | -1 | -1 | -1 | -1 | 1 | 1 | 1 | 1 | -1 | 1 | 1 | 1 | 1 | 1 | |
| 2 | 1 | -1 | -1 | -1 | 1 | 1 | 1 | 1 | 1 | -1 | -1 | 1 | 1 | 1 | |
| 3 | -1 | 1 | -1 | -1 | 1 | 1 | 1 | 1 | -1 | 1 | 1 | -1 | -1 | 1 | |
| 4 | 1 | 1 | -1 | -1 | 1 | 1 | 1 | 1 | 1 | -1 | -1 | -1 | -1 | 1 | |
| 5 | -1 | -1 | 1 | -1 | 1 | 1 | 1 | 1 | -1 | -1 | 1 | -1 | 1 | -1 | |
| 6 | 1 | -1 | 1 | -1 | 1 | 1 | 1 | 1 | 1 | 1 | -1 | -1 | 1 | -1 | |
| 7 | -1 | 1 | 1 | -1 | 1 | 1 | 1 | 1 | -1 | -1 | 1 | 1 | -1 | -1 | |
| 8 | 1 | 1 | 1 | -1 | 1 | 1 | 1 | 1 | 1 | 1 | -1 | 1 | -1 | -1 | |
| 9 | -1 | -1 | -1 | 1 | 1 | 1 | 1 | 1 | -1 | 1 | -1 | 1 | -1 | -1 | |
| 10 | 1 | -1 | -1 | 1 | 1 | 1 | 1 | 1 | 1 | -1 | 1 | 1 | -1 | -1 | |
| 11 | -1 | 1 | -1 | 1 | 1 | 1 | 1 | 1 | -1 | 1 | -1 | -1 | 1 | -1 | |
| 12 | 1 | 1 | -1 | 1 | 1 | 1 | 1 | 1 | 1 | -1 | 1 | -1 | 1 | -1 | |
| 13 | -1 | -1 | 1 | 1 | 1 | 1 | 1 | 1 | -1 | -1 | -1 | -1 | -1 | 1 | |
| 14 | 1 | -1 | 1 | 1 | 1 | 1 | 1 | 1 | 1 | 1 | 1 | -1 | -1 | 1 | |
| 15 | -1 | 1 | 1 | 1 | 1 | 1 | 1 | 1 | -1 | -1 | -1 | 1 | 1 | 1 | |
| 16 | 1 | 1 | 1 | 1 | 1 | 1 | 1 | 1 | 1 | 1 | 1 | 1 | 1 | 1 | |
| 17 | -2.0 | 0 | 0 | 0 | 4.0 | 0 | 0 | 0 | 0 | 0 | 0 | 0 | 0 | 0 | |
| 18 | 2.0 | 0 | 0 | 0 | 4.0 | 0 | 0 | 0 | 0 | 0 | 0 | 0 | 0 | 0 | |
| 19 | 0 | -2.0 | 0 | 0 | 0 | 4.0 | 0 | 0 | 0 | 0 | 0 | 0 | 0 | 0 | |
| 20 | 0 | 2.0 | 0 | 0 | 0 | 4.0 | 0 | 0 | 0 | 0 | 0 | 0 | 0 | 0 | |
| 21 | 0 | 0 | -2.0 | 0 | 0 | 0 | 4.0 | 0 | 0 | 0 | 0 | 0 | 0 | 0 | |
| 22 | 0 | 0 | 2.0 | 0 | 0 | 0 | 4.0 | 0 | 0 | 0 | 0 | 0 | 0 | 0 | |
| 23 | 0 | 0 | 0 | -2.0 | 0 | 0 | 0 | 4.0 | 0 | 0 | 0 | 0 | 0 | 0 | |
| 24 | 0 | 0 | 0 | 2.0 | 0 | 0 | 0 | 4.0 | 0 | 0 | 0 | 0 | 0 | 0 | |
| 25 | 0 | 0 | 0 | 0 | 0 | 0 | 0 | 0 | 0 | 0 | 0 | 0 | 0 | 0 | |
| 26 | 0 | 0 | 0 | 0 | 0 | 0 | 0 | 0 | 0 | 0 | 0 | 0 | 0 | 0 | |
| 27 | 0 | 0 | 0 | 0 | 0 | 0 | 0 | 0 | 0 | 0 | 0 | 0 | 0 | 0 | |
| 28 | 0 | 0 | 0 | 0 | 0 | 0 | 0 | 0 | 0 | 0 | 0 | 0 | 0 | 0 | |

| | | | | | | | | | | | | | | |
|---|---|---|---|---|---|---|---|---|---|---|---|---|---|---|
| 29 | 0 | 0 | 0 | 0 | 0 | 0 | 0 | 0 | 0 | 0 | 0 | 0 | 0 | 0 | |
| 30 | 0 | 0 | 0 | 0 | 0 | 0 | 0 | 0 | 0 | 0 | 0 | 0 | 0 | 0 | |
| 31 | 0 | 0 | 0 | 0 | 0 | 0 | 0 | 0 | 0 | 0 | 0 | 0 | 0 | 0 | |

## Table A.2 Material removal measurements

($p_e$, $N$, $R_e$, and $C$ indicate extrusion pressure in bar, number of cycles, reduction ratio and percentage concentration of abrasives in media respectively)

| Ex No | $p_e$ | $N$ | $R_e$ % | $C$ % | Weight before machining, g | | Weight after machining, g | | Difference, g |
|---|---|---|---|---|---|---|---|---|---|
| | | | | | | Avg. | | Avg | |
| 1 | 50 | 15 | 90 50 | 56 | 94.0520<br>94 0510<br>94.0520 | 96 0517 | 94.0380<br>94.0380<br>94.0360 | 94.0370 | 0 0147 |
| 2. | 35 | 10 | 87.25 | 61 | 91.9040<br>91.9040<br>91.9040 | 91.9040 | 91.8940<br>91.8950<br>91.8940 | 91.8950 | 0.0090 |
| 3. | 65 | 10 | 87 25 | 61 | 87.0040<br>87.0020<br>87.0020 | 87.0026 | 86.8980<br>86.8980<br>86.8980 | 86.8980 | 0.0146 |
| 4 | 35 | 20 | 87.25 | 61 | 97.5510<br>97.5500<br>97.5490 | 97.5500 | 97.5320<br>97.5320<br>97.5330 | 97 5323 | 0.0177 |
| 5. | 65 | 20 | 87.25 | 61 | 92.1980<br>92.2000<br>92.2010 | 92.1997 | 92.1760<br>92.1740<br>92.1770 | 95.1756 | 0.0241 |
| 6. | 35 | 10 | 93.75 | 61 | 39.4630<br>39.4620<br>39.4630 | 39.4626 | 39.4500<br>39.4510<br>39.4500 | 39.4503 | 0 0123 |
| 7. | 65 | 10 | 93.75 | 61 | 37 5990<br>37.5990<br>37.5990 | 37.5990 | 37.5830<br>37.5820<br>37.5820 | 37.5823 | 0.0167 |
| 8. | 35 | 20 | 93.75 | 61 | 39.5530<br>39.5540<br>39.5530 | 39.5530 | 39.5310<br>39.5320<br>39.5320 | 39.5316 | 0.0214 |
| 9. | 65 | 20 | 93.75 | 61 | 36.5010<br>36 5000<br>36.5000 | 36.5003 | 36.4690<br>36.4710<br>36.4710 | 36.4706 | 0.0297 |

| Ex No | $p_e$ | $N$ | $R_e$ % | $C$ % | Weight before machining, g | | Weight after machining, g | | Difference, g |
|---|---|---|---|---|---|---|---|---|---|
| | | | | | | Avg. | | Avg | |
| 10. | 20 | 15 | 90 50 | 66 | 94 9521<br>94.9521<br>94 9521 | 94 9521 | 94 9448<br>94 9444<br>94 9446 | 94 9446 | 0 0075 |
| 11 | 80 | 15 | 90.50 | 68 | 92 1396<br>92.1395<br>92.1395 | 95 1395 | 92.1120<br>92.1110<br>92 1110 | 92.1113 | 0.0282 |
| 12 | 50 | 5 | 90 50 | 66 | 96.3125<br>96 3125<br>96.3125 | 96.3125 | 96 3060<br>96.3060<br>96.3060 | 96.3060 | 0.0065 |
| 13. | 50 | 25 | 90 50 | 66 | 95.4890<br>95.4890<br>95.4890 | 95.4890 | 95.4620<br>95.4610<br>95.4620 | 95 4616 | 0.0274 |
| 14 | 50 | 15 | 84 0 | 66 | 292.5302<br>292.5304<br>292.5302 | 292 5303 | 292.5240<br>292.5241<br>292 5240 | 292 5240 | 0 0063 |
| 15. | 50 | 15 | 97.0 | 66 | 79.5836<br>79.5836<br>79.5837 | 79 5836 | 79.5341<br>79.5341<br>79.5341 | 79 5341 | 0.0495 |
| 16. | 50 | 15 | 90.50 | 66 | 89.4158<br>89.4159<br>89.4159 | 89.4159 | 89 3941<br>89.3943<br>89.3941 | 89.3942 | 0.0217 |
| 17. | 50 | 15 | 90.50 | 66 | 87.3387<br>87.3388<br>87.3389 | 87.3388 | 87.3161<br>87.3158<br>87.3158 | 87.3159 | 0.0229 |
| 18. | 50 | 15 | 90.50 | 66 | 89 4856<br>89.4859<br>89.4859 | 89 4858 | 89.4692<br>89.4691<br>89.4691 | 89 4624 | 0 0234 |
| 19 | 50 | 15 | 90.50 | 66 | 85 1182<br>85.1181<br>85.1182 | 85 1182 | 85 0974<br>85 0968<br>85.0970 | 85 0971 | 0 0211 |

| Ex No | $P$ | $N$ | $R_e$ % | $C$ % | Weight before machining, g | Avg | Weight after machining, g | Avg. | Difference, g |
|---|---|---|---|---|---|---|---|---|---|
| 20 | 50 | 15 | 90 50 | 66 | 84.9865<br>84 9865<br>84 9864 | 84.9865 | 84 9656<br>84.9657<br>84.9657 | 84 9657 | 0.0208 |
| 21 | 50 | 15 | 90 50 | 66 | 86 8612<br>86 8611<br>86.8611 | 86 8611 | 86 8406<br>86.8407<br>86.8405 | 86.8406 | 0.0205 |
| 22 | 50 | 15 | 90 50 | 66 | 87 5408<br>87.5409<br>87.5409 | 87.5409 | 87.5193<br>87.5193<br>87.5193 | 87.5193 | 0.0216 |
| 23. | 35 | 10 | 87.25 | 71 | 102 7951<br>102.7958<br>102.7959 | 102.7956 | 102.7839<br>102.7839<br>102.7839 | 102.7839 | 0.0117 |
| 24 | 65 | 10 | 87.25 | 71 | 99.3567<br>99.3561<br>99.3562 | 99.3563 | 99.3378<br>99.3379<br>99.3378 | 99.3377 | 0.0186 |
| 25 | 35 | 20 | 87.25 | 71 | 104.0585<br>104.0586<br>104.0586 | 104.0586 | 104.0390<br>104.0388<br>104.0388 | 104.0389 | 0.0197 |
| 26 | 65 | 20 | 87 25 | 71 | 100.8124<br>100.8125<br>100.8124 | 100 8124 | 100.7839<br>100.7839<br>100.7839 | 100.7839 | 0.0285 |
| 27 | 35 | 10 | 93.75 | 71 | 42.1224<br>42.1223<br>42.1224 | 42.1224 | 42 1015<br>42.1015<br>42.1015 | 42.1015 | 0.0209 |
| 28 | 65 | 10 | 93.75 | 71 | 44.0382<br>44.0382<br>44.0382 | 44.0382 | 44.0047<br>44.0047<br>44.0046 | 44.0047 | 0.0335 |
| 29 | 35 | 20 | 93.75 | 71 | 43.1297<br>43.1298<br>43.1298 | 43.1298 | 43.0934<br>43.0936<br>43.0935 | 43.0935 | 0.0363 |

| Ex No | $p_e$ | $N$ | $R_e$ % | $C$ % | Weight before machining, g | | Weight after machining, g | | Difference, g |
|---|---|---|---|---|---|---|---|---|---|
| | | | | | | Avg | | Avg. | |
| 30 | 65 | 20 | 93.75 | 71 | 43 4407<br>43 4407<br>43 4407 | 43 4407 | 43.3942<br>43 3942<br>43.3942 | 43.3942 | 0 0465 |
| 31 | 50 | 15 | 90 50 | 76 | 84.0064<br>84 0066<br>84.0063 | 84.0064 | 83.9785<br>83 9785<br>83.9785 | 83 9785 | 0 0279 |

## Table A.3 Surface roughness measurements

| Ex No | $p_e$ | $N$ | $R_e$ % | $C$ % | Surface Roughness Before Machining, $\mu m$ | | | | | | Surface Roughness After Machining, $\mu m$ | | | | | |
|---|---|---|---|---|---|---|---|---|---|---|---|---|---|---|---|---|
| | | | | | $R_a$ | | $R_y$ | | $R_{tm}$ | | $R_a$ | | $R_y$ | | $R_{tm}$ | |
| 1 | 50 | 15 | 90 50 | 56 | 2 34 | 2 27 | 16.32 | 15 37 | 11 87 | 10 82 | 1 98 | 1.84 | 11 82 | 11.40 | 9.65 | 8 37 |
| | | | | | 2 30 | | 15 45 | | 12 20 | | 1.87 | | 11.07 | | 9.02 | |
| | | | | | 2 22 | | 14 78 | | 9 66 | | 1 75 | | 11 82 | | 7.87 | |
| | | | | | 2 21 | | 14 93 | | 10 57 | | 1 78 | | 10 92 | | 6 95 | |
| 2 | 35 | 10 | 87 25 | 61 | 1 52 | 1.71 | 11.41 | 13.51 | 9 77 | 11 24 | 1 28 | 1.36 | 11 61 | 11 01 | 8 29 | 9 19 |
| | | | | | 1.77 | | 13 49 | | 12 05 | | 1 23 | | 10 28 | | 7.64 | |
| | | | | | 1 87 | | 16 52 | | 12 21 | | 1 48 | | 10.61 | | 10 49 | |
| | | | | | 1 71 | | 12 62 | | 10.93 | | 1.47 | | 11 56 | | 10.36 | |
| 3 | 65 | 10 | 87 25 | 61 | 1.32 | 1 31 | 15.42 | 15 49 | 8.57 | 9.18 | 0.84 | 0.81 | 12.30 | 12.00 | 5 89 | 6 00 |
| | | | | | 1.27 | | 14 92 | | 10 70 | | 0.90 | | 13.21 | | 6.79 | |
| | | | | | 1 39 | | 16 73 | | 11.35 | | 0 70 | | 11.18 | | 5.71 | |
| | | | | | 1 25 | | 14 89 | | 9 10 | | 0.77 | | 12.32 | | 5 63 | |
| 4 | 35 | 20 | 87 25 | 61 | 1.81 | 1.85 | 17.37 | 17.18 | 12.10 | 11.76 | 1.33 | 1.33 | 11.35 | 11.48 | 9.71 | 8.47 |
| | | | | | 1 95 | | 16.92 | | 11 44 | | 1 44 | | 11.97 | | 8.59 | |
| | | | | | 1.73 | | 16.81 | | 11 30 | | 1.21 | | 10.34 | | 7.53 | |
| | | | | | 1.92 | | 17.85 | | 12.20 | | 1.37 | | 12.26 | | 8.05 | |
| 5 | 65 | 20 | 87.25 | 61 | 2.06 | 2.01 | 23.11 | 18 89 | 14.72 | 13.85 | 1.14 | 1.24 | 13.01 | 13.39 | 10.43 | 10.15 |
| | | | | | 1.88 | | 17 12 | | 12.43 | | 1.16 | | 11.84 | | 9.20 | |
| | | | | | 2.15 | | 18.21 | | 15.31 | | 1.31 | | 14.12 | | 10 87 | |
| | | | | | 1.93 | | 17.54 | | 12.97 | | 1.37 | | 14.59 | | 10.13 | |
| 6 | 35 | 10 | 93.75 | 61 | 2.19 | 2.08 | 15.58 | 15 11 | 12.18 | 11.88 | 1 69 | 1 56 | 13 06 | 13.43 | 9.36 | 9.29 |
| | | | | | 2.17 | | 14.67 | | 11.09 | | 1.46 | | 13.94 | | 9.54 | |
| | | | | | 2.01 | | 16.54 | | 13 03 | | 1 56 | | 11.49 | | 8.52 | |
| | | | | | 1.95 | | 13.65 | | 11.24 | | 1.69 | | 15.24 | | 9.75 | |
| 7 | 65 | 10 | 93.75 | 61 | 2.11 | 2.15 | 17.63 | 17.60 | 12.60 | 13 29 | 1.45 | 1.46 | 11 04 | 10 79 | 8.02 | 8.25 |
| | | | | | 2.17 | | 18.25 | | 13.17 | | 1.53 | | 11 62 | | 8.34 | |
| | | | | | 2.05 | | 16.63 | | 13.12 | | 1 39 | | 10.06 | | 7.65 | |
| | | | | | 2.26 | | 17.92 | | 14 30 | | 1.47 | | 10.44 | | 9.02 | |
| 8 | 35 | 20 | 93.75 | 61 | 1.65 | 1.70 | 14.73 | 14.06 | 9.46. | 9.92 | 0.90. | 0.97 | 8.57 | 8.72 | 6 63 | 6.95 |
| | | | | | 1.56 | | 12.30 | | 8 33 | | 0.9 | | 8.32 | | 5.00 | |
| | | | | | 1.84 | | 15.41 | | 11.78 | | 1.17 | | 11.92 | | 9.10 | |
| | | | | | 1.75 | | 13.83 | | 10.14 | | 0 87 | | 6.10 | | 7.10 | |
| 9 | 65 | 20 | 93.75 | 61 | 1.89 | 1.93 | 14.00 | 13.98 | 10.10 | 9.94 | 0 91 | 0 99 | 6.89 | 8.59 | 4.85 | 5.32 |
| | | | | | 1.90 | | 13.58 | | 9.74 | | 1.02 | | 8 72 | | 5.74 | |
| | | | | | 1.99 | | 13.51 | | 9 49 | | 1.04 | | 9.86 | | 5.11 | |
| | | | | | 1.94 | | 14.83 | | 10.43 | | 0.98 | | 8.79 | | 5.79 | |
| 10 | 20 | 15 | 90 50 | 66 | 2.34 | 2.31 | 14.51 | 13.93 | 12.25 | 12.13 | 1.98 | 1.99 | 12.34 | 12.62 | 10 12 | 10.59 |
| | | | | | 2.28 | | 14.56 | | 13.45 | | 2.08 | | 13.35 | | 11.16 | |
| | | | | | 2.37 | | 13.26 | | 11.25 | | 1.76 | | 11.83 | | 9.66 | |
| | | | | | 2.25 | | 13 42 | | 11.59 | | 2.13 | | 12.97 | | 11.44 | |

| Ex N | $p_e$ | $N$ | $R_e$ | $C$ | Surface Roughness Before Machining, $\mu m$ | | | | | | Surface Roughness After Machining, $\mu m$ | | | | | |
|---|---|---|---|---|---|---|---|---|---|---|---|---|---|---|---|---|
| | | | | | $R_a$ | | $R_y$ | | $R_{tm}$ | | $R_a$ | | $R_y$ | | $R_{tm}$ | |
| 11 | 80 | 15 | 90 50 | 66 | 2.29 | 2 21 | 20.30 | 18.16 | 14 65 | 13 71 | 1 50 | 1 47 | 11 75 | 12 16 | 9 24 | 9.73 |
| | | | | | 2 33 | | 18.75 | | 13 23 | | 1 43 | | 11 97 | | 9 12 | |
| | | | | | 2 07 | | 16 27 | | 13.21 | | 1 40 | | 12 23 | | 9 62 | |
| | | | | | 2 13 | | 17 34 | | 13.75 | | 1.57 | | 12 71 | | 10 97 | |
| 12 | 50 | 5 | 90 50 | 66 | 1.82 | 1 82 | 14 65 | 14 01 | 9 97 | 9 80 | 1 43 | 1 51 | 10 71 | 11.37 | 8 23 | 8 26 |
| | | | | | 1 86 | | 14.41 | | 10.24 | | 1 45 | | 11 08 | | 8 17 | |
| | | | | | 1 83 | | 15 12 | | 9 67 | | 1 53 | | 11 66 | | 8 66 | |
| | | | | | 1 78 | | 11.89 | | 9 33 | | 1 61 | | 12.03 | | 7 98 | |
| 13 | 50 | 25 | 90 50 | 66 | 2 32 | 2 17 | 13 67 | 13.21 | 11.04 | 10.84 | 1 40 | 1 40 | 8 08 | 7 92 | 6.97 | 6.74 |
| | | | | | 2 10 | | 12.78 | | 11 07 | | 1 37 | | 6 62 | | 6 18 | |
| | | | | | 2.09 | | 12 76 | | 10 23 | | 1 39 | | 7 77 | | 6 64 | |
| | | | | | 2 17 | | 13.65 | | 11.02 | | 1 45 | | 9 21 | | 7.19 | |
| 14 | 50 | 15 | 84.0 | 66 | 1.99 | 2 01 | 14 12 | 15.18 | 10 90 | 11 16 | 1 77 | 1 65 | 10 58 | 11.34 | 9 36 | 8.52 |
| | | | | | 2.01 | | 17.50 | | 11 09 | | 1 74 | | 10 91 | | 8.76 | |
| | | | | | 2.07 | | 16.01 | | 11 82 | | 1 53 | | 11 07 | | 8 16 | |
| | | | | | 1.95 | | 13.12 | | 10.84 | | 1 58 | | 12 81 | | 8 02 | |
| 15. | 50 | 15 | 97.0 | 66 | 1.64 | 1.63 | 8.48 | 9.20 | 7.88 | 8 22 | 0 62 | 0 62 | 4 51 | 3 96 | 2 76 | 2 66 |
| | | | | | 1 62 | | 9.50 | | 8.72 | | 0 56 | | 3 64 | | 2.82 | |
| | | | | | 1 57 | | 8.92 | | 8.21 | | 0 61 | | 3 15 | | 2.40 | |
| | | | | | 1.70 | | 9 90 | | 8 10 | | 0 69 | | 4 55 | | 2 68 | |
| 16 | 50 | 15 | 90 50 | 66 | 1 85 | 1 88 | 14 56 | 11 80 | 9 6[illegible] | 8 [illegible] | 1 24 | 1 2[illegible] | [illegible] | 8 81 | 6 05 | 6.06 |
| | | | | | 1.96 | | 9 54 | | 8.39 | | 1 23 | | 7 60 | | 5.86 | |
| | | | | | 1.83 | | 11 31 | | 9 51 | | 1 27 | | 8 40 | | 5 94 | |
| | | | | | 1.88 | | 11.80 | | 8.29 | | 1 36 | | 11 67 | | 6.41 | |
| 17 | 50 | 15 | 90.50 | 66 | 1.52 | 1 70 | 12.48 | 12 71 | 10 62 | 7 84 | 1 13 | 1 16 | 8 12 | 8 82 | 5 33 | 5.21 |
| | | | | | 1.76 | | 11 60 | | 9 74 | | 1 05 | | 8 77 | | 4.84 | |
| | | | | | 1.71 | | 13.81 | | 9 89 | | 1 31 | | 8 55 | | 5 33 | |
| | | | | | 1.80 | | 12.95 | | 1.11 | | 1 15 | | 9 85 | | 5 37 | |
| 18 | 50 | 15 | 90.50 | 66 | 1.46 | 1 46 | 10 55 | 10 23 | 8 97 | 8 55 | 1 07 | 0 96 | 6 78 | 6 73 | 5 60 | 5.04 |
| | | | | | 1.58 | | 10.98 | | 9 03 | | 1 09 | | 7 33 | | 4.22 | |
| | | | | | 1.42 | | 9.73 | | 8 21 | | 0 90 | | 6 91 | | 5.52 | |
| | | | | | 1.37 | | 9.66 | | 8.01 | | 0 80 | | 5 93 | | 4.85 | |
| 19 | 50 | 15 | 90.50 | 66 | 2.05 | 2.12 | 11.65 | 14 89 | 13 70 | 12 55 | 1 5[illegible] | 1 5[illegible] | 10 [illegible] | 10 58 | 8 73 | 8 95 |
| | | | | | 2 13 | | 16.64 | | 14.05 | | 1 46 | | 10 44 | | 9.02 | |
| | | | | | 2.18 | | 15.10 | | 10.97 | | 1.49 | | 9 92 | | 9.10 | |
| | | | | | 2.12 | | 16.19 | | 11.51 | | 1.61 | | 11.61 | | 8.95 | |
| 20 | 50 | 15 | 90.50 | 66 | 2.15 | 2.08 | 14.12 | 14.49 | 11.14 | 11.15 | 1.21 | 1.35 | 8.66 | 9.44 | 5.04 | 6.44 |
| | | | | | 2.02 | | 12.65 | | 10 51 | | 1.39 | | 10 42 | | 8.81 | |
| | | | | | 2.15 | | 16.88 | | 11.63 | | 1 51 | | 10 25 | | 6.75 | |
| | | | | | 2.01 | | 14.34 | | 11 34 | | 1 30 | | 8 43 | | 5.19 | |

| Ex N | $p_e$ | $N$ | $R_e$ % | $C$ % | Surface Roughness Before Machining, $\mu m$ | | | | | | Surface Roughness After Machining, $\mu m$ | | | | | |
|---|---|---|---|---|---|---|---|---|---|---|---|---|---|---|---|---|
| | | | | | $R_a$ | | $R_y$ | | $R_{tm}$ | | $R_a$ | | $R_y$ | | $R_{tm}$ | |
| 21 | 50 | 15 | 90.50 | 66 | 2 34 | 2.22 | 15.32 | 14 52 | 11 28 | 11.19 | 1.66 | 1 58 | 12 53 | 12 02 | 9 01 | 8.72 |
| | | | | | 2 26 | | 13.54 | | 10 29 | | 1 55 | | 11.89 | | 8 85 | |
| | | | | | 2 10 | | 15.13 | | 12 63 | | 1 61 | | 12 65 | | 8 98 | |
| | | | | | 2 16 | | 14 11 | | 10 57 | | 1.49 | | 11 02 | | 8 06 | |
| 22 | 50 | 15 | 90 50 | 66 | 1 98 | 1 99 | 13 24 | 14 46 | 10 43 | 10 97 | 1 26 | 1 28 | 9.25 | 10 23 | 8 00 | 8 08 |
| | | | | | 1 87 | | 12 97 | | 9 78 | | 1.33 | | 10 32 | | 8 47 | |
| | | | | | 2 02 | | 15 68 | | 12 02 | | 1 15 | | 10 10 | | 7.36 | |
| | | | | | 2 12 | | 15 98 | | 11.68 | | 1 38 | | 11 24 | | 8 53 | |
| 23 | 35 | 10 | 87.25 | 71 | 1 12 | 1 05 | 9 58 | 9.07 | 6 63 | 6 63 | 0 45 | 0.60 | 5.85 | 5.87 | 4.71 | 4 58 |
| | | | | | 0 95 | | 8.56 | | 6 66 | | 0 69 | | 6.56 | | 4.44 | |
| | | | | | 1.14 | | 9 24 | | 6.22 | | 0.59 | | 5.48 | | 3.55 | |
| | | | | | 0 98 | | 8 93 | | 7.00 | | 0 67 | | 6.58 | | 4.62 | |
| 24 | 65 | 10 | 87 25 | 71 | 1 47 | 1.45 | 13.96 | 13.06 | 8.32 | 8.55 | 0.78 | 0 88 | 7 49 | 9.34 | 4.08 | 4 71 |
| | | | | | 1 29 | | 11.65 | | 7.88 | | 0.86 | | 8.81 | | 4.77 | |
| | | | | | 1 50 | | 12 96 | | 8 69 | | 0.96 | | 10 05 | | 5.10 | |
| | | | | | 1 54 | | 13 67 | | 9.32 | | 0.92 | | 11 04 | | 4 91 | |
| 25 | 35 | 20 | 87.25 | 71 | 1.61 | 1.63 | 13 76 | 13.66 | 9 14 | 9.95 | 1.02 | 0.98 | 9.96 | 8 60 | 6.14 | 5.98 |
| | | | | | 1 69 | | 12.74 | | 11.46 | | 0.84 | | 7.69 | | 5.59 | |
| | | | | | 1.63 | | 15.94 | | 9 66 | | 1.12 | | 8.86 | | 6.33 | |
| | | | | | 1.60 | | 13.22 | | 9.55 | | 0 95 | | 7.93 | | 5.86 | |
| 26 | 65 | 20 | 87.25 | 71 | 1.52 | 1.52 | 13.45 | 14.12 | 10 02 | 10 04 | 0.64 | 0.63 | 4.51 | 6.69 | 4 13 | 4 19 |
| | | | | | 1.47 | | 13 03 | | 9 86 | | 0.59 | | 5.68 | | 4.19 | |
| | | | | | 1.47 | | 14.17 | | 9.95 | | 0 54 | | 6.16 | | 4.05 | |
| | | | | | 1 63 | | 15 83 | | 10.34 | | 0.73 | | 6 40 | | 4.40 | |
| 27 | 35 | 10 | 93.75 | 71 | 1.51 | 1.48 | 9.52 | 9 51 | 8 81 | 8.42 | 1.05 | 0.94 | 7.84 | 6.10 | 5.14 | 4 55 |
| | | | | | 1.48 | | 9.49 | | 8.55 | | 1.02 | | 6 57 | | 5.22 | |
| | | | | | 1 40 | | 10.58 | | 7.41 | | 0.89 | | 4 68 | | 4.40 | |
| | | | | | 1.55 | | 8.47 | | 8.92 | | 0 79 | | 5.32 | | 3.45 | |
| 28 | 65 | 10 | 93.75 | 71 | 1.59 | 1.60 | 13.15 | 11.99 | 9.04 | 8 40 | 0.78 | 0 89 | 5 49 | 5.08 | 4.44 | 4 27 |
| | | | | | 1.58 | | 12.99 | | 7.71 | | 0 90 | | 5.13 | | 4.15 | |
| | | | | | 1.69 | | 11.09 | | 8.51 | | 0.86 | | 4 92 | | 4.06 | |
| | | | | | 1 56 | | 10 76 | | 8 33 | | 1.01 | | 4 80 | | 4.42 | |
| 29 | 35 | 20 | 93.75 | 71 | 1 74 | 1 68 | 11 30 | 10 83 | 9.40 | 8 64 | 0.86 | 0.89 | 4 46 | 4 76 | 3.40 | 3 75 |
| | | | | | 1.71 | | 10 05 | | 8.12 | | 0.86 | | 4.42 | | 3.80 | |
| | | | | | 1.72 | | 10 69 | | 8.91 | | 0.94 | | 5.37 | | 3.90 | |
| | | | | | 1.56 | | 11.28 | | 9.15 | | 0 92 | | 5.88 | | 4.20 | |
| 30 | 65 | 20 | 93 75 | 71 | 2.01 | 1 91 | 14.56 | 11 34 | 9.22 | 8 11 | 0.89 | 0 88 | 5.19 | 5.37 | 3.71 | 3.91 |
| | | | | | 1.84 | | 9.83 | | 7.03 | | 0.91 | | 6.02 | | 4.79 | |
| | | | | | 1.87 | | 12 10 | | 8.86 | | 0.77 | | 5 01 | | 3.16 | |
| | | | | | 1.93 | | 8.90 | | 7.36 | | 0.97 | | 5.27 | | 4.01 | |
| 31 | 50 | 15 | 90.50 | 76 | 1.92 | 1 81 | 14 81 | 14.71 | 10.89 | 10.58 | 1 01 | 0.96 | 8.61 | 7 22 | 6.01 | 5 35 |
| | | | | | 1 85 | | 14.53 | | 10.46 | | 1.10 | | 7.35 | | 6.57 | |
| | | | | | 1.58 | | 13.53 | | 9.78 | | 0.89 | | 6.52 | | 4.05 | |
| | | | | | 1.89 | | 15.98 | | 11.22 | | 0.82 | | 6.42 | | 4.80 | |

**Table A.4 Change in Surface roughness**

| Ex. No. | $p_e$ | $N$ | $R_e$ % | $C$ % | $\Delta R_a$ (μm) | $\Delta R_y$ (μm) | $\Delta R_{tm}$ (μm) |
|---|---|---|---|---|---|---|---|
| 1 | 50 | 15 | 90.50 | 56 | 0.43 | 3.92 | 2.55 |
| 2 | 35 | 10 | 87 25 | 61 | 0.35 | 2 50 | 2.05 |
| 3 | 65 | 10 | 87.25 | 61 | 0.50 | 3.49 | 3 18 |
| 4 | 35 | 20 | 87.25 | 61 | 0 52 | 5 70 | 3 29 |
| 5 | 65 | 20 | 87 25 | 61 | 0.77 | 5.6 | 3.70 |
| 6 | 35 | 10 | 93.75 | 61 | 0 56 | 1.68 | 2.59 |
| 7 | 65 | 10 | 93.75 | 61 | 0.69 | 5.34 | 5.04 |
| 8 | 35 | 20 | 93 75 | 61 | 0.73 | 5 34 | 2.97 |
| 9 | 65 | 20 | 93.75 | 61 | 0.94 | 5 39 | 4.57 |
| 10 | 20 | 15 | 90.50 | 66 | 0.32 | 1.31 | 1.54 |
| 11 | 80 | 15 | 90.50 | 66 | 0.74 | 6.00 | 3.89 |
| 12 | 50 | 5 | 90.50 | 66 | 0 31 | 2.64 | 1 54 |
| 13 | 50 | 25 | 90.50 | 66 | 0.77 | 5.92 | 4.2 |
| 14 | 50 | 15 | 84.0 | 66 | 0 36 | 3.84 | 2.64 |
| 15 | 50 | 15 | 97.0 | 66 | 1.01 | 5.24 | 5 66 |
| 16 | 50 | 15 | 90.50 | 66 | 0.61 | 2.99 | 2.90 |
| 17 | 50 | 15 | 90.50 | 66 | 0.54 | 3.89 | 2.63 |
| 18 | 50 | 15 | 90.50 | 66 | 0.50 | 3.50 | 3.51 |
| 19 | 50 | 15 | 90.50 | 66 | 0.59 | 4.31 | 3.60 |
| 20 | 50 | 15 | 90.50 | 66 | 0.73 | 5.05 | 4.70 |
| 21 | 50 | 15 | 90.50 | 66 | 0.64 | 2.50 | 2.47 |
| 22 | 50 | 15 | 90.50 | 66 | 0.71 | 4.23 | 2.88 |
| 23 | 35 | 10 | 87.25 | 71 | 0.45 | 3.20 | 2.05 |
| 24 | 65 | 10 | 87.25 | 71 | 0.57 | 3.72 | 3.84 |
| 25 | 35 | 20 | 87.25 | 71 | 0.65 | 5.04 | 3.97 |
| 26 | 65 | 20 | 87.25 | 71 | 0.89 | 7.43 | 5.84 |
| 27 | 35 | 10 | 93.75 | 71 | 0.54 | 3.41 | 3.87 |
| 28 | 65 | 10 | 93.75 | 71 | 0.71 | 6.91 | 4 13 |
| 29 | 35 | 20 | 93.75 | 71 | 0.79 | 6.07 | 4.89 |
| 30 | 65 | 20 | 93.75 | 71 | 1.03 | 5.97 | 4.20 |
| 31 | 50 | 15 | 90.50 | 76 | 0.85 | 7.49 | 5.23 |

**Table A.5 Active grain density for various concentrations of abrasives and mesh sizes**

| Carrier | $M_{av}$ | $C$ % | Active grain density per mm$^2$ | | | | Average active grain density per mm$^2$ |
|---|---|---|---|---|---|---|---|
| **Polyborosi-loxane** | 55 | 56 | 1.50 | 1.63 | 1 63 | 1.37 | 1.53 |
| | 55 | 61 | 1.75 | 2 00 | 1.87 | 1.87 | 1.87 |
| | 55 | 66 | 2.12 | 2.25 | 2.00 | 2.12 | 2.12 |
| | 55 | 71 | 2.37 | 2.50 | 2.50 | 2.62 | 2.50 |
| | 55 | 76 | 3.00 | 3.25 | 2.75 | 3.25 | 3.06 |
| **Putty** | 100 | 20 | 1.80 | 1.55 | 1.55 | 2.06 | 1.81 |
| | 100 | 40 | 2.83 | 3.09 | 2.58 | 3.35 | 2.96 |
| | 100 | 60 | 4.38 | 4.12 | 3.60 | 3.83 | 3.99 |
| | 100 | 80 | 6.44 | 6.95 | 6.70 | 6.44 | 6.63 |
| | 150 | 20 | 2.06 | 2.31 | 2.06 | 2.31 | 2.18 |
| | 150 | 40 | 3.85 | 3.59 | 3.65 | 3.33 | 3.65 |
| | 150 | 60 | 5.15 | 4 89 | 5.52 | 5.15 | 5.18 |
| | 150 | 80 | 8.76 | 8.50 | 9.02 | 9.02 | 8.82 |
| | 180 | 20 | 3.83 | 4.09 | 4.35 | 4.09 | 4.09 |
| | 180 | 40 | 6.60 | 6.86 | 6.60 | 6.86 | 6.73 |
| | 180 | 60 | 9.92 | 9.67 | 10 18 | 9.67 | 9.86 |
| | 180 | 80 | 15.05 | 15.30 | 14.54 | 14.79 | 14.92 |

**Table A.6 Measurements of temperatures at workpiece surface**

| Ex No. | Probe No | Temperature at workpiece surface , $^0$C | | | | | | Total temp rise, $^0$C |
|---|---|---|---|---|---|---|---|---|
| | | $N$ =0 | $N$ =5 | $N$ =10 | $N$ =15 | $N$ =20 | $N$ =25 | |
| 1. | 1 | 25 4 | 25 8-25.9 | 26.6 | 27.1 | | | 1 70 |
| | 2. | 25 4 | 25.8 | 26.5 | 27.1 | | | 1 70 |
| 2. | 1. | 25 9 | 26.1-26 2 | 26 4 | | | | 0.45 |
| | 2. | 25.9 | 26.1-26 2 | 26 3-26.4 | | | | 0.40 |
| 3 | 1 | 25 3-25 4 | 26.1-26.2 | 26.9-27 0 | | | | 1 60 |
| | 2 | 25 3-25.4 | 26 2 | 27 1 | | | | 1.80 |
| 4 | 1 | 25 7-25 8 | 26 1-26 2 | 26.4-26.5 | 26.8-26.9 | 27.1-27.2 | | 1.30 |
| | 2 | 25 7 | 26 1-26.2 | 26.3-26.4 | 26.5-26.6 | 26.8-26 9 | | 1.10 |
| 5 | 1 | 26.0 | 26.5-26 6 | 26.9-27.3 | 27.8-27.9 | 28.4-28.5 | | 2.25 |
| | 2 | 26.0 | 26 5-26.7 | 27 0-27.1 | 27.8 | 28.3 | | 2.10 |
| 6 | 1 | 26.0 | 26.3 | 26.5-26.6 | | | | 0 55 |
| | 2 | 26 0 | 26 3 | 26.5-26.6 | | | | 0.55 |
| 7 | 1 | 25.9-26.0 | 26.7 | 27.0 | | | | 1 05 |
| | 2 | 25.9-26.0 | 26.7 | 27.0 | | | | 1 05 |
| 8 | 1 | 26 2 | 26.6-26.7 | 26.8 | 27.0 | 27.2 | | 1.00 |
| | 2 | 26.2 | 26.6 | 26.8 | 27.0 | 27.1 | | 0.90 |
| 9 | 1 | 25.3-25.4 | 26.0-26.1 | 26.6 | 27.0 | 27.5 | | 2.25 |
| | 2 | 25 3-25.4 | 26.1 | 26.6 | 27.0 | 27.5-27.6 | | 2.30 |
| 10 | 1 | 25.5 | 25.7 | 25.8 | 26.3 | | | 0.80 |
| | 2 | 25.5-25.6 | 25.7-25.8 | 25.9 | 26.3-26.4 | | | 0.80 |
| 11 | 1 | 25.8 | 27.1 | 28.2 | 29.4 | | | 3.60 |
| | 2 | 25.8 | 27.1 | 28 2 | 29.4 | | | 3.60 |
| 12 | 1 | 25.5 | 26.1 | | | | | 0 60 |
| | 2 | 25.5 | 26.1 | | | | | 0.60 |
| 13 | 1 | 25.6 | 26.3 | 26.9 | 27.4 | 27.8 | 28.2 | 2.60 |
| | 2 | 25.6 | 26.3 | 26.8-26.9 | 27.4 | 27.8 | 28.2 | 2.60 |
| 14 | 1 | 26.0 | 26.4 - 26.5 | 26.9-27.0 | 27.4-27.5 | | | 1.45 |
| | 2 | 26.0 | 26 4 | 26.9 | 27.3-27.4 | | | 1.35 |
| 15 | 1 | 25.8 | 26.7-27.8 | 26.8-26.9 | 27.4 | | | 1.60 |
| | 2 | 25.8 | 26.6 | 26.8-26.9 | 27.2 | | | 1.40 |
| 16 | 1 | 26.1 | 26.4-26.5 | 27.4 | 27.9 | | | 1.80 |
| | 2 | 26.2 | 26.5-26.6 | 27 5 | 28.0 | | | 1.80 |

| Ex. No. | Probe No. | Temperature at workpiece surface, $^0$ C | | | | | | Total temp rise, $^0$C |
|---|---|---|---|---|---|---|---|---|
| | | $N$ =0 | $N$ =5 | $N$ =10 | $N$ =15 | $N$ =20 | $N$ =25 | |
| 17 | 1 | 26.2-26.3 | 26.9 | 27.4-27.5 | 28 2-28.3 | | | 2.00 |
| | 2 | 26 3-26.4 | 27 0-27.1 | 27.5-27 6 | 28.3-28.4 | | | 2.00 |
| 18 | 1 | 26.1-26.2 | 26.7-26.8 | 27.3-27 4 | 27.9-28 0 | | | 1 80 |
| | 2 | 26.1-26.2 | 26.9-27.0 | 27.4-27.5 | 28.0-28.1 | | | 1 90 |
| 19 | 1 | 26.4-26.5 | 27.2-27.3 | 27.8-27.9 | 28.3-28.4 | | | 1.90 |
| | 2 | 26.4-26.5 | 27.3-27 4 | 27.8-27.9 | 28.4-28.5 | | | 2.00 |
| 20 | 1 | 26.1 | 26.9 | 27.5 | 28.0 | | | 1.90 |
| | 2 | 26.1 | 26.9 | 27.5 | 28.0 | | | 1.90 |
| 21 | 1 | 26.2 | 26.9 | 27.4 | 28.2 | | | 2.00 |
| | 2 | 26.2 | 27.0 | 27.5 | 28.3 | | | 2.10 |
| 22 | 1 | 26 1 | 26.8 | 27.4 | 28.0 | | | 1.90 |
| | 2 | 26.1 | 26.8 | 27.4 | 28.0 | | | 1.90 |
| 23 | 1 | 26 5-26.6 | 26.7-26.8 | 27.4-27.5 | | | | 0.90 |
| | 2 | 26.6-26 7 | 26.6-26 7 | 27.4-27.5 | | | | 0.90 |
| 24 | 1 | 26.6 | 27.4 | 28.2 | | | | 1.60 |
| | 2 | 26 5 | 27.2 | 28.0 | | | | 1.50 |
| 25 | 1 | 26.1 | 26 5 | 26.8 | 27.2 | 27.6 | | 1.50 |
| | 2 | 26.1 | 26.5 | 26.8 | 27.2 | 27 6 | | 1.50 |
| 26 | 1 | 26.2 | 27.1 | 27.7 | 28.2 | 28.8-28.9 | | 2.65 |
| | 2 | 26.2 | 27.1 | 27.7 | 28.2 | 28.8 | | 2.60 |
| 27 | 1 | 26.1 | 26.3-26 4 | 26.8-26.9 | | | | 0.75 |
| | 2 | 26.2 | 26.4-26.5 | 26.9-27.0 | | | | 0.75 |
| 28 | 1 | 26.1 | 27.3 | 27.9 | | | | 1.80 |
| | 2 | 26.1 | 27.2 | 27.8 | | | | 1.70 |
| 29 | 1 | 26.1 | 26.6 | 27.0 | 27.3 | 27.5 | | 1.40 |
| | 2 | 26.1 | 26.6 | 27.0 | 27 3 | 27 5 | | 1.40 |
| 30 | 1 | 26.0 | 27.1 | 28.0 | 28.4 | 28 7 | | 2.70 |
| | 2 | 26 0 | 27.1 | 28.0 | 28 4 | 28.7 | | 2.70 |
| 31 | 1 | 26.1 | 26.9 | 27.7 | 28.3 | | | 2.20 |
| | 2 | 26.1 | 26.9 | 27.7 | 28.3 | | | 2.20 |

# Appendix B

# Viscosity of Media

## B.1 Introduction

Viscosity of media plays an important role in the performance of AFM process. At a particular velocity of piston, the viscosity of media affects the material removal and final surface roughness. The viscosity of media depends on type, mesh size and percentage concentration of abrasives, and type of carrier. From the literature survey, it is evident that there is a lack of investigation with regards to evaluation of rheological properties of the media. There is need to generate the data for viscosity of media of different types, mesh sizes and percentage concentrations of abrasives. The purpose of the present experimentation is to determine data for viscosity of media used in the AFM experiments reported in chapter 2 These viscosity experiments are necessary to calculate the material removal and surface roughness by theoretical model and simulation presented in chapters 3 and 4.

## B.2 Capillary Viscometry

In order to determine the rheological properties of the non-Newtonian fluids, many experimental methods have been developed. The viscometer developed based on the principle of capillary viscometry is the one used to determine the viscosity of the fluids in the present case. Hagan-Poiseuille studied capillary flow problems and derived relations between the flow rate and pressure drop considering the steady axial flow of an incompressible fluid in a circular tube [72].

In capillary viscometry (Fig.B.1), the media is forced through a fine-bore tube and the viscosity of the media is determined from the volumetric flow rate, applied pressure and tube dimensions.

The following assumptions have been made in capillary viscometry

- The flow is steady, incompressible, laminar, unidirectional and fully developed.

- There is no slippage at the wall (this condition postulates that axial velocity, v = 0 at $r = r_t$, where $r_t$ is inner radius of the tube).
- There are no external forces.
- The tube is sufficiently long such that end effects are negligible.

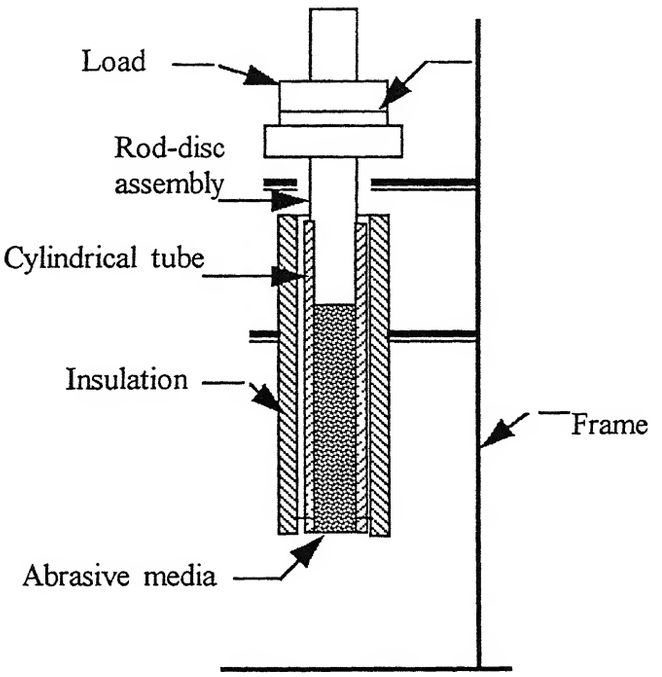


**Fig. B.1 Schematic diagram of a capillary viscometer**

For the fully developed laminar steady flow the expression for the two rheological functions, the shear stress and shear rate, are given by [72],

$$\tau' = \frac{\Delta p\, r}{2 l_t} \qquad \text{(B 1)}$$

$$\dot{\gamma} = -\frac{d\mathrm{v}}{dr} = f(\tau') \qquad \text{(B.2)}$$

Where, $\tau'$ is shear stress in $N/m^2$, $l_t$ is length of the tube in m, $\Delta p$ is pressure drop across the capillary in $N/m^2$ and $u$ is axial velocity of the fluid in the tube in m/s

It is convenient to define the shear stress and shear rate at the wall of the tube ($r = r_t$) in terms of measurable quantities

$$\tau'_w = \frac{\Delta p\, r_t}{2l_t} \tag{B 3}$$

$$\dot{\gamma}_w = \frac{4\dot{Q}}{\pi r_t^3} \tag{B 4}$$

The flow of abrasive media starts after an initial shear stress $\tau'_o$ is applied on it Hence, the expression for viscosity of media is given by

$$\mu = \frac{\tau' - \tau'_o}{\dot{\gamma}_w} \tag{B.5}$$

The initial shear stress $\tau'_o$ of the material to initiate flow in the tube is found out by plotting the graph between the wall shear rate and wall shear stress (Fig.B.2) Using the method of least squares for fitting the data to a straight line, the initial stress $\tau'_o$ is determined by extrapolating the straight line onto the x-axis. The intercept made on the x-axis at zero shear rate gives the value of $\tau'_o$. The slope of the straight line gives the reciprocal of viscosity.

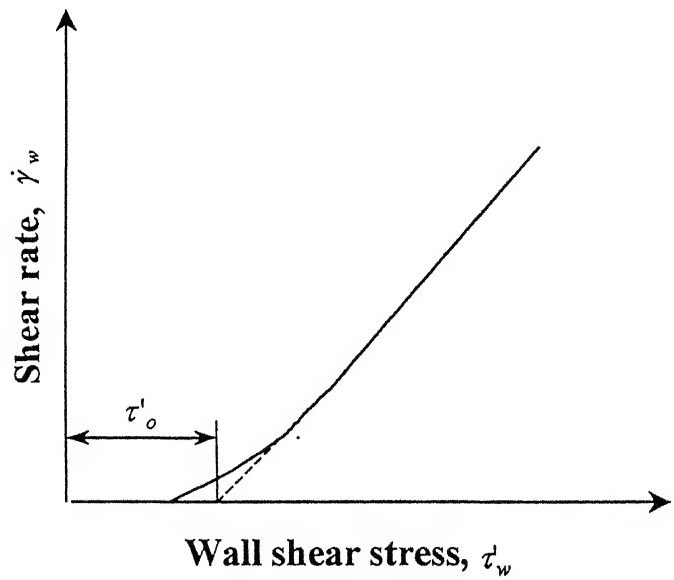


**Fig. B.2 Relationship between wall shear stress and shear rate**

## B.3 Experimentation

Media is filled into the tube of viscometer set-up upto its three-fourth length. Before filling the media into the tube, it is closed at the bottom by cylindrical cup. The media is then compacted by placing the 20 kg weight on the rod-disc assembly (Fig.B1) which acts as a piston to force the media inside the cylindrical tube, for about half an hour. This procedure is repeated until the tube is filled with the media upto three-fourth of its length After properly filling the media in tube, the cylindrical cup is removed. Afterwards, the pressure is applied on the media by placing weights on the rod-disc assembly. Then, length of the extruded material is measured for a time interval of 2.5 minutes. This procedure is repeated at different pressures. Table B.1 shows the conditions under which the experiments have been conducted.

Table B.1 Experimental parameters used in calculation

| |
|---|
| Radius of the tube = 4 7 mm |
| time interval =2.5 min |
| Temperature = 30 5 °C |

## B.4 Calculation of viscosity

Total Pressure gradient ($\Delta p$) across the length of media is given by

$$\Delta p = \frac{w}{\pi r_t^2} \tag{B.6}$$

where, $w$ is weight applied on the media which includes weight of rod-disc assembly.

As extrusion starts, the pressure gradient changes across the length of the tube, because the length of the media filled in the tube initially, does not remain constant as soon as the load is applied.

Assuming linear variation of $l_t$ with time as $l_t(t) = l_{ti} - bt$. (B.7)

where, $l_t(t)$ = length of media in the tube after the time interval 't', and b is a constant.

As $l_t$ varies with time, $l_t$ is integrated over the interval 0 to t min.

So, the actual value of $l_t = \frac{1}{t}\int_0^t (l_{tt} - bt)dt$ (B.8)

This actual value of '$l_t$' is used in the calculation of viscosity of media The constant b is determined by putting the measured value of $l_t$ at 0 and 2 5 min in eqn (B.7)

If $l_{em}$ is extruded length of media in time $t$, then volumetric flow rate is given by following expression

$$\dot{Q} = \frac{\pi r_t^2 l_{em}}{t} \quad \text{(B.9)}$$

The values of shear stress and shear rate at wall at different pressures is determined by eqns (B 3) and (B 4) after substituting the values of $\Delta p$ and $\dot{Q}$. The initial stress $\tau'_o$ is found out by plotting a graph between wall shear stress and shear rate as explained in sections B2 The viscosity of media is determined by eqn (B 5) after substituting values of $\tau'_w$, $\dot{\gamma}_w$ and $\tau'_o$

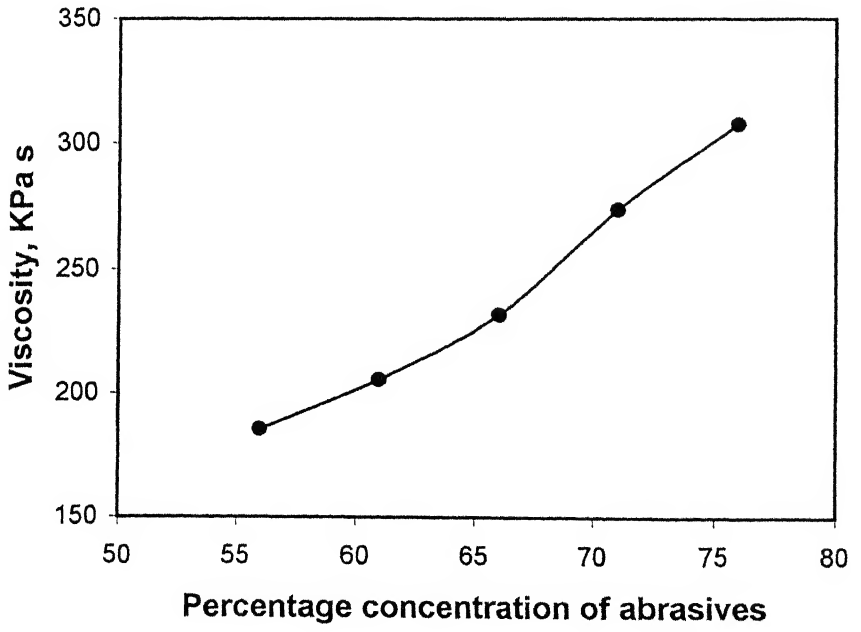


**Fig. B.3 Effect of percentage concentration of abrasives on viscosity of media**

## B.5 Results and Discussion

The experiments are conducted on a capillary viscometer to determine the viscosity of the abrasive media at different concentrations It is evident from the Fig.B 3 that viscosity of media increases with increase in percentage concentration of abrasives. This can be explained as follows· As the % concentration of the abrasives in the media increases, it decreases mobility of the particles migrating from the tube wall Due to this, the amount of material extruded from the tube decreases with increase in percentage concentration of the abrasives in the media, which ultimately decreases volumetric flow rate and the wall shear. There is a decrease in shear rate due to decrease in the volumetric flow rate Due to this reason, there is an increase in viscosity with increase in percentage concentration of abrasives in the media.

## B6. Experimental Data

**Abrasive concentration = 56 %**

Room temperature = 30 5 $^{0}$C

Initial stress = 13 74 KN/m$^2$

| S No | Load Applied (kg) | Extruded length m. | Average length of the media $\bar{L}$ (m) | Wall shear stress $\tau'_w$ (KN/m$^2$) | Shear rate $\dot{\gamma}$ (s$^{-1}$) | Viscosity $\mu$ (KN-s/m$^2$) | Av. Viscosity (KN-s/m$^2$) |
|---|---|---|---|---|---|---|---|
| 1. | 53 7 | 0 0250 | 0.4705 | 39.37 | 0.1418 | 182.72 | 185 40 |
| 2 | 58 7 | 0.0275 | 0 4670 | 43.49 | 0.1560 | 190.68 | |
| 3. | 63 7 | 0.0315 | 0.4680 | 47.30 | 0 1787 | 187.77 | |
| 4 | 68.7 | 0.0360 | 0.4650 | 51.61 | 0.2042 | 185.41 | |

**Abrasive concentration = 61 %**

Room temperature = 30 5 $^0$C

Initial stress = 14 78 KN/m$^2$

| S No. | Load Applied (kg). | Extruded length m. | Average length of the media $\bar{L}$ (m) | Wall shear stress $\tau'_w$ (KN/m$^2$) | Shear rate $\gamma$ (s$^{-1}$) | Viscosity $\mu$ (KN-s/m$^2$) | Av Viscosity (KN-s/m$^2$) |
|---|---|---|---|---|---|---|---|
| 1. | 53.7 | 0 0205 | 0 4735 | 36.92 | 0 1163 | 207.61 | 205.60 |
| 2 | 58 7 | 0.0240 | 0 4705 | 42 99 | 0.1361 | 207.19 | |
| 3 | 63 7 | 0 0280 | 0 4680 | 47.11 | 0.1588 | 203.55 | |
| 4 | 68 7 | 0.0315 | 0 4640 | 51.46 | 0.1787 | 205 28 | |

**Abrasive concentration = 66 %**

Room temperature = 30.0 $^0$C

Initial stress = 15.50 KN/m$^2$

| S. No. | Load Applied (kg). | Extrude d length m. | Average length of the media $\bar{L}$ (m) | Wall shear stress $\tau'_w$ (KN/m$^2$) | Shear rate $\dot{\gamma}$ (s$^{-1}$) | Viscosity $\mu$ (KN-s/m$^2$) | Av. Viscosity (KN-s/m$^2$) |
|---|---|---|---|---|---|---|---|
| 1. | 53.7 | 0.0175 | 0 4760 | 38.59 | 0 0992 | 232.59 | 231.87 |
| 2. | 58.7 | 0.0200 | 0.4740 | 42.48 | 0.1134 | 237.79 | |
| 3. | 63.7 | 0.0240 | 0.4720 | 46.50 | 0.1362 | 227.68 | |
| 4. | 68 7 | 0 0270 | 0.4690 | 50.67 | 0.1532 | 229.44 | |

**Abrasive concentration = 71 %**

Room temperature = 30.5 $^0$C

Initial shear stress = 16.78 KN/m$^2$.

| S. No. | Load Applied (kg). | Extruded length m. | Average length of the media $\bar{L}$ (m) | Wall shear stress $\tau'_w$ (KN/m$^2$) | Shear rate $\dot{\gamma}$ (s$^{-1}$) | Viscosity $\mu$ (KN-s/m$^2$) | Av Viscosity (KN-s/m$^2$) |
|---|---|---|---|---|---|---|---|
| 1. | 53.7 | 0.0140 | 0.4685 | 39.07 | 0.0794 | 280.68 | 273.35 |
| 2. | 58.7 | 0.0165 | 0.4750 | 42.23 | 0.0936 | 271.89 | |
| 3. | 63.7 | 0.0195 | 0.4720 | 46.28 | 0.1106 | 266.61 | |
| 4. | 68.7 | 0.0215 | 0.4700 | 50.23 | 0.1219 | 274.26 | |

**Abrasive concentration = 76 %**

Room temperature = 30.0 $^0$C

Initial shear stress = 17.66 KN/m$^2$

| S No. | Load Applied (kg). | Extruded length m. | Average length of the media $\bar{L}$ (m) | Wall shear stress $\tau'_w$ (KN/m$^2$) | Shear rate $\dot{\gamma}$ (s$^{-1}$) | Viscosity $\mu$ (KN-s/m$^2$) | Av. Viscosity (KN-s/m$^2$) |
|---|---|---|---|---|---|---|---|
| 1 | 53.7 | 0.0115 | 0.4740 | 38.51 | 0.0652 | 319.58 | 308.07 |
| 2. | 58.7 | 0.0145 | 0.4710 | 42.50 | 0.0822 | 302.01 | |
| 3. | 63.7 | 0.0165 | 0.4700 | 46.32 | 0.0936 | 306 22 | |
| 4. | 68.7 | 0.0190 | 0.4665 | 50.48 | 0.1078 | 304.47 | |

# Appendix C

## Specifications

| | |
|---|---|
| **Workpiece** | Material = mild steel (0.25C), $H_w$ = 2177.80 N/mm$^2$, $l_w$ = 38.5 mm, $c_{pw}$ = 43.40 J/kg-K, $k_w$ = 60.5 W/m-K, $\rho_w$ = 7854.0 kg/m$^3$ |
| **Abrasive [40]** | Type = SiC, $M$ = 50 – 60, $M_{av}$ = 55, $c_{pa}$ = 1400.0 J/kg-K, $k_a$ = 100.0 W/m-K, $\rho_a$ = 3220 0 kg/m$^3$ |
| **Carrier – Polyborosiloxane [22]** | $c_{pc}$ = 434.0 J/kg-K, $k_c$ = 0.22 W/m-K, $\rho_c$ = 985.0 kg/m$^3$, |
| **Media Cylinder** | $r_c$ = 43.75 mm, $l_s$ = 80.0 mm |
| **Assumed value of coefficient of friction** | $f$ = 0.2 [41] |
| **Relaxation time** | $\lambda$ = 0.002 s [33] |

# Appendix D

## Data from AFM experiments [19]

| S N. | $v_p$ | $C$ % | $M$ | $N$ | MRR | $R_a$ |
|---|---|---|---|---|---|---|
| 1 | 40.60 | 45.0 | 100 0 | 50 | 1.464 | 1 63 |
| 2 | 51 50 | 45 0 | 100.0 | 50 | 2.270 | 1.08 |
| 3 | 65 20 | 45 0 | 100 0 | 50 | 3 260 | 0.70 |
| 4 | 81.20 | 45 0 | 100 0 | 50 | 5.684 | 0.47 |
| 5 | 51 50 | 45 0 | 150 0 | 50 | 1.957 | 1 14 |
| 6 | 51 50 | 45 0 | 180 0 | 50 | 1.442 | 1.18 |
| 7 | 51.50 | 45.0 | 240.0 | 50 | 1.236 | 1.23 |
| 8 | 40.60 | 41.0 | 150.0 | 80 | 0.869 | 1.80 |
| 9 | 65.20 | 41 0 | 150.0 | 40 | 2.147 | 0.88 |
| 10 | 51.50 | 33 0 | 100.0 | 20 | 1 545 | 1.94 |
| 11 | 51.50 | 33.0 | 100.0 | 40 | 0 901 | 1.54 |
| 12 | 51.50 | 33 0 | 100 0 | 60 | 0.858 | 1.52 |
| 13 | 51.50 | 33.0 | 100.0 | 80 | 0 837 | 1.48 |
| 14 | 51 50 | 33.0 | 100.0 | 100 | 0.772 | 1.42 |
| 15 | 40.60 | 45 0 | 150.0 | 80 | 1.149 | 1.59 |
| 16 | 65 20 | 35.0 | 180.0 | 40 | 1 111 | 1.12 |
| 17 | 81 20 | 35 0 | 240 0 | 60 | 1.119 | 0.71 |
| 18 | 51.50 | 37 0 | 100.0 | 20 | 1.802 | 1.75 |
| 19 | 51.50 | 37 0 | 100.0 | 40 | 1.545 | 1.44 |
| 20 | 51.50 | 37.0 | 100.0 | 60 | 1.459 | 1.48 |
| 21 | 51.50 | 37.0 | 100.0 | 80 | 1.481 | 1.33 |
| 22 | 51.50 | 37 0 | 100.0 | 100 | 1.442 | 1.25 |
| 23 | 40.60 | 45 0 | 150.0 | 100 | 1.102 | 1.51 |
| 24 | 65.20 | 33 0 | 180.0 | 80 | 0 814 | 1.03 |
| 25 | 81.20 | 33 0 | 240.0 | 40 | 1.017 | 0 84 |
| 26 | 51 50 | 41 0 | 100.0 | 40 | 2.704 | 1 34 |
| 27 | 51.50 | 41.0 | 100.0 | 60 | 2 661 | 1.15 |
| 28 | 51.50 | 41.0 | 100.0 | 80 | 2 511 | 1.09 |
| 29 | 51 50 | 41.0 | 100.0 | 100 | 2.214 | 1 04 |
| 30 | 65.20 | 35 0 | 150.0 | 60 | 1.222 | 1.01 |
| 31 | 81 20 | 41.0 | 180.0 | 20 | 2 692 | 0.72 |
| 32 | 51.50 | 45.0 | 100.0 | 40 | 2 832 | 1.28 |
| 33 | 51.50 | 45 0 | 100.0 | 60 | 2 575 | 1.03 |
| 34 | 51.50 | 45 0 | 100.0 | 80 | 2.446 | 0.95 |
| 35 | 51.50 | 45 0 | 100 0 | 100 | 2.369 | 0.87 |

where, $v_p$ is piston velocity in cm/min, $M$ is mesh size of abrasive grains, $C$ is percentage concentration of abrasives by weight, $N$ is number of cycles, MRR is material removal rate in g/min$\times 10^{-4}$, and $R_a$ is surface roughness in $\mu$m.

# blications from the Present Work

ain R K and Jain V K, Abrasive finishing processes- A review, *International ournal for Manufacturing Science and Production*, **2**, 1999, 55-68

ain R K, Jain V. K Jain and Kalra P K, Modeling of abrasive flow machining rocess - A neural network approach, *Wear* (Accepted for publication)

ain R. K, Jain V. K Jain and Dixit P. M, Modeling of material removal and surface nish in abrasive flow machining process, *International Journal of Machine Tools nd Manufacture* (Accepted for publication)

ain R. K and Jain V. K., Simulation of surface generated in abrasive flow machining rocess, Advances in Product and Process Development (Accepted for publication).

ain R. K., and Jain V. K, Optimum selection of machining conditions in Abrasive low Machining Process using Neural Network (submitted).